



**HAL**  
open science

## Synthesis of new tetrazines functionalized with photoactive and electroactive groups

Qing Zhou

► **To cite this version:**

Qing Zhou. Synthesis of new tetrazines functionalized with photoactive and electroactive groups. Other. École normale supérieure de Cachan - ENS Cachan, 2012. English. NNT : 2012DENS0039 . tel-00796461

**HAL Id: tel-00796461**

**<https://theses.hal.science/tel-00796461>**

Submitted on 4 Mar 2013

**HAL** is a multi-disciplinary open access archive for the deposit and dissemination of scientific research documents, whether they are published or not. The documents may come from teaching and research institutions in France or abroad, or from public or private research centers.

L'archive ouverte pluridisciplinaire **HAL**, est destinée au dépôt et à la diffusion de documents scientifiques de niveau recherche, publiés ou non, émanant des établissements d'enseignement et de recherche français ou étrangers, des laboratoires publics ou privés.

**ENSC-(n° d'ordre)**

**THESE DE DOCTORAT**

**DE L'ECOLE NORMALE SUPERIEURE DE CACHAN**

Présentée par

QING ZHOU

**pour obtenir le grade de**

**DOCTEUR DE L'ECOLE NORMALE SUPERIEURE DE CACHAN**

Domaine :

**CHIMIE**

**Sujet de la thèse :**

**Synthesis of new tetrazines functionalized with photoactive and electroactive groups**

Thèse présentée et soutenue à Cachan le 20/07/2012 devant le jury composé de :

Jean-Christophe LACROIX	Professeur (Université Paris Diderot)
Jean-Manuel RAIMUNDO	Maître de conférences (Université Aix-Marseille)
Céline FROCHOT	Directeur de Recherche CNRS
Pierre AUDEBERT	Professeur (ENS-CACHAN)
Gilles CLAVIER	Chargé de recherche CNRS
Fan YANG	Professeur (ECNU-Shanghai)
Fabien MIOMANDRE	Maître de conférences (ENS-CACHAN)
Jie TANG	Professeur (ECNU-Shanghai)

Laboratoire de Photophysique et Photochimie Supramoléculaires et

Macromoléculaire-PPSM

ENS CACHAN/CNRS/UMR 8531

61, avenue du Président Wilson, 94235 CACHAN CEDEX (France)



# Table of Contents

<b>Table of Contents</b> .....	3
<b>Acronyms</b> .....	7
<b>General Introduction</b> .....	9
<b>Chapter 1 Introduction of 1,2,4,5-tetrazine: chemistry and application</b> .....	13
1.1 Introduction of 1,2,4,5-tetrazine.....	13
1.2 Synthesis of <i>s</i> -tetrazines .....	14
1.2.1 Pinner synthesis .....	15
1.2.2 Modification of Pinner synthesis for aliphatic <i>s</i> -tetrazine .....	17
1.2.3 Synthesis of dichlorotetrazine .....	20
1.3 Reactivity of tetrazine .....	22
1.3.1 Inverse electron-demand Diels-Alder reaction .....	22
1.3.2 Cross-coupling reactions with terminal alkynes .....	26
1.3.3 Aromatic nucleophilic substitution ( $S_NAr$ reaction) .....	28
1.3.4 Azaphilic addition with carbanions .....	34
1.4 Physical chemistry of <i>s</i> -tetrazine .....	36
1.4.1 Electrochemistry of <i>s</i> -tetrazine .....	36
1.4.1.1 Introduction of electrochemistry .....	36
1.4.1.2 Electrochemistry of tetrazines .....	37
1.4.2 Photophysical properties of <i>s</i> -tetrazines .....	40
1.4.2.1 Introduction to photophysical chemistry .....	40
1.4.2.2 Photophysical properties of tetrazines .....	44
1.4.3 Computational chemistry on tetrazines.....	47
1.5 Applications of <i>s</i> -tetrazines.....	50
1.5.1 Energetic materials from tetrazines .....	50
1.5.2 Pharmaceuticals from tetrazines .....	51
1.5.3 Efficient solar cells .....	52
1.5.4 NLO-phore with tetrazine .....	53
1.6 Conclusions .....	54
<b>Chapter 2 New <i>s</i>-tetrazines derivatives as the ion pair receptors</b> .....	63
2.1 Introduction .....	63
2.1.1 Supramolecular chemistry and ion pair receptor .....	63
2.1.2 Fluorescent molecular sensors and electrochemical sensors .....	64
2.1.3 Experimental evidence of anion-tetrazine interactions .....	66
2.1.4 Anion- $\pi$ interactions .....	68
2.2 Molecular design of ion pair receptors .....	72
2.3 Molecular synthesis .....	77
2.3.1 Preparation of 3,6-dichloro-1,2,4,5-tetrazine .....	77
2.3.2 Preparation of ion-pair receptors .....	78
2.3.3 Selection and synthesis of ion pairs .....	79
2.4 Screening for ion-pairs .....	80
2.5 NMR studies of ion pair receptors .....	81

2.5.1 <sup>1</sup> H NMR titration .....	81
2.5.2 Job plot .....	88
2.5.3 Determination of binding constant .....	89
2.6 Fluorescence studies of ion pair receptors .....	91
2.6.1 Spectroscopic properties of receptors .....	91
2.6.2 Titration studies .....	92
2.7 UV-vis absorption studies of ion pair receptors .....	97
2.8 Conclusions .....	100

### **Chapter 3 Studies of tetrazines with bulky or electron withdrawing substituents.107**

3.1 Studies of tetrazines with bulky or electron withdrawing substituents .....	107
3.1.1 Molecular design .....	107
3.1.2 Synthesis .....	108
3.1.3 Absorption and fluorescence properties .....	111
3.1.4 Electrochemical properties .....	113
3.2 New alkyl-s-tetrazines from an unexpected reaction .....	116
3.2.1 Introduction .....	116
3.2.2 Optimization and extension of the scope of the reaction.....	117
3.2.3 Spectroscopic studies .....	119
3.2.4 Electrochemical studies .....	123
3.3 Toward s-tetrazine based fluorescent dyads.....	125
3.3.1 Molecular design .....	125
3.3.2 Synthesis .....	127
3.3.3 Spectroscopic studies .....	132
3.3.4 Electrochemical studies .....	135
3.4 Tetrazines benzimidazole dyads .....	138
3.4.1 Molecular design .....	138
3.4.2 Synthesis .....	139
3.4.3 Spectroscopic studies .....	141
3.4.4 Electrochemical studies .....	143
3.5 Concluding remarks .....	144

### **Chapter 4 New brightly fluorescent s-tetrazines .....**

4.1 Resonant Energy transfer .....	149
4.2 Molecular design and synthesis .....	153
4.2.1 Molecular design .....	153
4.2.2 Preparation of the novel s-tetrazines n-ads .....	155
4.3 Spectroscopic studies of N-(2-(6-chloro-s-tetrazine-3-yloxy)ethyl)- 2-trifluoromethylbenzimidazole 143 .....	160
4.3.1 Electrochemical study .....	160
4.3.2 Absorption and fluorescence studies .....	161
4.3.3 Study of the energy transfer in 143 .....	163
4.4 Spectroscopic and electrochemical studies of NITZ .....	166
4.4.1 Electrochemical study .....	166

4.4.2 Absorption and fluorescence studies .....	167
4.4.3 Study of the energy transfer .....	169
4.5 Spectroscopic studies of 145 .....	175
4.5.1 Absorption and fluorescence studies .....	175
4.5.2 Energy transfer study .....	177
4.5.3 Color analysis of 2NITZ fluorescence.....	183
4.6 Spectroscopic studies for 146 .....	184
4.6.1 Absorption and fluorescence studies .....	184
4.6.2 Energy transfer studies for 3NITZ.....	185
4.7 Application of NITZ: three colors electrofluorochromic cell .....	189
4.8 Conclusions .....	193
<b>General conclusion and perspectives.....</b>	<b>195</b>
<b>Chapter 5 Experimental Section .....</b>	<b>197</b>
<b>Publication .....</b>	<b>241</b>
<b>Acknowledgement .....</b>	<b>261</b>



# Acronyms

CV: cyclic voltammogram

D-A: Diels-Alder

DCM: dichloromethane

DMF: dimethylformamide

EA: ethyl acetate

HEDMs: high-energy density materials

HOMO: highest occupied molecular orbital

LUMO: lowest unoccupied molecular orbital

NLO: nonlinear optical

NI: naphthalimide

PE: petroleum ether

PE(2) : photoelectron spectroscopy (1.4.1.2)

PET: photoelectron spectroscopy

PEO: polyethylene glycol

THF: tetrahydrofuran

TZ: 1,2,4,5-tetrazine

UV: ultra-violet





# General Introduction

The quest for new original organic fluorophores is still active in the scientific community, because of the many applications of these compounds in the fields of light generation, sensors, biosensors, and so on<sup>1,2</sup>. Among new organic fluorophores, *s*-tetrazines play a special role because their fluorescence stems from a normally forbidden  $n-\pi^*$  transition, localized on the *s*-tetrazine ring. Because of this, *s*-tetrazines are indeed the smallest organic fluorophores known to date. In addition, they have a strong electron withdrawing character, and consequently their excited state is a strong oxidant ( $E^\circ$  in the +2V range) and their fluorescence is therefore quenched by a variety of electron donors, which opens the way to the realization of original fluorescent sensors. In addition, these molecules are fluorescent both in the liquid and solid state, which is a chemical rarity. In the former years, the team lead by Pr Audebert in the ENS Cachan has started to study extensively *s*-tetrazine derivatives, especially their fluorescence<sup>1</sup> as well as the electrochemically triggered fluorescence switching (electrofluorochromism)<sup>3</sup>. And not the least, most *s*-tetrazine synthesis are relatively easy, starting from the classical dichloro-*s*-tetrazine, now routinely produced in the laboratory on several-grams scale.

*s*-Tetrazines are also electroactive molecules, which can be reversibly transformed into a stable anion-radical, and whose fluorescence can be efficiently switched on and off by electrochemical conversion. They can be inserted into larger molecular assemblies in order to develop low bandgap polymers and related materials<sup>4</sup>. Due to all these outstanding properties, *s*-tetrazines are an extremely promising target in the field of synthetic and physical chemistry.

Chapter 1 of this manuscript is devoted to the bibliographic analysis, describing the state of the knowledge in the field of *s*-tetrazines, replacing it in the larger domain of the fluorescent and electroactive organic fluorophores.

The main body of work aimed at the synthesis and studies new *s*-tetrazines, in order to match different goals and to improve the efficiency of these molecules, especially in the field of fluorescence and chemical sensing. First of all, an interesting point to investigate was the possibility to prepare anion-sensing molecules, because some theoretical works have proposed that *s*-tetrazine<sup>5</sup> should be able to form stable adducts with some anions, in particular halide anions. In addition, these adducts could be non-fluorescent, or at least have a quite different emission spectrum. Although initial findings from the ENS Cachan group had not permitted

to observe any favorable interaction between *s*-tetrazines and halides, only experiences in solution had been performed, where only random encounter between *s*-tetrazines and the substrate could occur, without trying to favor the proximity of the *s*-tetrazine ring with the anion that was supposed to interact. We wished therefore to develop supramolecular *s*-tetrazines, where an ions pair would be forced to sit close to the *s*-tetrazine ring, in order to get an interaction between them. To achieve this goal, a straightforward path was to connect *s*-tetrazine with a cation binder. If a cation could be locked very close to the *s*-tetrazine, then in turn the counteranion would also be obliged to stay in the vicinity, therefore enhancing the possibility of an interaction between the two partners. Thus, we have introduced a polyethylene oxide chain substituted on both ends by *s*-tetrazine rings. We describe the synthesis of some of these compounds, as well as the analytical studies in the presence of various ions pairs. We have analyzed the complexation efficiency with various salts and more especially the influence of the anion, using NMR, UV-vis. absorption and fluorescence spectroscopies as tools. We have found that in the case of these particular *s*-tetrazines, the nature of the anion influenced the NMR and fluorescence data. We have also found that, in the presence of iodide or bromide, photooxidation took place. This is related in chapter 2.

We have prepared *s*-tetrazines with bulky or electron withdrawing substituents in order to check if the fluorescence quantum yield could be improved. Indeed it is known that free rotation of substituents around the fluorophore in the excited state often causes the fluorescence intensity to decrease and bulky groups might counter this effect. Another point of concern was that the only efficiently fluorescent *s*-tetrazines known when our work was started were the chloroalkoxy-*s*-tetrazines. We have, during the course of the PhD, found a methodology to prepare new chloroalkyl and dialkyl *s*-tetrazines which are fluorescent, through simple aromatic nucleophilic substitution, although this reaction had been previously claimed not to work in the *s*-tetrazine series. This is related in chapter 3

Finally, we aimed at fighting one the major drawbacks of *s*-tetrazines, their relatively low absorption coefficients (around 500 L.mol<sup>-1</sup>.cm<sup>-1</sup> in the visible range and 1500 in the UV range). Actually, because the optical properties of *s*-tetrazines stem from a normally forbidden electronic transition, their absorption coefficient is unfortunately relatively low, compared to standard fluorophores (coumarins<sup>6</sup> displays values in the 30000 L.mol<sup>-1</sup>.cm<sup>-1</sup> range and fluorescein<sup>7</sup>, one of the best fluorophores, reaches 140000 L.mol<sup>-1</sup>.cm<sup>-1</sup>), but they perform much better than diacetyls, the only other class of fluorophores working after a n-π\* transition,

which have an extremely low in the 10-15 L.mol<sup>-1</sup>.cm<sup>-1</sup> range. This situation could be in principle solved by introducing “antennas” close to the *s*-tetrazine ring, consisting in another fluorophore able to absorb light with a much better efficiency and then transfer the energy onto the *s*-tetrazine, which can in turn emit fluorescence. However, the choice of the partner fluorophore is not trivial, since only efficient energy transfer has to occur, and detrimental processes have to be avoided, especially undesirable photoinduced electron transfer which leads on the other hand to fluorescence quenching, or non-radiative deactivation processes. This has been achieved by introducing electron-deficient fluorophores, and especially naphthalimides have proved to display excellent energy transfer with a high efficiency. Initial synthetic work is the final subject presented in chapter 3, and full spectroscopic studies results are given in chapter 4.

## Reference

1. Clavier, G.; Audebert, P., *s*-Tetrazines as Building Blocks for New Functional Molecules and Molecular Materials. *Chem Rev* **2010**, *110* (6), 3299-3314.
2. Devaraj, N. K.; Weissleder, R., Biomedical Applications of Tetrazine Cycloadditions. *Accounts Chem Res* **2011**, *44* (9), 816-827.
3. Kim, Y.; Do, J.; Kim, E.; Clavier, G.; Galmiche, L.; Audebert, P., Tetrazine-based electrofluorochromic windows: Modulation of the fluorescence through applied potential. *J Electroanal Chem* **2009**, *632* (1-2), 201-205.
4. Quinton, C.; Alain-Rizzo, V.; Dumas-Verdes, C.; Clavier, G.; Miomandre, F.; Audebert, P., Design of New Tetrazine-Triphenylamine Bichromophores - Fluorescent Switching by Chemical Oxidation. *Eur J Org Chem* **2012**, (7), 1394-1403.
5. Garau, C.; Quinonero, D.; Frontera, A.; Costa, A.; Ballester, P.; Deya, P. M., *s*-Tetrazine as a new binding unit in molecular recognition of anions. *Chem Phys Lett* **2003**, *370* (1-2), 7-13.
6. Hrdlovic, P.; Donovalova, J.; Stankovicova, H.; Gaplovsky, A., Influence of Polarity of Solvents on the Spectral Properties of Bichromophoric Coumarins. *Molecules* **2010**, *15* (12), 8915-8932.
7. Bogdanova, L. N.; Mchedlov-Petrossyan, N. O.; Vodolazkaya, N. A.; Lebed, A. V., The influence of beta-cyclodextrin on acid-base and tautomeric equilibrium of fluorescein dyes in aqueous solution. *Carbohydr Res* **2010**, *345* (13), 1882-1890.



# Chapter I Introduction of 1,2,4,5-tetrazine: chemistry and applications

## 1.1 Introduction of 1,2,4,5-tetrazine

Tetrazine (Figure 1.1) is a benzene like molecule with four CH units replaced by nitrogen atoms. The first two isomers, 1,2,3,4- and 1,2,3,5-tetrazine, have been the subject of synthetic studies<sup>1,2</sup>. Unfortunately few unequivocal products have been demonstrated, while 1,2,4,5-tetrazine (or *s*-tetrazine) has been unambiguously characterized experimentally<sup>3,4,5</sup>.

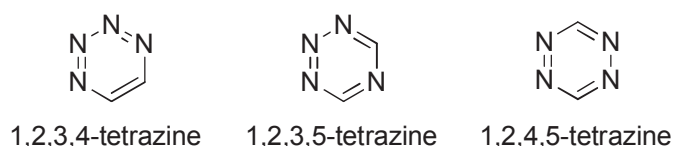


Figure 1.1. Tetrazine isomers.

The first report of *s*-tetrazine dates back to the end of the 19th century by Pinner<sup>6</sup>. He prepared several *s*-tetrazines, but did not go into many further investigations on their properties. Over the years, there have been more and more scientists interested in the *s*-tetrazines chemistry<sup>7,8</sup>. A lot of new *s*-tetrazines derivatives were synthesized by different ways<sup>9</sup>, including symmetrical tetrazines and unsymmetrical ones<sup>7</sup> (Figure 1.2).

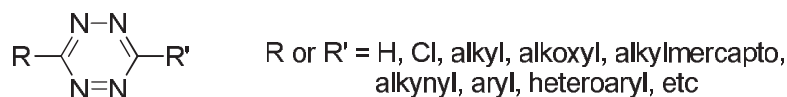


Figure 1.2. 1,2,4,5-Tetrazine derivatives.

As mentioned before, four CH groups are replaced by four more electronegative nitrogen atoms on the prototypical aromatic ring, which confer a high electron affinity to *s*-tetrazines. Hence they are the electron poorest C-N heterocycles, and can be reduced at high to very high potentials (-0.8~-0.4V vs Ag<sup>+</sup>/Ag). In addition, high nitrogen content makes *s*-tetrazines good candidates for energetic materials<sup>10,11</sup>.

The other distinct character of *s*-tetrazines is their low-lying  $\pi^*$  orbital (Figure 1.3), resulting in an  $n\text{-}\pi^*$  transition in the visible range. Thus, all *s*-tetrazines have a deep color ranging from purple to orange to red.

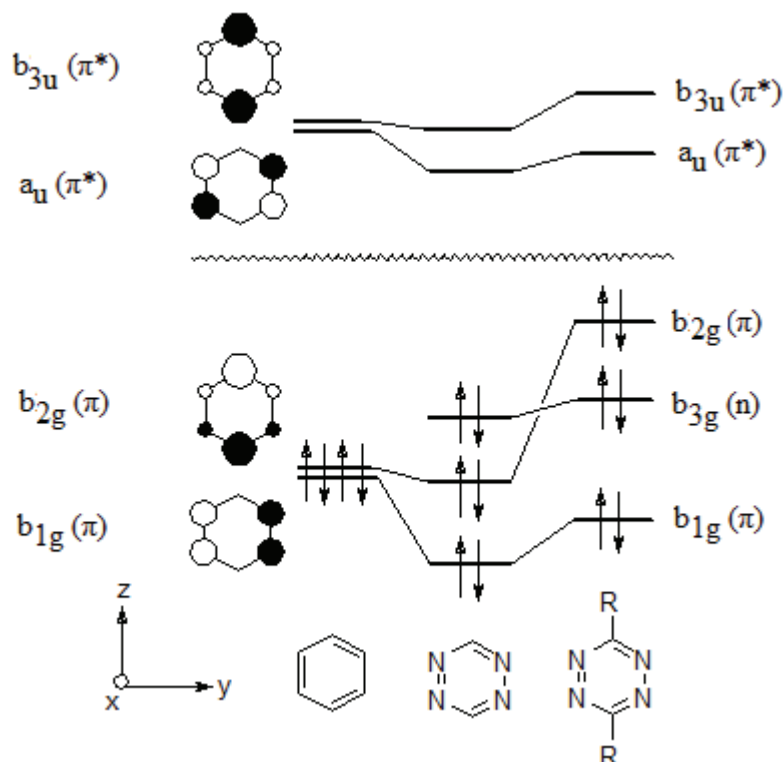


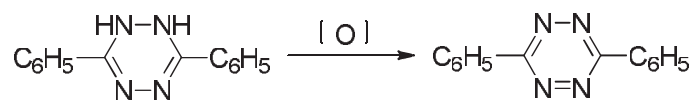
Figure 1.3. Qualitative diagram illustrating the energy shifts of the frontier orbitals of benzene and *s*-tetrazine as a result of 1,2,4,5-tetraaza replacement and 3,6-disubstitution by electron donating groups R.

The development of 1,2,4,5-tetrazine chemistry has been steady since 1996, not only owing to their structure and their reactivity, but also due to potential applications in various fields. The group of Professor Pierre Audebert and others paid more attention to the optical and electrochemical properties of new 1,2,4,5-tetrazines compounds given their outstanding photophysical and electron accepting properties.

## 1.2 Synthesis of *s*-tetrazines

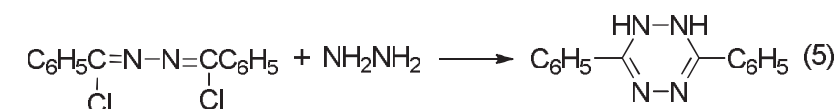
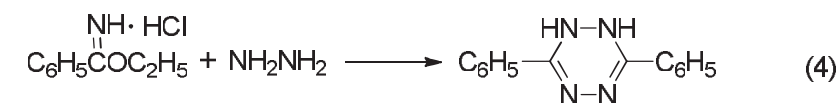
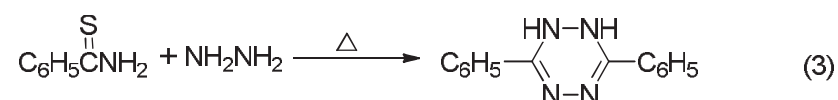
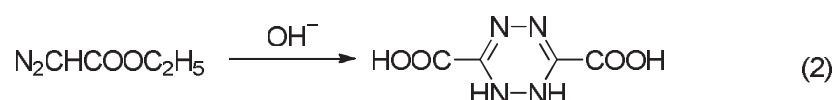
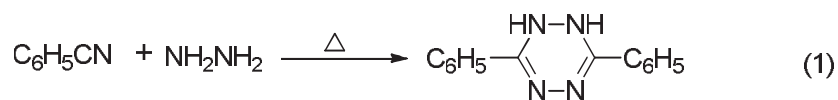
There is no direct synthesis of the *s*-tetrazine ring. It is always obtained by oxidation of its 1,2- or 1,4-dihydro (or even in very few cases its tetrahydro) counterpart (Scheme 1.1) by mild oxidizing agents, such as nitrites, bromine, air,

ferric chloride, hydrogen peroxide or chromic oxide<sup>9</sup>.



Scheme 1.1. Oxidation of diphenyl-1,2-dihydro-*s*-tetrazine.

Dihydro-*s*-tetrazine can be obtained by various methods. However, five main different ones are commonly used (Scheme 1.2)<sup>12</sup>. As the first reported method, the Pinner synthesis has been the object of several modifications as well as a number of special procedures. Most of the procedures presented have been shown to work for aromatic compounds. Only methods 1 and 4 can be used to prepare 3,6-dialkyl-1,2-dihydro-*s*-tetrazines.

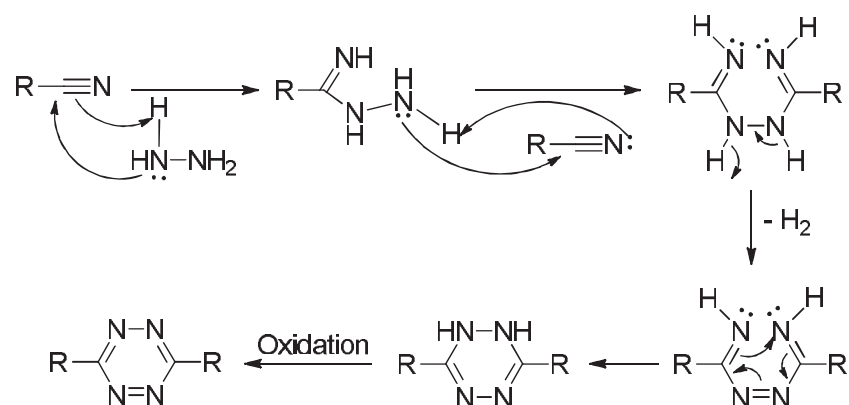


Scheme 1.2. Main preparation of dihydro-*s*-tetrazine.

### 1.2.1 Pinner synthesis

Pinner synthesis<sup>6</sup> plays an important role in the *s*-tetrazine chemistry. Original Pinner synthesis of dihydro-*s*-tetrazines has been shown in scheme 2(1): the aromatic nitrile is reacted with hydrazine in an aqueous solution of ammonium hydroxide, and the dihydro-*s*-tetrazines obtained is further oxidized into *s*-tetrazines. The mechanism of formation of *s*-tetrazines via Pinner synthesis is described in Scheme 1.3.





This synthetic route is effective for most of the aromatic symmetrical *s*-tetrazine where the nitrile is not sterically crowded. Wiley and co-workers<sup>13</sup> have improved the syntheses by carrying out the reaction under anhydrous conditions in a mixture of methanol and triethylamine. Some 3,6-diaryl-1,2,4,5-tetrazines (**1** and **2** in figure 1.4) and 3,6-di-*p*-biphenyl-1,2,4,5-tetraines (**3** in figure 1.4) were obtained in moderate yields. Using the same protocol, Soloduch<sup>14</sup> and his colleagues have synthesized a series of novel linear tetrazines, bis(pyrrolyl)tetrazines (**4** in figure 1.4) and bis(phenyl)tetrazines (**5,6,7** in figure 1.4). At the same time, Audebert<sup>4</sup> and his colleagues have synthesized some new original tetrazines substituted by heterocyclic rings (**8,9** in figure 1.4) using a related protocol and submitted them to electropolymerization.

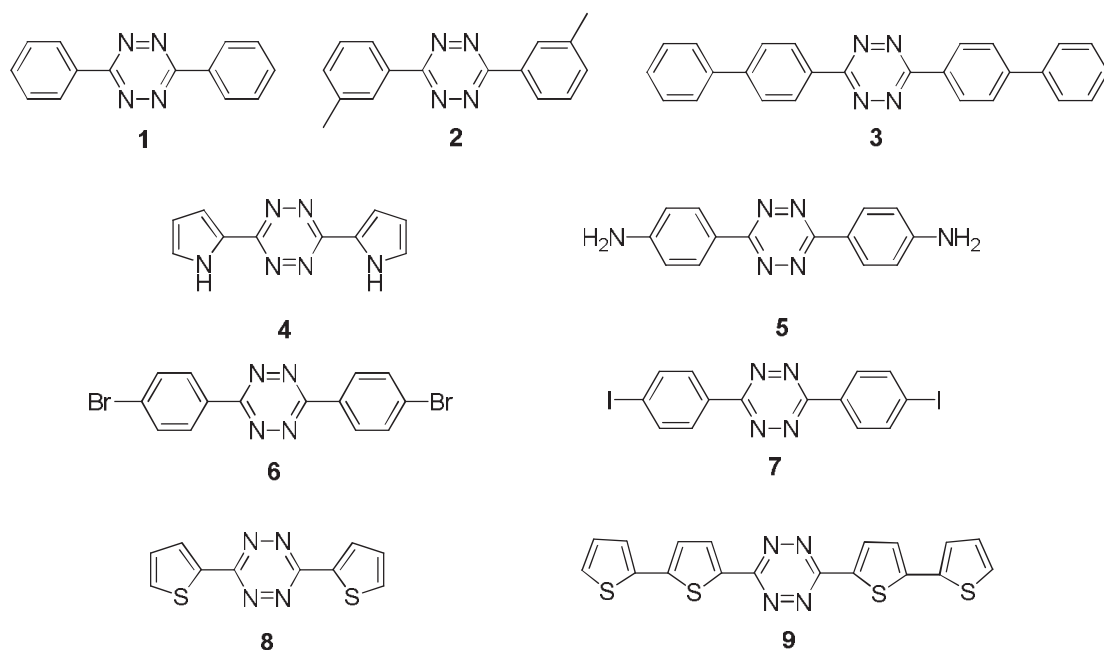
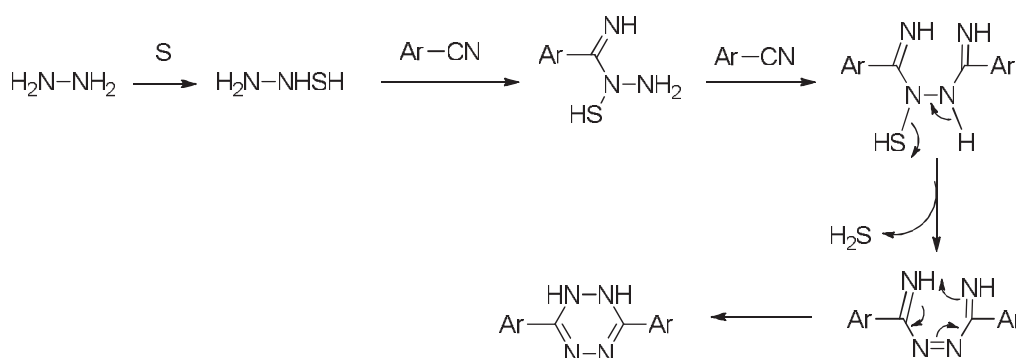


Figure 1.4. Examples of symmetrical aromatic *s*-tetrazines obtained by the modified Pinner synthesis.

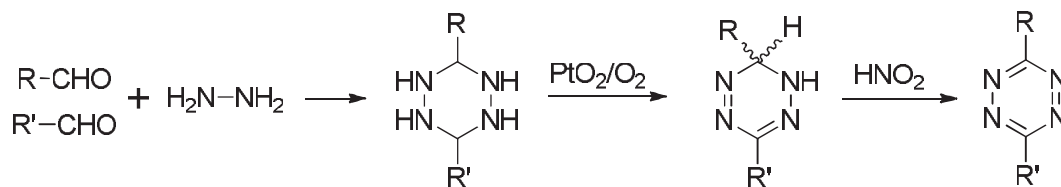
One of the most efficient modification of Pinner synthesis have been the discovery that the presence of sulfur in the reaction could lead to the formation of dihydro-*s*-tetrazine from aromatic nitrile in good yield<sup>12</sup>. Audebert's group<sup>8</sup> has proposed a reasonable mechanism on the basis of phenomenon observed during the course of the reaction (Scheme 1.4): the color of the solution changed from colorless to light orange, and vigorous production of H<sub>2</sub>S was detected through out of the reaction. This suggests that the active nucleophile is the addition product of sulfur on hydrazine (H<sub>2</sub>N-NH-SH).



Scheme 1.4. Mechanism of formation of aromatic tetrazines proposed by Audebert et al.

## 1.2.2 Modification of Pinner synthesis for aliphatic *s*-tetrazines

Pinner synthesis is effective for most of the symmetrical aromatic *s*-tetrazines, but does not work or does work in very low yields for aliphatic ones<sup>7,15</sup>. No clear explanation has been proposed for this observation, but could be likely due to confusion between the intermediate 1,2-dihydro-*s*-tetrazines and isomeric 4-amino-1,2,4-triazoles. In the case of aliphatic derivatives, the nitrile can be replaced by an aldehyde to give the hexahydro-*s*-tetrazine, which can be oxidized to *s*-tetrazine in two steps albeit in an overall low yield<sup>16,17</sup> (Scheme 1.5). However, aliphatic *s*-tetrazines are highly volatile, can easily sublime (some at atmospheric pressure and room temperature), and are difficult to isolate.

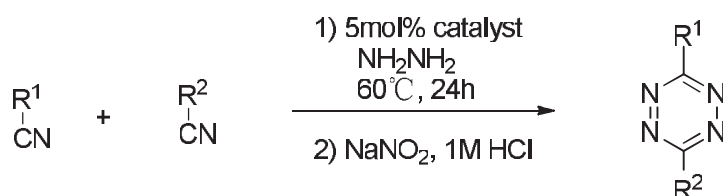


R=R'=Me, Et, *n*-Pr, *i*-Pr, *t*-Bu, *n*-C<sub>11</sub>H<sub>13</sub>  
 or R=Me, R'=Et  
 R=Me, R'=*i*-Pr  
 R=Me, R'=*t*-Bu  
 R=Et, R'=*i*-Pr

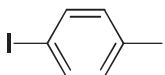
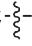
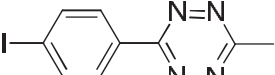
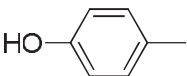
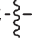
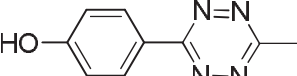
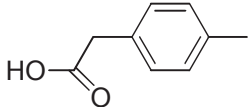
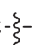
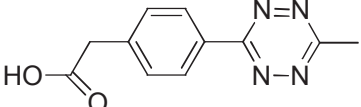
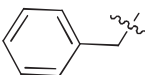
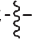
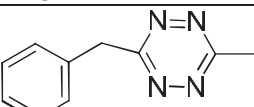
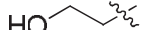
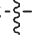
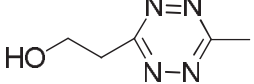

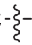
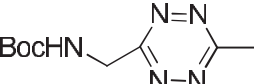
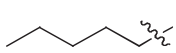
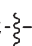
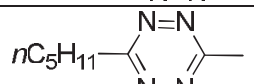
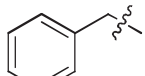

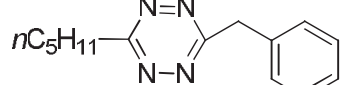
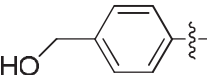
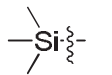
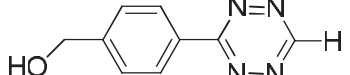
Scheme 1.5. Preparation of 3,6-dialkyl-1,2,4,5-tetrazines from the corresponding aldehyde.

Recently, Neal's group<sup>18</sup> reported the metal-catalyzed one-pot synthesis of *s*-tetrazines directly from aliphatic nitriles and hydrazine. They used the reaction of benzyl cyanide with neat hydrazine to survey a range of Lewis acid catalysts at 5mol% loading. Finally, the addition of 5mol% nickel triflate (Ni(OTf)<sub>2</sub>) led to near quantitative yield (95%) of 3,6-dibenzyl-*s*-tetrazine, and zinc triflate (Zn(OTf)<sub>2</sub>) gave good yields (70%). Then with these metal-catalysts, several *s*-tetrazines were synthesized directly from nitriles (Table 1.1). The scope of this method extends to asymmetric 3,6-disubstituted-*s*-tetrazines, which are among the most challenging *s*-tetrazines to synthesize. Although one of them (entry 15) was obtained in lower yield (about 12%), most of them have been synthesized in good to excellent yields (30%-70%).

Table 1.1. Synthesis of *s*-tetrazines directly from nitriles catalyzed by Ni(OTf)<sub>2</sub> and Zn(OTf)<sub>2</sub>.



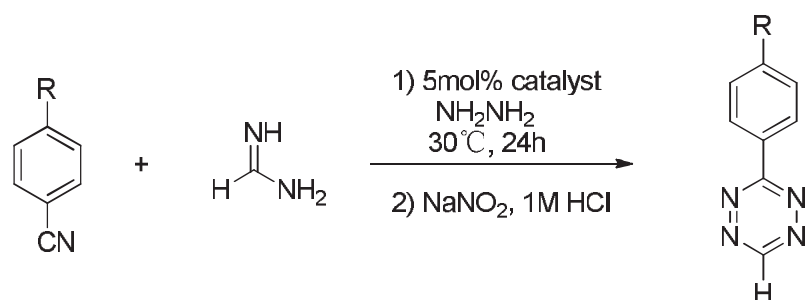
Entry	R <sup>1</sup>	R <sup>2</sup>	Cat	Product	Yield [%] <sup>a</sup>
1			Ni		95
2			Zn		59
3			Zn		24
4			Zn		32
5 <sup>b</sup>			Ni		58
6			Ni		68
7			Ni		66

8		$\text{H}_3\text{C}$ 	Ni		41
9		$\text{H}_3\text{C}$ 	Zn		43
10		$\text{H}_3\text{C}$ 	Ni		70
11		$\text{H}_3\text{C}$ 	Zn		40
12 <sup>c</sup>		$\text{H}_3\text{C}$ 	Zn		36
13		$\text{H}_3\text{C}$ 	Ni		36
14		$\text{H}_3\text{C}$ 	Zn		40
15			Zn		12
16 <sup>b</sup>			Zn		30

a. Yields reported after isolation by silica flash chromatography. b. The protective groups were lost during oxidative workup. c. Reaction required 36h.

Additionally, they explored the effect of Ni (OTf)<sub>2</sub> and Zn (OTf)<sub>2</sub> on the synthesis of *s*-tetrazine from aromatic nitriles and formamidine salts (Table 1.2). The metal ions could promote the reaction and increase the yield of *s*-tetrazine, which was between 60%-74%.

Table 1.2. Metal-catalyzed synthesis of *s*-tetrazines from aromatic nitriles and formamidine.



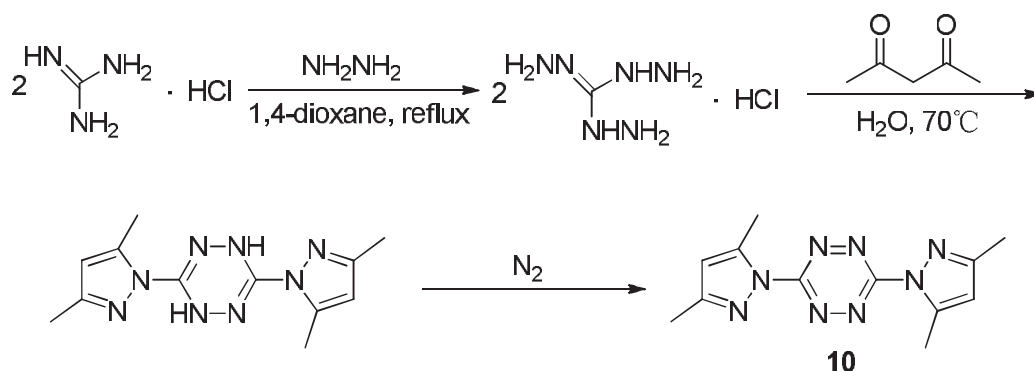
Entry	R	Cat.	Product	Yield [%] <sup>a</sup>
1		Ni		74
2		Ni		64
3 <sup>b</sup>		Zn		70

- a. Yields reported after isolation by silica flash chromatography.  
 b. Required use of DMF as cosolvent and 36h of reaction.

These modifications of Pinner's synthesis of *s*-tetrazine are helpful to obtain new *s*-tetrazines. Especially, the metal-catalyzed one-pot synthesis of *s*-tetrazines broadens the range of accessible substituted *s*-tetrazines. Consequently, it could benefit to many applications of *s*-tetrazines to various fields, such as, materials science, total synthesis and coordination chemistry.

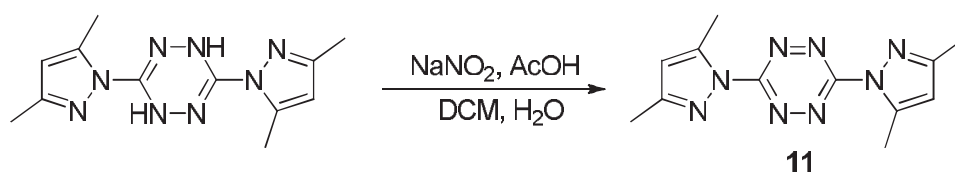
### 1.2.3 Synthesis of dichlorotetrazine

Dichloro-*s*-tetrazine, is an important intermediate for my research, and deserves particular attention. The synthetic work of Hiskey's<sup>19,20</sup> group is of utmost importance for the development of new *s*-tetrazines. They introduced an easy and quasi-quantitative procedure (Scheme 1.6) for the production of 3,6-bis(3,5-dimethyl-1H-pyrazol-1-yl)-*s*-tetrazine (**10**), which is a major intermediate to prepare dichloro-*s*-tetrazine.



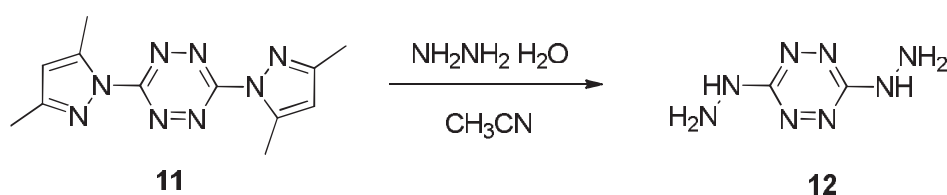
Scheme 1.6. Preparation of 3,6-bis(3,5-dimethyl-1H-pyrazol-1-yl)-*s*-tetrazine.

Audebert and colleagues<sup>8</sup> also contributed to this synthetic scheme by substituting the nitrous gas originally used in the oxidation step of the dihydro-*s*-tetrazine by the less cumbersome sodium nitrite (Scheme 1.7).



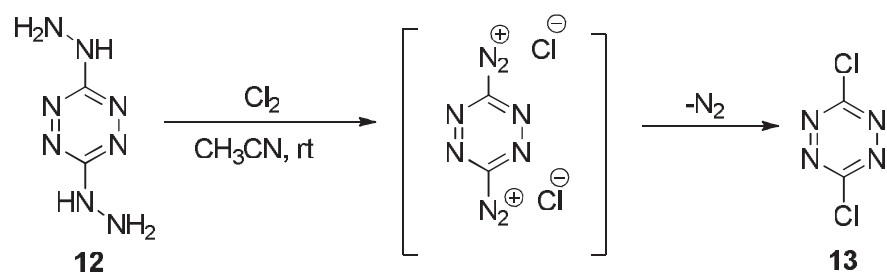
Scheme 1.7. Oxidation of bis(dimethylpyrazolyl)-dihydro-s-tetrazine with sodium nitrite.

The pyrazolyl moieties of **11** act as soft leaving groups, allowing a large range of substituents to be introduced on the *s*-tetrazine ring, provided that the basic character of the entering nucleophile is not too strong and its hardness of medium strength<sup>21,19</sup>. This has been done with hydrazine to give compound **12** (Scheme 1.8).



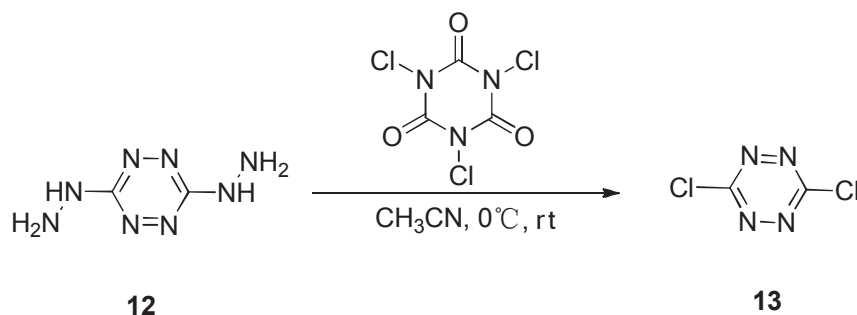
Scheme 1.8. Substitution of bis(dimethylpyrazolyl)-*s*-tetrazine with hydrazine.

Then, compound **12** can be used to prepare 3,6-dichloro-*s*-tetrazine in two steps with an overall yield *ca.* 80% and no tedious purification during the process (a very short chromatography is however required if very pure dichloro-*s*-tetrazine is needed). Hiskey<sup>22</sup> *et al.* investigated this reaction with chlorine gas (Scheme 1.9).



Scheme 1.9. Preparation of dichloro-*s*-tetrazine with chlorine gas.

Recently more convenient reaction conditions for this transformation were proposed by Harrity *et al.*, who replaced chlorine gas by the less dangerous trichloroisocyanuric acid<sup>23</sup> (Scheme 1.10).



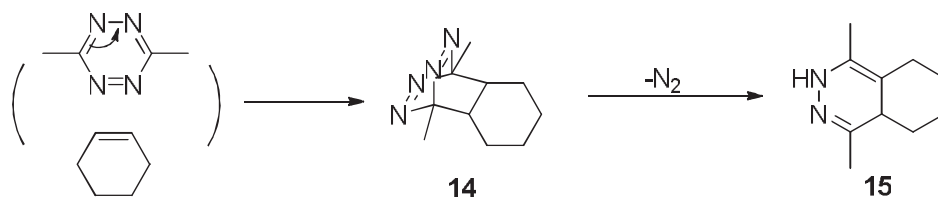
Scheme 1.10. Preparation of dichloro-*s*-tetrazine with trichloroisocyanuric acid.

In conclusion, the original Pinner synthesis is the main method to obtain *s*-tetrazines, especially for the aromatic substituted symmetrical derivatives. However, it can give aliphatic ones after modification. Based on the importance of dichloro-*s*-tetrazine in our research, we introduced its recently developed improved synthesis.

## 1.3 Reactivity of *s*-tetrazine

### 1.3.1 Inverse electron-demand Diels-Alder reaction

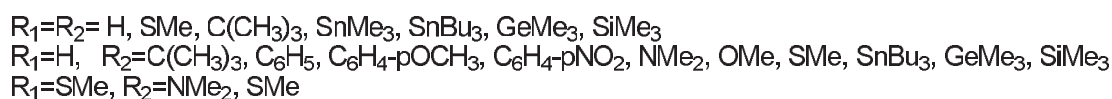
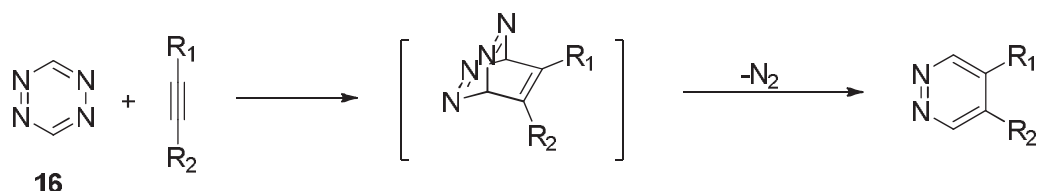
Until now, one of the main purposes for the *s*-tetrazines' research was preparation of tailored molecules and their implication in inverse demand Diels-Alder cycloaddition reactions<sup>24,25</sup> to make new pyridazines. The first observation was made by Carboni and Linsey<sup>26</sup> in 1959, while studying the synthesis of *s*-tetrazines from fluoroolefins and hydrazine. They discovered that *s*-tetrazines reacted readily with a variety of unsaturated compounds releasing one mole of nitrogen and yielding either dihydropyridazines or pyridazines depending on the dienophile reactant. It has since been determined that *s*-tetrazines react through a formal [4+2] Diels-Alder cycloaddition with numerous dienophiles. For example, 3,6-dimethyl-1,2,4,5-tetrazine can react with dienophiles such as alkenes and alkynes, forming formal [4+2] Diels-Alder adducts. These adducts instantly undergo a retro Diels-Alder step, releasing nitrogen. In the case of alkenes, after rearrangement, isomeric dihydropyridazines are typically formed. For example, the adduct (**14**, which has not been observed.) immediately undergoes an irreversible retro Diels-Alder step, which is responsible for the release of nitrogen to give 1,4-dihydro-pyridazine **15**<sup>27,28</sup> (Scheme 1.11).



Scheme 1.11. Example of a *s*-tetrazine Diels-Alder cycloaddition.

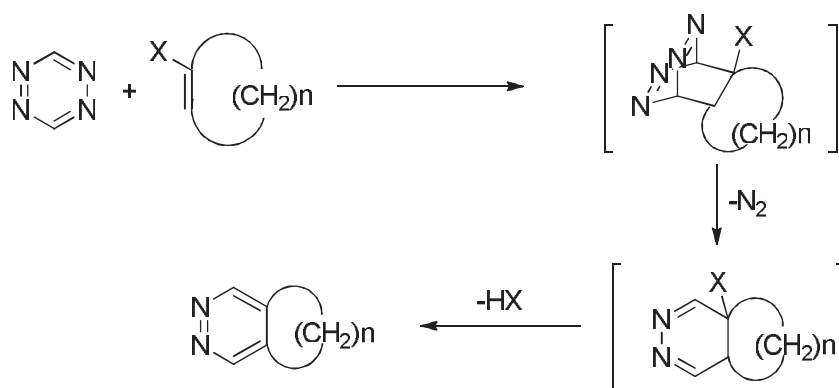
This application became the most developed to date, with large contributions from the groups of Sauer and Boger<sup>29,30,31,32</sup>. Tetrazines reaction with dienophiles can be followed spectroscopically by observing the disappearance of the visible absorption band usually found between 510 and 550nm. Sauer and co-workers performed extensive kinetic studies of the cycloaddition of various 3,6-substituted *s*-tetrazines with numerous dienophiles with this technique. The [4+2] cycloadditions of 1,2,4,5-tetrazine (**16**) with different dienophiles (alkynes, cyclic alkenes, ketene amins and so on) have been the object of studies to improve the conditions, yields and obtain supplementary kinetic data(Scheme 1.12).

Cycloadditions with electron-rich alkynes<sup>27</sup> afforded the expected donor-substituted pyridazines. All reactions proceed cleanly, side reactions are not observed and yields are generally high.



Scheme 1.12. [4+2] Cycloadditions of 1,2,4,5-tetrazines with alkynes.

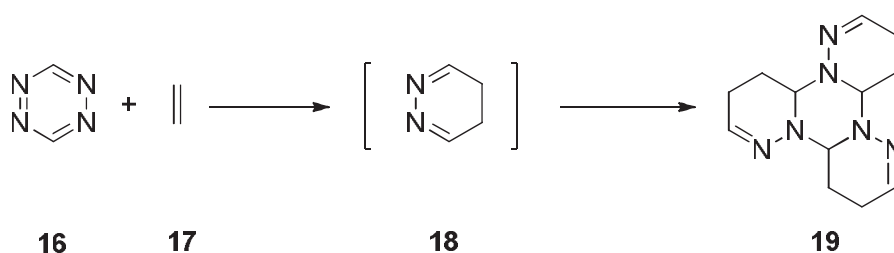
The reactions with cyclic alkenes (Scheme 1.13) are somewhat more complicated, due to different subsequent reactions being possible<sup>29</sup>. The mode of these subsequent reactions depends on the structure of the dienophile, as well as on the substituents in the 3- and 6- positions of the 1,2,4,5-tetrazine.



Scheme 1.13. [4+2] Cycloadditions of 1,2,4,5-tetrazine with cyclic alkenes.



For open-chain alkenes (Scheme 1.14), the modes of subsequent reactions also depend on the substituents of the alkene. For example, when ethylene (**17**) is the dienophile, the initially formed 4,5-dihydropyridazine (**18**) undergoes immediate trimerization to a mixture of stereoisomers (**19**) with respect to the central 1,3,5-triazane ring system.



Scheme 1.14. [4+2] Cycloadditions of 1,2,4,5-tetrazine with ethylene.

Boger and co-workers also reported the relative reactivity of tetrazines (**20-24**) toward N-vinyl pyrrolidinone<sup>33</sup> (Figure 1.5). The corresponding experiments indicated that the reactivity of *s*-tetrazine (**20**) is greater than that of the others. The experimental findings were consistent with Austin model 1 computational studies of a full range of substituted 1,2,4,5-tetrazines, where the LUMO of both **21** and **22** was at a higher energy than that of 3,6-dicarbomethoxy-1,2,4,5-tetrazine, but lower than **23** and **24**.

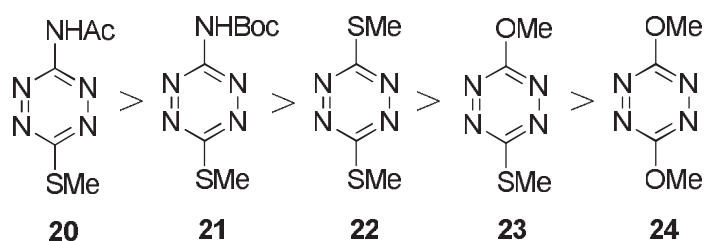
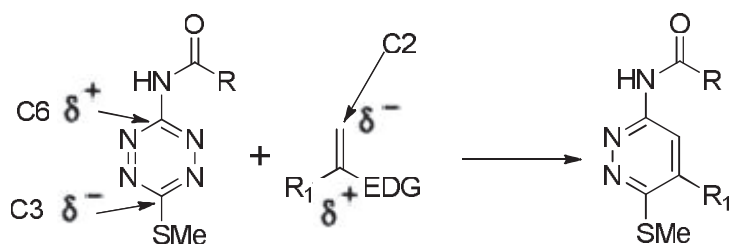


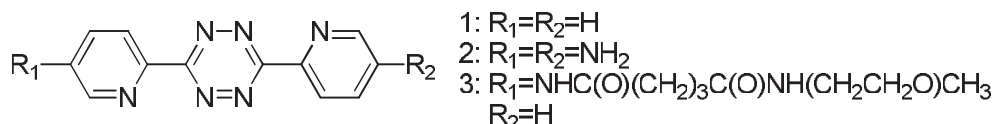
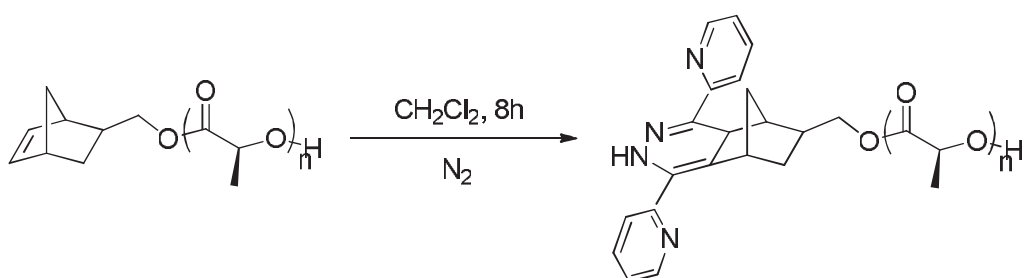
Figure 1.5. Order of reactivity of a series of *s*-tetrazines in inverse electron demand Diels-Alder reactions with electron-rich dienophiles.

They also found that the cycloaddition regioselectivity is consistent with the polarization of the diene and the ability of the methylthio group to stabilize a partial negative charge at C-3, and the N-acylamino group to stabilize a partial positive charge at C-6 (Scheme 1.15).



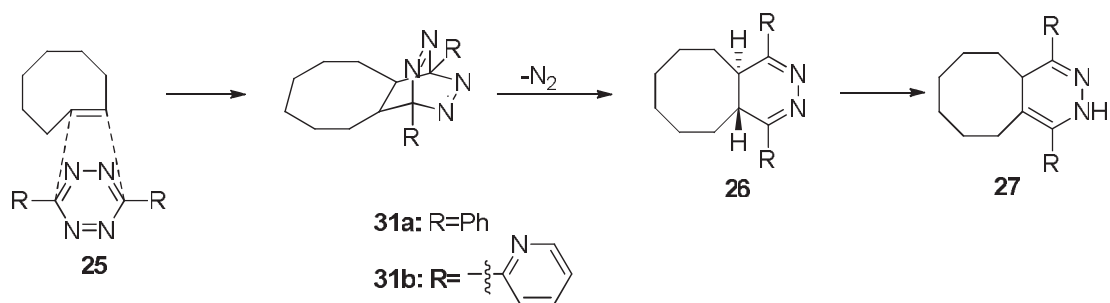
Scheme 1.15. The cycloaddition regioselectivity of 3-acylamino-6-methylthio-*s*-tetrazine in inverse electron demand D-A reaction.

Recently, the Diels-Alder reactions of *s*-tetrazine have been widely used. For instance, Dove<sup>34</sup> and co-workers used *s*-tetrazine-norbornene click reactions to functionalize degradable polymers derived from lactide (Scheme 1.16). This methodology, using the click reaction between *s*-tetrazine and norbornene, provides a versatile approach to widening the available pool of renewable polymeric materials.



Scheme 1.16. Reaction of 3,6-di-2-pyridyl-*s*-tetrazine with norbornene end-functional poly(L-lactide).

Furthermore, Joseph's group<sup>35,36</sup> introduced the *s*-tetrazine-trans-cyclooctene ligation (Scheme 1.17), a new bioorthogonal reaction with unusually fast rates that is based on the cycloaddition of *s*-tetrazines and trans-cyclooctene<sup>37</sup>. The development of this bioorthogonal reaction was enabled by a photochemical flow-reaction for the efficient preparation of trans-cyclooctene<sup>37-38</sup>. The results showed that 3,6-diaryl-*s*-tetrazines offer an excellent combination of fast reaction rates and stability for both the starting material and conjugation products.



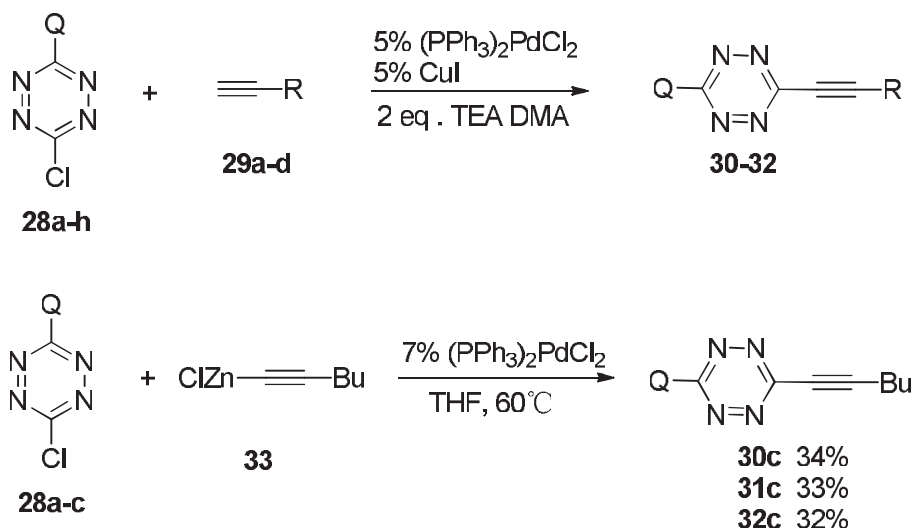
Scheme 1.17. Diels-Alder reaction of *s*-tetrazines with trans-cyclooctene.

Joseph and co-workers<sup>35</sup> designed a trans-cyclooctene derivative with enhanced reactivity in the *s*-tetrazine-trans-cyclooctene ligation by computational methods. The strained trans-cyclooctene derivative not only displays better reactivity but also can be easily derivatized, and bioconjugation to the protein thioredoxin has been demonstrated.

Today, the Diels-Alder reaction of *s*-tetrazine has gained more and more attention from researchers. This is due to the valuable applications in certain fields, particularly in biomedical application and total synthesis of natural compounds. On the other hand, heterocyclic aromatic rings can be synthesized by this kind of reaction. So it would be a potential subject of future development to obtain functional materials with the Diels-Alder reaction of *s*-tetrazine.

### 1.3.2 Cross-coupling reactions with terminal alkynes

The nonsymmetrically substituted *s*-tetrazines have been reported in limited number, because of their uneasy preparation. Until recently, the yield for their direct from the appropriate intermediates was low and the product difficult to purify from the symmetric ones always obtained as side products. On the other hand, the frequently utilized nucleophilic substitution reactions (see next paragraph) have been mostly limited to amines and alcohols. Kotschy's<sup>39</sup> group prepared a series of substituted chloro-*s*-tetrazines, which were reacted with different terminal alkynes under Sonogashira or Negishi coupling conditions (Scheme 1.18) to furnish alkynyl-*s*-tetrazines in moderate to good yields. The electron-donating property of the substituent on the tetrazine core was found to have a significant influence on the success of the reaction. The results constitute the first example of cross-coupling reactions on *s*-tetrazines.



Scheme 1.18. Cross-Coupling of various chloro-*s*-tetrazines with alkynes (the structures of R and Q are given in table 1.3).

Most aminotetrazines (**28a-c**) furnished the expected products (Table 1.3), but reaction with trimethylsilylacetylene (**29d**) was unsuccessful, as only decomposition was observed. Compounds bearing a secondary (**28d**) or primary amine (**28e**) scarcely reacted even after prolonged heating or changing the catalyst. More electron-deficient chloro-*s*-tetrazines (**28f-h**) were extremely sensitive and led only to decomposition products.

Table 1.3. Sonogashira coupling of various chlorotetrazines with acetylene derivatives.

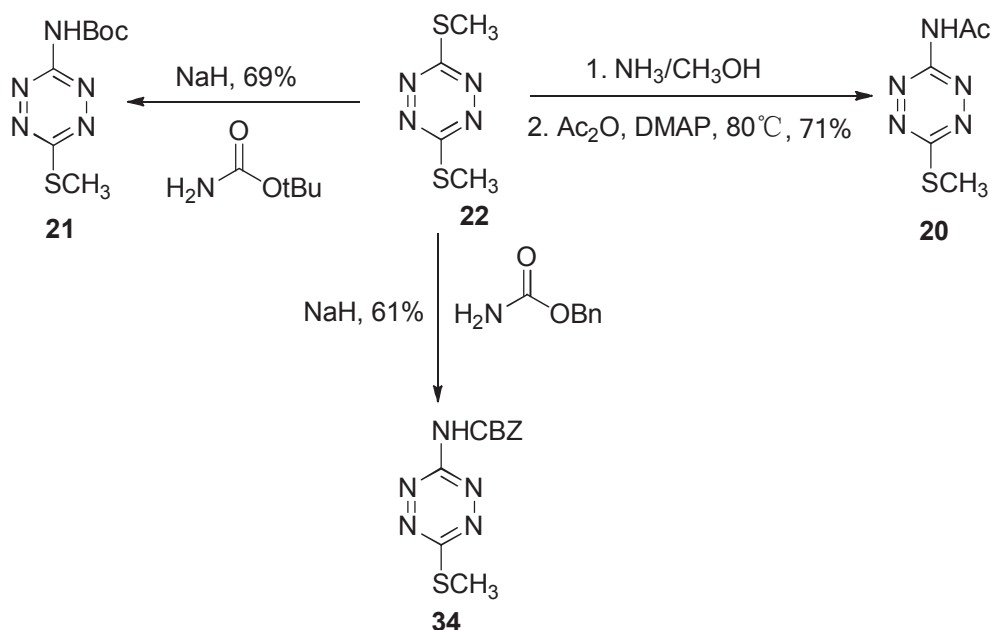
entry	Q	R	Yield(%) <sup>a</sup>
1	Morpholinyl ( <b>28a</b> )	C(CH <sub>3</sub> ) <sub>2</sub> OH ( <b>29a</b> )	57 ( <b>30a</b> )
2		Ph ( <b>29b</b> )	56 ( <b>30b</b> )
3		C <sub>4</sub> H <sub>9</sub> ( <b>29c</b> )	29 ( <b>30c</b> )
4		TMS ( <b>29d</b> )	dec <sup>b</sup>
5	Pyrrolidinyl ( <b>28b</b> )	<b>29a</b>	52 ( <b>31a</b> )
6		<b>29b</b>	23 ( <b>31b</b> )
7		<b>29c</b>	56 ( <b>31c</b> )
8	Diethylamino ( <b>28c</b> )	<b>29a</b>	30 ( <b>32a</b> )
9		<b>29b</b>	48 ( <b>32b</b> )
10		<b>29c</b>	65 ( <b>32c</b> )
11	Butylamino ( <b>28d</b> )	<b>29c</b>	traces
12	Amino ( <b>28e</b> )	<b>29a-c</b>	starting materials
13	Dimethylpyrazolyl ( <b>28f</b> )	<b>29a-c</b>	dec
14	Methoxy ( <b>28g</b> )	<b>29a</b>	dec
15	Chloro ( <b>28h</b> )	<b>29a</b>	dec

a. Isolated yield of analytically pure product.

### 1.3.3 Aromatic nucleophilic substitution ( $S_NAr$ reaction)

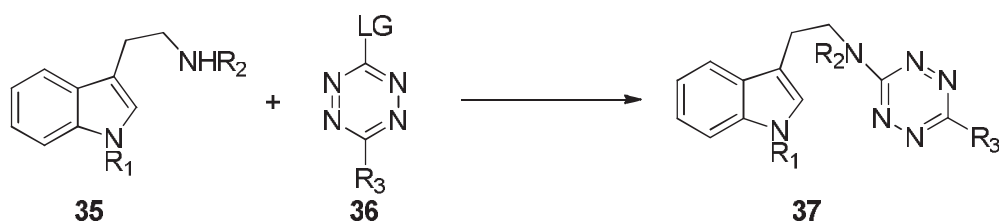
Besides the formation of the *s*-tetrazine ring directly from Pinner synthesis, a very important route toward functional *s*-tetrazines relies on their functionalization through nucleophilic aromatic substitution ( $S_NAr$ ), starting from an adequate precursor. For this purpose, bis(thiomethyl)-*s*-tetrazine was initially the compound of choice because of its relatively easy synthesis<sup>40</sup>.

Boger's group<sup>33</sup> reported three unsymmetrical *s*-tetrazines (**20**, **21** and **34**) for regioselective Diels-Alder reactions studies, which were anticipated to be accessible through the selective displacement of one methylthio group of 3,6-bis-(methylthio)-1,2,4,5-tetrazine (**22**) with the anions of tert-butyl carbamate, acetamide, or benzyl carbamate in one step procedure (Scheme 1.19). While this route proved successful, an alternative approach enlisting first the addition of ammonia and subsequent acylation of the resulting 6-amino-3-(methylthio)-1,2,4,5-tetrazine was also examined thus providing two methods for their preparation applicable to other unsymmetrically substituted tetrazines.



Scheme 1.19. Nucleophilic substitution on dimethylthio-*s*-tetrazine.

Snyder's group<sup>41</sup> also did some research in this field. For getting various heterocyclic compounds, they prepared tryptamine-tethered *s*-tetrazines by the displacements of methylthiolate from *s*-tetrazines in excellent yields (Scheme 1.20 and Table 1.4).



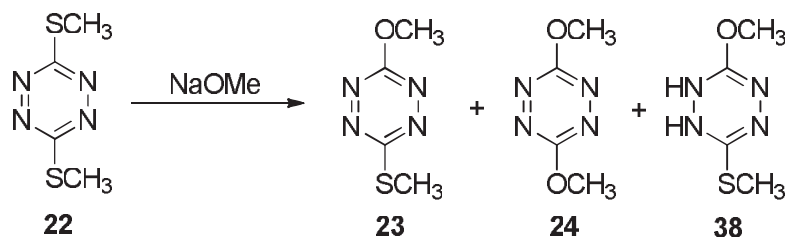
Scheme 1.20. Preparation of tryptamine-tethered *s*-tetrazines.

Table 1.4. Tethering of 1,2,4,5-tetrazines to tryptamine.

item	indole	R <sub>1</sub>	R <sub>2</sub>	tetrazine	R <sub>3</sub>	LG	conditions <sup>a</sup>	Product/yield
1	<b>35a</b>	H	H	<b>36a</b>	SCH <sub>3</sub>	SCH <sub>3</sub>	A	<b>37a</b> /94%
2	<b>35b</b>	Bn	H	<b>36a</b>	SCH <sub>3</sub>	SCH <sub>3</sub>	A	<b>37b</b> /95%
3	<b>35c</b>	Bn	Ac	<b>36a</b>	SCH <sub>3</sub>	SCH <sub>3</sub>	B	<b>37c</b> /60%
4	<b>35a</b>	H	H	<b>36b</b>	H	SCH <sub>3</sub>	A	<b>37d</b> /86%
5	<b>35b</b>	Bn	H	<b>36b</b>	H	SCH <sub>3</sub>	A	<b>37e</b> /85%
6	<b>35b</b>	Bn	H	<b>36c</b>	CH <sub>3</sub>	SCH <sub>3</sub>	A	<b>37f</b> /85%
7	<b>35b</b>	Bn	H	<b>36d</b>	Cl	Cl	C	<b>37g</b> /83%

a: A=reflux in MeOH; B= *n*-BuLi in THF, -30°C; C= reflux in CH<sub>2</sub>Cl<sub>2</sub>

In order to investigate the Diels-Alder reactions of the unsymmetrically disubstituted 3-methoxy-6-methylthio-1,2,4,5-tetrazine **23**, Sakya's group<sup>42</sup> prepared it from 3,6-bis(methylthio)-1,2,4,5-tetrazine **22** and catalytic sodium methoxide in methanol (Scheme 1.21). Compared to the previously reported use of phosgene and diazomethane<sup>43</sup>, to synthesize *s*-tetrazine **24** from this method is technically more convenient (Table 1.5).



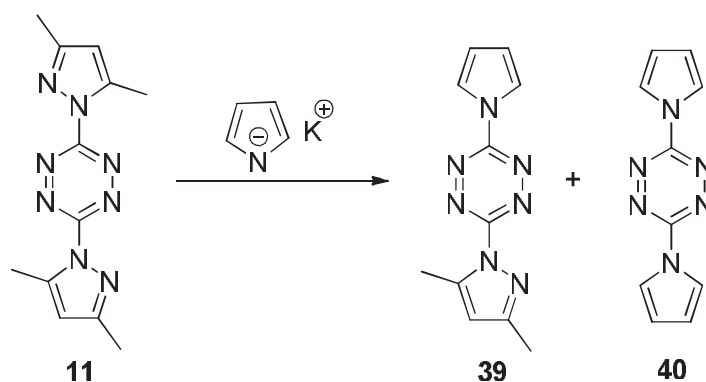
Scheme 1.21. Substitution of dimethylthio-*s*-tetrazine with sodium methoxide.

Table 1.5. Selective preparation of **23** and **24**.

NaOMe equiv.	solvent	temperatures	time	23	24
1.2	THF	0°C	20min	<5%	22%
1.1	THF	-78°C, -30°C	2h, 1h	60%	22%
0.1	MeOH	-15°C, 0°C	2h, 1h	<5%	56%

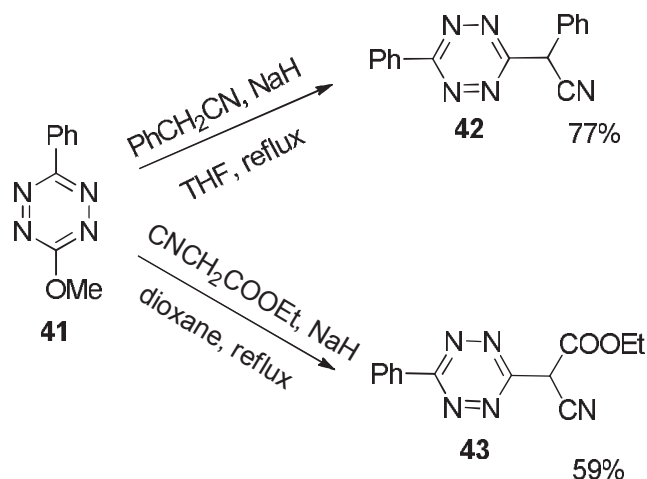
0.1	MeOH	-15°C	3h	65%	<5%
0.1	MeOH	-15°C, 0°C, RT	2h, 16h, 2h	7%	63%
0.1	MeOH	-78°C, -30°C	24h, 4h	72%	5%

Besides dimethylthio-*s*-tetrazine **22**, bis (dimethylpyrazolyl)-*s*-tetrazine **11** was another candidate for preparation of unsymmetrical *s*-tetrazines through nucleophilic aromatic substitution. Since pyrazolyl moiety acts as a soft leaving group, a large range of substituents could be introduced on *s*-tetrazine **11**. Audebert and colleagues<sup>44</sup> have prepared mono- and bis- *N*-pyrrolyl tetrazine **39** and **40** based on the S<sub>N</sub>Ar reaction of **11** with the anion *N*-pyrrolate anion, and investigated their electrochemical and spectroscopic features (Scheme 1.22).



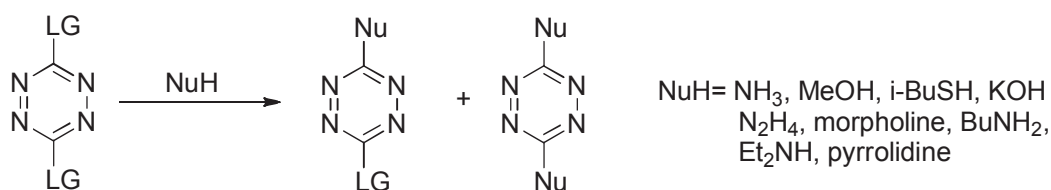
Scheme 1.22. Synthesis of compounds **39** and **40**.

As mentioned, these reactions have been mostly limited to nitrogen<sup>45,46</sup> and oxygen nucleophiles. There are only a few reports on the use of carbon nucleophile. Yamanaka and co-workers<sup>47</sup> studied the reaction of methoxy-*N*-heteroaromatics with phenylacetonitrile or ethyl cyanoacetate under basic conditions. They obtained unsymmetrically disubstituted *s*-tetrazines **42** and **43** in tetrahydrofuran in the presence of sodium hydride. The respective yields are 77% and 59% (Scheme 1.23).



Scheme 1.23. The reaction of 6-methoxy-3-phenyl-*s*-tetrazine with phenylacetonitrile or ethyl cyanoacetate.

Some of the intermediates formed through nucleophilic addition also require a subsequent oxidation to the aromatic product, which limits the number of substituents that are tolerated<sup>48</sup>. An optimal solution to this problem would be the use of *s*-tetrazines bearing good leaving groups which on treatment with nucleophiles, could undergo sequential displacement. Kotschy's group<sup>49</sup> has explored the selectivity of nucleophilic substitutions on various *s*-tetrazines. The three symmetrical *s*-tetrazine derivatives selected for the reactions with a series of nucleophiles, included 3,6-dichloro-*s*-tetrazine **13**, 3,6-bis(3,5-dimethylpyrazol-1-yl)-*s*-tetrazine **11**, and 3,6-bis(4-bromo-3,5-dimethylpyrazol-1-yl)-*s*-tetrazine **44** (Scheme 1.24).



LG= chloro, 3,5-dimethylpyrazol-1-yl, 4-bromo-3,5-dimethylpyrazol-1-yl

Scheme 1.24. Substitution of *s*-tetrazines by various nucleophiles.

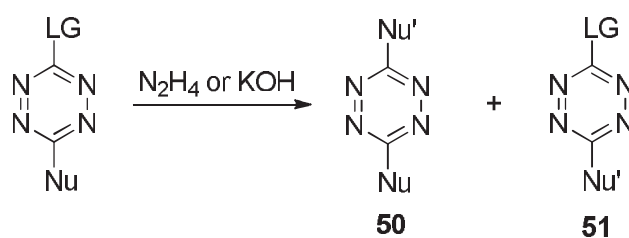
As expected, the chlorine atoms of 3,6-dichloro-*s*-tetrazine are both good leaving groups although the introduction of electron donating substituents led to a marked decrease of reactivity, which in turn allowed for the isolation of selectively mono substituted derivatives. Especially, *s*-tetrazines showed a marked tendency for disubstitution, when methanol or isobutyl mercaptan were used as the nucleophiles (Table 1.6).



Table 1.6. Preparation of *s*-tetrazines by nucleophilic substitution. Isolated yields of the mono- and disubstituted *s*-tetrazines from the reaction of **13**, **11** and **44**.

<i>s</i> -tetrazine/LG	NuH	monosubstitution	disubstitution
<b>13</b> /Chloro	NH <sub>3</sub>	78%	
	MeOH	52%	39%
	<i>i</i> -BuSH	5%	76%
	morpholine	83%	
	BuNH <sub>2</sub>	65%	
	Et <sub>2</sub> NH	89%	
	pyrrolidine	68%	
<b>11</b> /3,5-dimethylpyrazol-1-yl	NH <sub>3</sub>	96%	
	MeOH	80%	3%
	<i>i</i> -BuSH	66%	12%
	KOH	78%	
	N <sub>2</sub> H <sub>4</sub>	85%	
	morpholine	77%	
	BuNH <sub>2</sub>	91%	
	Et <sub>2</sub> NH	46%	
	pyrrolidine	74%	
<b>44</b> /4-bromo-3,5-dimethylpyrazol-1-yl	NH <sub>3</sub>	72%	
	MeOH	63%	8%
	<i>i</i> -BuSH	23%	43%
	KOH	81%	
	N <sub>2</sub> H <sub>4</sub>	67%	
	morpholine	83%	

After establishing the selective substitution on symmetrical *s*-tetrazines, the reactivity and selectivity of substitution on unsymmetrical ones towards nucleophiles was also examined (Scheme 1.25).



LG1= chloro,  
 LG2=3,5-dimethylpyrazol-1-yl,  
 LG3=4-bromo-3,5-dimethylpyrazol-1-yl  
 Nu= NH<sub>2</sub>, OMe, *i*-BuS

Scheme 1.25. Substitution on unsymmetrically by various nucleophiles.

The chloro-*s*-tetrazines gave only decomposition when reacted with soft hydrazine or hard potassium hydroxide. However, the other two *s*-tetrazines showed outstanding reactivity, and the course of the process depended both on the nature of the reagent and the leaving group. The reactivity of the leaving groups toward

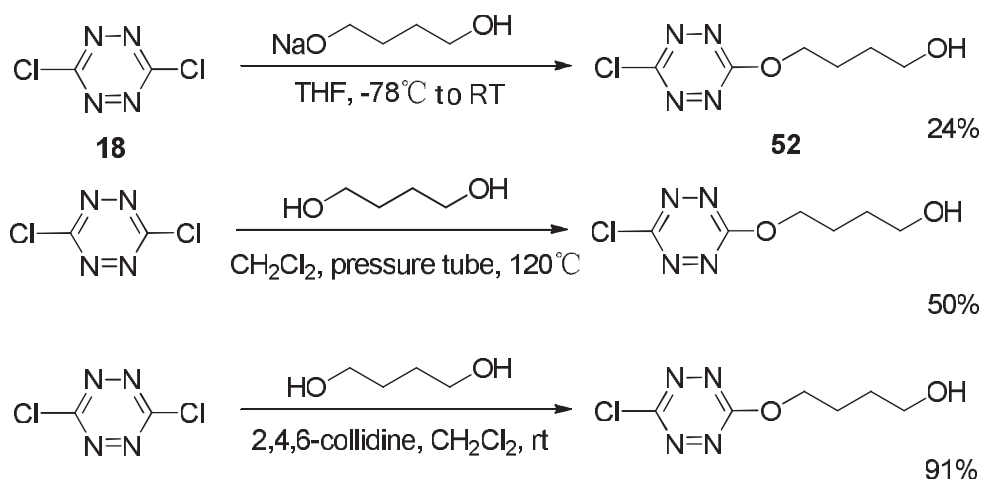
hydrazine decreased in the order: methoxy > pyrazolyl > amino, while towards the potassium hydroxide, it is methoxy, amino > bromopyrazolyl > mercapto > pyrazolyl (Table 1.7).

Table 1.7. Product distribution in the reaction of some selected *s*-tetrazine with different nucleophiles. (the yield were determined by NMR spectral investigation of the crude product).

LG	Nu	Nu'H	Normal substitution ( <b>50</b> )	Ipsosubstitution ( <b>51</b> )
chloro	NH <sub>2</sub>	N <sub>2</sub> H <sub>4</sub>	decomposition	Decomposition
	MeO		decomposition	decomposition
	<i>i</i> -BuS		Decomposition	Decomposition
	NH <sub>2</sub>	KOH	Decomposition	Decomposition
	MeO		Decomposition	Decomposition
	<i>i</i> -BuS		Decomposition	Decomposition
3,5-dimethyl Pyrazol-1-yl	NH <sub>2</sub>	N <sub>2</sub> H <sub>4</sub>	100%	
	MeO			100%
	<i>i</i> -BuS		100%	
	NH <sub>2</sub>	KOH		100%
	MeO			100%
	<i>i</i> -BuS		34%	66%
4-bromo- 3,5-dimethyl Pyrazol-1-yl	NH <sub>2</sub>	N <sub>2</sub> H <sub>4</sub>	100%	
	MeO			100%
	<i>i</i> -BuS		100%	
	NH <sub>2</sub>	KOH		100%
	MeO			100%
	<i>i</i> -BuS		66%	34%

Audebert's group<sup>4,50</sup> optimized the reaction conditions for the mono- and disubstitution of dichloro-*s*-tetrazine with alcohols (Scheme 1.26). Alcoholates proved to be too reactive as a lot of degradation took place and the desired products were obtained only in moderate yields. The reaction yield was improved by using the alcohol directly in a pressure tube. Addition of 2,4,6-collidine at room temperature gave the highest conversion to the monosubstituted derivative.

Disubstitution with the same alcohol can be done in good yield when using a combination of 2,4,6-collidine and pressure tube<sup>51</sup>. Unsymmetrical *s*-tetrazines can also be prepared from the monoether, but an alcoholate must be used in this case again and, the yield is about 25%.

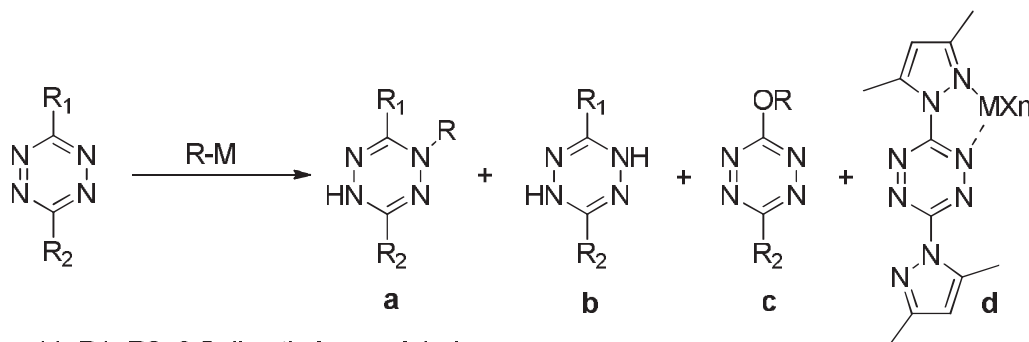


Scheme 1.26. Study of the  $S_NAr$  reaction conditions for the monosubstitution of **13** with butane-1,4-diol.

### 1.3.4 Azaphilic addition with carbanions

When reactive carbon nucleophiles such as organolithium or Grignard reagents<sup>52</sup> were used in an attempt to substitute 3,6-bis (methylthio)-*s*-tetrazine, the organic groups only added onto a ring nitrogen atom, giving “azaphilic addition” transformation, and not the  $S_NAr$  reaction. This is quite unprecedented for nitrogen containing heterocycles, but had been reported previously for 3,6-diphenyl-*s*-tetrazine.

Kotschy’s group<sup>53</sup> has prepared different *s*-tetrazine derivatives and reacted them with a series of organometallic reagents (Scheme 1.27), Azaphilic addition (a), reduction (b) or nucleophilic displacement (c) were observed. They noticed that the more polar organometallic reagents, especially lithium, magnesium and zinc derivatives, showed a marked affinity towards the nitrogen atom of the *s*-tetrazine core, a behavior fairly unusual in heterocyclic chemistry. The oxidative rearrangement of the azaphilic adducts to alkoxy/aryloxy tetrazines was also observed in certain cases (Table 1.8).



- 11: R1=R2=3,5-dimethylpyrazol-1-yl  
 22: R1=R2=methylthio  
 52: R1=R2=3-pyridyl  
 53: R1=3,5-dimethylpyrazol-1-yl, R2=morpholino  
 54: R1=morpholino, R2=chloro

Scheme 1.27. Product distribution in the azaphilic addition of organometallic carbanions to *s*-tetrazines.

Table 1.8. Results of azaphilic addition reactions of *s*-tetrazines with carbanions (yield %).

Entry.	tetrazine	R-M	a (%)	b (%)	c (%)	d (%)
1	11	BuLi	70			
2	11	PhLi	62			
3	11	PhMeCl	85			
4	11	BuCuLiI	60			40
5	11	BuZnBr	85			15
6	11	PhZnBr	90			
7	11	PhZnBr	45			35
8	11	(C <sub>3</sub> H <sub>5</sub> ) <sub>3</sub> In <sub>2</sub> Br <sub>3</sub>	60			
9	11	(C <sub>3</sub> H <sub>5</sub> ) <sub>3</sub> In <sub>2</sub> Br <sub>3</sub>	50	50		
10	52	BuLi	13	32		
11	52	BuMgI	96			
12	52	PhLi	35	25		
13	52	PhMeCl	58			
14	53	BuLi	13		80	
15	53	BuMgI	43		56	
16	53	PhLi	85			
17	53	PhMeCl	90			
18	22	BuLi	90			
19	22	PhLi	80			
20	22	PhMeCl	94			
21	54	PhMeCl	dec			

In conclusion, the study of reactivity of *s*-tetrazine mainly aimed at the synthesis of large variety of new compounds, such as, pyridazines or symmetrical and unsymmetrical *s*-tetrazines, S<sub>N</sub>Ar reaction was widely used by us to obtain new *s*-tetrazines derivatives since they display original fluorescence and electrochemical properties.

## 1.4 Physical chemistry of *s*-tetrazine

### 1.4.1 Electrochemistry of *s*-tetrazine

#### 1.4.1.1 Introduction to electrochemistry

Electrochemistry is a branch of chemistry that studies chemical reactions which take place in a solution at the interface of an electron conductor (a metal or a semiconductor) and an ionic conductor (the electrolyte), and which involve electron transfer between the electrode and the electrolyte or species in solution<sup>54</sup>.

Electroanalytical methods are a class of techniques in analytical chemistry which study an analyte by measuring the potential (volts) and current (amperes) in an electrochemical cell<sup>55,56</sup>. These methods can be classified into several categories depending on which aspects of the cell are controlled and which are measured. The three main categories are: potentiometry, coulometry and voltammetry. Voltammetry applies a constant or varying potential at an electrode's surface and measure the resulting current with a three electrodes system. This method can reveal the reduction or oxidation potential of an analyte and its electrochemical reactivity. This method in practical term is nondestructive since only a very small amount of the analyte is consumed at the two-dimensional surface of the working and auxiliary electrodes.

Cyclic voltammetry<sup>56,57,58</sup>(CV) is a type of potentiodynamic electrochemical measurement. In a cyclic voltammetry experiment the working electrode potential is ramped linearly versus time as shown in figure 1.6. The ramping is known as the experiment's scan rate (V/s). The potential is applied between the reference electrode and the working electrode while the current is measured between the working electrode and the counter electrode.

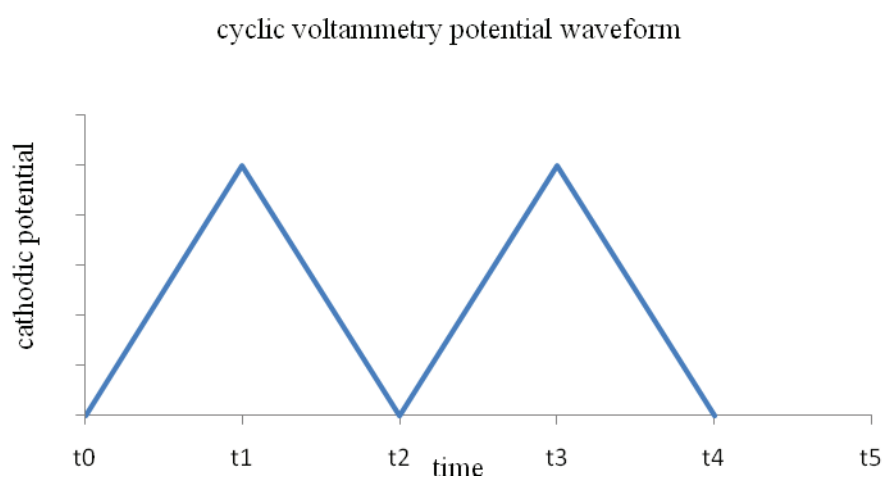


Figure 1.6. Cyclic voltammetry potential waveform.

As the waveform shows, the forward scan produces a current peak for any analytes that can be reduced (or oxidized depending on the initial scan direction) through the range of the potential scanned. The current will increase as the potential reaches the reduction potential of the analyte, but then falls off as the concentration of the analyte is depleted close to the electrode surface. If the redox couple is reversible then when the applied potential is reversed, it will reach the potential that will reoxidize (re-reduce) the product formed in the first reduction (oxydation) reaction, and produces a current of reverse polarity from the forward scan. This backward peak will usually have a similar shape to the forward one. Figure 1.7 display a typical cyclic voltammogram where  $i_{pc}$  and  $i_{pa}$  show the peak cathodic and anodic current respectively for a reversible reaction. Cyclic Voltammetry is generally used to study the electrochemical properties of an analyte in solution.

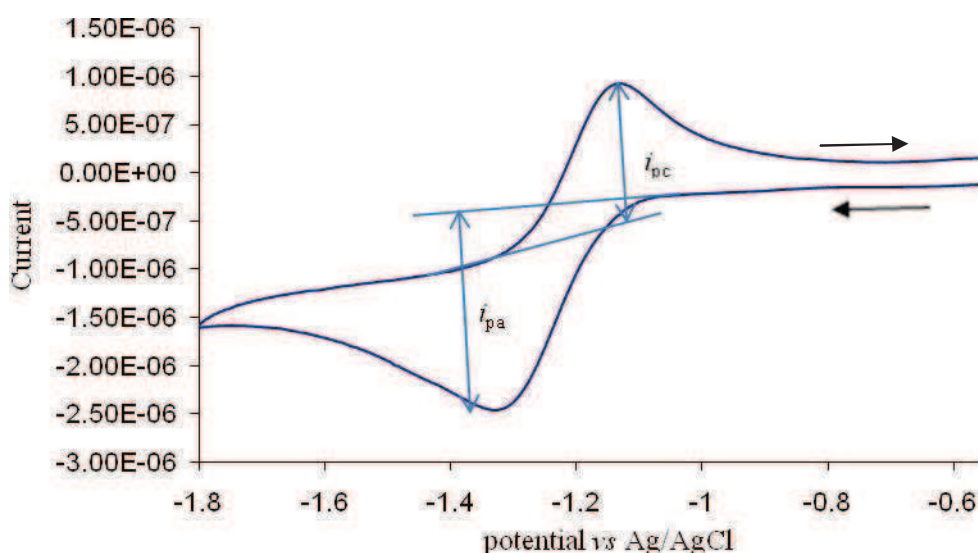


Figure 1.7. Example of cyclic voltammetry curve.

#### 1.4.1.2 Electrochemistry of *s*-tetrazines

The easy reduction of *s*-tetrazines (compared to other polyazines) was reported by Stone *et al.* as soon as 1963<sup>59</sup>. Subsequently their electrochemical reversibility was mentioned several times<sup>60</sup>. Then a paper by Neugebauer *et al.* gathered newly recorded along with ancient data from his group and former works<sup>61</sup>. Notably, fundamental experiments of photoelectron spectroscopy (PE) of *s*-tetrazines due to Gleiter *et al.*<sup>62,63</sup>, who studied a large number of donor or acceptor-substituted

*s*-tetrazines in order to find out the influence of  $\pi$ -electron donating and accepting groups on the ionization energies and the level ordering of *s*-tetrazines were included in the investigation. These PE measurements were combined with an electrochemical study ( $E_{1/2}$ ) and HAM/3 calculations to correlate PE bands and calculated the HAM/3 electron affinities. It should be mentioned that this interesting and relatively complete work reports a measurement on the very interesting compound difluoro-*s*-tetrazine, the synthesis of which was never subsequently reported. The anion radicals of various *s*-tetrazines have also been studied by ESR spectroscopy.

Aubedert's group studied many *s*-tetrazine derivatives, to decipher the factors governing the electrochemical properties<sup>44,50,51</sup>. All *s*-tetrazines examined which are substituted by heteroatoms or aromatics can be reversibly reduced in organic solvents, because of their electron-deficient character, accepting one electron to give an anion radical, very stable in the absence of acids (Figure 1.8). The differences in  $E_{1/2}$  values for the reversible reduction to the corresponding anion radicals reflect the electronic influence of the substituents. Thus, the variation of the potential  $E^0$  can be easily correlated to the electron withdrawing or donating character of the substituent (Table 1.9).

Table 1.9. Half-wave reduction potential (V vs Fc/Fc<sup>+</sup>) of *s*-tetrazine in dichloromethane.

No.	Substituent X, Y	$E^0$	No.	Substituent X, Y	$E^0$
1	Phenyl, phenyl	-1.21	18	Cl, Cl	-0.68
2	Pyrrol-2-yl, pyrrol-2-yl	-1.31	19	Cl, OMe	-0.99
3	2-thienyl, 2-thienyl	-1.24	20	Cl, naphthalene-1-yloxy	-0.97
4	2,2'-bithienyl-5-yl, 2,2'-bithienyl-5-yl	-1.25	21	Cl, pyrrolidine-1-yl	-1.35
5	4-ferrocenylphenyl, 4-ferrocenylpheny	-1.32	22	Cl, 2,3-diphenylaziridin-1-yl	-1.04
6	Cl, borneol	-0.74	23	OMe, OMe	-1.25
7	SMe, SMe	-1.20	24	OMe, SMe	-1.23
8	Cl, 9H-fluoren-9-ylmethoxy	-0.75	25	Cl, paracyclophan-4-ylmethoxy	-0.82
9	Cl, adamantan-2-yloxy	-0.79	26	Cl, adamantan-1-ylmethoxy	-0.85
10	Cl, pentachlorophenoxy	-0.54	27	Cl, N-phtalimidyl	-0.51
11	Adamantan-1-ylmethoxy, admantan-1-ylmethoxy	-1.13	28	Pyrrolidin-1-yl, pyrrolidin- 1-yl	-1.73
12	3,5-dimethyl-1H-pyrazol- 1-yl, OMe	-0.89	29	3,5-dimethyl-1H-pyrazol-1- yl, pyrrol-1-yl	-0.97
13	Pyrrol-1-yl,	-1.07	30	ferrocenyl,	-1.28

	pyrrol-1-yl			ferrocenyl	
14	3,5-dimethyl-1H-pyrazol-1-yl, 3,5-dimethyl-1H-pyrazol-1-yl,	-0.96	31	s-tetrazine	-1.16
15	difluorotetrazine	-0.56	32	dicyanotetrazine	-0.31
16	Bis(methylamino)tetrazine	-1.51	33	Bis(dimethylamino)tetrazine	-1.55
17	dimethyltetrazine	-1.32	34	Bis(aziridyl)tetrazine	-1.25

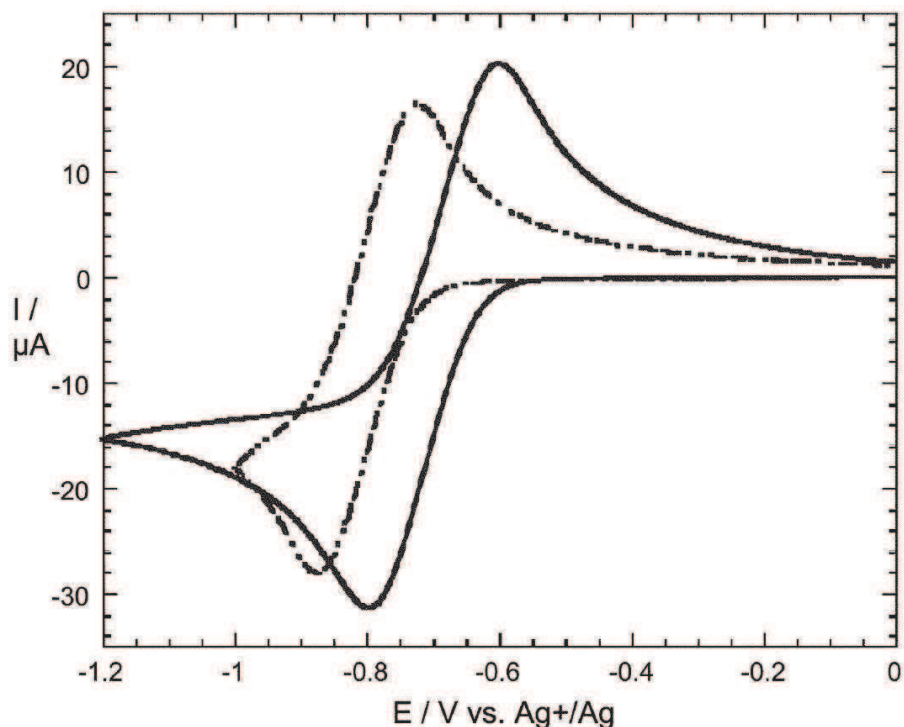


Figure 1.8. Cyclic voltammograms of bis-substituted tetrazines in dichloromethane (+0.1 M TBAP) on a platinum electrode: bis(N-pyrrolyl)-tetrazine (solid line) and bis(thienyl)tetrazine (dashed line).

Most of the tetrazine derivatives can also accept a second electron, despite the fact that this process is not electrochemically reversible in standard conditions. However, this latter process is chemically reversible (with the exception of dichloro-*s*-tetrazine), as demonstrated by the cyclic voltammogram of compound **8** in figure 1.9. Despite the fact that the second electron transfer does not give a stable dianion (which is probably very basic and reacts with traces of water or protic impurities), a stable species is formed and is sluggishly reoxidized into the original anion radical, which is completely restored. It is probable that the reduced species formed is the known dihydrotetrazine, or more likely its monoanion.



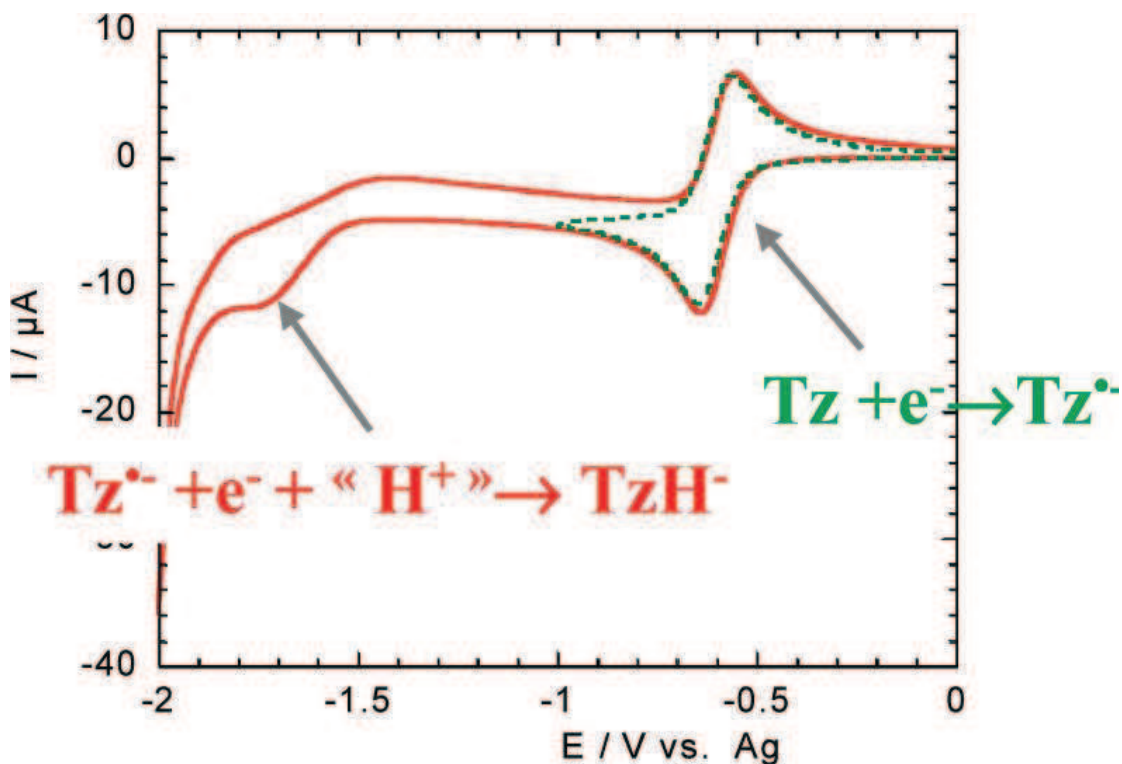


Figure 1.9. Cyclic voltammograms of **9** showing the first and second reductions.

## 1.4.2 Photophysical properties of *s*-tetrazines

### 1.4.2.1 Introduction to photophysical chemistry

The aim of this part is to recall the basic principles of UV-visible absorption and fluorescence emission.

#### (1) Absorption of UV-visible light

An electronic transition consists in the promotion of an electron from an orbital of a molecule in its ground state to an unoccupied orbital by absorption of a photon. There are several kinds of molecular orbitals which can give different types of electronic transitions (Figure 1.10).

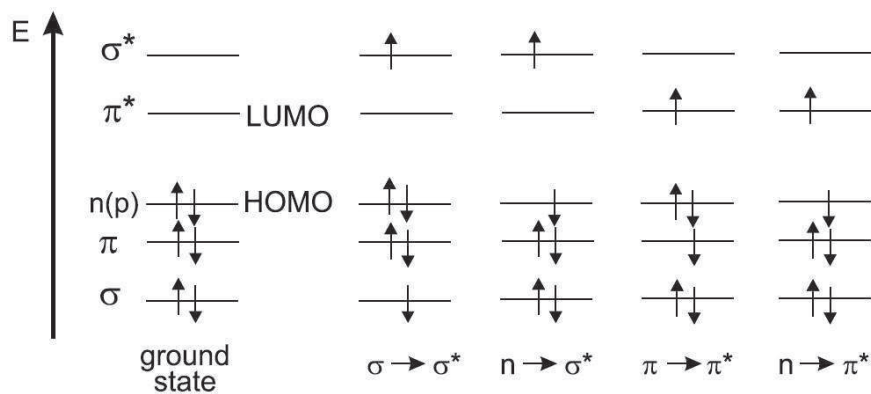


Figure 1.10. Energy levels of molecular orbitals in formaldehyde and possible electronic transition.

The energy of these electronic transitions is generally as follow:  $n \rightarrow \pi^* < \pi \rightarrow \pi^* < n \rightarrow \sigma^* < \sigma \rightarrow \sigma^*$ . In absorption and fluorescence spectroscopy, two important types of orbitals are considered: the Highest Occupied Molecular Orbitals (HOMO) and the Lowest Unoccupied Molecular Orbitals (LUMO). The energy difference between the HOMO and LUMO is termed the HOMO-LUMO gap, and the spectrum is decided by this gap. Both refer to the ground state of molecule.

The efficiency of light absorption is expressed by the molar absorption coefficient ( $\epsilon$ ), which can be calculated by the Beer-Lambert Law (Equation 1.1).

$$A(\lambda) = \log \frac{I_0}{I_\lambda} = \epsilon(\lambda)lc$$

Equation 1.1. The Beer-Lambert Law.

## (2) Fluorescence emission

Once a molecule is excited by absorption of a photo, it returns to the ground state by various possible de-excitation pathways (Figure 1.11): emission of fluorescence, internal conversion (direct return to the ground state without emission of fluorescence), intersystem crossing (possibly followed by emission of phosphorescence), conformational changes. Interactions in the excited state with other molecules may also open other pathways: electron transfer, proton transfer, energy transfer, excimer or exciplex formation, intermolecular charge transfer<sup>64</sup> which competes with intramolecular de-excitation processes.

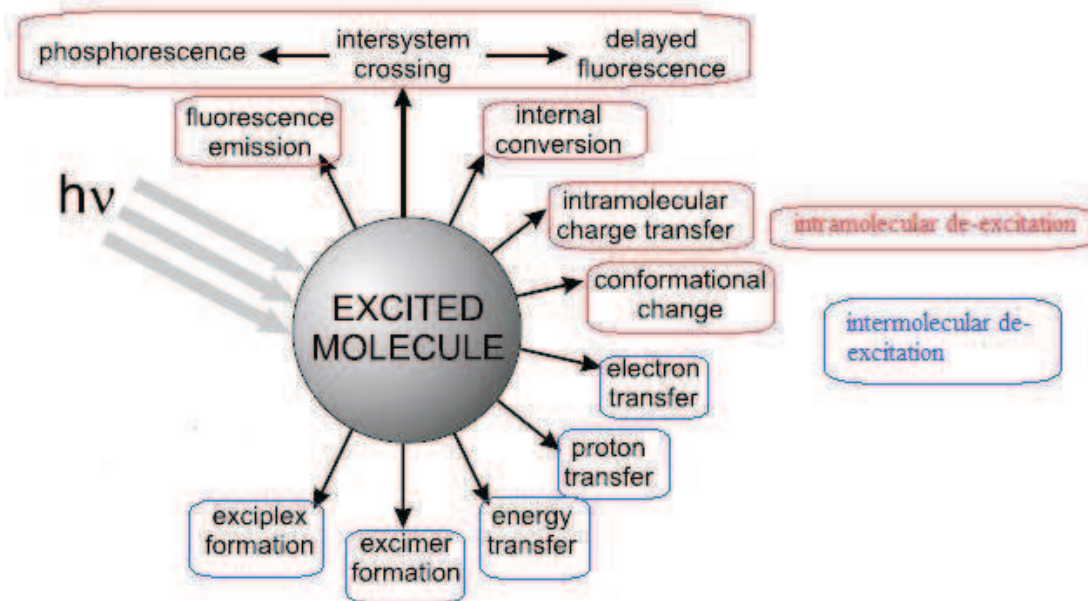


Figure 1.11. De-excitation pathways for an excited molecule.

Generally, emission of photons accompanying the  $S_1 \rightarrow S_0$  relaxation is called fluorescence (Figure 1.12), and the fluorescence spectrum is located at higher wavelengths (lower energy) than the absorption spectrum because of the energy loss in the excited state due to vibrational relaxation.

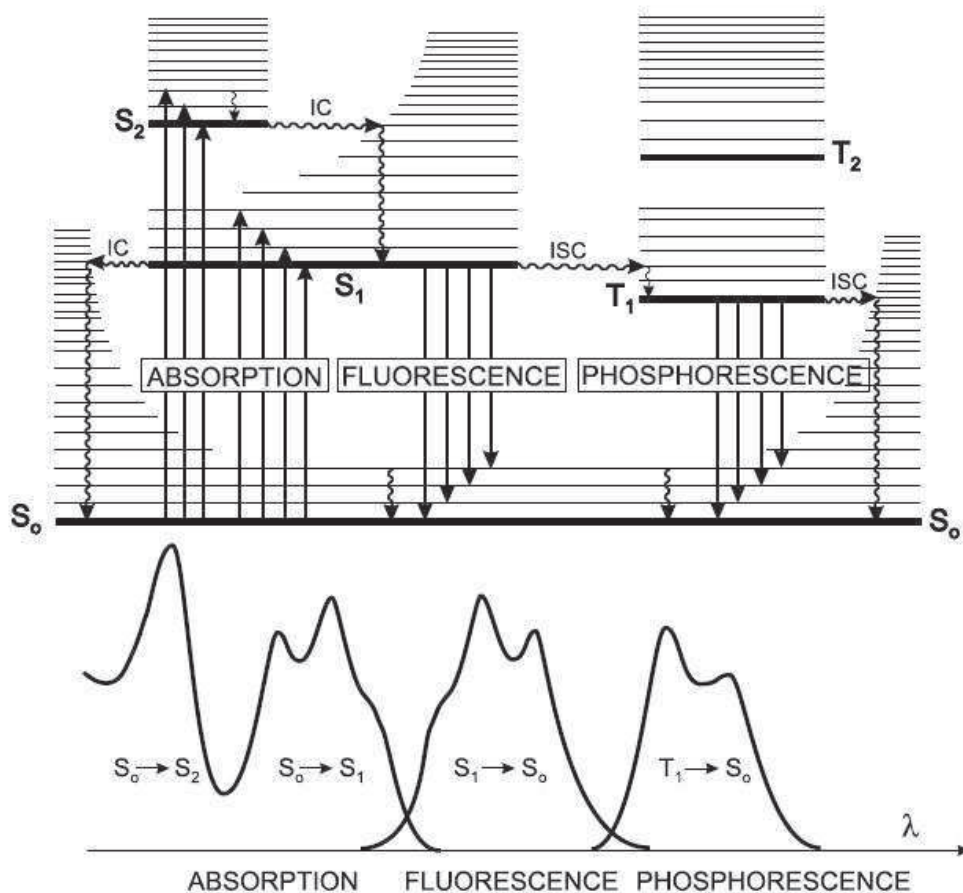


Figure 1.12. The Perrin-Jablonski diagram (top) and illustration of the relative positions of absorption, fluorescence and phosphorescence spectra (bottom).

### (3) Lifetimes and quantum yields

The lifetime is the average time during which the molecules stay in the excited state before emitting one photon. The fluorescence decays time  $\tau_s$ , is one of the most important characteristics of a fluorescent molecule because it defines the time window of observation of dynamic phenomena.

The fluorescence quantum yield  $\Phi_F$  is the fraction of excited molecules that return to the ground state  $S_0$  with emission of fluorescence photons. It is equal to the ratio of the number of emitted photons to the number of absorbed photons. It also can be written by using the radiative lifetime (Equation 1.2). It gives the efficiency of the fluorescence process.  $K_r^F$  is the rate constant for radiative deactivation  $S_1 \rightarrow S_0$  with emission of fluorescence;  $K_{nr}^F$  is the rate constant for all the non-radiative (internal conversion  $S_1 \rightarrow S_0$ , intersystem crossing).  $\tau_r$  introduces the excited state lifetime of fluorophore.  $\tau_r$  is called radiative lifetime on the condition that the only way of de-excitation  $S_1 \rightarrow S_0$  was fluorescence emission.

$$\Phi_F = \frac{K_r^s}{K_f^s + K_{nr}^s} = \frac{\tau_s}{\tau_r}$$

Equation 1.2. Fluorescence quantum yield.

In order to obtain this value, a comparative method is widely used. This method relies on the use of fluorescence standards with known fluorescence quantum yields and is really only applicable to solution phase measurements. So the experiment should be prepared under the same excited wavelength. Hence, it can be written as equation 1.3.

$$\Phi_x = \Phi_s * \frac{A_x}{A_s} * \frac{F_s}{F_x} * \left(\frac{n_x}{n_s}\right)^2$$

Equation 1.3. Equation for estimation of fluorescence quantum yield.

“X” represents the compound of interest while “S” is the standard compound. “F” is the integrated area under the corrected fluorescence spectrum. “A” is the absorbance of the solution, and it should not exceed 0.1 at any wavelength longer than the excitation wavelength. This recommendation is made so as to minimize any effects due to re-absorption of the fluorescence. “n” is the refractive indice of the solvent used for the two solutions.

### 1.4.2.2 Photophysical properties of tetrazines

Based on the structure of 1,2,4,5-tetrazine, this molecule not only has  $\pi^*$  orbitals, but also non bonding n orbitals. So these orbitals contributes to two kinds of transition:  $n \rightarrow \pi^*$  transition and  $\pi \rightarrow \pi^*$  transition. This is another outstanding character of *s*-tetrazine. The vapor spectrum of *s*-tetrazine was first studied by Koenigsberger and Vogt, and later by Lin et al<sup>65</sup>. Glenn<sup>66,67</sup> reported a series of researches that dealt with the infrared, visible, and ultraviolet spectra of *s*-tetrazine, and in particular, with the understanding of the energetic of the four lone pairs of nitrogen nonbonding electrons.

From the early report<sup>68</sup> of the absorption spectra, *s*-tetrazine vapor shows two main singlet absorption systems: a first is around 250nm which corresponds to the  $\pi \rightarrow \pi^*$  transition analogue to benzene and a second system is around 500nm which is due to the  $n \rightarrow \pi^*$  transition. Mason has assigned the broad absorption in the region of 350nm in solutions to an additional  $n \rightarrow \pi^*$  transition. These results are identical with the recent research.

In addition, Mason<sup>69</sup> *et al.* pointed out, that the position of the absorption band corresponding to the  $n \rightarrow \pi^*$  transition is weakly influenced by the nature of the substituents and was shown not to be solvatochromic. The molar extinction coefficient associated with this transition is low, about  $500\text{-}1000\text{L}\cdot\text{mol}^{-1}\cdot\text{cm}^{-1}$ . Contrary, the position of  $\pi \rightarrow \pi^*$  transition strongly depends on the substituents nature, it correlates linearly with their electron-donating or withdrawing character. Figure 1.13 shows the absorption spectra<sup>8</sup> of different *s*-tetrazines, **13** (green), 3-chloro-6-methoxy-1,2,4,5-tetrazine **55** (blue), **24** (red), which clearly present this influence.

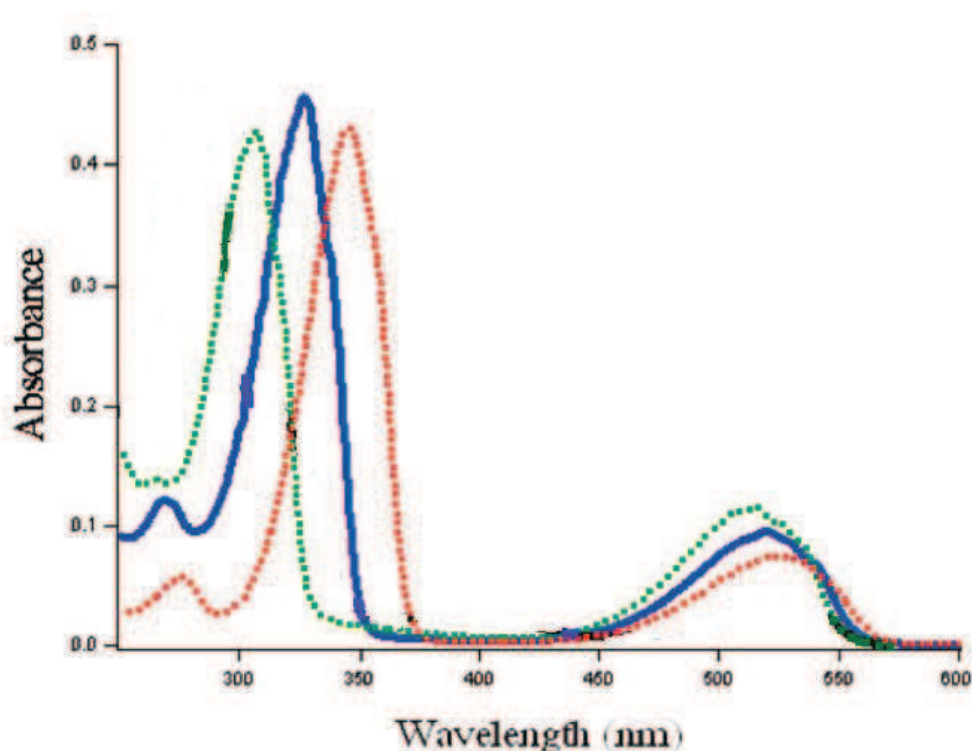


Figure 1.13. Absorption spectra of compounds **13** (green), **55** (blue), **24** (red).

The first report of fluorescence of *s*-tetrazines was from Mihir and Lionel<sup>70</sup>. Fluorescence of *s*-tetrazine and dimethyl-*s*-tetrazine were studied at different temperatures: 77K for *s*-tetrazine and room temperature for dimethyl-*s*-tetrazine. In fact, these two compounds are photochemically unstable; they decomposed to nitrogen and cyanuric acid or acetonitrile. Then the following studies showed that increasing the size of the substituents can improve the photostability. For instance, diphenyl-*s*-tetrazines is stable upon light irradiation.

A series of new substituted *s*-tetrazines were prepared by Audebert's group (figure 1.14), and their photophysical properties were also observed. Generally, the color range of *s*-tetrazine is from purple to orange to red, but not all of them are fluorescent (Figure 1.15).

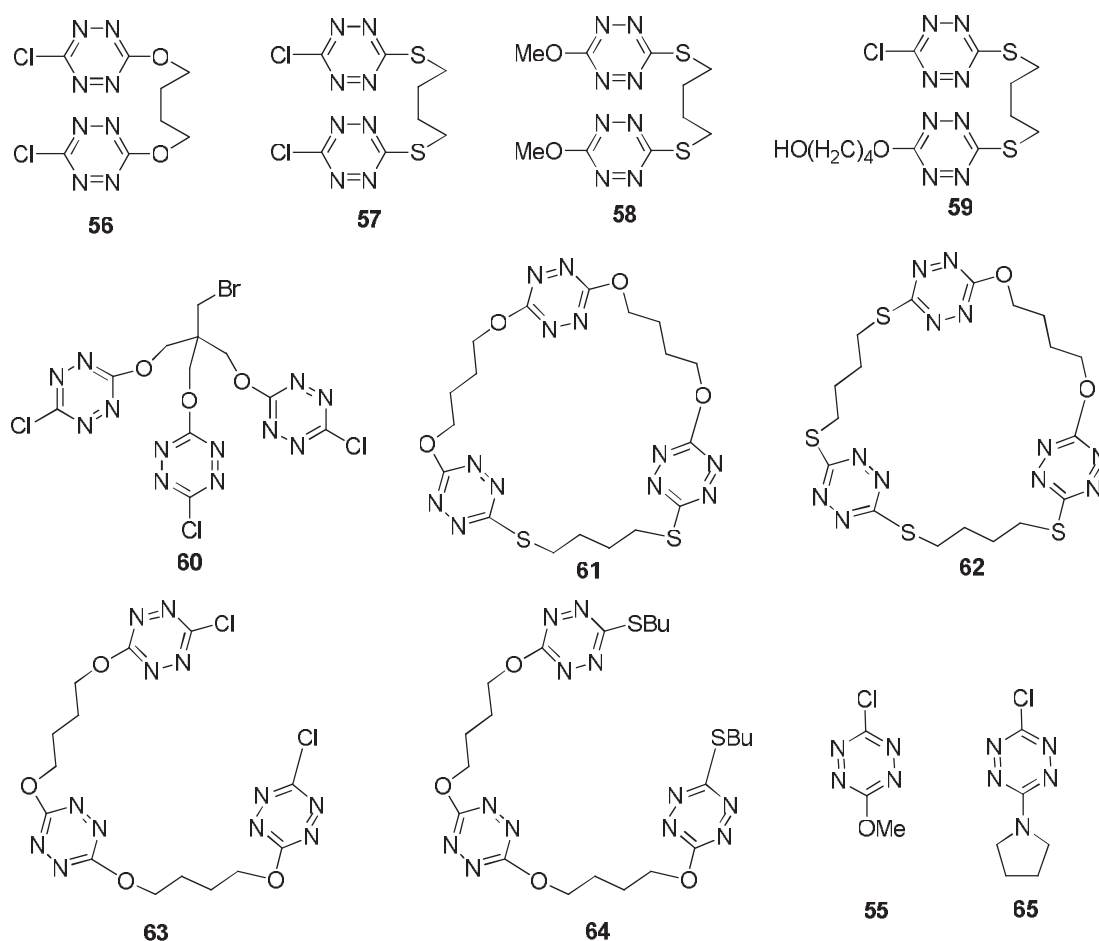


Figure 1.14. New *s*-tetrazines from Audebert's group.

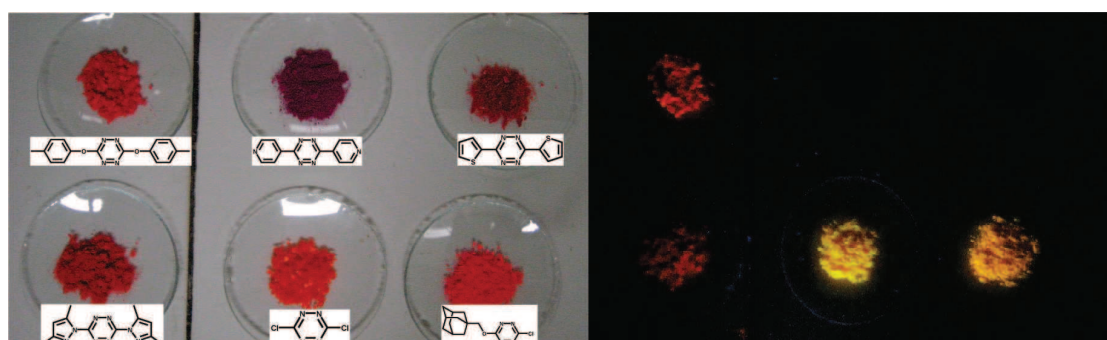


Figure 1.15. Left: photograph under ambient light of selected tetrazines with their corresponding formulas. Right: same sample irradiated at 365nm.

The lifetime of *s*-tetrazine is very dependent on the nature of the substituents (table 1.10). The longest one was reported for 3-chloro-6-methoxy-*s*-tetrazine (**55**) about 160ns, while the lifetime of dimethoxytetrazine (**29**) is just 49ns. Furthermore, the molecules with the longest lifetimes also have the highest quantum yields.

Table 1.10. Absorption and fluorescence maxima of tetrazines recorded in dichloromethane.

tetrazine	UV-vis absorption			fluorescence		
	$\lambda_1$	$\lambda_2$	$\lambda_3$	$\lambda_{\max}^a$	$\phi^b$	$\tau(\text{ns})^c$
<b>1</b>	544	295		602		<0.5
<b>11</b>	524	383	278			
<b>13</b>	515	307		551,567	0.14	58
<b>24</b>	524	345	275	575	0.11	49
<b>56</b>	521	328	270	572	0.36	144
<b>57</b>	522	391	273	576	0.025	12.8,6.3
<b>58</b>	529	396	258	580	$5 \times 10^{-3}$	7.1, 1.93
<b>59</b>	524	394	263	577	$5 \times 10^{-3}$	$5.39^d$
<b>60</b>	518	323	269	565	0.29	150
<b>61</b>	528	397,349	257	585	$6 \times 10^{-3}$	
<b>62</b>	529	403	288	585	$2 \times 10^{-3}$	
<b>63</b>	522	330	269	570	0.126	59
<b>64</b>	528.5	398, 348	259	575	$6 \times 10^{-3}$	10
<b>55</b>	520	327	269	567	0.38	160
<i>s</i> -tetrazine	542	320	252	575	$6 \times 10^{-4}$	1.5

a.  $\lambda_{\text{ex}} = \lambda_1$ , b.  $\phi \pm 8\%$ , c.  $\tau \pm 2\%$ , d. average of a multiexponential decline

### 1.4.3 Computational chemistry on tetrazines

In order to understand the origin of the differences in fluorescence properties, systematic quantum chemical studies have been conducted<sup>4</sup>. It has been found that in many cases the HOMO of the *s*-tetrazine is a combination of the four nonbonding *n* electrons of the nitrogen atoms. However, a  $\pi$  orbital lies frequently very close to this *n* orbital, and according to the substituent nature their order can be exchanged. In other words, the  $\pi$  orbital becomes the HOMO of the molecule. Figure 1.16 shows the HOMO and HOMO-1 obtained by DFT calculations in the two antagonist cases of the pyrrolidine and the aziridine substituents.



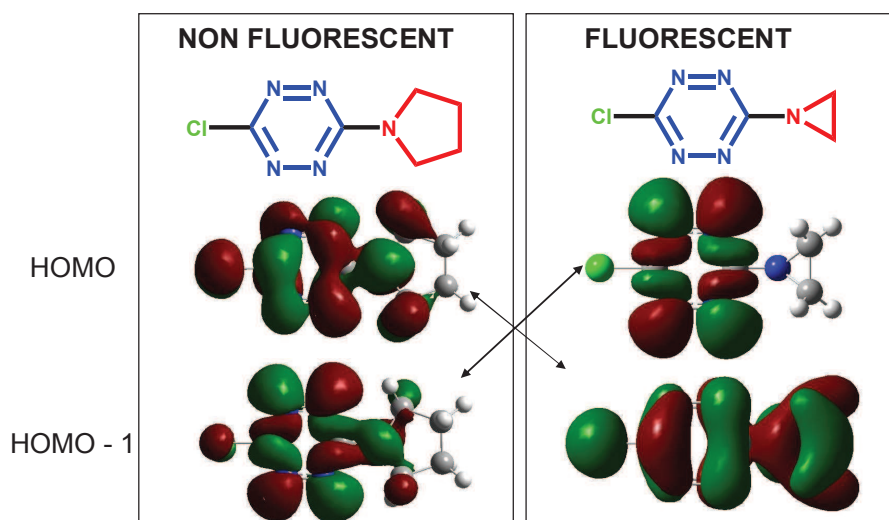


Figure 1.16. Calculated structures of the HOMO and HOMO-1 of tetraziens.

The results show in particular that fluorescence occurs when the HOMO orbital has a nonbonding n character, but is absent if the HOMO is a  $\pi$  orbital. Extension of this calculation to other derivatives confirms that trend (Figure 1.17). Hence, the occurrence of the fluorescence properties of *s*-tetrazine can be predicted through such theoretical approach.

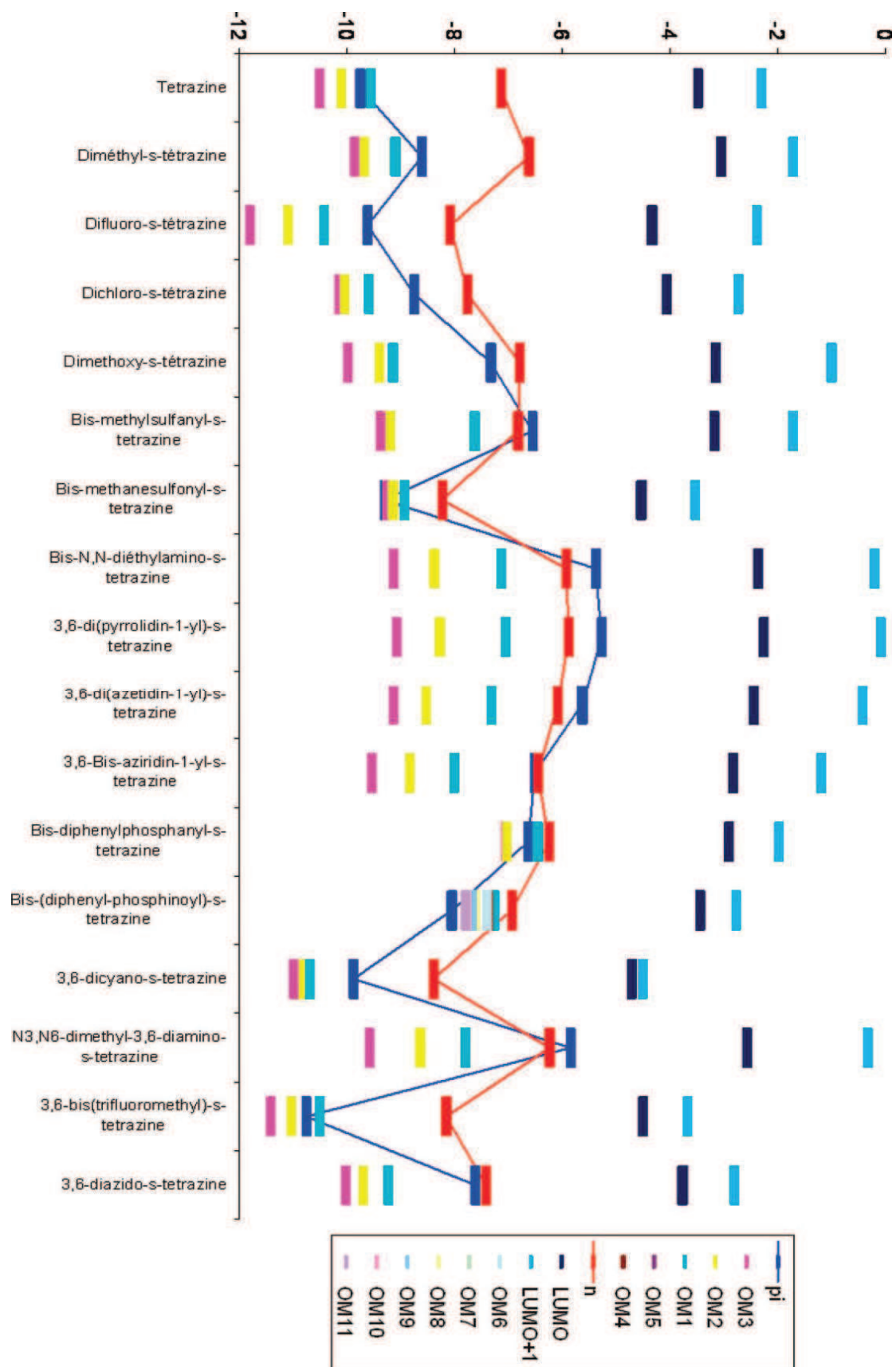


Figure 1.17. Orbital energies of symmetric *s*-tetrazines with heteroatomic substituents.

The calculations also allow a good estimation of the relative position of the reduction potentials of the tetrazines. It is directly linked to the relative LUMO position, as could be expected (Table 1.11) (Figure 1.18).

Table 1.11. Values of differences between standard potentials and the differences between LUMO levels compared with tetrazine **18** as the standard.

compound	Measured $\Delta E^0$ [V]	Measured $\Delta E_{\text{LUMO}}$ [eV]
<b>55</b>	0.31	0.28
<b>65</b>	0.67	0.70
<b>24</b>	0.57	0.55
<b>40</b>	1.05	1.27

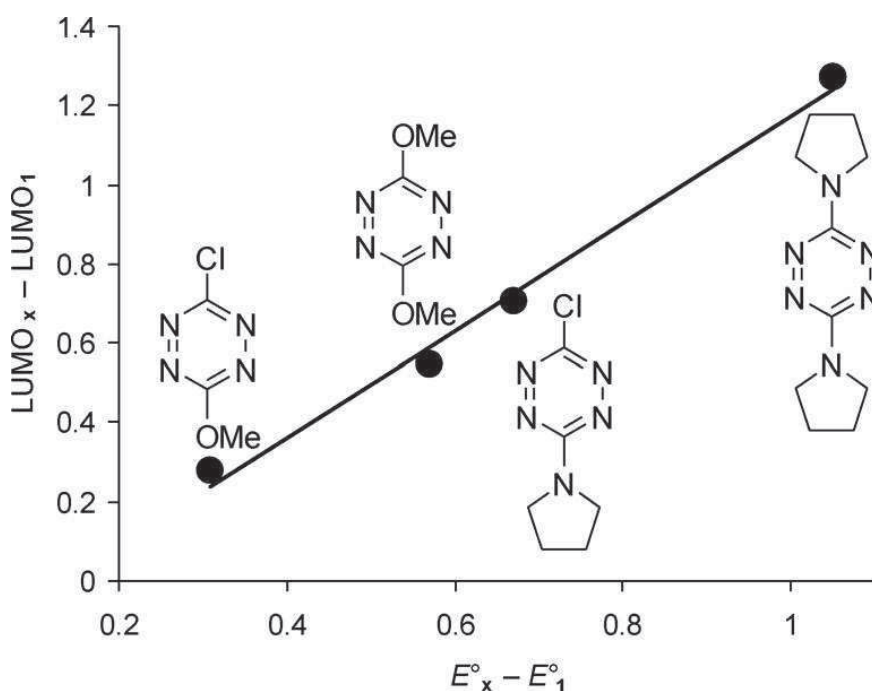


Figure 1.18. Correlation between the differences in the LUMO energies of *s*-tetrazines (**55,65,24,40**) relative to **18** and the differences of their standard potentials ( $R^2=0.9904$ ).

## 1.5 Applications of *s*-tetrazines

### 1.5.1 Energetic materials from tetrazines

High-energy density materials (HEDMs) offer distinct advantages to conventional carbon-based energetic materials. Due to a large number of N-N and C-N bonds, they possess large positive heats of formation<sup>71,72</sup>. Hence energetic high-nitrogen organic compounds are promising candidates for HEDMs. The low percentage of carbon and hydrogen in these compounds has a double positive effect: enhancement of density<sup>73,11</sup> and thermal stability<sup>74</sup>. Thanks to this special properties,

there are a lot of *s*-tetrazine derivatives which have been synthesized and characterized by Los Alamos National Laboratory<sup>75</sup>, Xiao's group<sup>76</sup> and Talawar's group (Figure 1.19).

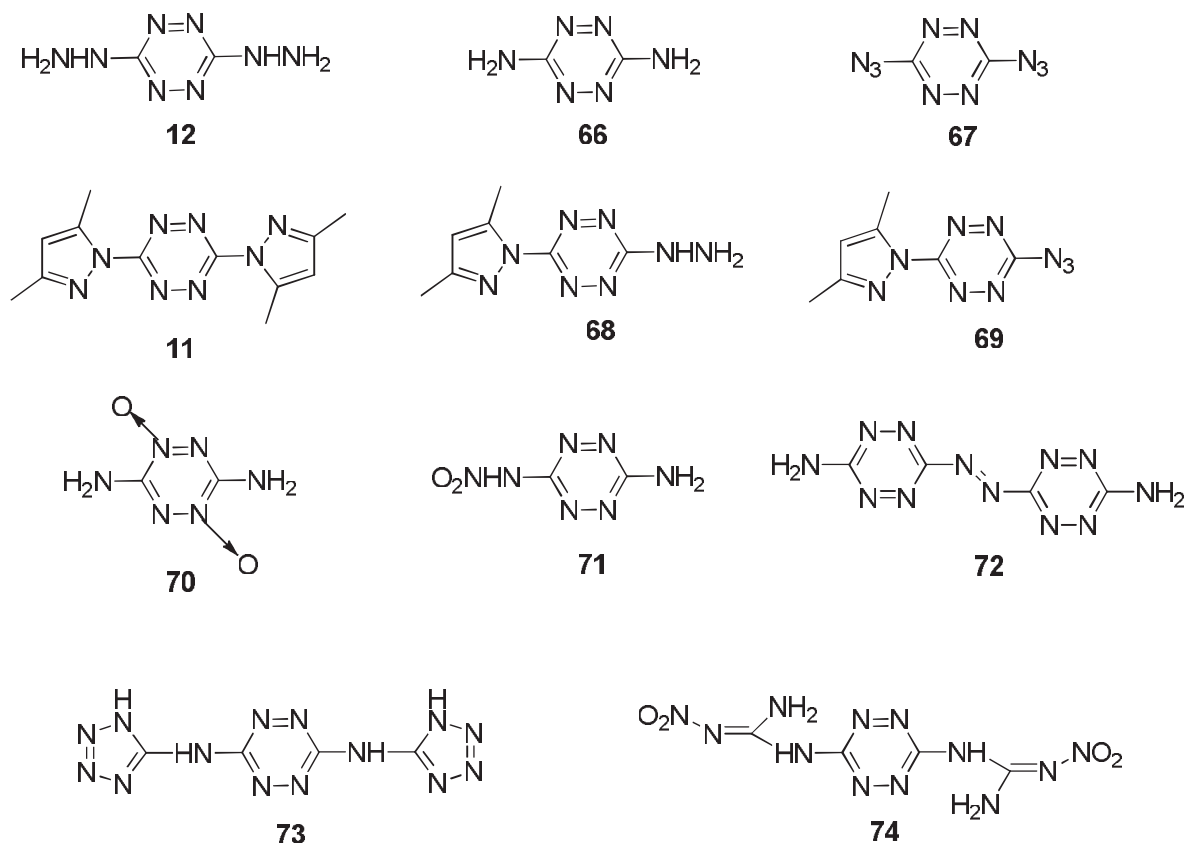


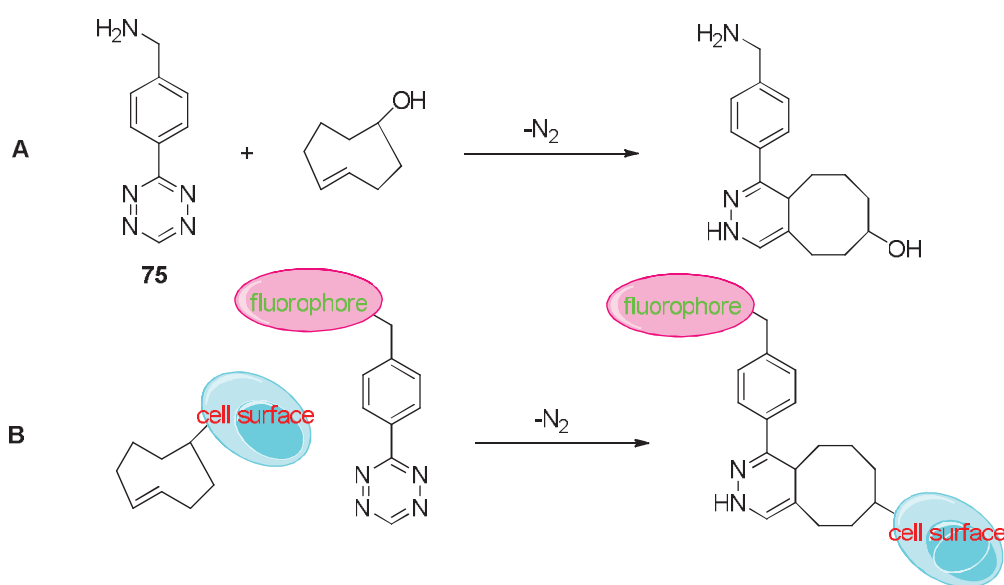
Figure 1.19. High nitrogen content *s*-tetrazine derivatives for energetic material applications.

### 1.5.2 Pharmaceuticals from *s*-tetrazines

1,2,4,5-tetrazine derivatives or their *n*-hydro form have a high potential for biological activity, possessing a wide range of antiviral and antitumor properties. These derivatives have also been widely used in pesticides and herbicides. According to the literature, 1,2,4,5-tetramethyl-3,6-bis(phenylethynyl)-1,2,4,5-tetrazine has been suggested as an antitumor agent<sup>77,78,79</sup>; 3-amino-6-aryl-1,2,4,5-tetrazines showed modest antimalarial activity<sup>80</sup> a series of tetrahydro-*s*-tetrazines have been evaluated for their antibacterial and antifungal activities<sup>81</sup>, and some hexahydro-*s*-tetrazines proved to have useful analgesic and anti-inflammatory activities.

Recently, in addition to Hu's and Werbel's group doing more research on the biological activity of *s*-tetrazine derivatives, Devaral and his colleagues used the inverse demand Diels-Alder reactivity of *s*-tetrazine to label biomarkers on live cells<sup>82,28,83</sup> (scheme 1.28). The main advantages of this reaction compared to

conventional bioorthogonal reactions are: (1) there is no requirement for a catalyst; (2) the bimolecular rate constants for reaction can be very high ( $>10^3 \text{ M}^{-1} \cdot \text{s}^{-1}$ ) with appropriate choice of *s*-tetrazine and strained dienophile; (3) certain *s*-tetrazine chromophores are fluorogenic upon cycloaddition, thus improving signal-to-background for fluorescence microscopy; (4) the reactants are straightforward to synthesize from commercial sources.



Scheme 1.28. A: reaction of benzylamino-*s*-tetrazine with trans-cyclooctenol is extremely rapid and leads to dihydropyridazine adducts; B: live cell multistep labeling of A549 human lung carcinoma cells using tetrazine cycloadditions.

### 1.5.3 Efficient solar cells

Due to its high electro-attractor effect, *s*-tetrazines can be used in solar cells. Ding's group<sup>84</sup> reported a new *s*-tetrazine based low-bandgap semiconducting polymer, PCPDTTz (Figure 1.20). This is the first solution-processable conjugated polymer with *s*-tetrazine in the main chain. This polymer shows good thermal stability and broad absorption covering 450-700 nm. The HOMO and LUMO energy levels were estimated to be -5.34 and -3.48 eV respectively, with an electrochemical bandgap of 1.86 eV. Simple polymer solar cells based on PCPDTTz and PC71BM exhibit a calibrated power conversion efficiency of 5.4%.

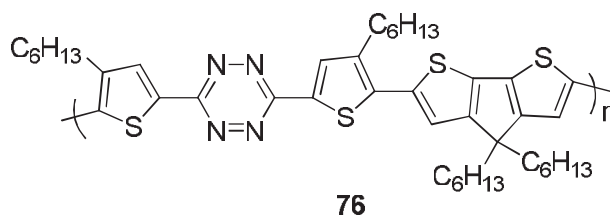


Figure 1.20. Structure of PCPDTTTz.

#### 1.5.4 NLO-phore with tetrazine

As the most electrodefficient aromatic heterocycle of the C-N family, *s*-tetrazine derivatives have appeared as promising targets for the design of new optically and electroactive molecules. Their strong electron affinity should also enhance the charge transfer in related conjugated molecules leading to enhanced nonlinear optical (NLO) properties. The *s*-tetrazine moiety can either serve as the attractor for a classical dipolar push-pull molecule or more interestingly contribute to the formation of a linear octupole, as proposed by Zyss *et al.* some years ago. Moreover, the reversible electrochemical reduction displayed by most *s*-tetrazines might constitute a useful feature for the achievement of electroswitchable NLO devices.

Even though researchers toward such structures have not been reported up to now, Audebert's group<sup>85</sup> has prepared two donor-acceptor-donor *s*-tetrazines containing ferrocene group as a donor unit and phenyl group unit as a  $\pi$ -bridge units (Figure 1.21). They studied their third order NLO properties. Even though researches toward such structures have not been reported today. From cyclic voltammetric study, the oxidation potential of ferrocene indicates that the separation of the charge in **77** is considerably greater than **78** in the ground state due to the presence of the phenyl linkage between the ferrocene and *s*-tetrazine moieties, which increases the electron density on the ferrocene units. On the other hand, UV-vis studies show an increase in the charge transfer due to the phenyl linkage between the ferrocene and tetrazine. Both *s*-tetrazines display reduction potentials in the same range, showing a much weaker influence of the ferrocene substituents on the *s*-tetrazines than the other way around. Their third-order NLO properties show that the ferrocenyl group does not play a highly positive role in the optimization of  $\gamma$  values. However, it evidences the possible role of metal-to-ligand charge transfer on third-order hyperpolarizability values, confirming the counteractive effect of the charge transfer process already reported for quadratic nonlinear responses.

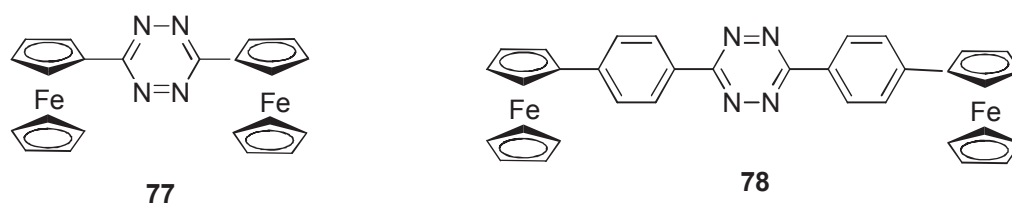


Figure 1.21. Third order NLO active tetrazine derivatives.

The former applications are still active, and more and more researchers are done in the field of active polymers containing *s*-tetrazines<sup>86,14</sup>, supermolecular *s*-tetrazines<sup>50,87,88</sup>, *s*-tetrazine-doped silica nanoparticles<sup>89</sup>, electrofluorescence switching of *s*-tetrazines<sup>90,91</sup>, good corrosion inhibitors<sup>92,93</sup>.

## 1.6 Conclusions

Despite is quite ancient discovery *s*-tetrazine has been far less used than many other heterocycles in synthetic chemistry and development of molecular materials. However, the recent discovery of easy and efficient synthetic accesses to important intermediates such as dichloro-*s*-tetrazine has given the impulse for a renewed interest in this aromatic ring. From, the literature survey presented in this chapter, it can be seen that many derivatives have now been synthesized and studied. The synthesis, reactivity and physico-chemical properties of simple derivatives are now well established and understood.

This body of knowledge opens up the possibility to design more elaborates *s*-tetrazine derivatives which will make good use of their outstanding photophysical and electrochemical properties for applications in various fields.

During my PhD, I have developed three axis of research. The first one was the use of *s*-tetrazine to synthesize new receptors for anions and ions pair. Their working principle will be based on the use of anion electron deficient aromatic ring interactions since *s*-tetrazine has been recognized as “the most electron deficient N heterocycle”.

The second axis was to try to improve the intrinsic photophysical properties of *s*-tetrazines through specific substituents which had not been tested before. For example, bulky or electro attracting groups have been used. During the course of this work, an unexpected new reactivity of *s*-tetrazines was also discovered.

Finally, the last part will deal with the synthesis and study of new original dyads containing *s*-tetrazine. Some of these molecules present an efficient intramolecular resonant energy transfer which confers a highly improved brightness to

*s*-tetrazine. One of these molecules has been the object of an original use in an electrofluorochromic cell.



## References

1. Churakov, A. M.; Tartakovsky, V. A., Progress in 1,2,3,4-tetrazine chemistry. *Chem Rev* **2004**, *104* (5), 2601-2616.
2. Dianez, M. J.; Estrada, M. D.; Lopezcastro, A.; Perezgarrido, S., Diethyl 6(R)-3-(4-Chlorophenyl)-6-(Tetra-O-Acetyl-D-Arabino-Threitol-1-Yl)-1,2,3,6-Tetrahydro-1,2,3,4-Tetrazine-1,2-Dicarboxylate, C<sub>26</sub>H<sub>33</sub>ClN<sub>4</sub>O<sub>12</sub>. *Acta Crystallogr C* **1994**, *50*, 1972-1974.
3. Audebert, P.; Miomandre, F.; Clavier, G.; Vernieres, M. C.; Badre, S.; Meallet-Renault, R., Synthesis and properties of new tetrazines substituted by heteroatoms: Towards the world's smallest organic fluorophores. *Chem-Eur J* **2005**, *11* (19), 5667-5673.
4. Gong, Y. H.; Miomandre, F.; Meallet-Renault, R.; Badre, S.; Galmiche, L.; Tang, J.; Audebert, P.; Clavier, G., Synthesis and Physical Chemistry of s-Tetrazines: Which Ones are Fluorescent and Why? *Eur J Org Chem* **2009**, (35), 6121-6128.
5. Son, S. F.; Berghout, H. L.; Bolme, C. A.; Chavez, D. E.; Naud, D.; Hiskey, M. A., Burn rate measurements of HMX, TATB, DHT, DAAF, and BTATz. *P Combust Inst* **2000**, *28*, 919-924.
6. Pinner, A., Ueber die Einwirkung von Hydrazin auf die Imidoäther. *Chemische Berichte* **1897**, *30*, 1871.
7. Saracoglu, N., Recent advances and applications in 1,2,4,5-tetrazine chemistry. *Tetrahedron* **2007**, *63* (20), 4199-4236.
8. Clavier, G.; Audebert, P., s-Tetrazines as Building Blocks for New Functional Molecules and Molecular Materials. *Chem Rev* **2010**, *110* (6), 3299-3314.
9. Erickson, J. G.; F., W. P.; Wystrach, V. P., The 1, 2, 3- and 1, 2, 4-triazines, tetrazines, and pentazines. In *The Chemistry of heterocyclic compounds; a series of monographs*, Interscience Publishers Inc.: New-York, 1956; pp 179-249.
10. Gao, H. X.; Wang, R. H.; Twamley, B.; Hiskey, M. A.; Shreeve, J. M., 3-amino-6-nitroamino-tetrazine (ANAT)-based energetic salts. *Chemical Communications* **2006**, (38), 4007-4009.
11. Chavez, D. E.; Hiskey, M. A.; Gilardi, R. D., 3,3'-azobis(6-amino-1,2,4,5-tetrazine): A novel high-nitrogen energetic material. *Angew Chem Int Edit* **2000**, *39* (10), 1791-+.
12. Abdelrah.Mo; Kira, M. A.; Tolba, M. N., A Direct Synthesis of Dihyrotetrazines. *Tetrahedron Lett* **1968**, (35), 3871-&.
13. Wiley, R. H.; Jarboe Jr., C. H.; Hayes, F. N., Heterocyclic Analogs of Terphenyl : 3,6-Diaryl-1,2,4,5-Tetrazines. *J Org Chem* **1957**, *22* (7), 835.
14. Soloduch, J.; Doskocz, J.; Cabaj, J.; Roszak, S., Practical synthesis of bis-substituted tetrazines with two pendant 2-pyrrolyl or 2-thienyl groups, precursors of new conjugated polymers. *Tetrahedron* **2003**, *59* (26), 4761-4766.
15. Larsen, C.; Binderup, E.; Moller, J., Mass Spectrometry of 1,2,4,5-Tetrazines. *Acta Chem Scand* **1967**, *21* (10), 2855-&.
16. Skorianetz, W.; Kovats, E. s., Eine neue Synthese von 3,6-Dialkyl-1,2,4,5-tetrazinen. *Helvetica Chimica Acta* **1971**, *54* (7), 1922.
17. Skorianetz, W.; Kovats, E. s., Dihydro- und Tetrahydroderivate des 3,6-Dimethyl-1,2,4,5-tetrazins. *Helvetica Chimica Acta* **1972**, *55* (5), 1404.
18. Jun Yang, M. R. K., Weilong Li, Swagat Sahu, and Neal K. Devaraj, Metal-Catalyzed One-Pot Synthesis of Tetrazines Directly from Aliphatic Nitriles and Hydrazine. *Angew. Chem. Int. Ed.* **2012**, *51*, 1-5.
19. Coburn, M. D.; Buntain, G. A.; Harris, B. W.; Hiskey, M. A.; Lee, K. Y.; Ott, D. G., An Improved Synthesis of 3,6-Diamino-1,2,4,5-Tetrazine .2. From

- Triaminoguanidine and 2,4-Pentanedione. *Journal of Heterocyclic Chemistry* **1991**, *28* (8), 2049-2050.
20. Bentiss, F.; Lagrenée, M.; Traisnel, M.; Mernari, B.; Elattari, H., A Simple One Step Synthesis of New 3,5-Disubstituted-4-amino-1,2,4-triazoles. *Journal of Heterocyclic Chemistry* **1999**, *36*, 149.
21. Coburn, M. D.; Hiskey, M. A.; Lee, K. Y.; Ott, D. G.; Stinecipher, M. M., Oxidations of 3,6-Diamino-1,2,4,5-Tetrazine and 3,6-Bis(S,S-Dimethylsulfilimino)-1,2,4,5-Tetrazine. *J Heterocyclic Chem* **1993**, *30* (6), 1593-1595.
22. Chavez, D. E.; Hiskey, M. A., Synthesis of the bi-heterocyclic parent ring system 1,2,4-triazolo[4,3-b][1,2,4,5]tetrazine and some 3,6-disubstituted derivatives. *J Heterocyclic Chem* **1998**, *35* (6), 1329-1332.
23. Helm, M. D.; Plant, A.; Harrity, J. P. A., A novel approach to functionalised pyridazinone arrays. *Organic & Biomolecular Chemistry* **2006**, *4* (23), 4278-4280.
24. Boger, D. L.; Panek, J. S., 1,2,4-Triazine Preparation Via Thermal Cycloaddition of Dimethyl "1,2,4,5-Tetrazine-3,6-Dicarboxylate with Aryl Thioimidates. *Tetrahedron Lett* **1983**, *24* (42), 4511-4514.
25. Boger, D. L., Diels-Alder Reactions of Heterocyclic Azadienes - Scope and Applications. *Chem Rev* **1986**, *86* (5), 781-793.
26. Carboni, R. A.; Lindsey Jr., R. V., Reaction of tetrazines with unsaturated compounds. a new synthesis of pyridazines. *J Am Chem Soc* **1959**, *81*, 4342.
27. Carboni, R. A.; Lindsey, R. V., Reactions of Tetrazines with Unsaturated Compounds - a New Synthesis of Pyridazines. *J Am Chem Soc* **1959**, *81* (16), 4342-4346.
28. Devaraj, N. K.; Weissleder, R., Biomedical Applications of Tetrazine Cycloadditions. *Accounts Chem Res* **2011**, *44* (9), 816-827.
29. Sauer, J.; Heldmann, D. K.; Hetzenegger, J.; Krauthan, J.; Sichert, H.; Schuster, J., 1,2,4,5-tetrazine: Synthesis and reactivity in 4+2 cycloadditions. *Eur J Org Chem* **1998**, (12), 2885-2896.
30. Thalhammer, F.; Wallfahner, U.; Sauer, J., Reactivity of Simple Open-Chain and Cyclic Dienophiles in Inverse-Type Diels-Alder Reactions. *Tetrahedron Lett* **1990**, *31* (47), 6851-6854.
31. Soenen, D. R.; Zimpleman, J. M.; Boger, D. L., Synthesis and inverse electron demand Diels-Alder reactions of 3,6-bis(3,4-dimethoxybenzoyl)-1,2,4,5-tetrazine. *J Org Chem* **2003**, *68* (9), 3593-3598.
32. Boger, D. L.; Coleman, R. S.; Panek, J. S.; Huber, F. X.; Sauer, J., A Detailed, Convenient Preparation of Dimethyl "1,2,4,5-Tetrazine-3,6-Dicarboxylate. *J Org Chem* **1985**, *50* (25), 5377-5379.
33. Boger, D. L.; Schaum, R. P.; Garbaccio, R. M., Regioselective inverse electron demand Diels-Alder reactions of N-acyl 6-amino-3-(methylthio)-1,2,4,5-tetrazines. *Journal of Organic Chemistry* **1998**, *63* (18), 6329-6337.
34. Barker, I. A.; Hall, D. J.; Hansell, C. F.; Du Prez, F. E.; O'Reilly, R. K.; Dove, A. P., Tetrazine-Norbornene Click Reactions to Functionalize Degradable Polymers Derived from Lactide. *Macromol Rapid Comm* **2011**, *32* (17), 1362-1366.
35. Taylor, M. T.; Blackman, M. L.; Dmitrenko, O.; Fox, J. M., Design and Synthesis of Highly Reactive Dienophiles for the Tetrazine trans-Cyclooctene Ligation. *J Am Chem Soc* **2011**, *133* (25), 9646-9649.
36. Blackman, M. L.; Royzen, M.; Fox, J. M., Tetrazine Ligation: Fast Bioconjugation Based on Inverse-Electron-Demand Diels-Alder Reactivity. *J. Am. Chem. Soc.* **2008**, *130* (41), 13518-13519.
37. Blackman, M. L.; Royzen, M.; Fox, J. M., Tetrazine ligation: Fast bioconjugation based on inverse-electron-demand Diels-Alder reactivity. *J Am Chem Soc* **2008**, *130* (41), 13518-+.

38. Royzen, M.; Yap, G. P. A.; Fox, J. M., A photochemical synthesis of functionalized trans-cyclooctenes driven by metal complexation. *J Am Chem Soc* **2008**, *130* (12), 3760-+.
39. Novak, Z.; Kotschy, A., First cross-coupling reactions on tetrazines. *Organic Letters* **2003**, *5* (19), 3495-3497.
40. Boger, D. L.; Sakya, S. M., Inverse Electron Demand Diels-Alder Reactions of 3,6-Bis(Methylthio)-1,2,4,5-Tetrazine - 1,2-Diazine Introduction and Direct Implementation of a Divergent 1,2,4,5-Tetrazine-]1,2-Diazine-]Benzene (Indoline Indole) Diels-Alder Strategy. *J Org Chem* **1988**, *53* (7), 1415-1423.
41. Benson, S. C.; Lee, L.; Yang, L.; Snyder, J. K., Intramolecular inverse electron demand Diels-Alder reactions of tryptamine with tethered heteroaromatic azadienes. *Tetrahedron* **2000**, *56* (9), 1165-1180.
42. Sakya, S. M.; Groskopf, K. K.; Boger, D. L., Preparation and inverse electron demand Diels-Alder reactions of 3-methoxy-6-methylthio-1,2,4,5-tetrazine. *Tetrahedron Letters* **1997**, *38* (22), 3805-3808.
43. Neugebauer, F., Union of the Textile Supply, Leather Supply, Tanning Substance and Raw-Material Washing Industry (Tegawa). *Melliand Textil Int* **1982**, *63* (5), 384-387.
44. Audebert, P.; Sadki, S.; Miomandre, F.; Clavier, G.; Vernieres, M. C.; Saoud, M.; Hapiot, P., Synthesis of new substituted tetrazines: electrochemical and spectroscopic properties. *New J Chem* **2004**, *28* (3), 387-392.
45. Latosh, N. I.; Rusinov, G. L.; Ganebnykh, I. N.; Chupakhin, O. N., Pyrazole as a leaving group during nucleophilic substitution in 3,6-bis(3,5-dimethyl-4-X-pyrazol-1-yl)-1,2,4,5-tetrazines. *Zh Org Khim+* **1999**, *35* (9), 1392-1400.
46. Glidewell, C.; Lightfoot, P.; Royles, B. J. L.; Smith, D. M., The 'inverse electron-demand' Diels-Alder reaction in polymer synthesis .4. The preparation and crystal structures of some bis(1,2,4,5-tetrazines). *Journal of the Chemical Society-Perkin Transactions 2* **1997**, (6), 1167-1174.
47. Yamanaka, H.; Ohba, S., Reaction of methoxy-N-heteroaromatics with phenylacetonitrile under basic conditions. *Heterocycles* **1990**, *31* (5), 895.
48. Counottepotman, A.; Vanderplas, H. C.; Vanveldhuizen, B., 1,6-Dihydro-1,2,4,5-Tetrazine, a Neutral Homoaromatic System .3. *J Org Chem* **1981**, *46* (10), 2138-2141.
49. Novak, Z.; Bostai, B.; Csekei, M.; Lorincz, K.; Kotschy, A., Selective nucleophilic substitutions on tetrazines. *Heterocycles* **2003**, *60* (12), 2653.
50. Gong, Y. H.; Audebert, P.; Tang, J.; Miomandre, F.; Clavier, G.; Badre, S.; Meallet-Renault, R.; Marrot, J., New tetrazines substituted by heteroatoms including the first tetrazine based cyclophane: Synthesis and electrochemical properties. *J Electroanal Chem* **2006**, *592* (2), 147-152.
51. Qing, Z.; Audebert, P.; Clavier, G.; Miomandre, F.; Tang, J.; Vu, T. T.; Meallet-Renault, R., Tetrazines with hindered or electron withdrawing substituents: Synthesis, electrochemical and fluorescence properties. *J Electroanal Chem* **2009**, *632* (1-2), 39-44.
52. Wilkes, M. C., Azaphilic Addition of Methyl Lithium to 3,6-Bisalkylthio-1,2,4,5-Tetrazines - a Remarkable Dichotomy. *J Heterocyclic Chem* **1991**, *28* (4), 1163-1164.
53. Farago, J.; Novak, Z.; Schlosser, G.; Csampai, A.; Kotschy, A., The azaphilic addition of organometallic reagents on tetrazines: scope and limitations. *Tetrahedron* **2004**, *60* (9), 1991-1996.
54. Skoog, D. A.; West, D. M.; Holler, F. J., *Fundamentals of analytical chemistry*. 7th ed.; Saunders College Pub.: Fort Worth, 1996.
55. Zoski, C. G., *Handbook of electrochemistry*. 1st ed.; Elsevier: Amsterdam ; Boston, 2007; p xx, 892 p., 19 p. of plates.

56. Bard, A. J.; Faulkner, L. R., *Electrochemical methods : fundamentals and applications*. 2nd ed.; Wiley: New York, 2001; p xxi, 833 p.
57. Nicholson, R. S.; Shain, I., Theory of Stationary Electrode Polarography - Single Scan + Cyclic Methods Applied to Reversible Irreversible + Kinetic Systems. *Anal Chem* **1964**, *36* (4), 706-&.
58. Heinze, J., Cyclic Voltammetry - Electrochemical Spectroscopy. *Angewandte Chemie-International Edition in English* **1984**, *23* (11), 831-847.
59. Stone, E. W.; Maki, A. H., ESR Study of Polyazine Anions. *J Chem Phys* **1963**, *39* (7), 1635-&.
60. Troll, T., Reduction Potentials of Substituted Asymmetric-Triazines and S-Tetrazines in Acetonitrile. *Electrochim Acta* **1982**, *27* (9), 1311-1314.
61. Gleiter, R.; Schehlmann, V.; Larsen, J. S.; Fischer, H.; Neugebauer, F. A., Pe Spectra of Disubstituted 1,2,4,5-Tetrazines. *J Org Chem* **1988**, *53* (24), 5756-5762.
62. Gleiter, R.; Hornung, V.; Heilbron, E., Applications of Photoelectron Spectroscopy .28. Photoelectron Spectra of Azabenzenes and Azanaphthalenes .1. Pyridine, Diazines, S-Triazine and S-Tetrazine. *Helv Chim Acta* **1972**, *55* (1), 255-&.
63. Thulstrup, E. W.; Spangetlarsen, J.; Gleiter, R., Electronic-Structure of Para-Terphenyl, 3,6-Diphenyl-Pyridazine and 3,6-Diphenyl-S-Tetrazine - Photoelectron and Polarized Absorption-Spectra. *Mol Phys* **1979**, *37* (5), 1381-1395.
64. Valeur, B., *Molecular fluorescence : principles and applications*. Wiley-VCH: Weinheim ; New York, 2002; p xiv, 387 p.
65. Brown, H. C.; Brewster, J. H.; Shechter, H., An Interpretation of the Chemical Behavior of 5-Membered and 6-Membered Ring Compounds. *J Am Chem Soc* **1954**, *76* (2), 467-474.
66. Spencer, G. H.; Cross, P. C.; Wiberg, K. B., S-Tetrazine .1. High-Resolution Vapor-Phase Study of Visible N-]Pi' Vibronic Absorption Band Systems. *J Chem Phys* **1961**, *35* (6), 1925-&.
67. Spencer, G. H.; Cross, P. C.; Wiberg, K. B., S-Tetrazine .2. Infrared Spectra. *J Chem Phys* **1961**, *35* (6), 1939-&.
68. Hochstra, Rm; King, D. S., Absorption, Fluorescence and Phosphorescence Spectra of Singlet and Triplet-States of S-Tetrazine in Crystal and in Mixed-Crystals at Low-Temperatures. *Chem Phys* **1974**, *5* (3), 439-447.
69. Mason, S. F., The Electronic Spectra of N-Heteroaromatic Systems .1. The N-]Pi Transitions of Monocyclic Azines. *J Chem Soc* **1959**, (Mar), 1240-1246.
70. Chowdhury, M.; Goodman, L., Fluorescence of S-Tetrazine. *J Chem Phys* **1962**, *36* (2), 548-&.
71. Neutz, J.; Grosshardt, O.; Schaufele, S.; Schuppler, H.; Schweikert, W., Synthesis, characterization and thermal behaviour of guanidinium-5-aminotetrazolate (GA) - A new nitrogen-rich compound. *Propell Explos Pyrot* **2003**, *28* (4), 181-188.
72. Huynh, M. H. V.; Hiskey, M. A.; Hartline, E. L.; Montoya, D. P.; Gilardi, R., Polyazido high-nitrogen compounds: Hydrazo- and azo-1,3,5-triazine. *Angew Chem Int Edit* **2004**, *43* (37), 4924-4928.
73. Kerth, J.; Lobbecke, S., Synthesis and characterization of 3,3'-azobis(6-amino-1,2,4,5-tetrazine) DAAT - A new promising nitrogen-rich compound. *Propell Explos Pyrot* **2002**, *27* (3), 111-118.
74. Churakov, A. M.; Smirnov, O. Y.; Ioffe, S. L.; Strelenko, Y. A.; Tartakovsky, V. A., Benzo-1,2,3,4-tetrazine 1,3-dioxides: Synthesis and NMR study. *Eur J Org Chem* **2002**, (14), 2342-2349.
75. Chavez, D. E.; Hiskey, M. A.; Naud, D. L., Tetrazine explosives. *Propell Explos Pyrot* **2004**, *29* (4), 209-215.

76. Wei, T.; Zhu, W. H.; Zhang, X. W.; Li, Y. F.; Xiao, H. M., Molecular Design of 1,2,4,5-Tetrazine-Based High-Energy Density Materials. *J Phys Chem A* **2009**, *113* (33), 9404-9412.
77. Yeremeyev, A. V.; Tikhomirov, D. A.; Tyusheva, V. A.; Liepinsh, E. E., "Acetylene-Alpha-Aziridinocarbinols in Reactions with Hydrazine and Methyl-Substituted Hydrazines. *Khim Geterotsikl+* **1978**, (6), 753-757.
78. Rao, G. W.; Hu, W. X., Synthesis, structure analysis, and antitumor activity of 3,6-disubstituted-1,4-dihydro-1,2,4,5-tetrazine derivatives. *Bioorg Med Chem Lett* **2006**, *16* (14), 3702-3705.
79. Hu, W. X.; Rao, G. W.; Sun, Y. Q., Synthesis and antitumor activity of s-tetrazine derivatives. *Bioorg Med Chem Lett* **2004**, *14* (5), 1177-1181.
80. Werbel, L. M.; Mcnamara, D. J.; Colbry, N. L.; Johnson, J. L.; Degnan, M. J.; Whitney, B., Anti-Malarial Drugs .42. Synthesis and Anti-Malarial Effects of N,N-Dialkyl-6-(Substituted Phenyl)-1,2,4,5-Tetrazin-3-Amines. *J Heterocyclic Chem* **1979**, *16* (5), 881-894.
81. Mohan, J., Facile Synthesis and Antimicrobial Activity of Spirobicyclo[3.2.1]Octane-2',3-(4h)-[2h]-Thiazolo[3,2-B]-S-Tetrazines. *Org Prep Proced Int* **1992**, *24* (5), 523-525.
82. Devaraj, N. K.; Weissleder, R.; Hilderbrand, S. A., Tetrazine-Based Cycloadditions: Application to Pretargeted Live Cell Imaging. *Bioconjugate Chem* **2008**, *19* (12), 2297-2299.
83. Devaraj, N. K.; Upadhyay, R.; Hatin, J. B.; Hilderbrand, S. A.; Weissleder, R., Fast and Sensitive Pretargeted Labeling of Cancer Cells through a Tetrazine/trans-Cyclooctene Cycloaddition. *Angew Chem Int Edit* **2009**, *48* (38), 7013-7016.
84. Li, Z.; Ding, J. F.; Song, N. H.; Lu, J. P.; Tao, Y., Development of a New s-Tetrazine-Based Copolymer for Efficient Solar Cells. *J Am Chem Soc* **2010**, *132* (38), 13160-13161.
85. Janowska, I.; Miomandre, F.; Clavier, G.; Audebert, P.; Zakrzewski, J.; Thi, K. H.; Ledoux-Rak, I., Donor-acceptor-donor tetrazines containing a ferrocene unit: Synthesis, electrochemical and spectroscopic properties. *J Phys Chem A* **2006**, *110* (47), 12971-12975.
86. Audebert, P.; Sadki, S.; Miomandre, F.; Clavier, G., First example of an electroactive polymer issued from an oligothiophene substituted tetrazine. *Electrochem Commun* **2004**, *6* (2), 144-147.
87. Gong, Y. H.; Audebert, P.; Clavier, G.; Miomandre, F.; Tang, J.; Badre, S.; Meallet-Renault, R.; Naidus, E., Preparation and physicochemical studies of new multiple rings s-tetrazines. *New J Chem* **2008**, *32* (7), 1235-1242.
88. Garau, C.; Quinonero, D.; Frontera, A.; Costa, A.; Ballester, P.; Deya, P. M., s-Tetrazine as a new binding unit in molecular recognition of anions. *Chem Phys Lett* **2003**, *370* (1-2), 7-13.
89. Malinge, J.; Allain, C.; Galmiche, L.; Miomandre, F.; Audebert, P., Preparation, Photophysical, Electrochemical, and Sensing Properties of Luminescent Tetrazine-Doped Silica Nanoparticles. *Chem Mater* **2011**, *23* (20), 4599-4605.
90. Kim, Y.; Kim, E.; Clavier, G.; Audebert, P., New tetrazine-based fluoro-electrochromic window; modulation of the fluorescence through applied potential. *Chem Commun* **2006**, (34), 3612-3614.
91. Kim, Y.; Do, J.; Kim, E.; Clavier, G.; Galmiche, L.; Audebert, P., Tetrazine-based electrofluorochromic windows: Modulation of the fluorescence through applied potential. *J Electroanal Chem* **2009**, *632* (1-2), 201-205.
92. Zucchi, F.; Trabanelli, G.; Brunoro, G., The Influence of the Chromium Content on the Inhibitive Efficiency of Some Organic-Compounds. *Corros Sci* **1992**, *33* (7), 1135-1139.

93. Elkadi, L.; Mernari, B.; Traisnel, M.; Bentiss, F.; Lagrenee, M., The inhibition action of 3,6-bis(2-methoxyphenyl)-1,2-dihydro-1,2,4,5-tetrazine on the corrosion of mild steel in acidic media. *Corros Sci* **2000**, 42 (4), 703-719.



# Chapter 2 New *s*-tetrazines derivatives as the ion pair receptors

## 2.1 Introduction

### 2.1.1 Supramolecular chemistry and ion pair receptor

“Supramolecular chemistry” is defined as “the chemistry of the intermolecular bond, covering the structures and functions of the entities formed by the association of two or more chemical species” by Jean-Marie Lehn who obtain the 1987 Nobel Prize. The forces responsible for the structure include hydrogen bonding, metal coordination, hydrophobic forces, van der Waals forces,  $\pi$ - $\pi$  interactions and electrostatic effects<sup>1,2</sup>.

Molecular recognition<sup>3,4</sup> is one concept of supramolecular chemistry, which is specific binding of a guest molecule to a complementary host molecule to form a host-guest complex. One of the earliest examples of such supramolecular entity is crown ethers which are capable of selectively binding specific cations. However, a number of artificial systems have since been established. The key applications of this field are the construction of molecular sensors and catalysis.

Over the past several decades, a large number of macrocyclic receptors have been synthesized and evaluated for their abilities to bind cations<sup>5</sup>. More recently, increased attention has been directed towards the design and construction of anion<sup>4,6</sup> receptors because of their important role in biological systems and environmental issues. Further development in the field has been the combination of these two types of receptors to bind both partners. Compared with simple ion receptors, ion pair receptors bearing both a cation and an anion recognition site offer the promise of binding ion pairs or pairs of ions strongly as the result of direct or indirect cooperative interactions between co-bound ions. Most ion pair receptors take advantage of hydrogen bonding donors (urea, amide, imidazolium, pyrrole and uranyl), Lewis acidic sites and positively charged polyammonium groups, for anion recognition. On the contrary, cation recognition relies on lone pair electron donors and  $\pi$ -electron donors.

Ion pair receptors can be classified by how they bind the cations and the anions of targeted ion pairs (Figure 2.1). In the first mold presented, the anion and the cation are in a direct contact; in the second, termed “solvent-bridged ion pair”, one or more solvent molecules bridge the gap between the anion and the co-bound cation; in the



last one, called “host-separated ion pair”, the anion and the cation are bound relatively far from another, usually by the receptor framework<sup>7,8</sup>.

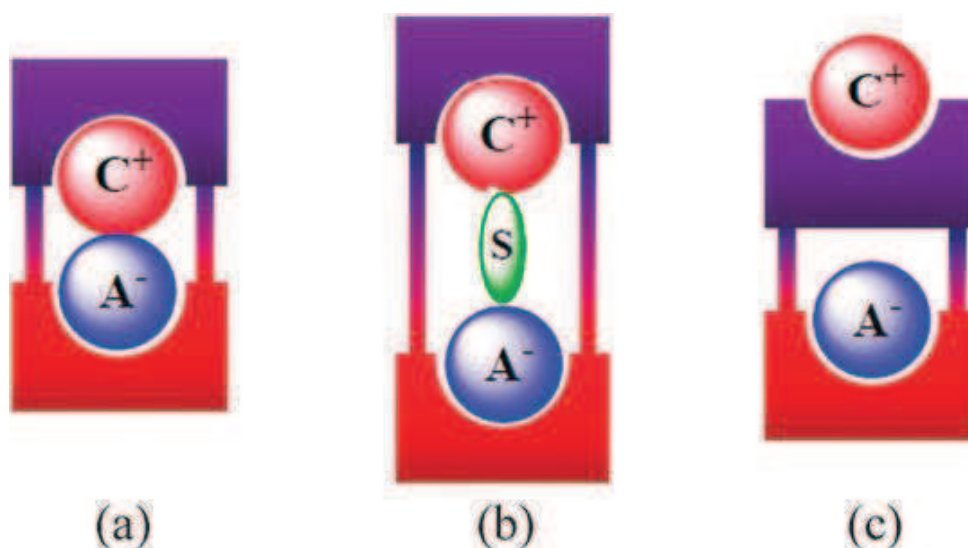


Figure 2.1. Limiting ion-pair interactions relevant to receptor-mediated ion-pair recognition: (a) contact, (b) solvent-bridged, and (c) host-separated. In this figure, the anion is shown as “A<sup>-</sup>”, the cation as “C<sup>+</sup>”, and the solvent is represented as “S”.

However, in spite of their potential applications in various fields, such as salt solubilization, extraction, and membrane transport, the number of well-characterized ion pair receptors remains limited<sup>9</sup>.

### 2.1.2 Fluorescent molecular sensors

Usually the structure of a sensor is a combination of a complexing part and a sensing part. The complexation of guest species with receptors can be monitored either by optical (colorimetric or fluorescent) changes or by changes in electrochemical behavior (resistance, conductivity, current, potential, capacity, etc).

Due to the high demand in analytical chemistry, clinical biochemistry, medicine, the environment, and so on, the design of fluorescent sensors is more and more important. Furthermore, numerous chemical and biochemical analytes can be detected by fluorescence methods: cations (H<sup>+</sup>, Li<sup>+</sup>, Na<sup>+</sup>, K<sup>+</sup>, Ca<sup>2+</sup>, Mg<sup>2+</sup>, Zn<sup>2+</sup>, Pb<sup>2+</sup>, Al<sup>3+</sup>, Cd<sup>2+</sup>, etc.) , neutral molecules (sugars, etc.) and gas (O<sub>2</sub>, CO<sub>2</sub>, NO, etc). In addition, fluorescent molecular sensors offer distinct advantages such as high sensitivity, selectivity, short response time, local observation, and the possibility for remote sensing.

Valeur has classified the fluorescent molecular sensors into three classes<sup>10</sup>

(Figure 2.2):

Class 1: fluorophores that undergo quenching upon collision with an analyte;

Class 2: fluorophores that can reversibly bind an analyte, of which the fluorescence can be either quenched (Chelation Enhancement of Quenching (CEQ) type) or enhanced (Chelation Enhancement of Fluorescence (CEF) type) upon binding;

Class 3: fluorophores linked, via a spacer or not, to a receptor. The design of such sensors, which are based on molecule or ion recognition by a receptor, requires special care in order to fulfill the criteria of affinity and selectivity, which are relevant to the field of supramolecular chemistry. The changes in photophysical properties of the fluorophore upon interaction with the bound analyte are due to the perturbation of photoinduced processes by the latter (electron transfer, charge transfer, energy transfer, excimer or exciplex formation or disappearance, etc.). Again, fluorescence can be quenched or enhanced.

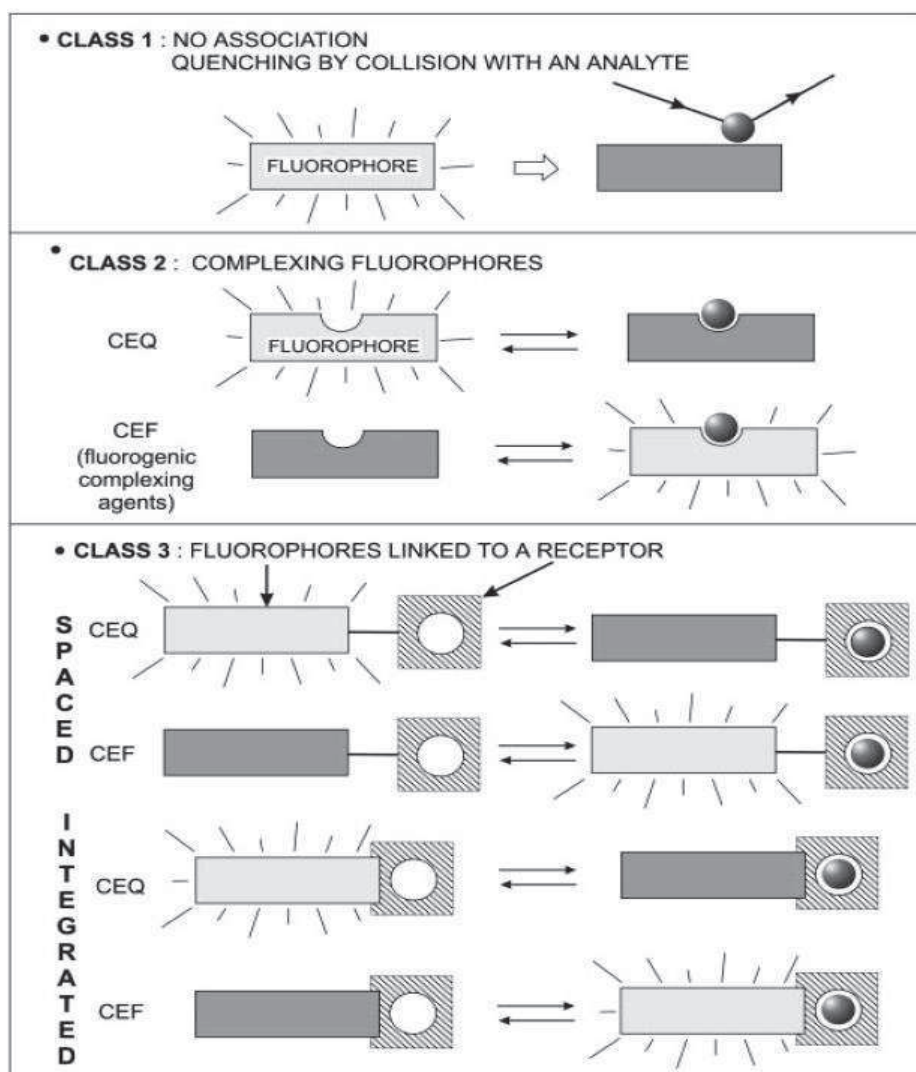


Figure 2.2. Main classes of fluorescent molecular sensors classified by Valeur (from ref. 10).

The discovery of crown ethers and cryptands in the late 1960s opened up new possibilities for cation recognition with improvement of selectivity, especially for alkali metal ions for which there was a lack of selective chelators. Then, the idea of coupling these ionophores to chromophores or fluorophores, leading to so-called chromoionophores and fluoroionophores, respectively, emerged some years later. In the design of a fluoroionophore, much attention is paid to the characteristics of the ionophore moiety and to the expected changes in fluorescence characteristics of the fluorophore moiety upon binding<sup>10</sup> (Figure 2.3). It is important to note that the same working principles can be applied to the development of fluorescent sensors for anions, ion pairs or neutral molecules.

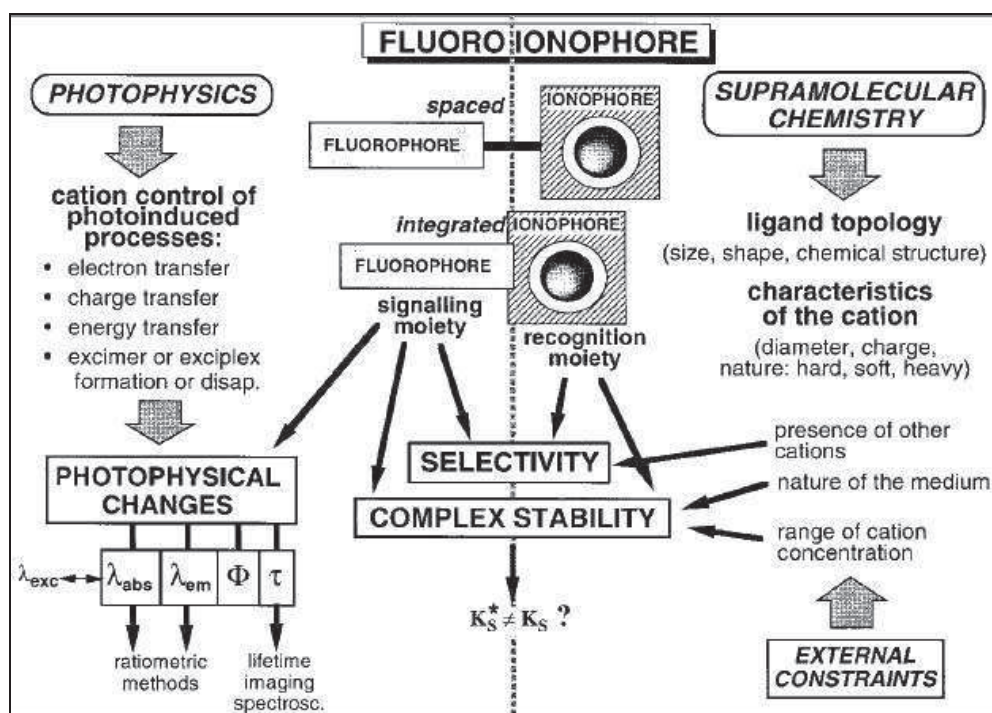


Figure 2.3. Main aspects of fluorescent molecular sensors for cation recognition (fluoroionophore) (from ref<sup>10</sup>).

There are other kinds of sensors in addition to fluorescent molecular sensors, for example, electrochemical sensors, which are based on changes of electrochemical behavior once the complex between redox-active receptor and analyte is formed<sup>11</sup>.

### 2.1.3 Experimental evidences of anion-*s*-tetrazine interactions

In 1999<sup>12</sup>, Dunbar's group reported a one-pot, high-yield synthesis of metallacyclophanes from 3,6-bis(2-pyridyl)-*s*-tetrazine and  $[\text{Ni}(\text{CH}_3\text{CN})_6]^{2+}$ , by anion template assembly with  $[\text{BF}_4]^-$ . This is the first experimental evidence for the use of *s*-tetrazine as a binding unit for the molecular recognition of anions. Then, they did further studies in this field<sup>13,14</sup>. And the results have shown that the formation of the various metallacyclophanes is influenced by the choice of the metal ions, anions, and solvents. Two examples have been retrieved from Cambridge Structural Database, which are shown in figure 2.4<sup>15</sup>. In LOGWOT, the encapsulated anion  $[\text{BF}_4]^-$  resides in the void space in the center of the cavity of the molecular square,  $\pi$ -interacting with the four electron deficient *s*-tetrazine rings. In QEZVIA, the  $[\text{SbF}_6]^-$  anion was used. A molecular pentagon has been obtained where the anion interacted with 5 electron deficient *s*-tetrazine rings.

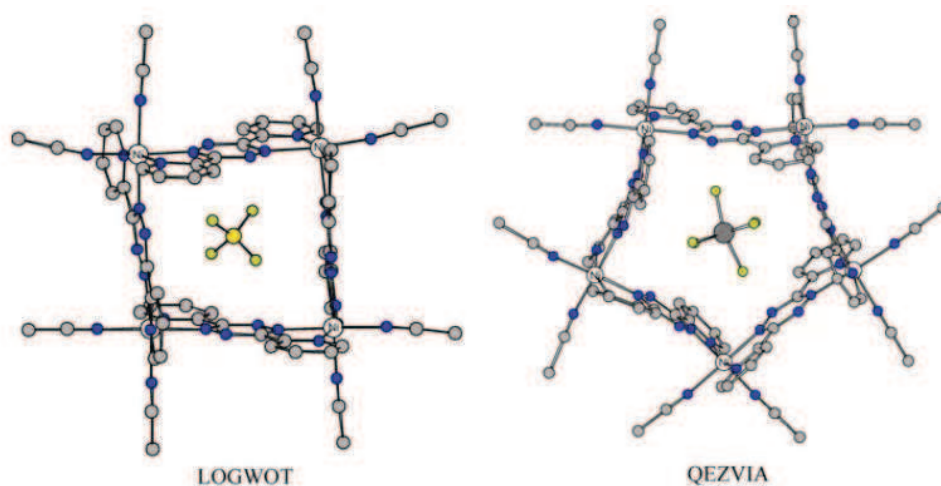


Figure 2.4. X-ray crystal structures of  $[\text{Ni}_4(\text{bptz})_4(\text{CH}_3\text{CN})_8]^{8+}$  with the encapsulated  $[\text{BF}_4]^-$  ion (LOGWOT) and  $[\text{Ni}_5(\text{bptz})_5(\text{CH}_3\text{CN})_{10}]^{10+}$  with the encapsulated  $[\text{SbF}_6]^-$  ion (QEZVIA).

Recently, Dunbar *et al.* reported a series of such attractive contacts between various polynuclear anions and the *s*-tetrazine-based ligand bis(2-pyridynyl)-*s*-tetrazine (bptz)<sup>16</sup>. For example,  $[\text{Ag}_2(\text{bptz})_2(\text{CH}_3\text{CN})_2](\text{PF}_6)_2$  owns strong binding interactions between the  $\text{PF}_6^-$  ions and the *s*-tetrazine rings (Figure 2.5).

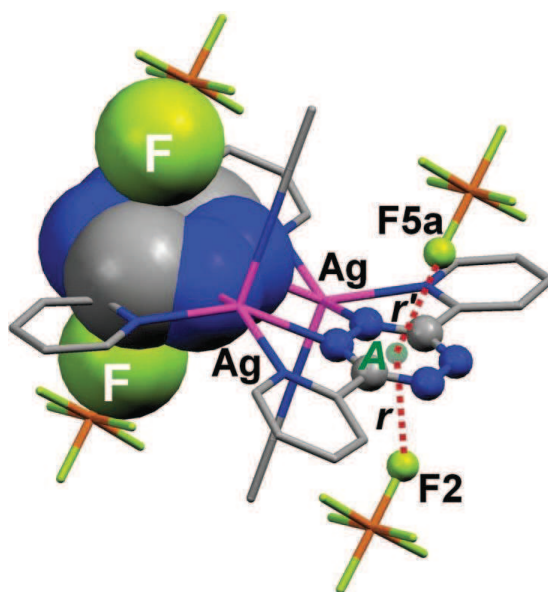


Figure 2.5. Representation of the complex  $[\text{Ag}_2(\text{bptz})_2(\text{CH}_3\text{CN})_2](\text{PF}_6)_2$  showing the hexafluorophosphate-*s*-tetrazine-hexafluorophosphate interactions. Distances between the *s*-tetrazine centroid A and the fluoride atoms F2 and F5a of hexafluorophosphate anions:  $r=2.806 \text{ \AA}$  and  $r'=2.835 \text{ \AA}$ , respectively.

In addition, they mentioned that there are close directional contacts between the anion and the central *s*-tetrazine ring of the bptz ligands. It could then be of interest to further explore the possibility of anion- $\pi$  interactions as a stabilizing factor in this kind of system and for the design of anion receptors.

#### 2.1.4 Anion- $\pi$ interactions

The anion- $\pi$  interaction has been reported by Frontera's group in the study of interactions between anions and hexafluorobenzene<sup>17</sup> or 1,3,5-trinitrobenzene<sup>18</sup>, and by Maascal *et al.*<sup>19</sup>.

Elegant studies have revealed that the anion- $\pi$  interaction is dominated by electrostatic and anion-induced polarization contributions<sup>17,20</sup>. The electrostatic component of the interaction is correlated to the permanent quadrupole moment,  $Q_{zz}$ , of the electron deficient aromatic ring. The quadrupole moment is a measure of the charge distribution of a molecule relative to a particular molecular axis.

Further studies indicated that, for molecules with a very positive  $Q_{zz}$ , *e.g.* 1,3,5-trinitrobenzene ( $Q_{zz} = +20\text{B}$ ), the anion- $\pi$  interaction is basically dominated by the electrostatic term, whereas for molecules with small  $Q_{zz}$  value, *e.g.* 1,2,4,5-tetrazine ( $Q_{zz} = +0.9\text{B}$ ), the anion-induced polarization correlates with the molecular polarizability,  $\alpha_{\parallel}$ , of the aromatic compound. This component has a significant

contribution to the anion- $\pi$  interaction for molecules with high  $\alpha_{\pi}$  values, for example,  $\alpha_{\pi}$  (*s*-tetrazine) = 58.7<sup>21</sup>.

A comprehensive crystallographic and theoretical study was undertaken by Dunbar's group<sup>16</sup> to probe the effect of anion- $\pi$  interactions on the preferred structural motifs of the Ag(I) complexes obtained from the reaction of the Ag(I)X salts (X = [PF<sub>6</sub>]<sup>-</sup>, [AsF<sub>6</sub>]<sup>-</sup>, [SbF<sub>6</sub>]<sup>-</sup> and [BF<sub>4</sub>]<sup>-</sup>) with 3,6-bis(2-pyridyl)-1,2,4,5-tetrazine (bptz)<sup>16</sup>. Figure 2.6 presents the geometry optimization and electrostatic potential (ESP) maps for bptz. Due to the four electron withdrawing nitrogen atoms in the central ring in bptz, a significantly electropositive area is observed in the tetrazine ring. The bptz reactions led to polymeric, dinuclear and propeller-type species, depending on the anion. In addition, multiple, shorter and stronger anion- $\pi$  interactions between the anions and *s*-tetrazine rings are established in the bptz complexes. Furthermore, all the Ag(I) bptz complexes have more than one *s*-tetrazine ring  $\pi$ -contacts per anion, in [Ag<sub>2</sub>(bptz)<sub>3</sub>][SbF<sub>6</sub>]<sub>2</sub>, each anion interacts with 3 *s*-tetrazine rings (Figure 2.6). Multiple anion- $\pi$  interactions per anion are established in the case of the bptz complexes. It is notable that this structure exhibits the first crystallographic example of an anion- $\pi_6$  system, *i.e.*, a system having six anion- $\pi$  interactions per participating [SbF<sub>6</sub>]<sup>-</sup> anion. Besides the anion- $\pi$  interactions, the central *s*-tetrazine ring of bptz participates in  $\pi$ - $\pi$  stacking interactions with another *s*-tetrazine ring (Figure 2.7).

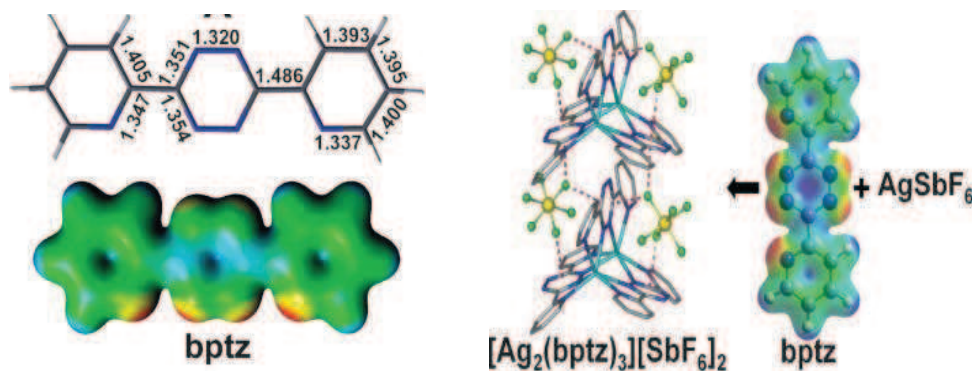


Figure 2.6. Right: BP86/TZP geometry optimization and ESP maps for bptz in the syn orientation. The ESP maps were generated with ADFView at an isodensity value of 0.02 and a color scale of +126 (blue) to -63 (red) kcal/mol. Left: a fragment of the [Ag<sub>2</sub>(bptz)<sub>3</sub>][SbF<sub>6</sub>]<sub>2</sub> structure depicting three anion- $\pi$  contacts between each [SbF<sub>6</sub>]<sup>-</sup> anion and *s*-tetrazine rings (from ref<sup>16</sup>).

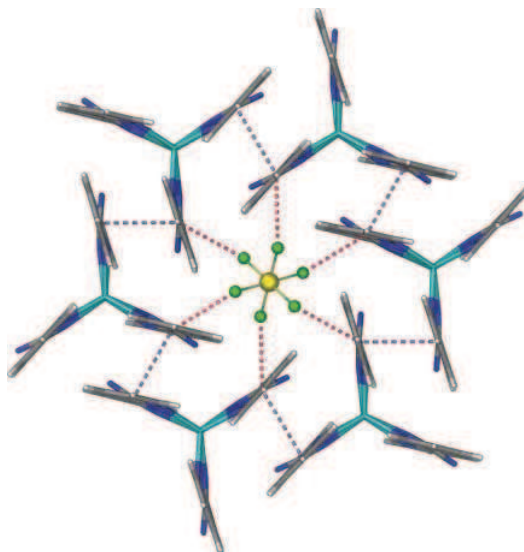


Figure 2.7. Anion- $\pi$  interactions between a  $[\text{SbF}_6]_2$  anion and six *s*-tetrazine rings in  $[\text{Ag}_2(\text{bptz})_3][\text{SbF}_6]_2$ . F-centroid distance = 3.265(3) Å (red dashed lines), F- *s*-tetrazine plane distance = 2.844 Å. The  $\pi$ - $\pi$  contacts (3.36 Å) are indicated with purple dashed lines.

The evidence gleaned from the solid state structures *vis-à-vis* the relative strength of the anion- $\pi$  interactions for bptz, was corroborated by DFT single point energy calculations on several of their Ag (I) complexes. In figure 2.8, the ESP maps for  $[\text{Ag}_2(\text{bptz})_2(\text{CH}_3\text{CN})_2][\text{AsF}_6]_2$  as (a) a dication and (b) a neutral species are shown. The dication demonstrates high electropositive character (more blue) on the central *s*-tetrazine rings, which is greatly diminished in  $[\text{Ag}_2(\text{bptz})_2(\text{CH}_3\text{CN})_2][\text{AsF}_6]_2$  due to a flow of electron density from the  $[\text{AsF}_6]^-$  anions to the bptz  $\pi$ -acidic central rings and the establishment of favorable anion- $\pi$  interactions between anion and *s*-tetrazine rings. In the singly-charged cation  $\{[\text{Ag}_2(\text{bptz})_2(\text{CH}_3\text{CN})_2][\text{AsF}_6]\}^+$ , the ring distal from anion is clearly more electropositive than the ring in close proximity to the  $[\text{AsF}_6]^-$  anion (Figure 2.9).

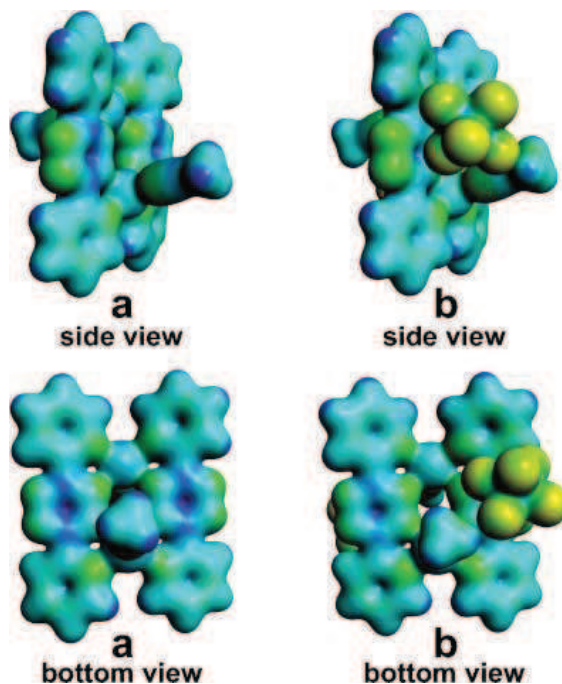


Figure 2.8. ESP map from the BP86/TZP SPE calculations of (a) dication  $[\text{Ag}_2(\text{bptz})_2(\text{CH}_3\text{CN})_2]^{2+}$  with a color scale of 220 (blue) to  $-31$  (red)  $\text{kcal mol}^{-1}$  and (b) neutral complex  $[\text{Ag}_2(\text{bptz})_2(\text{CH}_3\text{CN})_2][\text{AsF}_6]_2$  with a color scale of 126 (blue) to 2126 (red)  $\text{kcal mol}^{-1}$ . The maps were generated with ADFView at a 0.02 isodensity value. (from ref<sup>16</sup>).

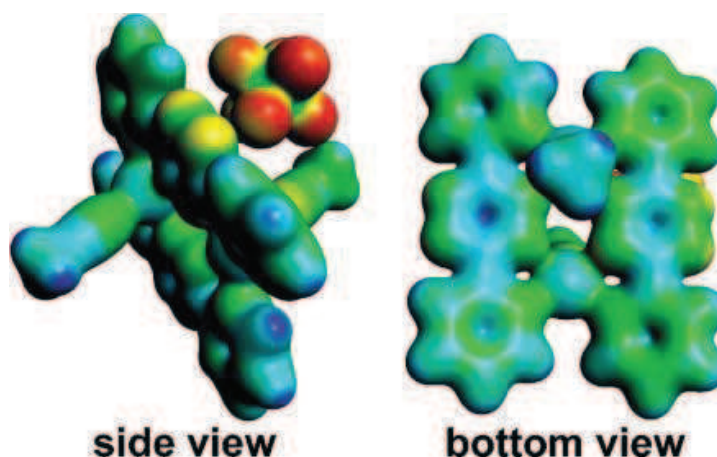


Figure 2.9. ESP map from the BP86/TZP SPE calculations for the singly charged cation  $\{[\text{Ag}_2(\text{bptz})_2(\text{CH}_3\text{CN})_2][\text{AsF}_6]\}^+$  with a color scale of 188 (blue) to 231 (red)  $\text{kcal mol}^{-1}$ . The maps were generated with ADFView at a 0.02 isodensity value (from ref<sup>16</sup>).

More recently, Frontera's<sup>15</sup> group has reported the results of high level *ab initio* calculations computed for several complexes of anions with urea, squaramide and *s*-tetrazine, to go deeper into the understanding of the binding forces entangled in both hydrogen bond and anion- $\pi$  interactions. For the electron deficient aromatic ring



*s*-tetrazine, calculations showed that the formation of a complex between *s*-tetrazine and fluoride (Figure 2.10) should be energetically favorable (calculated complexation energy  $E = -18.75 \text{ Kcal.mol}^{-1}$ ) and would be mainly governed by electrostatic and polarization energies. Comparably, complexation with chloride or bromide would be less favorable ( $E \approx -10 \text{ Kcal.mol}^{-1}$ ), and in principle, the halogen anions could be discriminated.

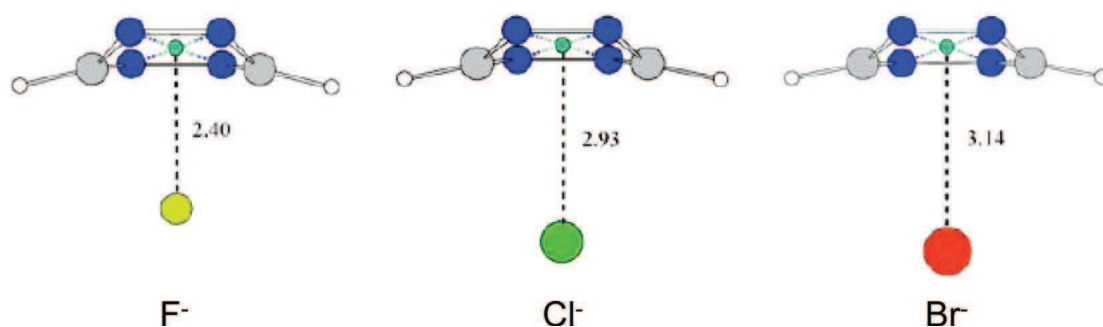


Figure 2.10. MP2-optimized geometries of *s*-tetrazine complexes with fluoride, chloride, and bromide. Distances are in angstroms, and the ring centroid is represented by a dummy atom.

## 2.2 Molecular design of ion pair receptors

Audebert's group<sup>22</sup> reported that the fluorescence of the bis-*s*-tetrazine **56** (Figure 2.11), can be efficiently quenched in the presence of electron-rich compounds such as triphenylamines, phenol or anisole. Figure 2.11 depicts the Stern-Volmer plots in the case of several quenchers. It is clear that the tendency is related to the electron affinity of the quenchers: the better electron donors lead to the higher quenching constants.

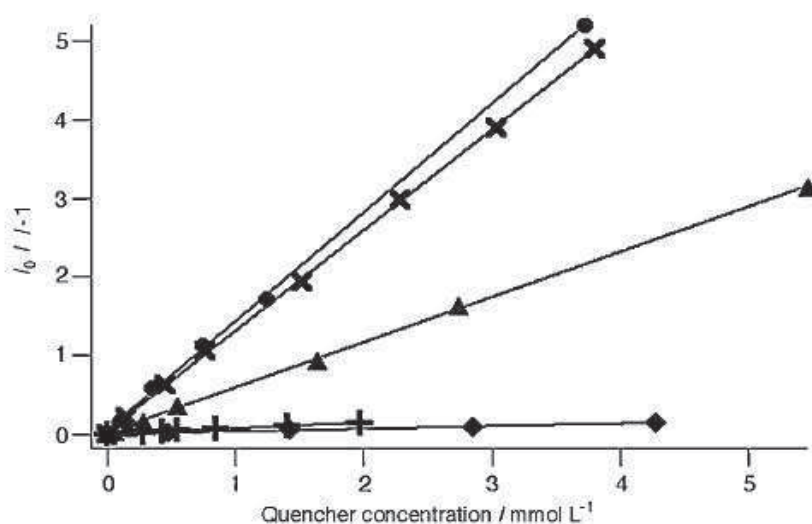
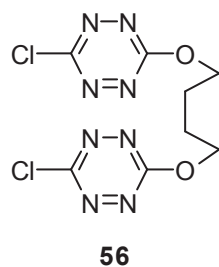


Figure 2.11. Stern–Volmer plots for compound **56** as functions of quencher concentrations for the various quenchers: ● triphenylamine; x tris-*p*-bromophenylamine; ▲ phenol; + 4-nitrophenol; ◆ anisole.

Later, they prepared new multi *s*-tetrazine derivatives **60**, **61**, **63** and **64** (Figure 2.12)<sup>23,24</sup>. The fluorescence of compound **60** and **63** is quenched by electron donors according to a charge transfer process (Figure 2.13). It confirms the potential of *s*-tetrazines for the sensing of aromatic electron rich compounds. Except in the case of the closed cyclophane **61**, the spatial arrangement of the *s*-tetrazine rings does not seem to influence noticeably the rate of the fluorescence quenching.

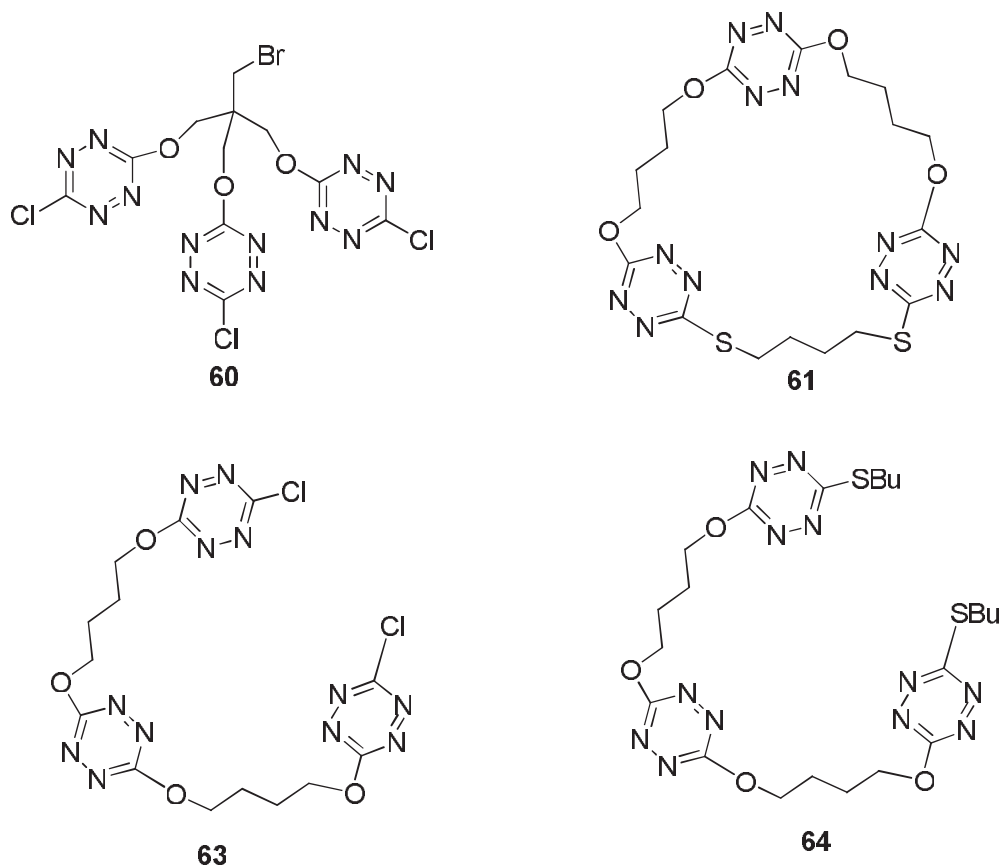


Figure 2.12. Multi *s*-tetrazine derivatives reported by Audebert's group.

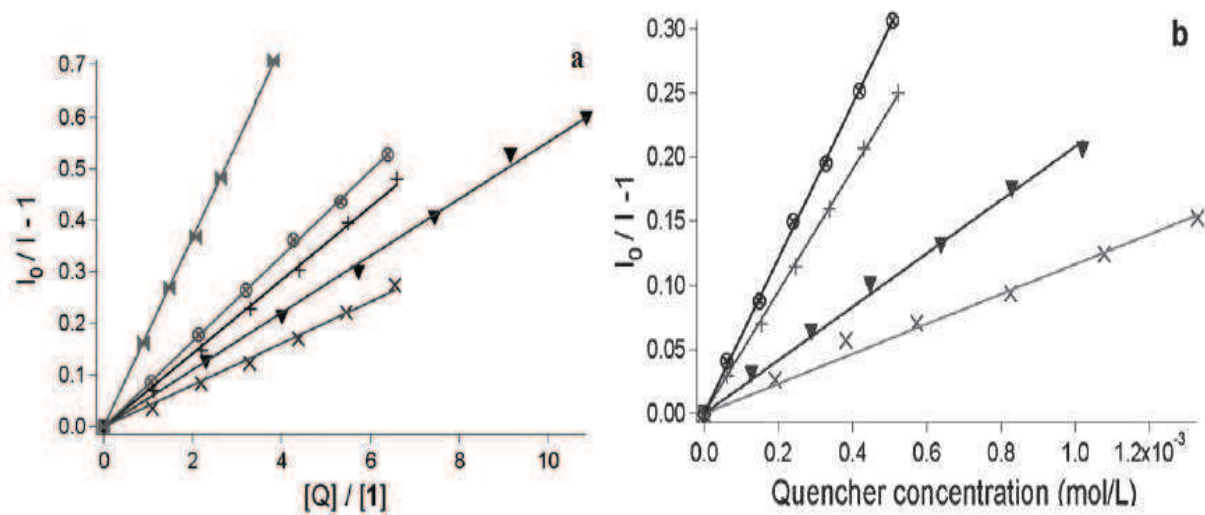


Figure 2.13. (a) Stern-Volmer plots for the quenching of compound **60** with five different quenchers (Q), namely tetrathiafulvalene (▶◀), triphenylamine (⊗), tri(4-bromophenyl)amine (+), pyrrole (♥) and 1,3,5-trimethoxybenzene (x). (b). Stern-Volmer plots for the quenching of



63 with triphenylamine, tri(4-bromophenyl)-amine (+), pyrrole (♥) and 1,3,5-trimethoxybenzene (x).

Recently, tetrazine **79** (Figure 2.14) have been prepared by Audebert's group<sup>25</sup>, and fluorescence quenching experiments were performed with aliphatic or aromatic amines. Each time, the addition of the pollutant leads to a diminution of the fluorescence intensity. The slopes of the Stern-Volmer plots are in good agreement with the electron density of each quencher, which is fully consistent with a quenching by electron transfer in the excited state. Additionally, this molecule has been grafted on silica nanoparticles. They show a bright fluorescence emission, albeit with some degree of quenching because of interchromophoric interactions and can also detect the same amines through fluorescence quenching.

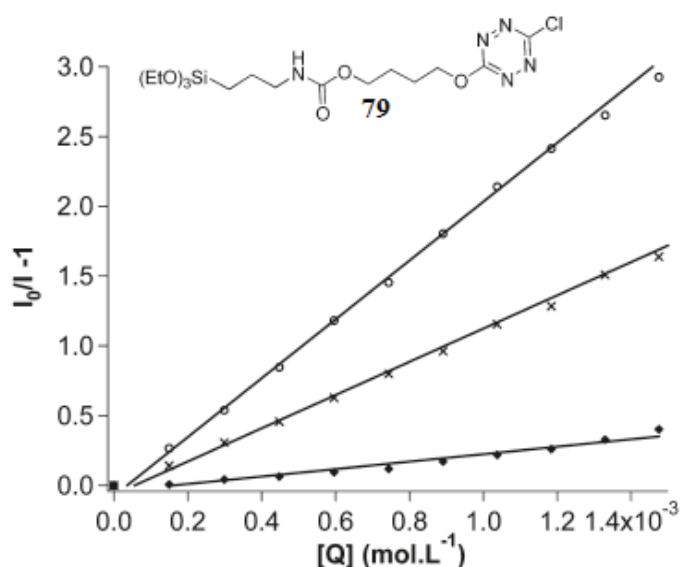


Figure 2.14. Stern-Volmer plots for the free dye **79** as function of quencher concentration for various quenchers: ○ DPA; ◆ EtOA; x TEA (excitation wavelength 340 nm).

Thus the interaction of *s*-tetrazines with electron rich aromatics in the excited state is well established. However, there is no experimental evidence of *s*-tetrazine-anion interactions in solution so far despite the calculations results from Frontera's group and the solid state observations from Dunbar's team. Preliminary tests conducted in Audebert's team did not show any significant evidence of interactions (fluorescence quenching, variation of reduction potential) of anions with *s*-tetrazines upon simple mixing. So the binding force between anions and *s*-tetrazine is probably too small. An alternative approach was pursued by designing an ion pair receptor where recognition of the anion would be favored by cooperative interactions between co-bound ions. For this purpose an open receptor was designed which contains a site

for interaction with cations: a polyethylene glycol chain and sites to bind anions through anion- $\pi$  interactions: *s*-tetrazines. In order to get the best spectroscopic response both sites should be as close as possible. So it was considered linking directly tetrazine to PEO chain (Figure 2.15). The open chain topology is usually less favorable for efficient binding but it was neither the less selected for two main reasons. First, nucleophilic substitution on alkoxy-*s*-tetrazines is unfavorable and second, dialkoxy-*s*-tetrazines are less fluorescent. In order to increase the probability of *s*-tetrazine interactions with anions, two *s*-tetrazines were included. Various PEO chain lengths have been used to try to obtain some selectivity.

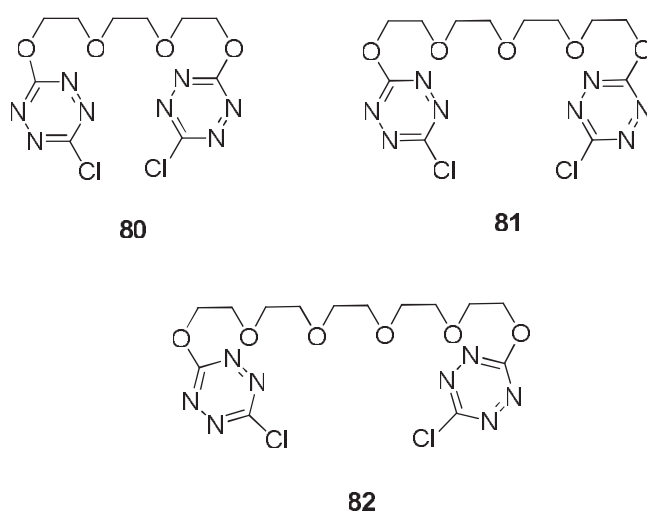


Figure 2.15. Ion pair receptors synthetic targets

The mode of action of the receptor is depicted in figure 2.16. The elongated PEO chain should wrap around the cation bringing both *s*-tetrazines close to each other. It is then expected that the anion will lie close to the cation and possibly be sandwiched by both *s*-tetrazines leading to a detectable fluorescence quenching.

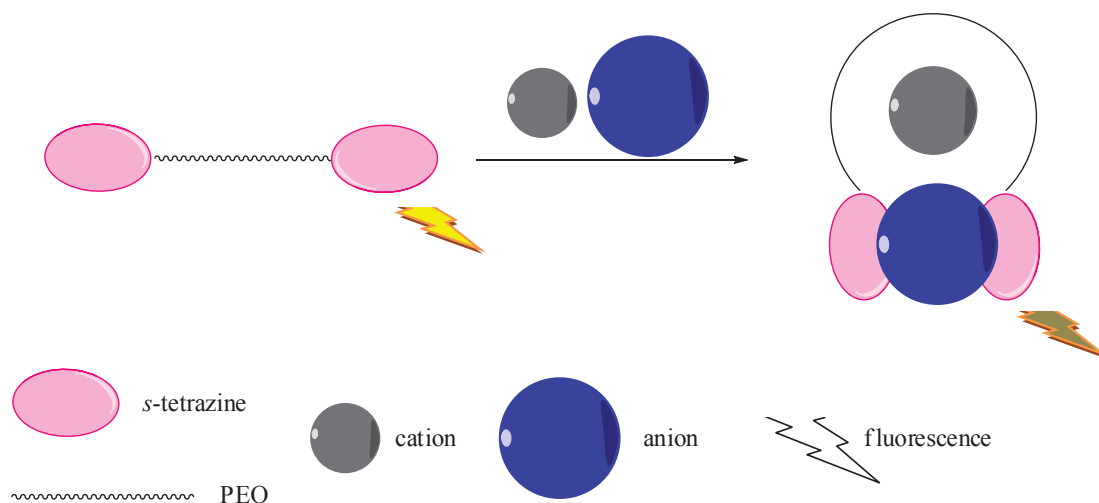


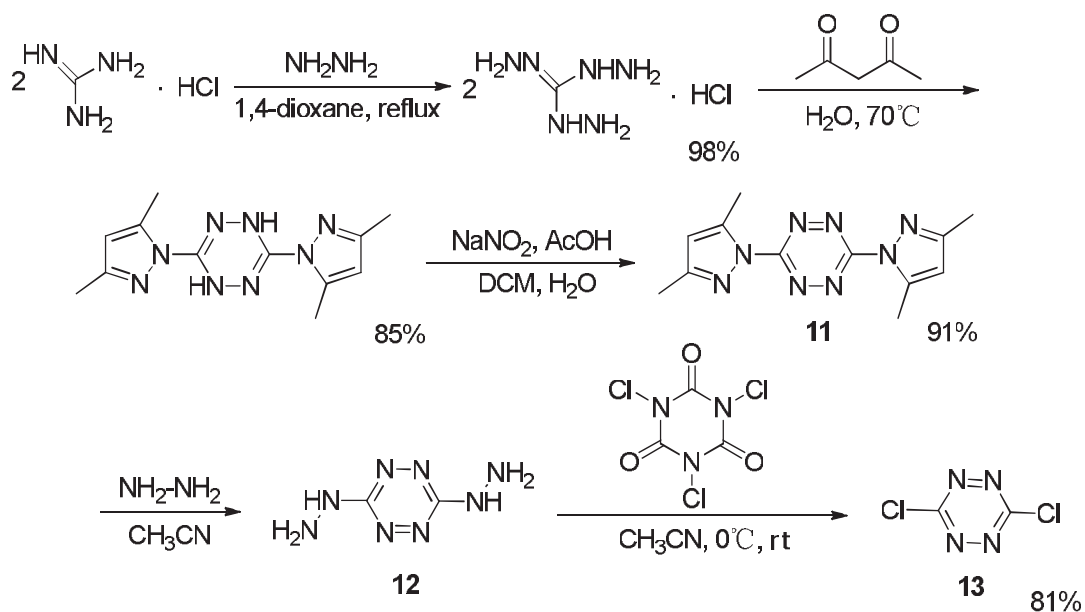
Figure 2.16. *s*-Tetrazine ion pair receptor working principle.

## 2.3 Synthesis

### 2.3.1 Preparation of 3,6-dichloro-1,2,4,5-tetrazine

Considering that 3,6-dichloro-1,2,4,5-tetrazine present a high reactivity toward various nucleophiles, we use it as the starting material for the preparation of the receptors. As mentioned in chapter one, this intermediate can be obtained in high yields in 5 steps (Scheme 2.1).

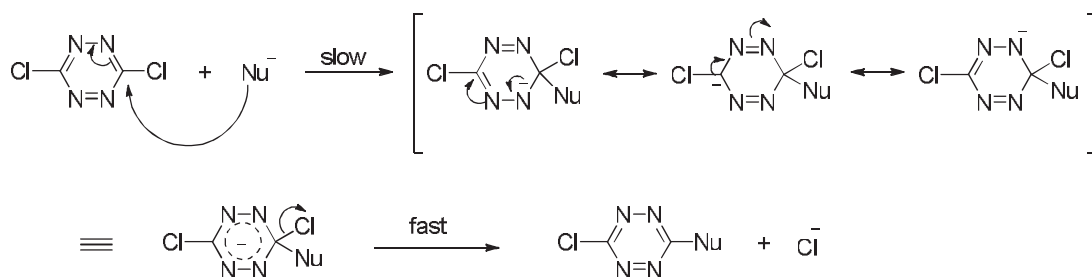
First of all, guanidine hydrochloride is refluxed with hydrazine monohydrate in 1,4-dioxane to give triaminoguanidine monohydrochloride in high yield (98%), which is then condensed with 2,4-pentanedione to afford 3,6-bis(3,5-dimethylpyrazol-1-yl)-1,2-dihydro-1,2,4,5-tetrazine in good yield (85%). Then the dihydro-*s*-tetrazine can be oxidized by using  $\text{NaNO}_2$  combined with acetic acid, and the reaction goes smoothly in water with a small amount of dichloromethane. Product **11** is obtained pure after washing the crude solid with dilute aqueous solution of potassium carbonate. After the oxidation, the bis-dimethylpyrazolyl-*s*-tetrazine is refluxed with hydrazine for a short time to give 3,6-dihydrazino-*s*-tetrazine (**12**). Lastly, trichloroisocyanuric acid as chlorination agent reacts with **12** at room temperature, and then dichloro-*s*-tetrazine (**13**) is obtained.



Scheme 2.1. Synthesis of dichloro-*s*-tetrazine.

### 2.3.2 Preparation of ion-pair receptors

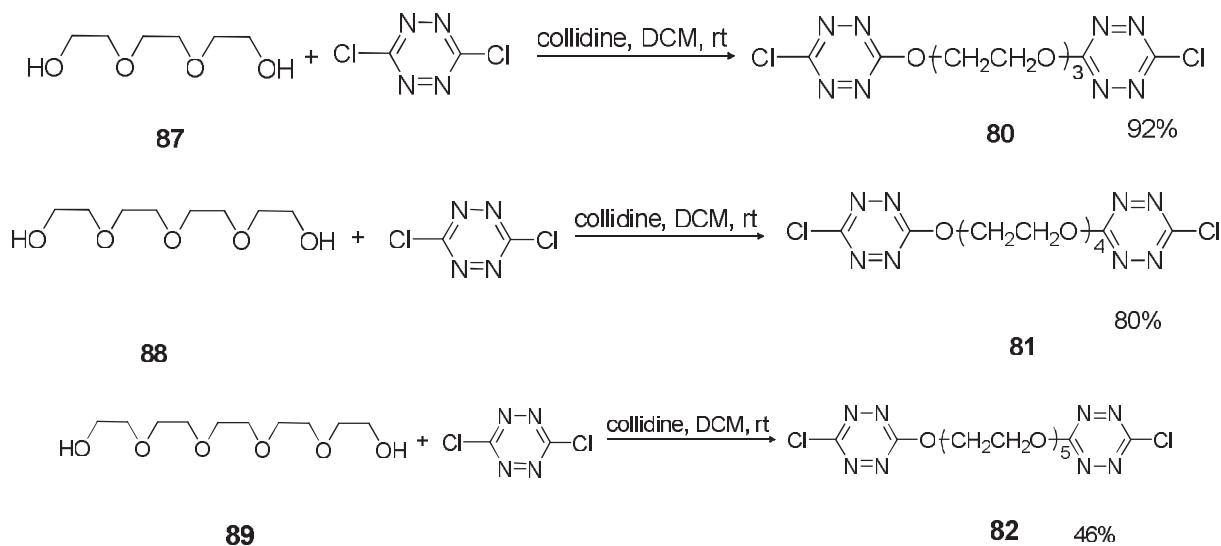
Because chlorine is a good leaving group, 3,6-dichloro-*s*-tetrazine is a good choice for aromatic nucleophilic substitution with a variety of nucleophiles. In addition, the mechanism of the  $S_NAr$  reaction of dichloro-*s*-tetrazine was described by Gong (Scheme 2.2)<sup>23</sup>.



Scheme 2.2.  $S_NAr$  mechanism with dichloro-*s*-tetrazine.

Efficient conditions for this reaction using alcohol as the nucleophile have been developed by our group. The reaction works perfectly well in dichloromethane and in the presence of 1 equivalent of *s*-collidine at room temperature. Typically yields for the monosubstitution range from 50% to 90% with primary alcohols, but drop significantly (10%-20%) with secondary alcohols<sup>26</sup>. Dialcohols **87**, **88**, and **89** were

selected as good nucleophiles. Mixing 2 equivalents of dichloro-*s*-tetrazine with the alcohol in the basic conditions gave the target compounds. The yields are as expected, above 50%.

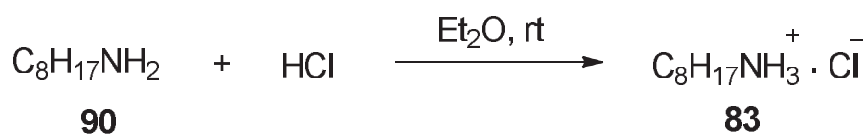


Scheme 2.3. Synthesis of ion pair receptors **80**, **81** and **82**.

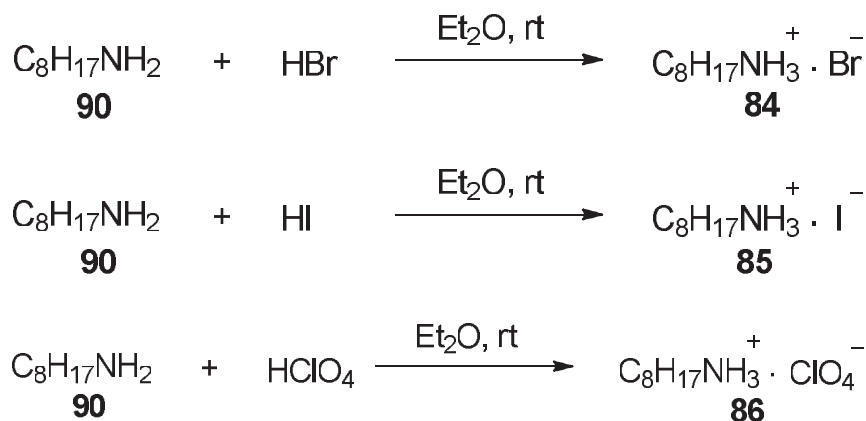
### 2.3.3 Selection and synthesis of ion pairs

In a first approach, simple alkali halides were tested and compared to alkali perchloric salts. However, a more elaborate one had also to be considered for solubility reason. Many complexes between crown ethers and cationic guest species have been reported. However, relatively few cases involving primary alkyl ammonium ions as the guest cation are known. But, in all these cases, this guest cation is bound principally through  $[N^+ \cdots H \cdots O]$  hydrogen bond to the host<sup>27</sup>. This situation was supposed to be favorable for our ion pair receptor. In addition, octylammonium halides are soluble in organic solvents and became a target of choice for our study.

Four ammonium salts have been prepared by the reaction of octylamine with the corresponding aqueous acid<sup>28</sup>, and then recrystallized from diethyl ether.







Scheme 2.4. Synthesis of ammonium ion-pairs.

## 2.4 Screening of ion-pairs

In order to investigate the selectivity of compounds **80-82** as receptors, fluorescence quenching studies were carried out by addition of different ion pairs.

Firstly, from the research of Frontera's group, calculations showed that the complex between *s*-tetrazine and fluoride should be energetically the most favorable followed by chloride and bromide. Since handling of fluoride ions is not always an easy task, NaCl and KCl became the first candidates as ion pairs. Unfortunately, they are weakly soluble in organic solvents, such as dichloromethane or acetonitrile. Furthermore, chloroalkoxy-*s*-tetrazines react with water or alcohols, so they can not be used as solvent. So several other candidates which can be dissolved in organic solvents have been chosen: NaClO<sub>4</sub> (soluble in CH<sub>3</sub>CN), LiClO<sub>4</sub> (soluble in CH<sub>3</sub>CN), C<sub>8</sub>H<sub>17</sub>NH<sub>3</sub><sup>+</sup>·Cl<sup>-</sup> (soluble in CHCl<sub>3</sub>), C<sub>8</sub>H<sub>17</sub>NH<sub>3</sub><sup>+</sup>·Br<sup>-</sup> (soluble in CHCl<sub>3</sub>), C<sub>8</sub>H<sub>17</sub>NH<sub>3</sub><sup>+</sup>·I<sup>-</sup> (soluble in CHCl<sub>3</sub>) and C<sub>8</sub>H<sub>17</sub>NH<sub>3</sub><sup>+</sup>·ClO<sub>4</sub><sup>-</sup> (soluble in CHCl<sub>3</sub>).

A series of simple screening experiments was handled first: salts were added to a solution of *s*-tetrazine directly and the fluorescence spectra were recorded. If the salts are recognized by the *s*-tetrazine receptor, there should be a change in the fluorescence spectra. Figure 2.17 present the results for *s*-tetrazine **80**. There is no obvious fluorescence variation by addition of NaClO<sub>4</sub> and LiClO<sub>4</sub>, and fluorescence quenching with C<sub>8</sub>H<sub>17</sub>NH<sub>3</sub><sup>+</sup>·Br<sup>-</sup>.

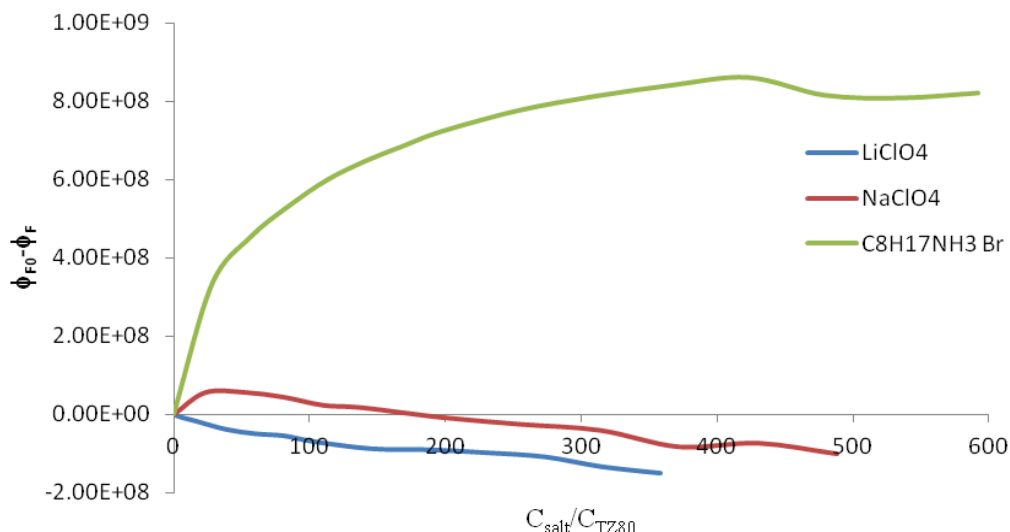


Figure 2.17. Fluorescence change upon addition of several ion pairs to *s*-tetrazine **80**

Similar results have been attained with compound **81**, so further screening was focused on the octylammonium salts. The three ammonium halides showed interactions with *s*-tetrazines **80**, **81** and **82** but not  $C_8H_{17}NH_3^+ \cdot ClO_4^-$  (Table 2.1).

Table 2.1. Screening of ammonium salts.

compounds	$C_8H_{17}NH_3^+ \cdot Cl^-$	$C_8H_{17}NH_3^+ \cdot Br^-$	$C_8H_{17}NH_3^+ \cdot I^-$	$C_8H_{17}NH_3^+ \cdot ClO_4^-$
<b>80</b>	○	+	+	○
<b>81</b>	○	+	+	○
<b>82</b>	○	+	+	○

+: quenching of fluorescence; ○: no effect

In conclusion, only the alkyl ammonium halogen salts induced a quenching of the fluorescence of receptors **80-82** in organic solvents. The complexation of these receptors with the three salts was thus studied in details by NMR, UV-vis. absorption and fluorescence spectroscopies.

## 2.5 NMR studies of ion pair receptors

### 2.5.1 $^1H$ NMR titration

Since the ammonium should interact with the polyethylene oxide chain of the receptors, it should be possible to follow the complexation by monitoring the change in chemical shifts of the methylenes of the PEO.

Upon addition of  $C_8H_{17}NH_3^+ \cdot I^-$ , the signal was found to gradually shift

downfield for all three receptors. Especially for **82**, the receptor's proton peaks found of  $\delta = 4.82\text{ppm}$  and  $\delta = 3.99\text{ppm}$  in the initial spectrum ultimately shift to  $\delta = 4.92\text{ppm}$  and  $\delta = 4.07\text{ppm}$  after addition of 24.7 equivalents of salt. The total shift is about  $0.1\text{ppm}$ , as indicated by the overlay of NMR spectra shown in figure 2.18.

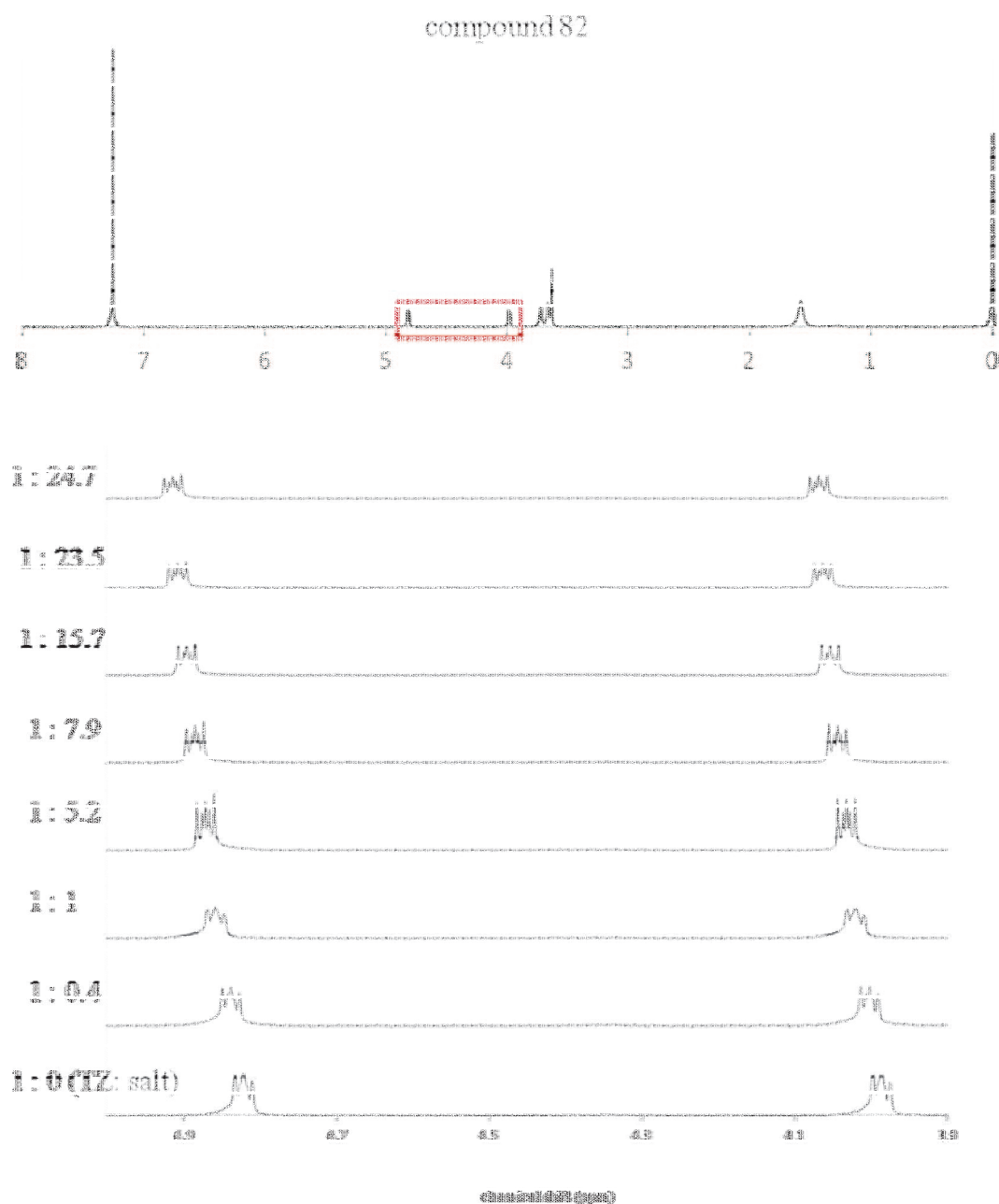


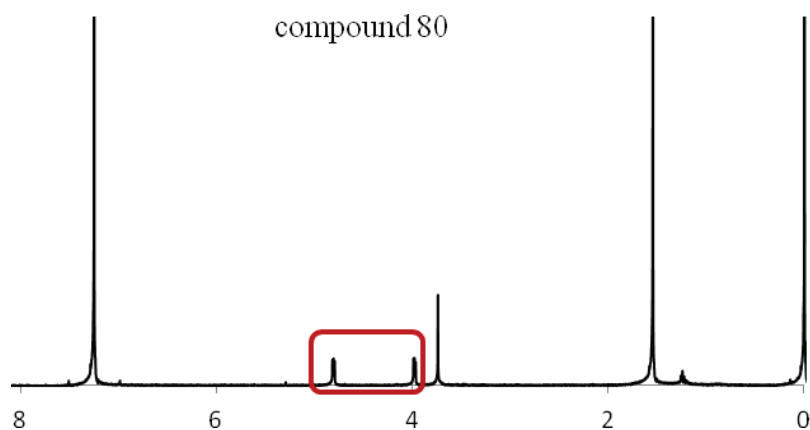
Figure 2.18.  $^1\text{H}$  NMR spectra obtained during the titration of host **82** with  $\text{C}_8\text{H}_{17}\text{NH}_3^+\cdot\text{I}^-$ . Up: full spectrum of **82**; Down: variation of the significant peaks upon addition of salt.

Titration of compound **82** with  $\text{C}_8\text{H}_{17}\text{NH}_3^+\cdot\text{Br}^-$  also leads to spectral shifts, but from  $\delta = 4.82\text{ppm}$  to  $\delta = 4.84\text{ppm}$  after addition of 125 equivalents of salt. The total of

chemical shifts is only  $\Delta\delta = 0.02\text{ppm}$ .

For compound **80**, the chemical shifts also change and it is less pronounced with bromide salt  $\Delta\delta = 0.003\text{ppm}$  (Figure 2.19) than with iodide salt  $\Delta\delta = 0.01\text{ppm}$  (Figure 2.20). In addition, the maximum value is attained at the ratio 18: 1 for iodide and at 450: 1 for bromide salt. That means that host **80** binds iodide salt stronger than bromide salt.

Furthermore, Dalcanale's group<sup>28</sup> reported that a low  $K_{\text{ass}}$  value in the case of octylammonium chloride as the ion pair. In our case, the changes in chemical shifts observed with  $\text{C}_8\text{H}_{17}\text{NH}_3^+\cdot\text{Br}^-$  are small (0.003ppm), and are close to the technical limit of NMR spectroscopy. So we did not run the NMR titration with  $\text{C}_8\text{H}_{17}\text{NH}_3^+\cdot\text{Cl}^-$ . But fluorescence which is a more sensitive technique allowed titration of  $\text{C}_8\text{H}_{17}\text{NH}_3^+\cdot\text{Cl}^-$  with our receptors (*vide infra*).



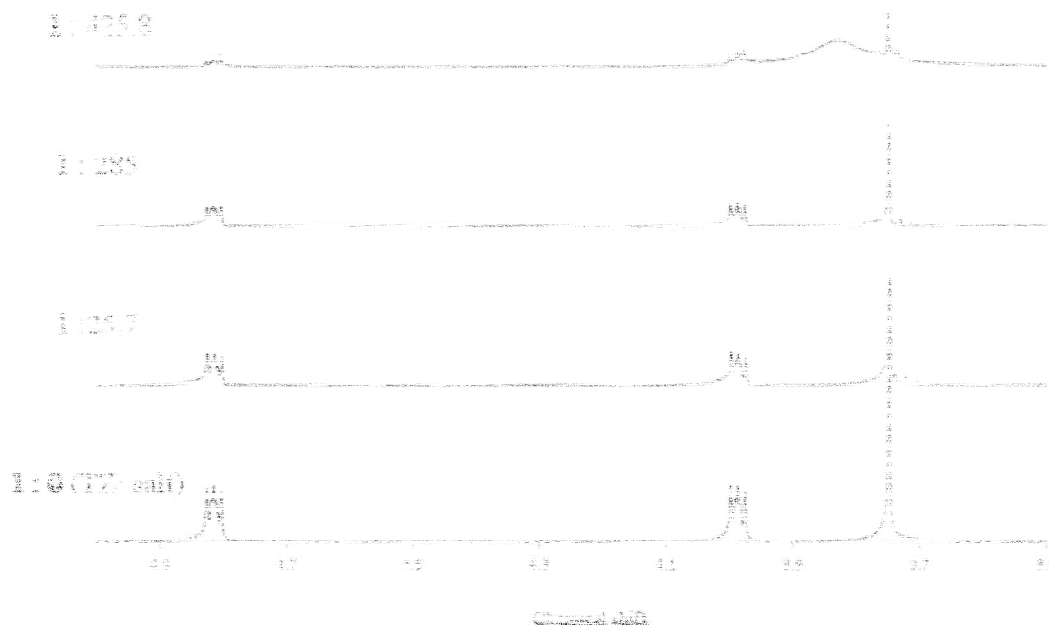


Figure 2.19.  $^1\text{H}$  NMR spectra obtained during the titration of host **80** with  $\text{C}_8\text{H}_{17}\text{NH}_3^+\cdot\text{Br}^-$ . Up: full spectrum of **80**; Down: variation of the significant peaks upon addition of salt.

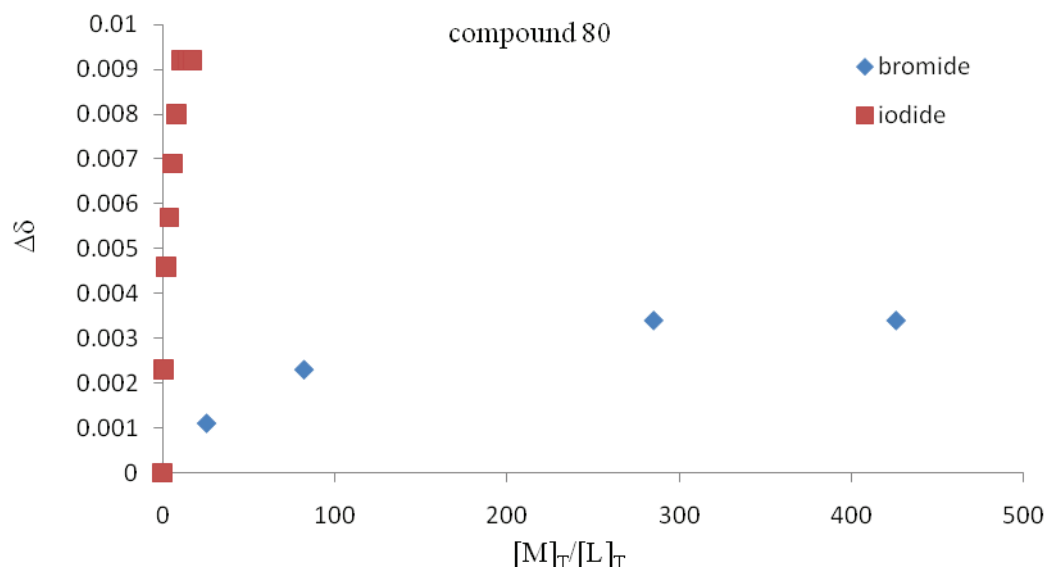


Figure 2.20. Binding curves resulting from the  $^1\text{H}$  NMR spectral shifts of the  $\text{CH}_2$  peak of **80** upon titration with  $\text{C}_8\text{H}_{17}\text{NH}_3^+\cdot\text{I}^-$  and  $\text{C}_8\text{H}_{17}\text{NH}_3^+\cdot\text{Br}^-$ .

Compound **81** also showed obvious chemical shift changes (Figure 2.21) in the presence of  $C_8H_{17}NH_3^+ \cdot I^-$  ( $\Delta\delta = 0.0384\text{ppm}$ ), and a smaller variation with addition of  $C_8H_{17}NH_3^+ \cdot Br^-$  ( $\Delta\delta = 0.0098\text{ppm}$ ). A maximum is attained after addition of 15 equivalents of the first salt and about 400 equivalents of the second.

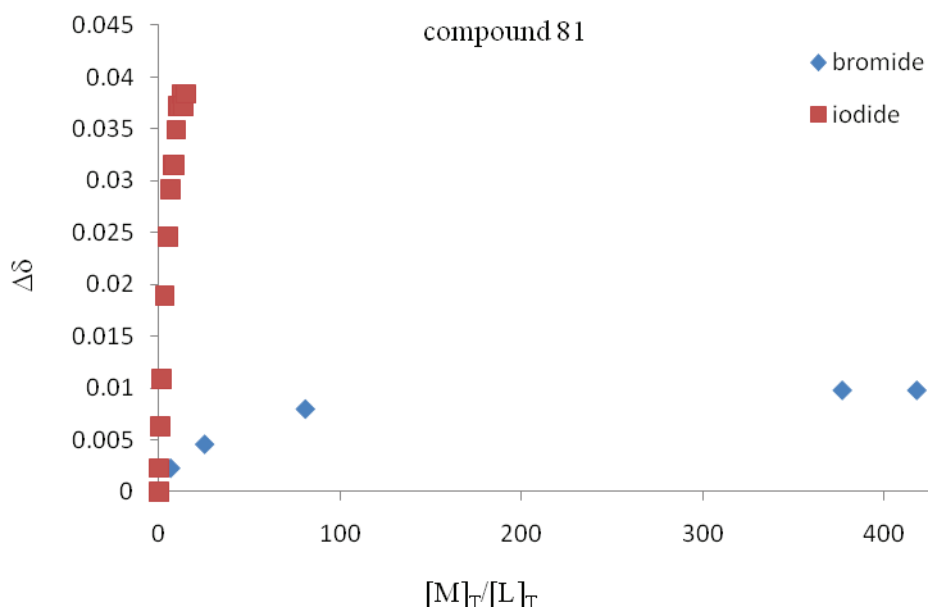


Figure 2.21. Binding curves resulting from the  $^1H$  NMR spectral shifts of the  $CH_2$  peak of **81** upon titration with  $C_8H_{17}NH_3^+ \cdot I^-$  and  $C_8H_{17}NH_3^+ \cdot Br^-$ .

Finally for compound **82**, a similar trend is observed (Figure 2.22): larger change of chemical shifts at smaller ratio with iodide compared to bromide.

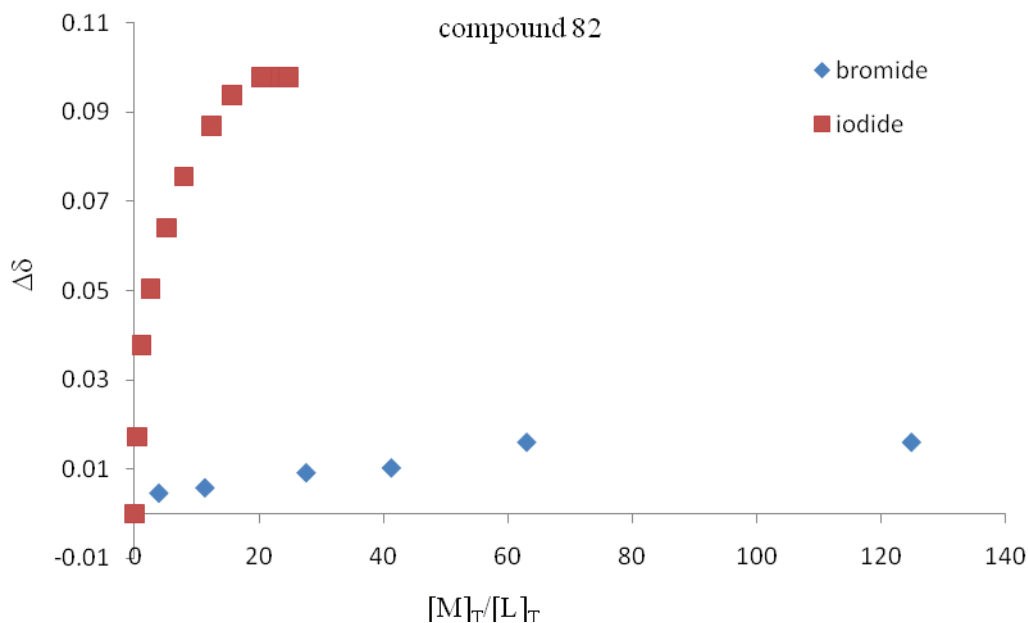


Figure 2.22. Binding curves resulting from the  $^1\text{H}$  NMR spectral shifts of the  $\text{CH}_2$  peak of **82** upon titration with  $\text{C}_8\text{H}_{17}\text{NH}_3^+\cdot\text{I}^-$  and  $\text{C}_8\text{H}_{17}\text{NH}_3^+\cdot\text{Br}^-$ .

Comparison of the results obtained with all three receptors clearly shows that  $\text{C}_8\text{H}_{17}\text{NH}_3^+\cdot\text{I}^-$  binds stronger than  $\text{C}_8\text{H}_{17}\text{NH}_3^+\cdot\text{Br}^-$ . Since the main difference between the three receptors is the cavity size, the systematic preference for iodide has to come from a specific interaction of the anion with *s*-tetrazine. It has been reported in the literature that *s*-tetrazine is a highly polarizable aromatic ring (see paragraph 2.1.4). It is then understandable it interacts better with the most polarizable anion  $\text{I}^-$ . Noteworthy, these findings are contradictory with the theoretical work of Frontera<sup>15</sup>.

The comparisons of the titrations of all three receptors with the same salt are presented in figure 2.23 for  $\text{Br}^-$  and figure 2.24 for  $\text{I}^-$ .

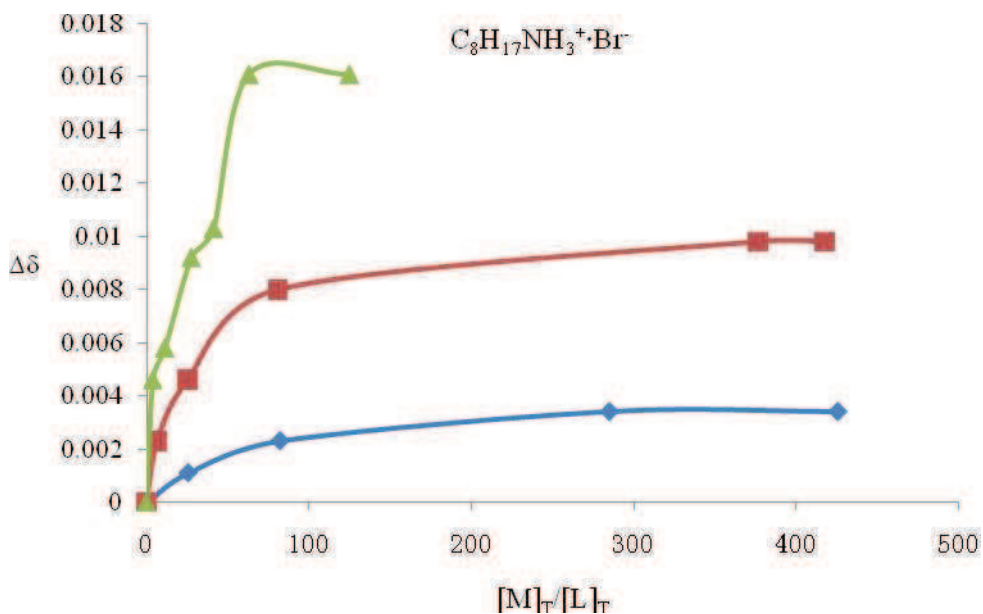


Figure 2.23. Binding curves resulting from the  $^1\text{H}$  NMR spectral shifts of the  $\text{CH}_2$  peak of **80** (blue), **81** (red) and **82** (green) upon titration with  $\text{C}_8\text{H}_{17}\text{NH}_3^+\cdot\text{Br}^-$ .

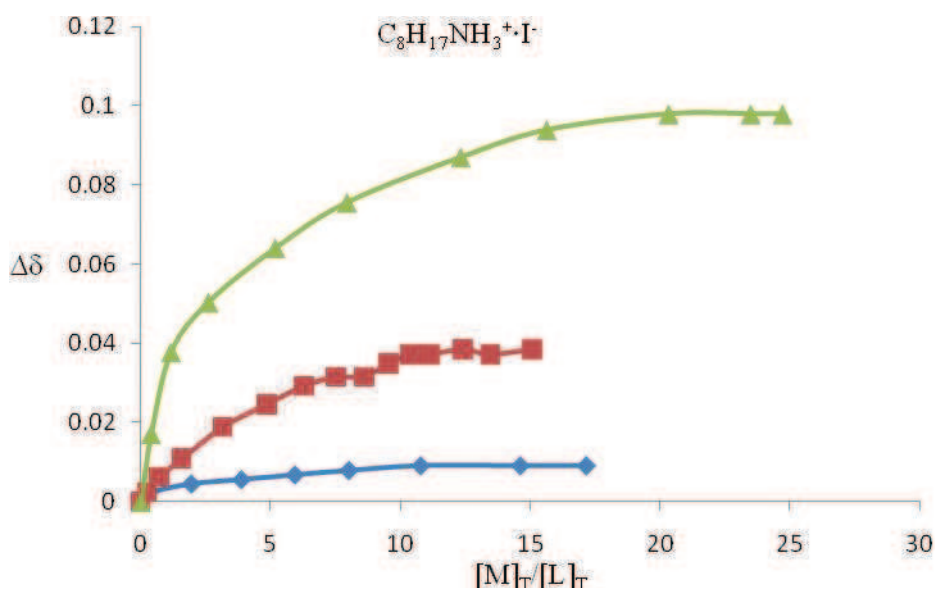


Figure 2.24. Binding curves resulting from the  $^1\text{H}$  NMR spectral shifts of the  $\text{CH}_2$  peak of **80** (blue), **81** (red) and **82** (green) upon titration with  $\text{C}_8\text{H}_{17}\text{NH}_3^+\cdot\text{I}^-$ .

For both salts, the same trend is observed: the binding strength follows the order: **82** > **81** > **80**. This tendency probably comes from a better ability of the pentaethylene glycol chain of **82** to form a stable complex with primary alkyl



ammonium salts than shorter PEO. This result can be related to the superior capacity of [18] crown-6 to bind primary alkyl ammonium salts stronger than smaller macrocycles<sup>29,27,30</sup>. It is then likely that receptor **82** can adopt a more favorable conformation to accommodate  $C_8H_{17}NH_3^+X^-$  salts than the two smaller **80** and **81** receptor.

Two conclusions can be drawn from the NMR titrations:

- 1) Receptor **82** comprising 6 oxygen atoms binds alkyl ammonium salts stronger than its shorter equivalents **80** and **81**.
- 2) The three tetrazine derivatives show selectivity for halogens in the order:  $I^- > Br^- \gg Cl^-$ .

### 2.5.2 Job plot

Job plot also known as the method of continuous variation or Job's method is used to determine the stoichiometry of a binding event. This method is widely used in analytical chemistry, instrumental analysis and advanced chemical equilibrium.

In our case,  $^1H$  NMR titration afforded plots of chemical shift changes vs. molar fraction of ammonium iodide. The Job's plot for the complex **81** with  $C_8H_{17}NH_3^+I^-$  presents a maximum for  $M/(M+L)=0.3$  (Figure 2.25) which corresponds to a  $M_1L_2$  stoichiometry ( $M= C_8H_{17}NH_3^+I^-$  and  $L=80$ ).

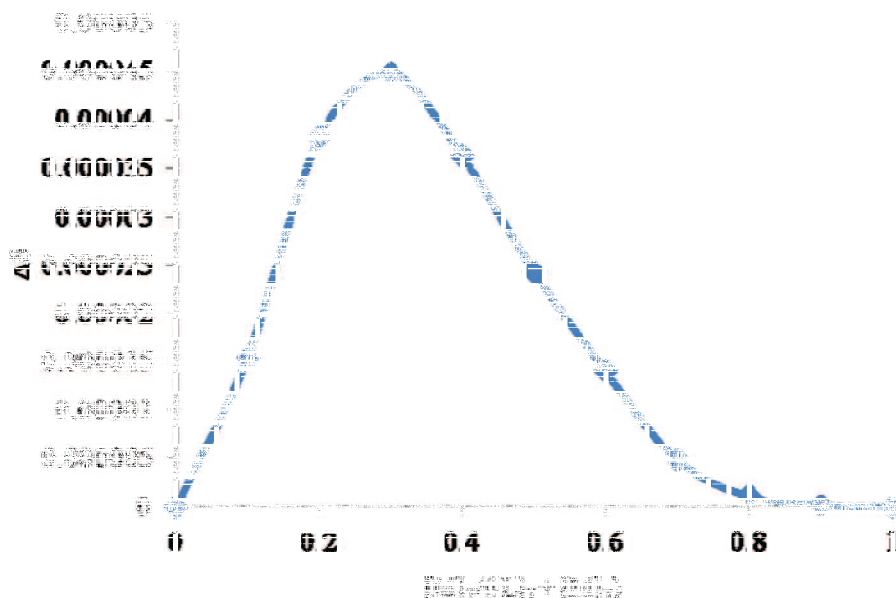


Figure 2.25. Job's plot of compound **81** (L) with  $C_8H_{17}NH_3^+I^-$  (M). The sum of total concentration  $[L]_T + [M]_T$  was 0.0156M in  $CDCl_3$ .  $\Delta\delta$  denotes changes in chemical shift of the ethoxyl protons of **81** upon complexation with ammonium salts.

The same experiment with **82** and  $C_8H_{17}NH_3^+ \cdot I^-$  (Figure 2.26) gives a different result since the plot presents a broad maximum between 0.5 and 0.6. It is then possible that in this case two stoichiometries coexist: ML and  $M_2L$ .

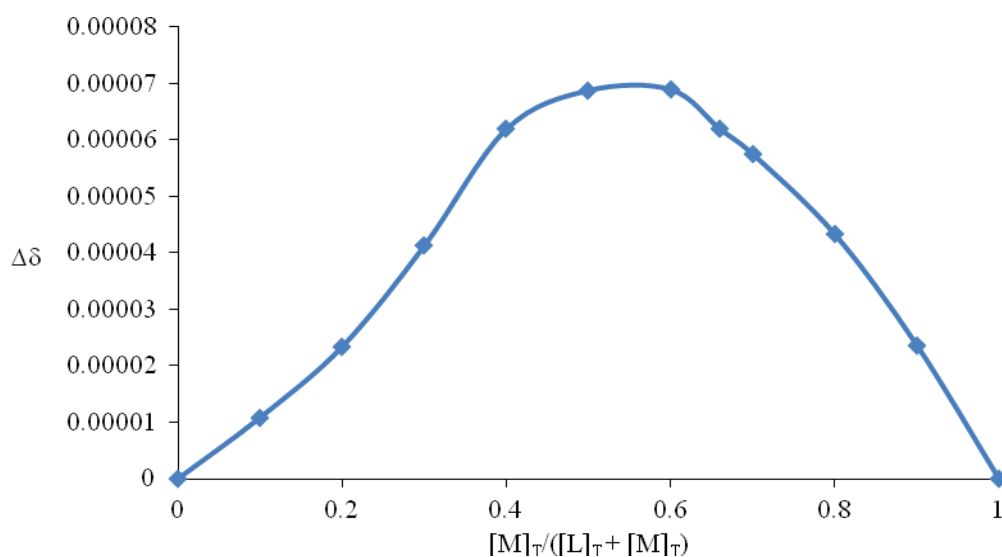


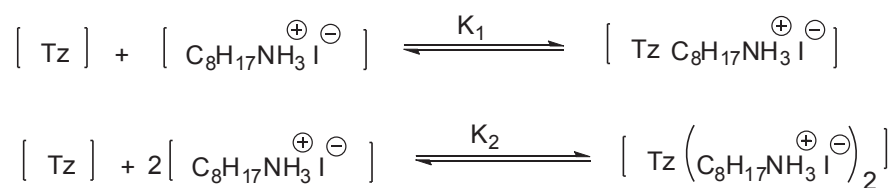
Figure 2.26. Job's plot of compound **82** (L) with  $C_8H_{17}NH_3^+ \cdot I^-$  (M). The sum of total concentration  $[L]_T + [M]_T$  was 0.0043M in  $CDCl_3$ .  $\Delta\delta$  denotes change in chemical shift of the ethoxyl protons of **82** upon complexation with ammonium salts.

### 2.5.3 Determination of binding constants

According to the NMR titrations, the ion pairs interact with *s*-tetrazines receptors **80-82**. Then the resulting titration data were analyzed by the winEQNMR2<sup>31</sup> computer program to attempt binding constant determination. Estimates for each binding constant and the limiting chemical shifts and the stoichiometry of the complex determined by the Job's Plot were included the input file. The various parameters were refined by non-linear least-squares analysis to achieve the best fit between observed chemical shifts and calculated chemical shifts. The program plots the observed and calculated chemical shifts versus guest concentration, which reveals the accuracy of the experimental data and the suitability of the model. It also gives the best fit values of the stability constants together with their errors. The parameters were varied until the values for the stability constants converged, and good visual similarity of the theoretical binding isotherm with the experimental one demonstrated that the model used was appropriate.

The Job's plot for the complex of **82** with the ammonium iodide gives a maximum value for  $x = 0.6$ , which corresponds to a stoichiometry of 1 *s*-tetrazine

receptor for 2 ammonium iodide salts. Hence, the binding of the ion pair to **82** can be written as two consecutive equilibria:



This model was used in the search for the best fit in winEQNMR2 and the values obtained for the association constants are  $K_1 = 665$  and  $K_2 = 1177$ . The experimental and calculated chemical shifts correlated well as seen in figure 2.27.

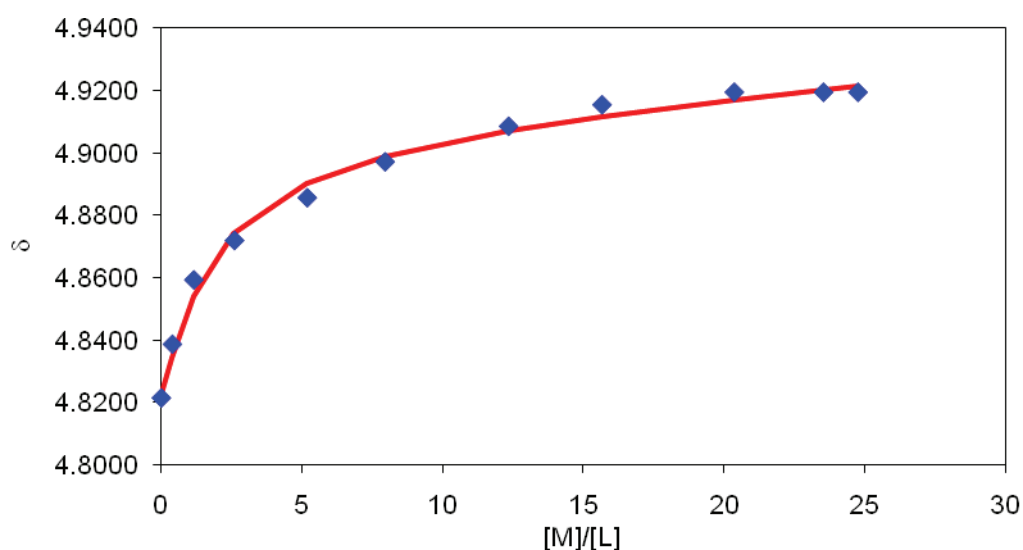
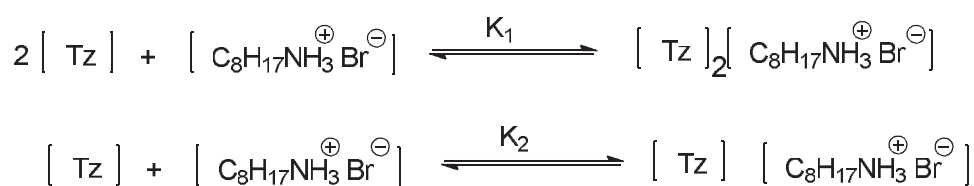


Figure 2.27. NMR titration curve and corresponding calculated isotherm for interaction of **82** with ammonium iodide.

The complex formation of **81** with ammonium iodide was also studied in the same way. The maximum value found in the Job's Plot is 0.3, which reveals the formation of a 2:1 complex beside a 1:1 complex. In this case the stepwise binding of the ion pair to **81** is:



Refinement of the data with this model gave:  $K_1 = 487$  and  $K_2 = 28$ . Again a good agreement between experiment and calculated data is observed (Figure 2.28).

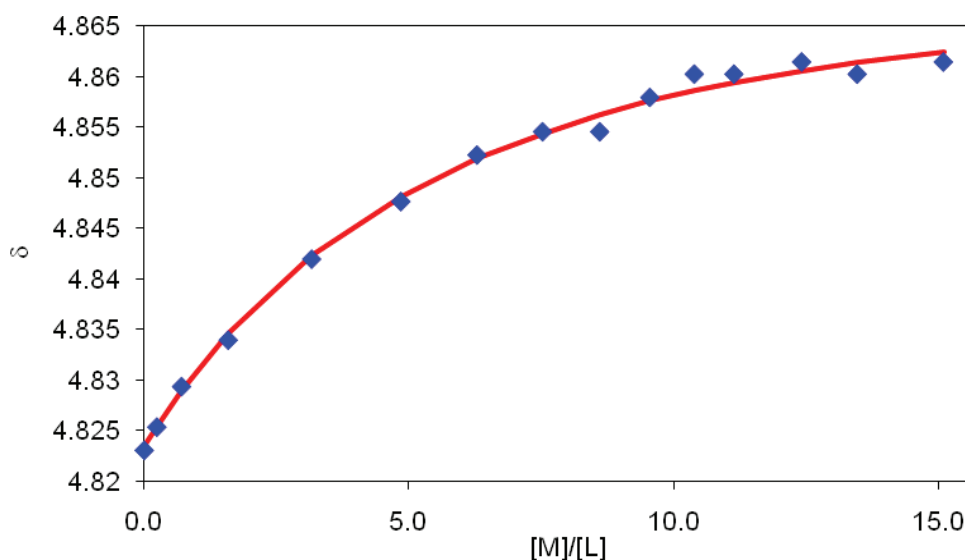


Figure 2.28. NMR titration curve and corresponding calculated isotherm for interaction of **81** with ammonium iodide.

This result confirms that *s*-tetrazine **82** is the best receptor for ammonium salts among the three derivatives. In addition, **81** and **82** form different complexes. This is possibly due to the steric hindrance effect between the receptor and ion pair. In other words, thanks to its longer PEO chains, *s*-tetrazine **82** can accommodate one and even two ammonium iodide salts. In contrast, shorter sized **81** led to lower binding constants and preferential formation of a 2 receptors for 1 anion complex.

## 2.6 Fluorescence studies of ion pair receptors

### 2.6.1 Spectroscopic properties of the receptors

Before photophysical studies of the ion pair – receptors interactions, we first set out to characterize the properties of compounds **80-82** alone (Figure 2.29 and Table 2.2).

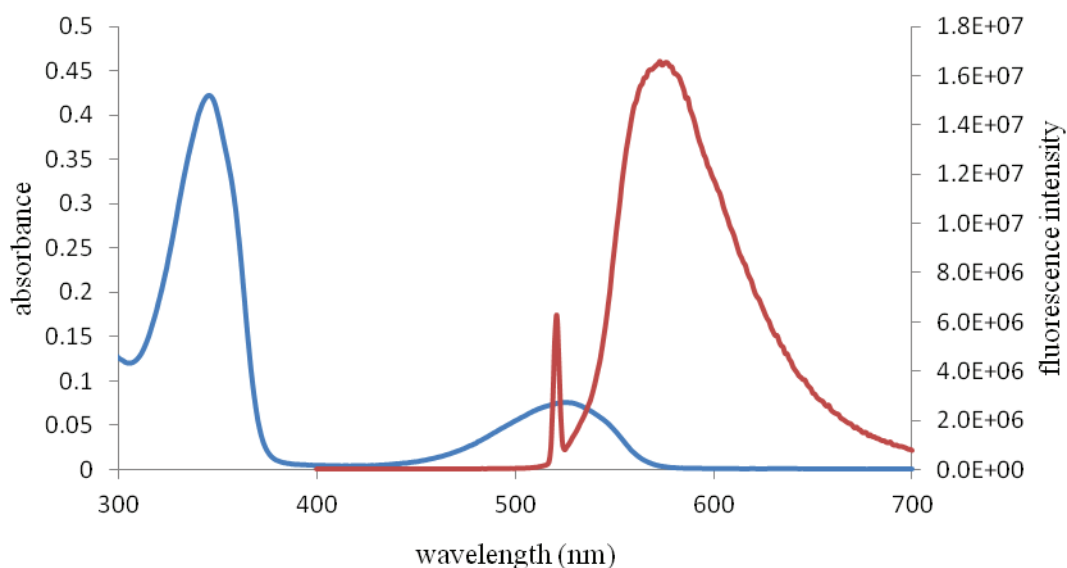


Figure 2.29. Absorbance (blue) and fluorescence (red) spectra of *s*-tetrazine **80** recorded in chloroform.

Table 2.2. Photophysical data for receptors **80-82** recorded in chloroform.

compound	$\lambda_{\text{abs, max}}$ [nm]	$\lambda_{\text{em, max}}$ [nm]	$\epsilon$ [L/(mol.cm)]	$\phi_{\text{F}}^{\text{a}}$
<b>80</b>	526	573	429	0.11
<b>81</b>	520	565	602	0.22
<b>82</b>	520	566	601	0.34

a.  $\lambda_{\text{ex}} = 520\text{nm}$

## 2.6.2 Titration studies

These studies were performed in chloroform, since it's a proper medium to assess host-guest binding. Firstly, addition of ammonium salts to compound **80** resulted in the spectra presented in figure 2.30. The intensity of the fluorescence band decreased upon addition of bromide (b) and iodide (c) confirming the modulation of emission properties in the presence of ion pairs. On the contrary, there is no variation with ammonium chloride (a). Compared to the  $^1\text{H}$  NMR titrations, the binding curves (d) showed the same trends: host **80** exhibited a stronger affinity for  $\text{C}_8\text{H}_{17}\text{NH}_3^+\cdot\text{I}^-$  than for  $\text{C}_8\text{H}_{17}\text{NH}_3^+\cdot\text{Br}^-$ . And there are no clear sign of interaction between **80** and  $\text{C}_8\text{H}_{17}\text{NH}_3^+\cdot\text{Cl}^-$ .

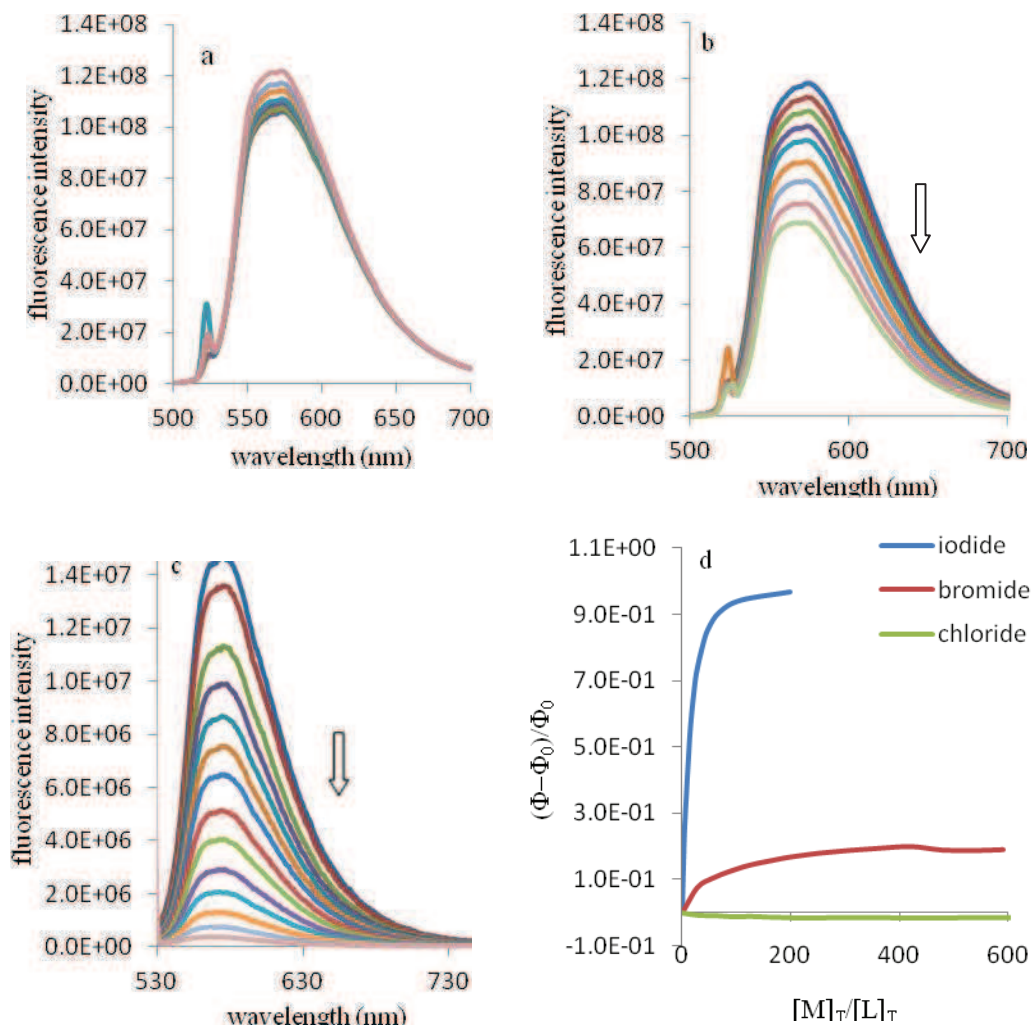


Figure 2.30. Changes in the emission spectra of host **80** upon titration with chloride (a), bromide (b) and iodide (c) in chloroform ( $\lambda_{\text{ex}}=522\text{nm}$ ). Binding curves resulting from the changes in the emission properties of host **80** upon titration with ammonium halides (d).

Secondly, addition of ammonium salts to compound **81** resulted in spectra shown in figure 2.31. The intensities of fluorescence peaks of *s*-tetrazines were found to decrease upon addition of bromide (b) and iodide (c), and the addition of  $\text{C}_8\text{H}_{17}\text{NH}_3^+\cdot\text{Cl}^-$  (a) does not change the intensity of *s*-tetrazine fluorescence.

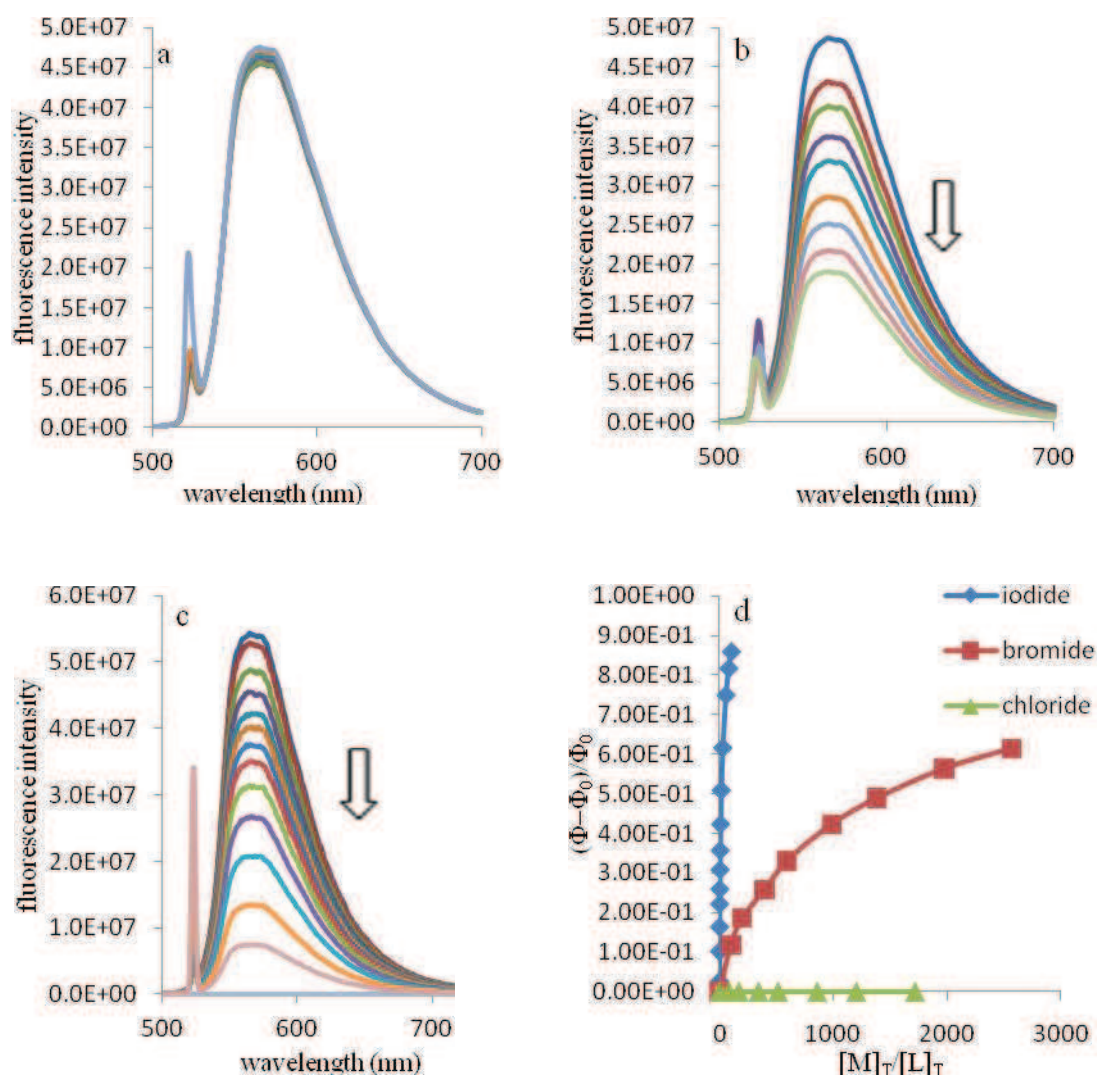


Figure 2.31. Changes in the emission spectra of host **81** upon titration with chloride (a), bromide (b) and iodide (c) in chloroform ( $\lambda_{ex}=522\text{nm}$ ). Binding curves resulting from the changes in the emission properties of host **81** upon titration with ammonium halide (d).

Binding curves for compound **82** are shown in figure 2.32. Emission studies with **82** reveal the same trend than for **80** and **81**: all of them exhibit stronger affinity for iodide salt than bromide one and no interaction with chloride.

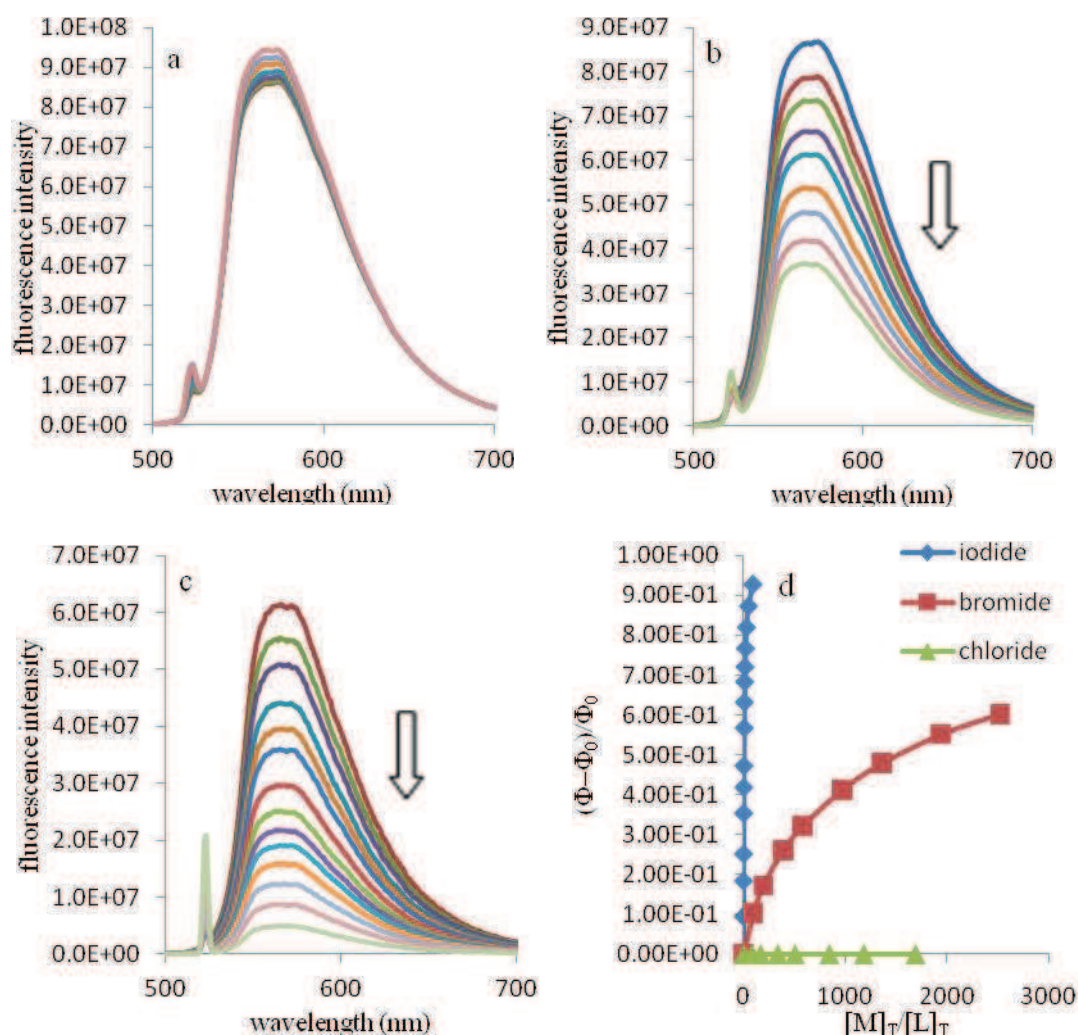


Figure 2.32. Changes in the emission spectra of host **82** upon titration with chloride (a), bromide (b) and iodide (c) in chloroform ( $\lambda_{\text{ex}}=522\text{nm}$ ). Binding curves resulting from the changes in the emission properties of host **82** upon titration with ammonium halide (d).

Fluorescence studies yield results similar to NMR titrations: all these receptors do not interact with  $\text{C}_8\text{H}_{17}\text{NH}_3^+\cdot\text{Cl}^-$  since no fluorescence quenching appears. However, they are quenched by both bromide and iodide, the second being more efficient.

These preferential selectivity for iodide, confirmed both by NMR and fluorescence, is quite surprising if one consider the theoretical calculations reported by Garou<sup>15</sup> *et al.* Indeed, they found that the selectivity should be  $\text{F}^- > \text{Cl}^- > \text{Br}^-$  (iodide was not mentioned). However, in more recent studies the same group showed that the quadrupole moment of the aromatic ring is not the only factor to consider and that anion- $\pi$  interactions depend also on the polarizability of the molecule.

The quadrupole moment of *s*-tetrazine is low while its polarizability is high (see paragraph 2.1.4). Furthermore, it was shown that polarizability is indeed the main



factor to consider to understand the selectivity of anion binding by *s*-triazine ring which is closely related to *s*-tetrazine. It is then likely that the better binding of iodide by our receptors comes from the high polarizability of both partners.

Comparison of the binding abilities of molecules **80**, **81** and **82** with the same salt as seen from the fluorescence studies are presented in figure 2.33 for I<sup>-</sup> and 2.34 for Br<sup>-</sup>.

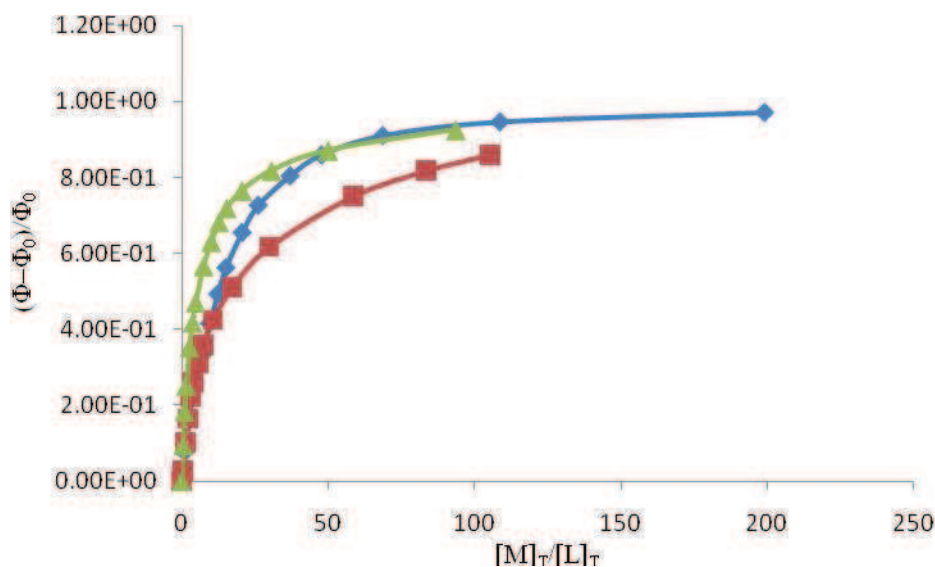


Figure 2.33. Binding curves resulting from the changes in the emission properties of host **80** (blue), **81** (red) and **82** (green) upon titration with C<sub>8</sub>H<sub>17</sub>NH<sub>3</sub><sup>+</sup>·I<sup>-</sup>

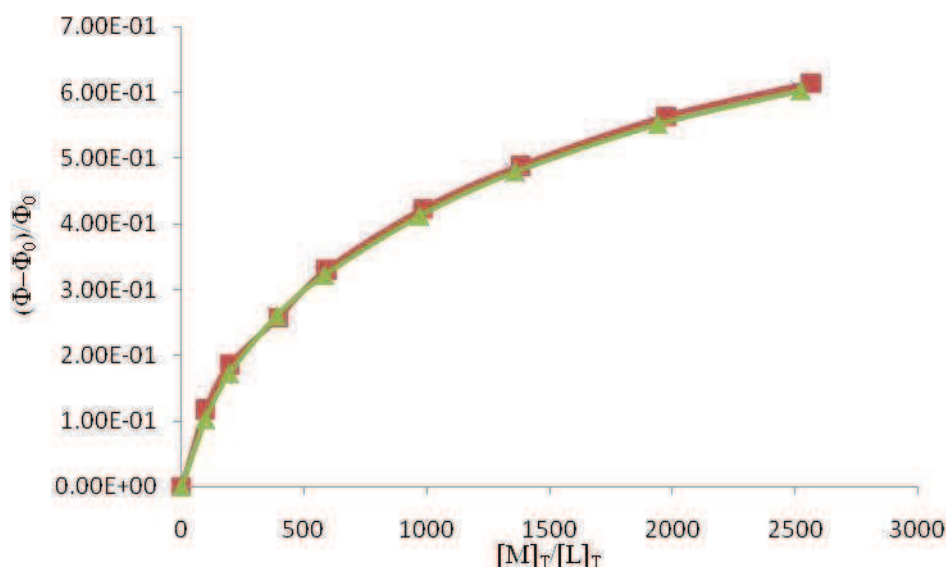


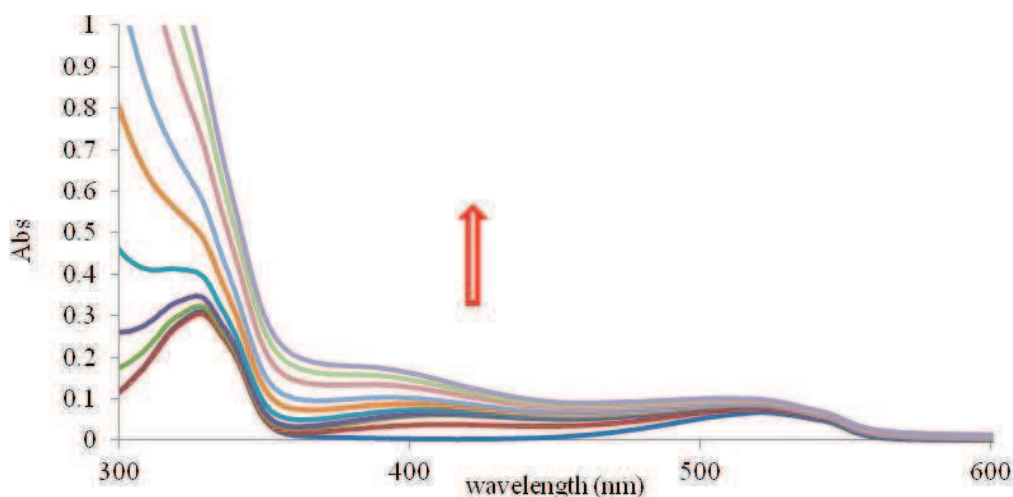
Figure 2.34. Binding curves resulting from the changes in the emission properties of host **81** and **82** upon titration with C<sub>8</sub>H<sub>17</sub>NH<sub>3</sub><sup>+</sup>·Br<sup>-</sup>

It is quite apparent that contrary to what was observed by NMR, no selectivity of the receptors for a given salt is observed here since all binding curves more or less overlap with  $C_8H_{17}NH_3^+ \cdot I^-$  or  $C_8H_{17}NH_3^+ \cdot Br^-$ . One possible explanation is that two different phenomenon are observed. In the NMR studies, the main interaction monitored is between the ammonium and the PEO chain while in fluorescence studies, it is the anion- $\pi$  one. Hence, both techniques could highlight two complementary selectivities: that of PEO chain for cation and that of *s*-tetrazine for anion.

However, it must be said that in the course of fluorescence titrations, a strong color change was also observed upon addition of either salt. It was then interesting to study the receptor ion pair interactions by absorption spectroscopy.

## 2.7 UV-vis. absorption studies of ion pair receptors

The changes in UV-vis. spectra when ion pair  $C_8H_{17}NH_3^+ \cdot Br^-$  was added to **82** are shown in figure 2.35. A new intense absorption band is observed between 250-300nm. Its intensity increases with the addition of octylammonium bromide. Concomitantly, a second broad band appears in the 300-600nm range. However, its intensity is less important than the first one.



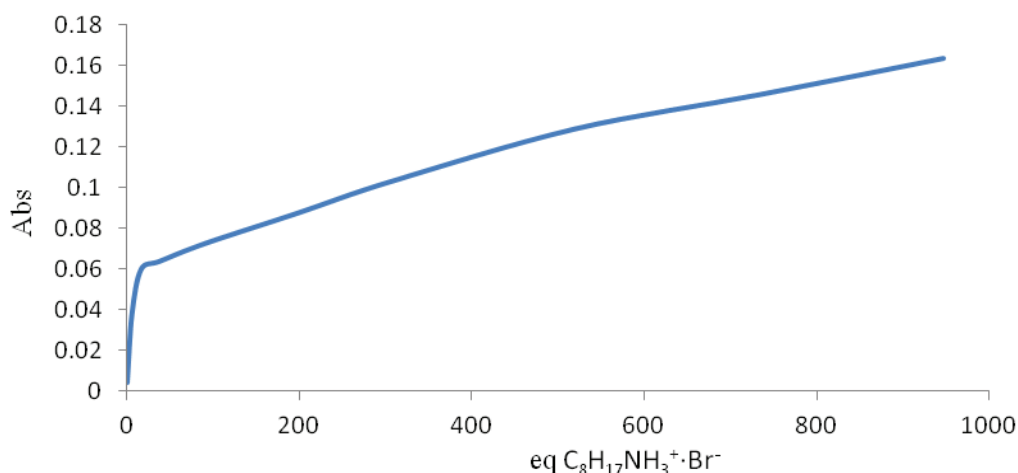


Figure 2.35. Top: changes in the UV-vis spectra of **82** upon titration of  $C_8H_{17}NH_3^+ \cdot Br^-$  in chloroform. Bottom: plot of  $Abs^{82}(400nm)$  as a function of the quantity of  $C_8H_{17}NH_3^+ \cdot Br^-$  added.

The plot of the variation of the absorbance at 400 nm where *s*-tetrazine does not absorb, clearly show a quick jump followed by a constant rise. It is noteworthy that the absorption band of *s*-tetrazine in the visible is unchanged. In order to gain insight into the origin of these new bands, absorption spectrum of  $Br_2$  in chloroform was recorded (Figure 2.36). The main feature of this spectrum is a broad band ranging from 350 to 550nm and centered at  $\sim 410nm$ .

This band is quite similar to the new one observed in the visible range during titration of **82** with  $C_8H_{17}NH_3^+ \cdot Br^-$ . It is then possible that  $Br_2$  is formed in the media. However, the origin of the sharp UV band at  $\sim 260nm$  is still unclear.

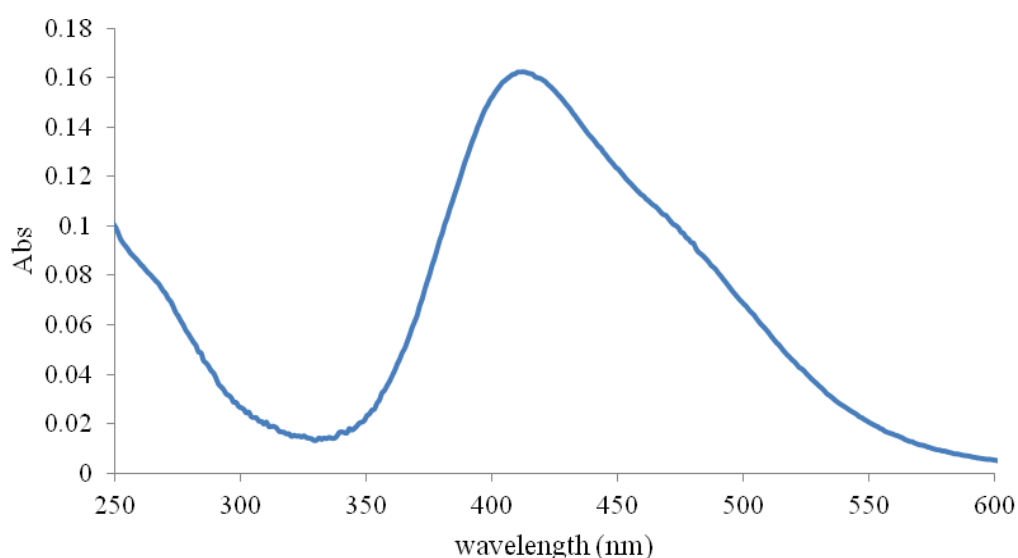


Figure 2.36. Absorption spectra of  $Br_2$  in chloroform.

A similar experiment was carried out with **82** and  $\text{C}_8\text{H}_{17}\text{NH}_3^+\text{I}^-$  in chloroform (Figure 2.37). Compared to absorption spectra of pure **82**, a new absorption band centered at  $\sim 500\text{nm}$  gradually appears in this case too.

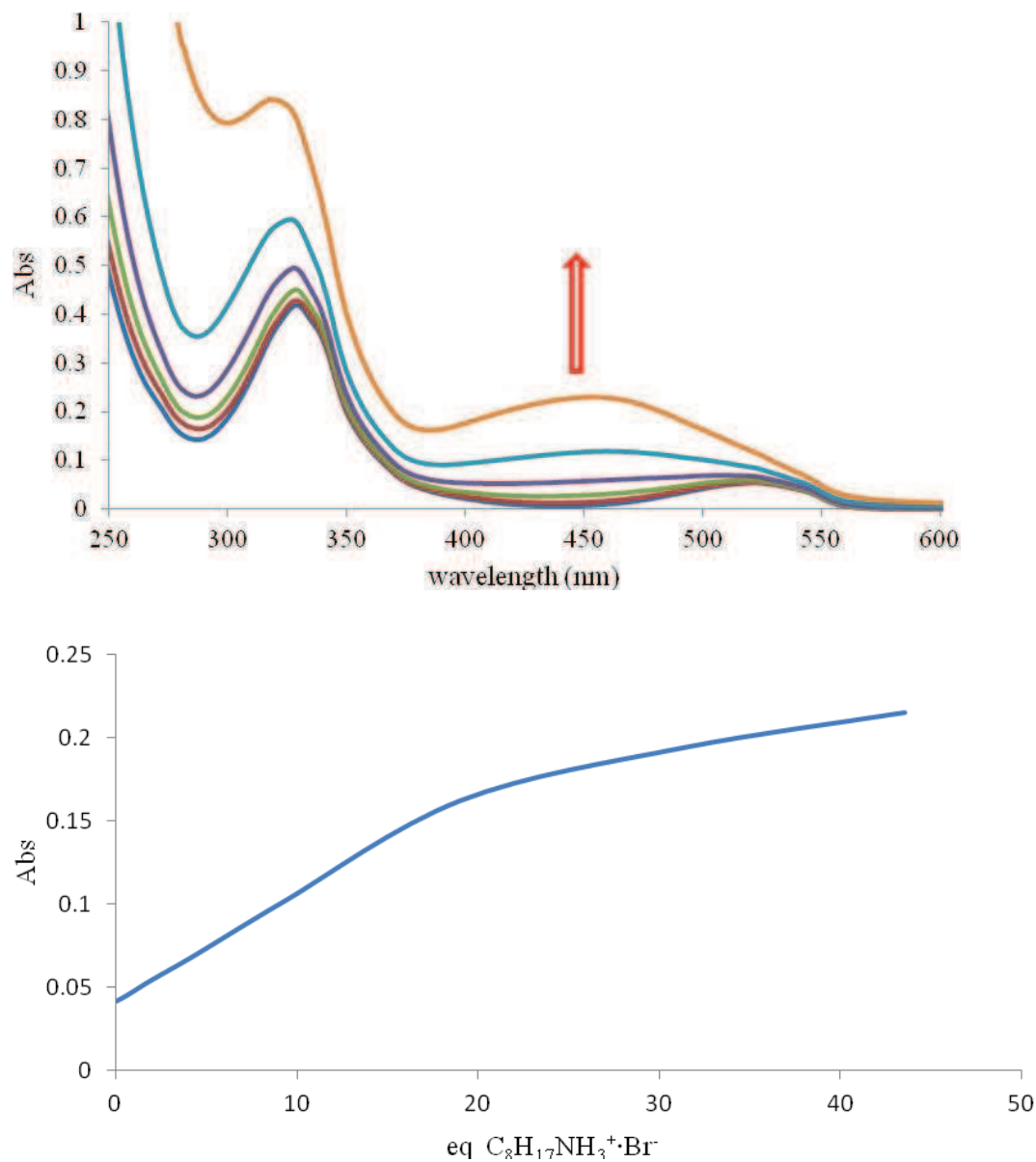


Figure 2.37. Top: changes in the UV/vis spectra of **82** upon titration by  $\text{C}_8\text{H}_{17}\text{NH}_3^+\text{I}^-$  in chloroform; Bottom: plot of  $\text{Abs}^{\text{82}}(500\text{nm})$  as a function of the quantity of  $\text{C}_8\text{H}_{17}\text{NH}_3^+\text{I}^-$  added.

The plot of the absorbance at 500 nm where *s*-tetrazine does absorb is not flat but clearly shows a constant rise despite the fact that the concentration of **82** was kept constant. The absorption spectrum of  $\text{I}_2$  in chloroform was also recorded (Figure 2.38).

It presents one main absorption band in the visible ranging from 400nm to 600nm, and centered at ~500nm.

A similarity in position and shape between this band and the one appearing during the titration of **82** with  $\Gamma$  can be noted. It is then reasonable to infer that  $I_2$  is formed in the media. However, it does not account for the sharper increase in absorption observed at  $\lambda < 300\text{nm}$ .

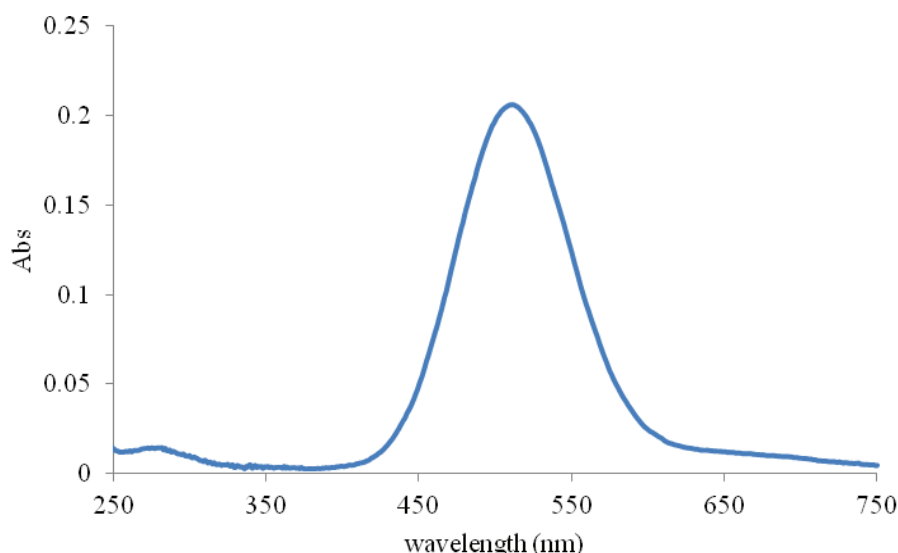


Figure 2.38. Absorption of  $I_2$  in chloroform.

In conclusion, the absorption experiments show that the interaction of *s*-tetrazine based receptors with halides is a more complex phenomenon than simple binding since it is highly likely that  $Br_2$  and  $I_2$  are formed upon irradiation.

## 2.8 Conclusion

We have designed and synthesized three *s*-tetrazine based receptors for ions pair recognition. The cation binding site is a polyethylene glycol chain whose length was varied. The anion complexation relies on the ability of *s*-tetrazine to establish anion- $\pi$  interactions which have been previously recognized in crystals or anticipated by theoretical calculations. The novelty of this approach lies in the fact that this type of interactions between aromatics and anion has been seldom observed in solution as well as in the fact that the receptors are neutral.

Preliminary experiments have shown that our receptors preferentially interact with octylammonium bromide or iodide salts in chloroform. NMR titration experiments have confirmed the formation of a complex between the ammonium and

the polyethylene glycol moiety for all three receptors and revealed a stronger interaction with iodide. The strongest binding was found with **82**, presumably because pentaethylene glycol has the best size to fit a primary ammonium salt. Furthermore, Job's plot and mathematical fitting of the binding curves proved that the stoichiometries of the complexes are  $ML_2$  and  $ML$  for **81** and  $ML$  and  $M_2L$  for **82** ( $M$  = salt and  $L$  = receptor). This also probably comes from the different sizes of the receptors.

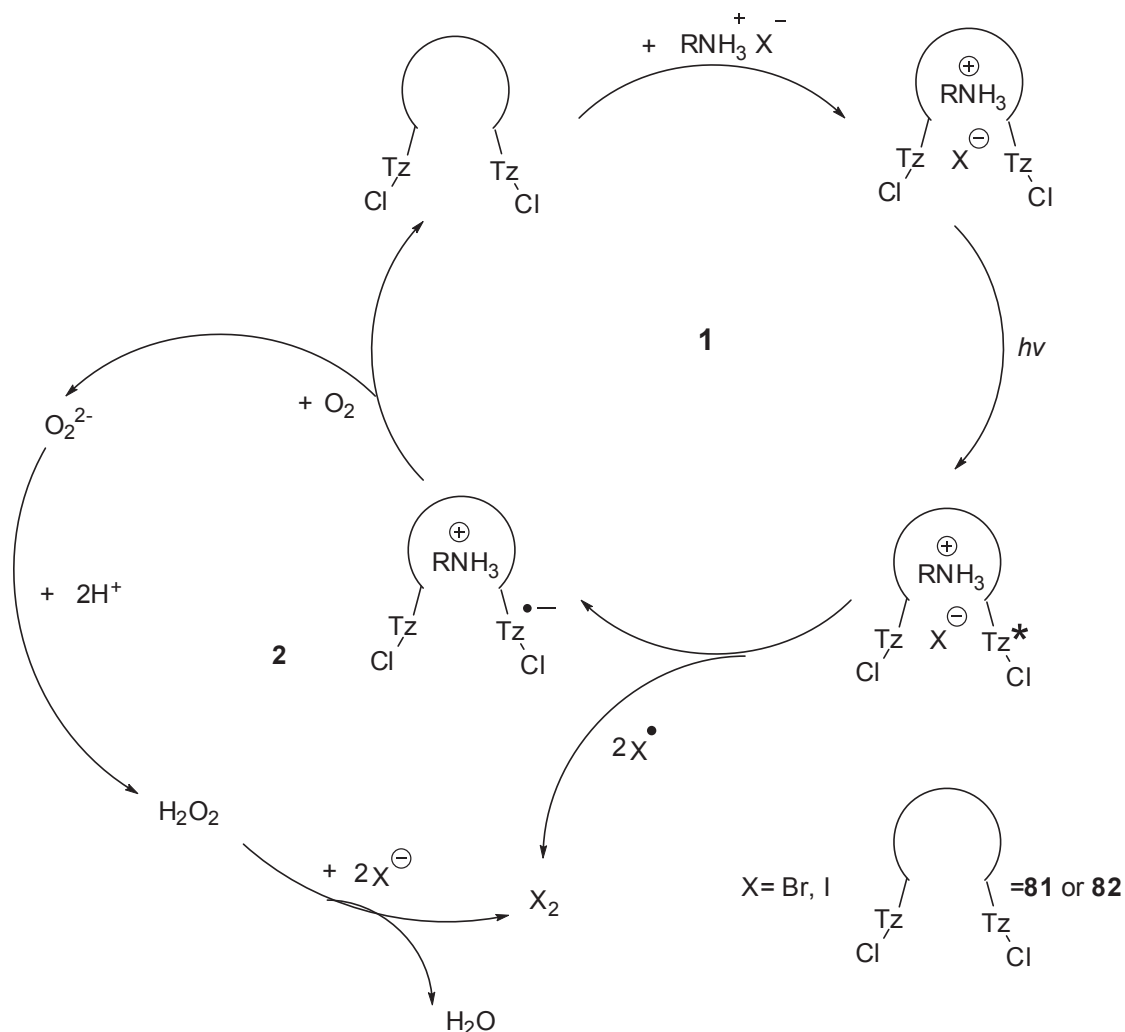
Fluorescence titrations also demonstrated that receptor-salt interactions take place, since addition of bromide or iodide leads to a quenching of the emission. Hence, it is likely that the anion lies close to the *s*-tetrazine rings in all receptors thanks to anion- $\pi$  interactions. Fluorescence experiments also confirmed that the receptors bind stronger to iodide than other halides. This is contradictory with reported results of *ab initio* calculations. However, it can be rationalized based on more recent work where it was demonstrated that polarizability is a main factor in anion- $\pi$  interactions.

But the most unexpected results were obtained from UV-vis. absorption experiments which suggested the formation of  $Br_2$  or  $I_2$  during the course of the titrations. The later is formed in larger quantity than the former. It is important to remind here that it was previously demonstrated in our group that *s*-tetrazine fluorescence is quenched in the presence of electron rich aromatics by photoinduced electron transfer. This is due to the very high oxidizing power of the *s*-tetrazine in its excited state. Inspection of the oxidation potentials of both  $Br^-$   $\Gamma$  and reduction potential of *s*-tetrazine (Table 2.3) shows that it is indeed possible to transfer an electron from the anion to the aromatic ring after absorption of a photon. However, *s*-tetrazine should be recovered since its absorption does not decrease during the titration.

Table 2.3. Standard redox potentials of compounds involved in the proposed mechanism.

reaction	$E^0 / V$
$I_2 + 2e \rightleftharpoons 2I^-$	0.54
$Br_2 + 2e \rightleftharpoons 2Br^-$	1.09
$Cl_2 + 2e \rightleftharpoons 2Cl^-$	1.36
$Tz + e \rightleftharpoons Tz^{\cdot-}$	-0.60
$Tz^* + e \rightleftharpoons Tz^{\cdot-}$	$\approx 1.2-1.4$
$O_2 + 2H^+ + 2e \rightleftharpoons H_2O_2$	0.70
$H_2O_2 + 2H^+ + 2e \rightleftharpoons 2H_2O$	1.78

Hence, a full mechanism for the formation of I<sub>2</sub> or Br<sub>2</sub> and subsequent reoxydation of *s*-tetrazine can be proposed (Scheme 2.5).



Scheme 2.5. Proposed mechanism of formation of X<sub>2</sub> from the ion pair-*s*-tetrazine complex.

In the first step the ion's pair – tetrazine receptor complex is formed as evidenced by NMR titrations. After absorption of a photon by tetrazine, the halide can transfer one electron to the aromatic ring yielding two radicals. On one hand, two halogen radicals X<sup>•</sup> can combine to form X<sub>2</sub>. On the other hand, two *s*-tetrazine anion radicals can react with the oxygen dissolved in the solution to give the neutral receptors back and O<sup>2-</sup>. This highly unstable species is transformed in hydrogen peroxide since there are a lot of acidic protons provided by the ammonium. Subsequently, the hydrogen peroxide can also react with halides to give dihalogens and water as proved by their respective redox potentials (Table 2.3).

This mechanism can explain how Br<sub>2</sub> or I<sub>2</sub> could be formed. However, additional experiments are needed to prove this mechanism solely based on the results of absorption spectra and consideration of redox potentials. For example, a complete irradiation of the mixture salt and receptor **82** could be done followed by analysis of the resulting products. It should be quite easy see if the ammonium has been transformed to its amine by NMR.

Future work on this system should aim at avoiding the side reaction uncovered in the course of our experiments by testing other polarizable anions that cannot be oxidized by *s*-tetrazine if sensing properties are pursued. But exploitation of the photoinduced oxidation of molecules or ions by *s*-tetrazine is another possible and interesting development. Indeed, photodegradation of pollutants is currently an area of research under development since it is an environmental friendly process.



## References

1. Lehn, J. M., Supramolecular Chemistry. *Science* **1993**, *260* (5115), 1762-1763.
2. Lehn, J. M., *Supramolecular chemistry : concepts and perspectives : a personal account built upon the George Fisher Baker lectures in chemistry at Cornell University [and] Lezioni Lincee, Accademia nazionale dei Lincei, Roma*. VCH: Weinheim ; New York, 1995; p x, 271 p.
3. Cosic, I., Macromolecular Bioactivity - Is It Resonant Interaction between Macromolecules - Theory and Applications. *Ieee T Bio-Med Eng* **1994**, *41* (12), 1101-1114.
4. Gellman, S. H., Introduction: Molecular recognition. *Chem Rev* **1997**, *97* (5), 1231-1232.
5. Atwood, J. L.; Lehn, J. M., *Comprehensive supramolecular chemistry*. 1st ed.; Pergamon: New York, 1996.
6. Gale, P. A., Anion receptor chemistry. *Chem Commun (Camb)* **2011**, *47* (1), 82-6.
7. Antonisse, M. M. G.; Reinhoudt, D. N., Neutral anion receptors: design and application. *Chem Commun* **1998**, (4), 443-448.
8. Kirkovits, G. J.; Shriver, J. A.; Gale, P. A.; Sessler, J. L., Synthetic ditopic receptors. *J Incl Phenom Macro* **2001**, *41* (1-4), 69-75.
9. Kim, S. K.; Sessler, J. L., Ion pair receptors. *Chem Soc Rev* **2010**, *39* (10), 3784-3809.
10. Valeur, B., *Molecular fluorescence : principles and applications*. Wiley-VCH: Weinheim ; New York, 2002; p xiv, 387 p.
11. Beer, P. D.; Gale, P. A., Anion recognition and sensing: The state of the art and future perspectives. *Angew Chem Int Edit* **2001**, *40* (3), 486-516.
12. Campos-Fernandez, C. S.; Clerac, R.; Dunbar, K. R., A one-pot, high-yield synthesis of a paramagnetic nickel square from divergent precursors by anion template assembly. *Angew Chem Int Edit* **1999**, *38* (23), 3477-3479.
13. Campos-Fernandez, C. S.; Clerac, R.; Koomen, J. M.; Russell, D. H.; Dunbar, K. R., Fine-tuning the ring-size of metallacyclophanes: A rational approach to molecular pentagons. *J Am Chem Soc* **2001**, *123* (4), 773-774.
14. Campos-Fernandez, C. S.; Schottel, B. L.; Chifotides, H. T.; Bera, J. K.; Bacsá, J.; Koomen, J. M.; Russell, D. H.; Dunbar, K. R., Anion template effect on the self-assembly and interconversion of metallacyclophanes. *J Am Chem Soc* **2005**, *127* (37), 12909-12923.
15. Garau, C.; Quinonero, D.; Frontera, A.; Costa, A.; Ballester, P.; Deya, P. M., s-Tetrazine as a new binding unit in molecular recognition of anions. *Chem Phys Lett* **2003**, *370* (1-2), 7-13.
16. Schottel, B. L.; Chifotides, H. T.; Shatruck, M.; Chouai, A.; Perez, L. M.; Bacsá, J.; Dunbar, K. R., Anion-pi interactions as controlling elements in self-assembly reactions of Ag(I) complexes with pi-acidic aromatic rings. *J Am Chem Soc* **2006**, *128* (17), 5895-5912.
17. Quinonero, D.; Garau, C.; Rotger, C.; Frontera, A.; Ballester, P.; Costa, A.; Deya, P. M., Anion-pi interactions: Do they exist? *Angew Chem Int Edit* **2002**, *41* (18), 3389-3392.

18. Quinonero, D.; Garau, C.; Frontera, A.; Ballester, P.; Costa, A.; Deya, P. M., Counterintuitive interaction of anions with benzene derivatives. *Chem Phys Lett* **2002**, *359* (5-6), 486-492.
19. Mascal, M.; Armstrong, A.; Bartberger, M. D., Anion-aromatic bonding: A case for anion recognition by pi-acidic rings. *J Am Chem Soc* **2002**, *124* (22), 6274-6276.
20. Garau, C.; Frontera, A.; Quinonero, D.; Ballester, P.; Costa, A.; Deya, P. M., A topological analysis of the electron density in anion - pi interactions. *Chemphyschem* **2003**, *4* (12), 1344-1348.
21. Garau, C.; Frontera, A.; Quinonero, D.; Ballester, P.; Costa, A.; Deya, P. M., Cation-pi versus anion-pi interactions: Energetic, charge transfer, and aromatic aspects. *J Phys Chem A* **2004**, *108* (43), 9423-9427.
22. Audebert, P.; Miomandre, F.; Clavier, G.; Vernieres, M. C.; Badre, S.; Meallet-Renault, R., Synthesis and properties of new tetrazines substituted by heteroatoms: Towards the world's smallest organic fluorophores. *Chem-Eur J* **2005**, *11* (19), 5667-5673.
23. Gong, Y. H.; Audebert, P.; Tang, J.; Miomandre, F.; Clavier, G.; Badre, S.; Meallet-Renault, R.; Marrot, J., New tetrazines substituted by heteroatoms including the first tetrazine based cyclophane: Synthesis and electrochemical properties. *J Electroanal Chem* **2006**, *592* (2), 147-152.
24. Gong, Y. H.; Audebert, P.; Clavier, G.; Miomandre, F.; Tang, J.; Badre, S.; Meallet-Renault, R.; Naidus, E., Preparation and physicochemical studies of new multiple rings s-tetrazines. *New J Chem* **2008**, *32* (7), 1235-1242.
25. Malinge, J.; Allain, C.; Galmiche, L.; Miomandre, F.; Audebert, P., Preparation, Photophysical, Electrochemical, and Sensing Properties of Luminescent Tetrazine-Doped Silica Nanoparticles. *Chem Mater* **2011**, *23* (20), 4599-4605.
26. Qing, Z.; Audebert, P.; Clavier, G.; Miomandre, F.; Tang, J.; Vu, T. T.; Meallet-Renault, R., Tetrazines with hindered or electron withdrawing substituents: Synthesis, electrochemical and fluorescence properties. *J Electroanal Chem* **2009**, *632* (1-2), 39-44.
27. Maud, J. M.; Stoddart, J. F.; Williams, D. J., A 1-1 Complex between 1,4,7,10,13,16-Hexaoxacyclooctadecane (18-Crown-6) and Phenacylammonium Hexafluorophosphate, C<sub>12</sub>H<sub>24</sub>O<sub>6</sub>.C<sub>6</sub>H<sub>5</sub>COCH<sub>2</sub>NH<sub>3</sub><sup>+</sup>.PF<sub>6</sub><sup>-</sup>. *Acta Crystallogr C* **1985**, *41* (Jan), 137-140.
28. Tancini, F.; Gottschalk, T.; Schweizer, W. B.; Diederich, F.; Dalcanale, E., Ion-Pair Complexation with a Cavitand Receptor. *Chem-Eur J* **2010**, *16* (26), 7813-7819.
29. Bovill, M. J.; Chadwick, D. J.; Sutherland, I. O.; Watkin, D., Molecular Mechanics Calculations for Ethers - the Conformations of Some Crown Ethers and the Structure of the Complex of 18-Crown-6 with Benzylammonium Thiocyanate. *J Chem Soc Perk T 2* **1980**, (10), 1529-1543.
30. Trueblood, K. N.; Knobler, C. B.; Lawrence, D. S.; Stevens, R. V., Structures of the 1-1 Complexes of 18-Crown-6 with Hydrazinium Perchlorate, Hydroxylammonium Perchlorate, and Methylammonium Perchlorate. *Journal of the American Chemical Society* **1982**, *104* (5), 1355-1362.
31. Hynes, M. J., Eqnmr - a Computer-Program for the Calculation of Stability-Constants from Nuclear-Magnetic-Resonance Chemical-Shift Data. *J Chem Soc Dalton* **1993**, (2), 311-312.



## Chapter 3 New *s*-tetrazines functionalized with electrochemically and optically active

*s*-Tetrazine is a rather unique nitrogen containing heterocycle since it is both reversibly electroactive and, in many instances, fluorescent. This last property is quite uncommon for six membered rings containing nitrogen and is even more interesting since the fluorescence quantum yields can be high (up to 0.4) and the fluorescence lifetime is very long for an organic molecule (up to 160 ns). The combination of these two properties has previously been used in the laboratory to develop, for example, an electrofluorochromic cell<sup>1</sup>. Despite the body of work done to understand these unique features<sup>2</sup>, it was still interesting to consider other factors that could control and improve the properties of *s*-tetrazine.

In this chapter, we will first introduce new derivatives where the size of the substituents or their electron affinity have been varied. Then, new original derivatives obtained by an unexpected reaction will be presented. Finally, exploratory work for the design of fluorescent dyads comprising *s*-tetrazine will be depicted with an emphasis on the nature of the energy donor and the nature of the link between the two moieties. In all cases, the photophysical and electrochemical properties of the derivatives have been studied to uncover the influence of the various substituents used on the physico-chemical properties of *s*-tetrazine.

### 3.1 Studies of tetrazines with bulky or electron withdrawing substituents

#### 3.1.1 Molecular design

Previous work in the laboratory demonstrated that the combination of a chlorine and an alkoxy substituent on *s*-tetrazine appears to maximize its fluorescence quantum yield ( $\phi_F \approx 0.4$ ) and lifetime ( $\tau_F \approx 160\text{ns}$ )<sup>2</sup>. However, the simple chloromethoxy-*s*-tetrazine easily sublimates even at room temperature which limits its applicability for the design of solid state devices. An attracting development to overcome this drawback was thus to prepare chloro-*s*-tetrazines with bulky alkoxy substituents (Figure 3.1). Since *s*-tetrazines are electroactive, their electrochemistry was also interesting, especially as far as the electron transfer rate can be depended on the substituents' size and nature.

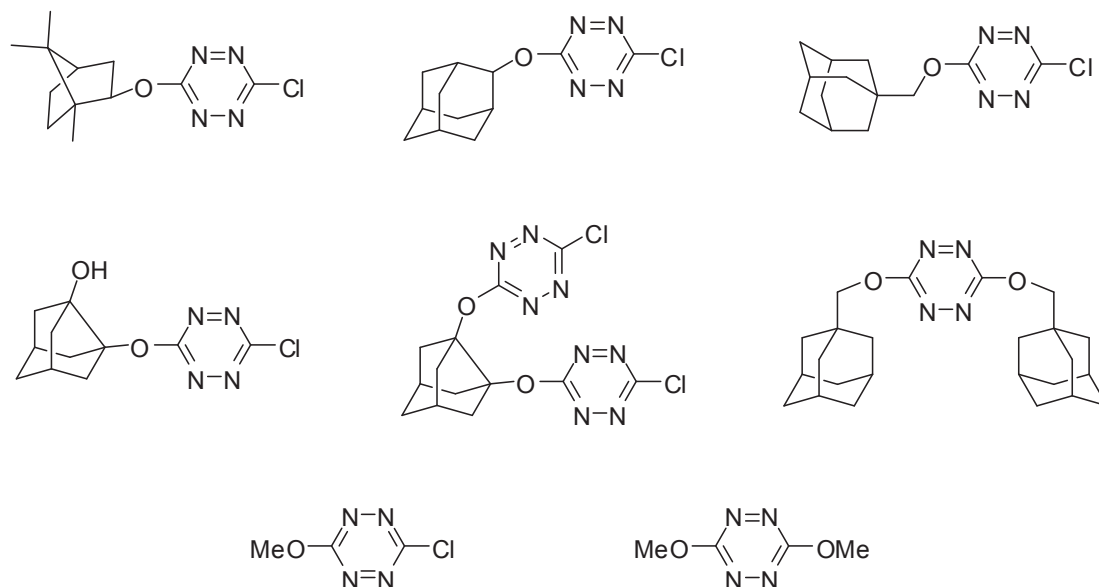


Figure 3.1. Synthetic targets for steric hindrance effect studies.

It has also been shown that fluorescence and electrochemistry properties are depended on the nature of the substituent. For example, *s*-tetrazines linked to aliphatic amines are not fluorescent. However, attachment of electron withdrawing has seldom been investigated. It was then interesting to investigate the replacement of the alkoxy by more imides (Figure 3.2). In addition, methoxyfluorene was also tested as a reference for electron donating group. This approach could also open up the possibility to prepare bichromophoric compounds.

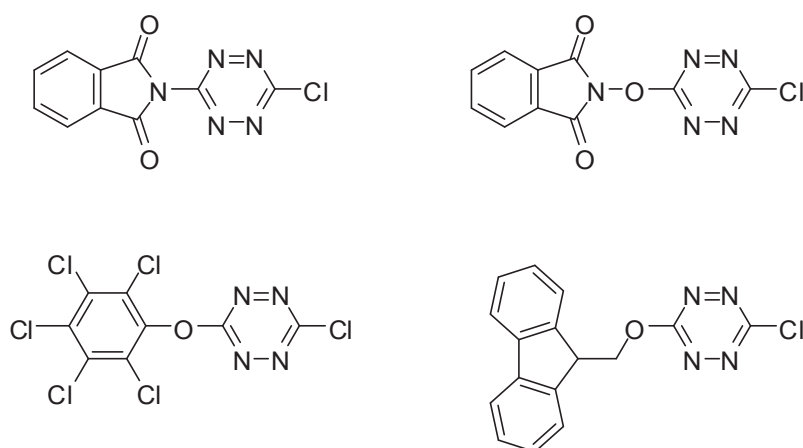
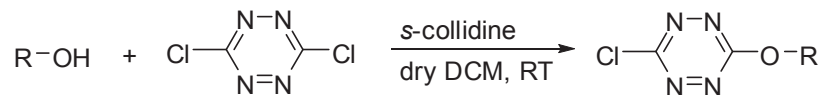


Figure 3.2. Synthetic targets for electron affinity effect studies.

### 3.1.2 Synthesis

As mentioned in chapter 2, most *s*-tetrazines substituted with one alkoxy group can be synthesized by reaction of the alcohol with dichloro-*s*-tetrazine in dry DCM in

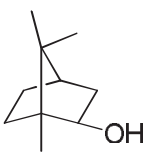
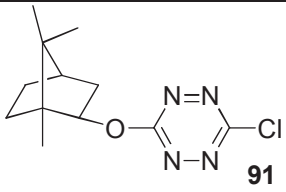
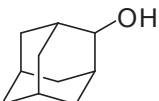
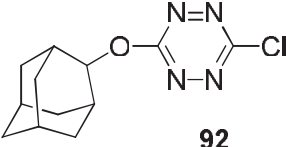
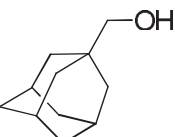
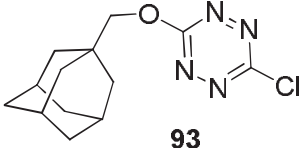
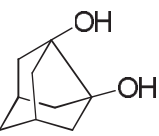
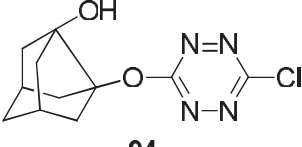
the presence of *s*-collidine. Hence, most of the targeted *s*-tetrazines were prepared accordingly (Scheme 3.1). The products were obtained pure by column chromatography.

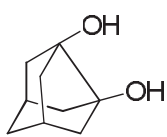
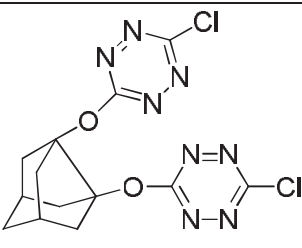
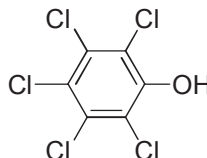
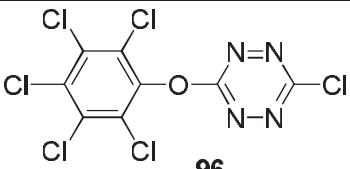
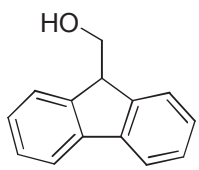
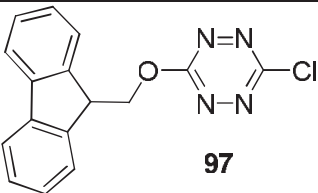


Scheme 3.1. Synthetic route for chloro-*s*-tetrazines substituted with one alkoxy group (for R substituents see Table 3.1).

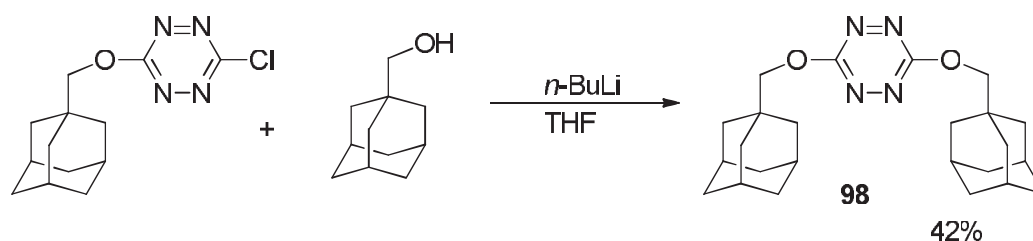
Most new *s*-tetrazines derivatives were obtained in good to excellent yields (40-90%; Table 3.1). However, *s*-tetrazine **94** and **95** were obtained in about 2% yields only, even when the reaction was done in a pressure tube or at high temperature or during longer reaction times. From these results, it can be seen that dichloro-*s*-tetrazine usually reacts better with phenols or primary alkyl alcohols than secondary alcohols.

Table 3.1. *s*-Tetrazines derivatives synthesized by S<sub>N</sub>Ar reaction.

alcohol	product	yield
		39%
		71%
		64%
		2%

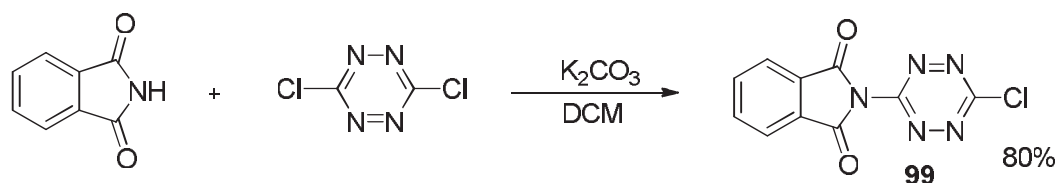
	 <b>95</b>	2%
	 <b>96</b>	92%
	 <b>97</b>	80%

The introduction of a second alkoxy substituent on *s*-tetrazine is always more difficult since the first substituent diminish the reactivity of the remaining chlorine<sup>3</sup>. Hence the preparation of compound **98** had to be carried out using the more reactive alcoholate which is obtained by action of *n*-butyl lithium (Scheme 3.2). Compound **98** was obtained in 42% yield after purification.



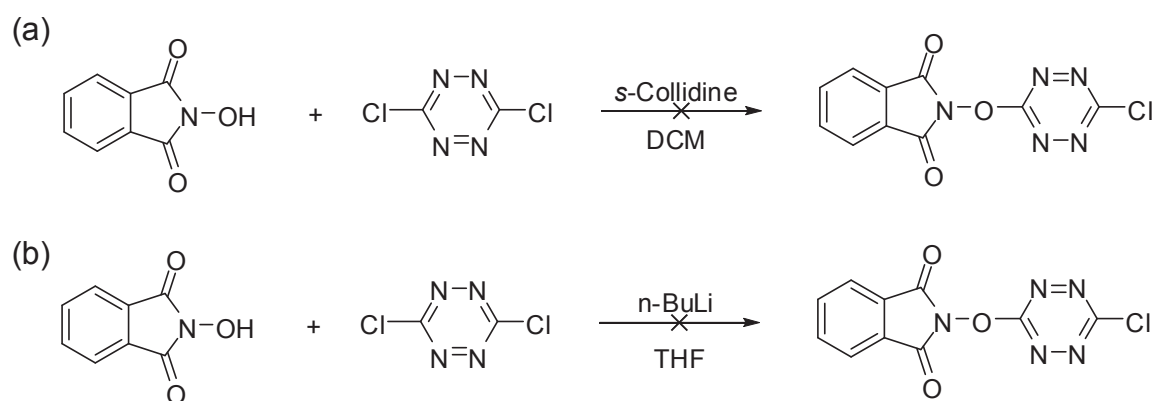
Scheme 3.2. Preparation of **98**.

The preparation of compound **99** was done using a procedure similar to that used for alcohols but *s*-collidine was replaced by potassium carbonate (Scheme 3.3). Compound **99** was obtained in 80% yield after purification.



Scheme 3.3. Preparation of **99**.

Unfortunately,  $S_NAr$  reaction between dichloro-*s*-tetrazine and *N*-hydroxyphthalimide failed to give *N*-(6-chloro-*s*-tetrazine-3-yloxy)-phthalimide (Scheme 3.4a). TLC showed that the 3,6-dichloro-*s*-tetrazine decomposed after stirring overnight at 50°C. As an alternative, *N*-hydroxyphthalimide was first reacted with *n*-butyl lithium (Scheme 3.4b) to produce the corresponding anion. However, after addition on 3,6-dichloro-*s*-tetrazine, decomposition also occurred and no new *s*-tetrazine was detected.



Scheme 3.4. Attempted preparation of *N*-(6-chloro-*s*-tetrazine-3-yloxy)phthalimide.

### 3.1.3 Absorption and fluorescence properties

As previously reported<sup>4,5,1</sup>, tetrazines bearing inductive electron-withdrawing substituents (like a chlorine or an alkoxy moiety) are fluorescent, both in solution but also in the solid state. Figure 3.3 shows the absorption and fluorescence spectrum of *s*-tetrazine **91** in solution (DCM), which is typical of a chloroalkoxy-*s*-tetrazine since they resemble the ones of the generic chloromethoxy-*s*-tetrazine. There are two absorption bands: one is found at about 330nm which is due to a  $\pi$ - $\pi^*$  transition and the other one around 520nm is caused by an  $n$ - $\pi^*$  transition. The same type of spectra was observed for all the other chloroalkoxy-*s*-tetrazines. All the chloroalkoxy-*s*-tetrazines synthesized are fluorescent in solution and emit around 560nm. However the phthalimide tetrazine **99** is not emissive.



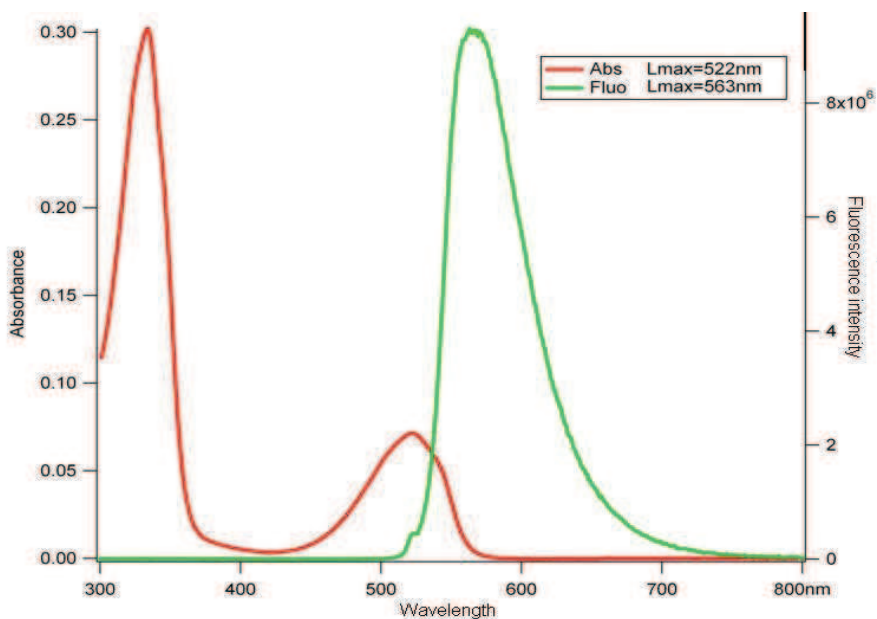


Figure 3.3. Absorption (red) and fluorescence (green) spectra of tetrazine **91** recorded in dichloromethane.

Table 3.2 displays the spectroscopic characteristics of *s*-tetrazines **91-99**. Quantum yields are very dependent on the nature of the substituent. In the case of bulky purely alkyloxy substituents, it was expected that the fluorescence quantum yields could be higher than for chloromethoxy-*s*-tetrazine because of some isolation of the fluorescent *s*-tetrazine core by the bulky inert alkyl groups. However, the yields are only very slightly higher, and therefore the size effect of the alkyl group appears to be weak.

The case of **97** bearing an electron rich aromatic group presents an unexpected result. Its fluorescence quantum yield is low, most likely because of a quenching by excited state electron transfer from the fluorene to the *s*-tetrazine. As reported<sup>4</sup>, the tetrazine fluorescence is quenched in the presence of good electron donors like triphenylamines. In the case of **97** the donor is weaker, since the oxidation potentials of triaryl amines are typically in the +1V (vs. SCE) range and fluorene group is oxidized at higher potential (+1.64V) in organic solvents. However, in this case, the proximity of the two groups in the same molecule may enhance the quenching efficiency, thus lowering the fluorescence quantum yield.

On the other hand, *s*-tetrazines **96** and **99** bearing electron attracting substituents display weak to very weak fluorescence quantum yields. This is somewhat surprising, especially in the case of the electron withdrawing pentachlorophenol, which owns a very low energy  $\pi^*$  orbital. Normally this should enhance the intensity of the  $n-\pi^*$  transition responsible for the fluorescence. However, somewhat similarly to the dichloro-*s*-tetrazine case, quantum yields decrease

compared to the chloroalkoxy-*s*-tetrazine. It might be therefore proposed that the existence of an appreciable dipolar moment is also a necessary condition for the existence of a relatively high fluorescence quantum yield. Finally, compound **98**, bearing two alkoxy substituents, displays a fluorescence yield slightly lower than the one of dimethoxy-*s*-tetrazine, and again the large size of the substituents does not lead to a rise of the fluorescence quantum yield.

Table 3.2. Spectroscopic data for *s*-tetrazine **91**, **93** and **96-99** measured in dichloromethane.

compound	$\lambda_{\text{abs, max}}$ [nm]	$\lambda_{\text{em, max}}$ [nm]	$\epsilon_{\text{vis}}$ [l/(mol.cm)] <sup>a</sup>	$\phi_{\text{F}}$
<b>91</b>	522 334	563	480	0.40
<b>93</b>	522 330	567	720	0.40
<b>96</b>	518 <300	566	820	0.09
<b>97</b>	519 328	563	620	0.08
<b>98</b>	530 351	579	590	0.07
<b>99</b>	518 311	546	450	0.006

a:  $\epsilon$  values measured at the maximum of the visible absorption band.

### 3.1.4 Electrochemical properties

The electrochemical behavior of the *s*-tetrazines has been investigated, looking at the substituent effects, and compared to the generic chloromethoxy-*s*-tetrazine. Figure 3.4 represents the cyclic voltammograms for three different tetrazines, two of them (**91** and **97**) bearing a donor alkoxy group, and an attractor imide group for the third one (**99**). It is clear that all of them show reversible CV's, with potentials depending on the electron affinity of the substituent, and not on its size as it could be expected.

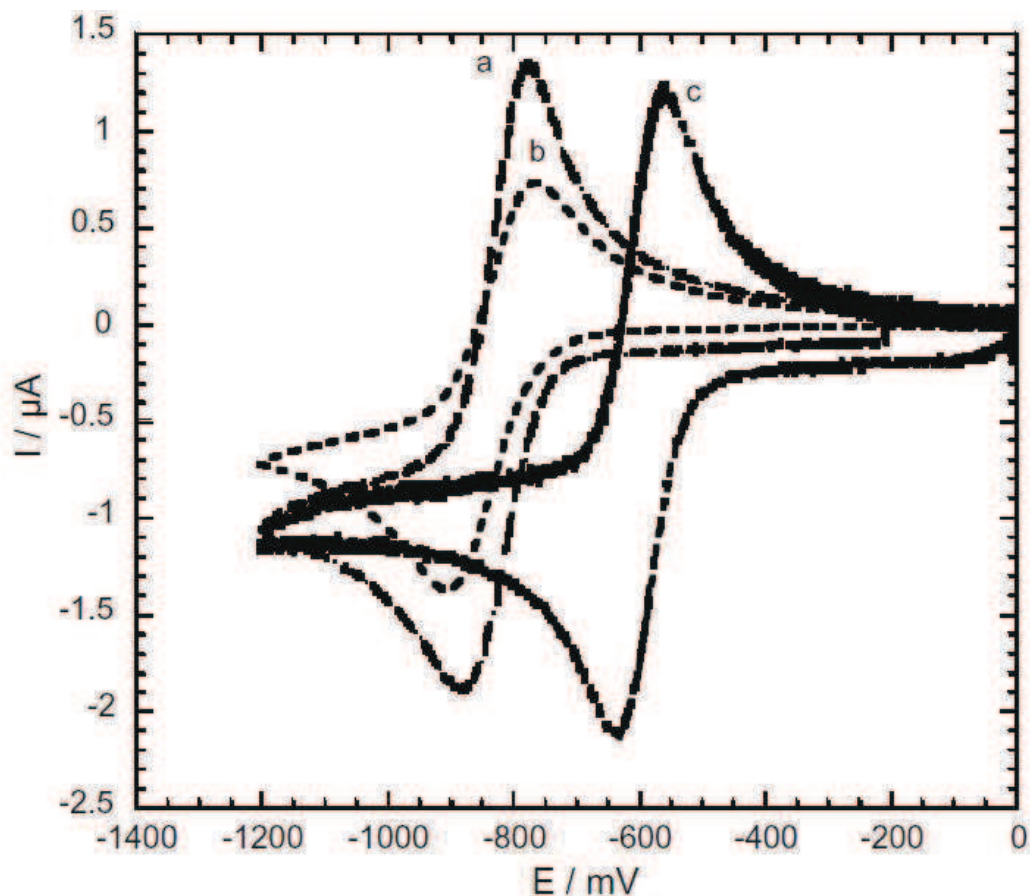


Figure 3.4. CV featuring the first reduction peak of resp. tetrazines **97** (curve a), **91** (curve b) and **99** (curve c).

Table 3.3 gathers the standard potential values for the first redox couple of *s*-tetrazines studied in this paragraph. While variations of the potential can be easily correlated to the electron withdrawing or donating character of the substituent, its steric hindrance appears to play a smaller role. All together the differences between the *s*-tetrazines bearing one chlorine and one alkoxy group appear very small, while the presence of two alkoxy groups in **98** noticeably decreases the potential. Considering the behavior of *s*-tetrazine **96** and **99**, the attracting groups, although much more withdrawing than a standard alkoxy, seem to exert a power slightly smaller than chlorine since both potentials are more negative than that of dichloro-*s*-tetrazine itself ( $E^0 = -0.68\text{V}$  for Cl-Tz-Cl). These results proved that the potential depends on the electron affinity of the substituent, but not on its size.

It should be noticed that electron transfer on *s*-tetrazine appears relatively slow, since the peak to peak separation values are all above 100mV/s. This is unexpected for aromatics, and especially for the smaller member of the series like chloromethoxy tetrazine.

Table 3.3. Standard reduction potentials and peak to peak separations for *s*-tetrazine derivatives **91-93** and **96-99** measured in DCM.

	<b>91</b>	<b>92</b>	<b>93</b>	<b>96</b>	<b>97</b>	<b>98</b>	<b>99</b>
$E^\circ / \text{V}$ vs. $\text{Ag}^+/\text{Ag}$	-0.83	-0.88	-0.94	-0.63	-0.84	-1.21	-0.60
$\Delta E_p / \text{mV}$	140	130	140	110	100	130	100

One of the most interesting characteristics of *s*-tetrazine derivatives is their ability to be electrochemically reduced through a two-electrons process (similarly to most quinones) without electrochemical, but however, chemical reversibility. Figure 3.5 presents the CV's of compound **91** at various negative inversion potentials. On the curves, the reoxidation of the anion radical is clearly visible whatever the negative potential limit scan. This means that the two electrons reduced electrogenerated species gives back the anion-radical in the course of the first reoxidation process.

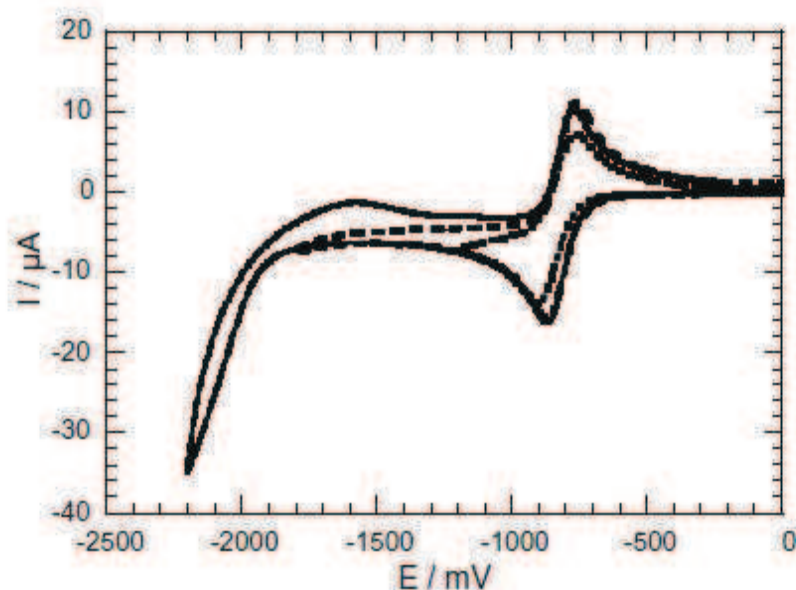


Figure 3.5. CV's of *s*-tetrazine **91** at different inversion potentials (Scan rate:  $100\text{mV s}^{-1}$ ).

In conclusion, new *s*-tetrazines substituted with bulky or electron withdrawing functional groups have been synthesized. All the mono substituted ones have been obtained by a  $\text{S}_{\text{N}}\text{Ar}$  reaction of an alcohol or imide with dichloro-*s*-tetrazine. The symmetric compound **98** was synthesized by reaction of **93** with a lithium alcoholate (ROLi).

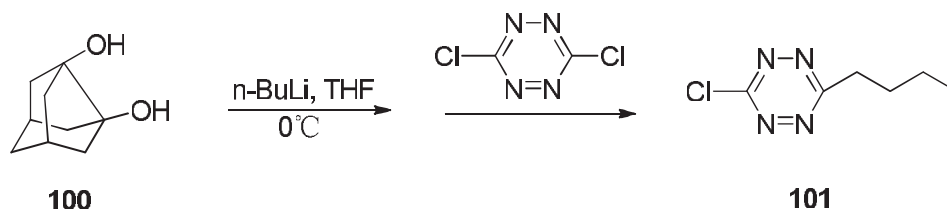
Particular attention was paid to the effect of the substituents on the electrochemical and fluorescence properties of these *s*-tetrazines. The results show that all the *s*-tetrazines have a classical absorption spectrum with two main bands located around 330 and 520nm. The fluorescence spectra of the *s*-tetrazines are weakly affected by the size of the substituent. However, its nature has a strong impact on the fluorescence quantum yields: they are high ( $\phi_F \approx 0.4$ ) when the substituent is an alkoxy, but drop dramatically ( $\phi_F < 0.1$ ) when it is an electron donor or acceptor group. This can be easily explained by a photoinduced electron transfer process in the case of an electron donor but was rather unexpected for electron acceptor substituents.

Finally, the study of the electrochemical properties shows that the reduction potential of the *s*-tetrazines depends on the electron affinity of the substituent, and not on its size. Furthermore, an uncommon slow electron exchange was also observed with these small organic molecules.

## 3.2 New alkyl-*s*-tetrazines from an unexpected reaction

### 3.2.1 Introduction

In the previous paragraph, it has been shown that the synthesis of compounds **94** and **95** proceeds poorly since each was obtained in only 2% yield following the classical conditions for the  $S_NAr$  reaction on dichloro-*s*-tetrazine. Thus, a different synthetic method was tried in order to improve the outcome of the reaction. It has been shown in previous works that in some cases, the use of the alcoholate instead of the alcohol in the  $S_NAr$  reaction gives better results. Hence, diol **100** was reacted with two equivalents of *n*-butyl lithium and the mixture added onto dichloro-*s*-tetrazine. However, this approach turned out not to be so successful for the synthesis of **94** or **95** but instead gave mainly an unexpected side product: *n*-butyl-chloro-*s*-tetrazine **101** (Scheme 3.5). It was also obtained in the absence of **100** and its structure was confirmed by NMR and mass spectrometry<sup>a</sup>.



<sup>a</sup> Further proof of the integrity of the *s*-tetrazine nucleus can be gained from the spectroscopic results (vide infra) since **101** retain the typical pink color and yellow fluorescence of *s*-tetrazine while dihydro-*s*-tetrazines are usually yellow and non fluorescent.

### Scheme 3.5. Unexpected synthesis of *s*-tetrazine **101**.

It is likely that the formation of the dianion of **100** is unfavorable since the two alcohols are very close. It is also possible that the anion on one oxygen atom is stabilized by the assistance of the remaining hydroxyl (Figure 3.6). Hence, one equivalent of *n*-butyl lithium would be still available in the medium to react with the dichloro-*s*-tetrazine.

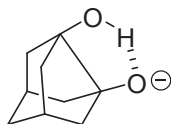
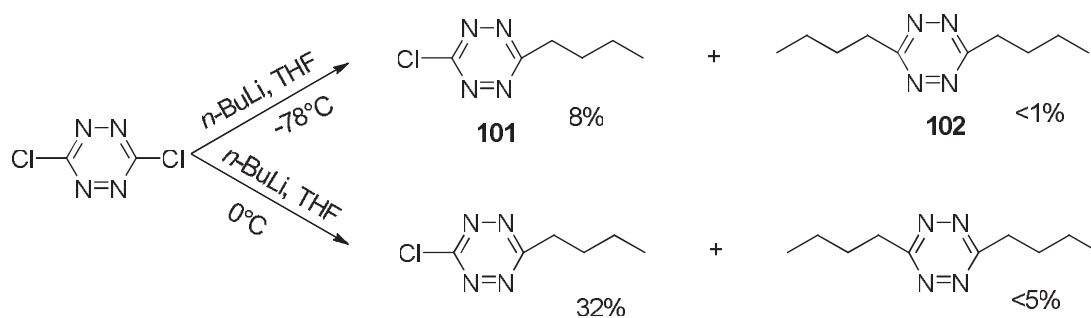


Figure 3.6. Possible stable structure for the anion of **100**.

However, it has been reported<sup>6</sup> that if soft carbanions, like the sodium salt of diethyl malonate, can undergo nucleophilic substitution with *s*-tetrazines, hard carbanions give azaphilic addition selectively. Kotschy *et al.* have shown that the azaphilic addition is always observed when *n*-butyl lithium reacts with various *s*-tetrazines. It is noteworthy that they did not test dichloro-*s*-tetrazine as starting compound but only 3-chloro-6-morpholino-*s*-tetrazine which decomposed in the presence of phenylmagnesium chloride. The nucleophilic substitution of *n*-butyl lithium on dichloro-*s*-tetrazine is then unique and the scope and limitation of this reaction was further investigated.

#### 3.2.2 Optimization and extension of the scope of the reaction

The first step was to find the best conditions for this reaction. The main factor tested was the temperature. Generally, reactions using *n*-butyl lithium are run at  $-78^{\circ}\text{C}$  but in our case compounds **101** and **102** were obtained in low yields (Scheme 3.6). When the same reaction was carried out at  $0^{\circ}\text{C}$  compounds **101** and **102** were obtained in 32% and less than 5% respectively. The low yields for **102** in both cases are easily explained since only 1.2 equivalents of *n*-butyl lithium were used. Hence, the mono substitution proceeds smoothly and in good yield at  $0^{\circ}\text{C}$ .



Scheme 3.6. Survey of effect of the temperature on the  $S_NAr$  reaction of *n*-butyl lithium with dichloro-*s*-tetrazine.

In a second step, the reaction was tested, using the same conditions, on various chloro-*s*-tetrazines already prepared in the laboratory (Table 3.4). It appears that this reaction is quite general since it works with several chloro-*s*-tetrazines bearing either electron withdrawing (entries 1, 2 and 4) or donating (entries 3, 5 and 6) groups regardless of their size. It is noteworthy that 3-chloro-6-morpholino-*s*-tetrazine (entry 6) reacts similarly and does not give any product coming from an azaphilic addition. The yields are also typically good (30%-50%), except in the case of compounds **102** (12%) and **104** (18%).

Table 3.4. Preparation of *n*-butyl -*s*-tetrazine<sup>a</sup>.

Entry	chloro- <i>s</i> -tetrazine	<i>n</i> -butyl- <i>s</i> -tetrazine	yield
1			35%
2			16% <sup>b</sup>
3			52%
4			30%
5			18%
6			45%

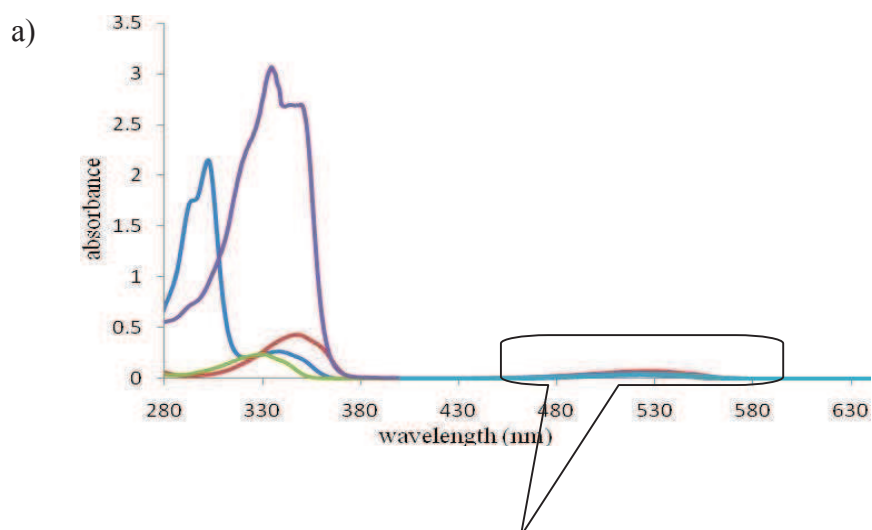
a: reaction conditions: *n*-BuLi (1.2 eq) in THF at 0°C; b: 2.4 equivalents of : *n*-BuLi were used.

The new reaction uncovered on dichloro-*s*-tetrazine is then rather general since *n*-butyl lithium reacts smoothly with other chloro-*s*-tetrazines. It is then demonstrated for the first time that alkyl substituted *s*-tetrazines can be directly obtained from the corresponding chloro-*s*-tetrazine. This is important for *s*-tetrazine chemistry because of the difficulty to synthesize alkyl substituted *s*-tetrazines. Indeed, unlike aryl nitriles, alkyl nitriles hardly give the corresponding *s*-tetrazine following the classical Pinner's synthesis. Other routes have been reported but suffer from many shortages. Very recently, Devaraj *et al.* proposed an efficient metal-catalyzed (Ni or Zn) one-pot synthesis which gives symmetrical and unsymmetrical alkyl(aryl)-*s*-tetrazines from the corresponding nitriles<sup>7</sup>. Our approach is complementary since it allows the synthesis of unsymmetrical *s*-tetrazines comprising a heteroatom on one side and an alkyl chain on the other.

### 3.2.3 Spectroscopic studies

The photophysical properties of the new *n*-butyl-*s*-tetrazines have been studied and compared to those of the starting chloro substituted equivalents in order to investigate the influence of the alkyl chain.

The absorption spectra of *s*-tetrazines **101-105** are shown in figure 3.7 and data are given in Table 3.5.





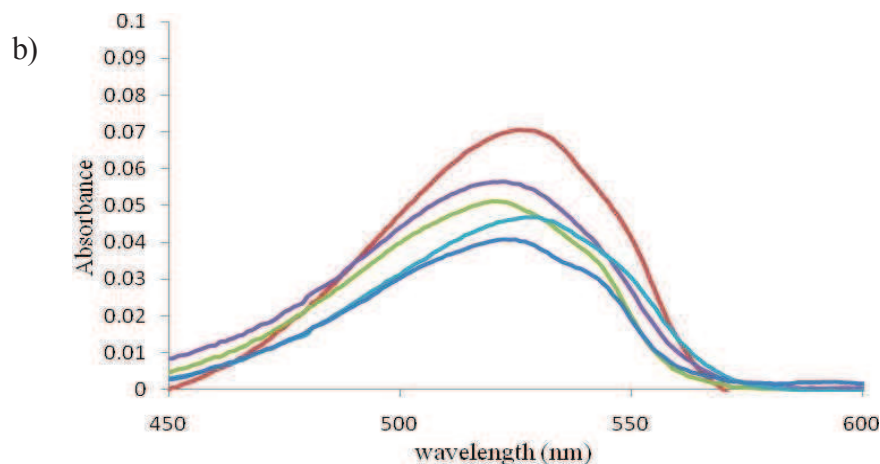


Figure 3.7. a) Full absorption spectra and b) zoom on the visible band of compounds **101** (green), **102** (light blue), **103** (red), **104** (blue), and **105** (purple) recorded in DCM.

All compounds display the two usual absorption bands of *s*-tetrazines: a weak absorption in the visible range centered on 520 nm and a stronger one in the UV around 350nm. However, compounds **104** and **105** have another intense absorption band in the UV region which is due to the substituent (pentachlorobenzene and naphthalimide respectively). Additionally, it is clear that upon replacing chlorine by *n*-butyl, the visible absorption band is red shifted by 5 to 9nm (Figure 3.8b). The same tendency but to a larger extent can also be observed on the UV band as seen for **101** and **102** (Figure 3.8a). This bathochromic shift for both  $\pi$ - $\pi^*$  and  $n$ - $\pi^*$  transitions comes from the electron donating ability of the butyl which stabilizes the orbitals of the *s*-tetrazine.

More importantly, the fluorescence properties of these new compounds have also been studied. Compounds **101-105** are all fluorescent when excited in their  $n$ - $\pi^*$  absorption band (Figure 3.8, Table 3.5).

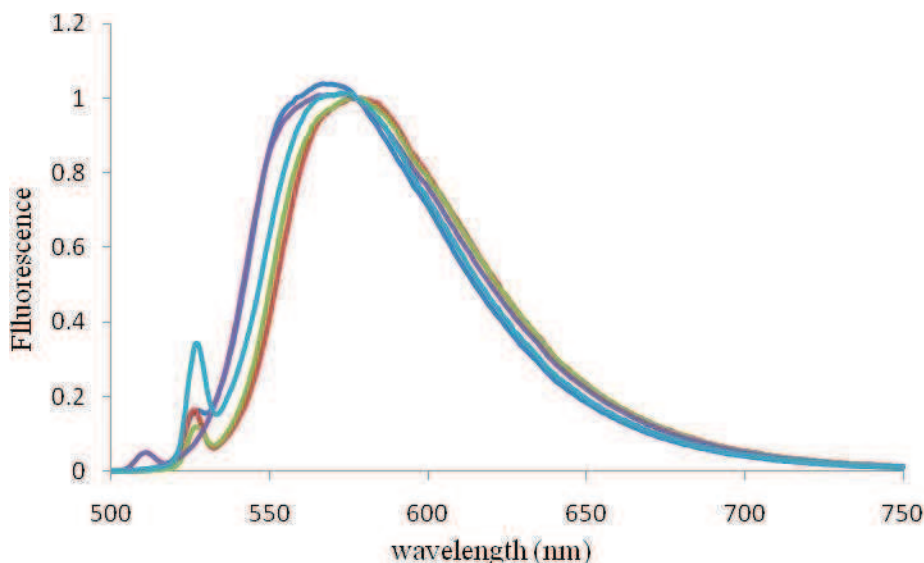
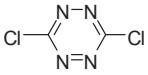
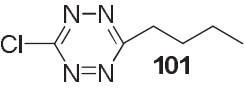
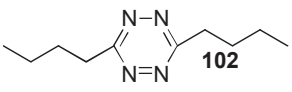
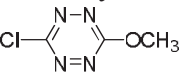
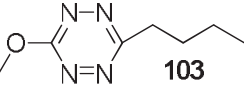
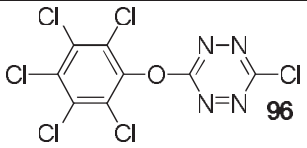
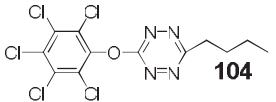
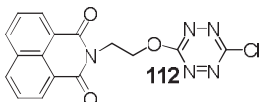
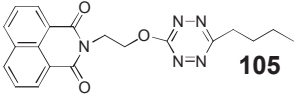
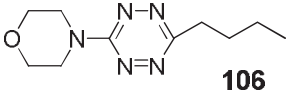


Figure 3.8. Fluorescence spectra of compounds **101** (purple), **102** (red), **103** (green), **104** (blue) and **105** (light blue) recorded in DCM.

The fluorescence band maxima are above 570 nm for all compounds but **101**. Similarly to what has been observed on the absorption spectra, the compounds experience a 6-13nm bathochromic shift upon substitution of chlorine by butyl. This shift is of the same order when methoxyl replaces chlorine. Hence butyl plays the same inductive donor role as methoxyl on *s*-tetrazine.

The more noticeable differences are observed on the fluorescence quantum yields and lifetimes. Compared to dichloro-*s*-tetrazine, fluorescence quantum yield and lifetime of compound **101** are increased 3.7 (from 0.14 to 0.52) and 2.7 (from 58ns to 158ns) times respectively. However, dichloro-*s*-tetrazine and dibutyl-*s*-tetrazine **102** have similar values for both parameters. This might originate from the combination of one electron donating and one electron withdrawing group on the *s*-tetrazine moiety. Indeed, it seems that *s*-tetrazines substituted with two groups of similar electron affinity are less fluorescent than the ones with substituents of opposing electron affinities. This has previously been observed on the 3-chloro-6-methoxy-*s*-tetrazine compared to either dichloro or dimethoxy-*s*-tetrazines<sup>1</sup>.

Table 3.5. Spectroscopic characteristics of butyl-*s*-tetrazines and their chloro counterparts.

compound	$\lambda_{\text{abs max}}$ (nm)	$\epsilon$ (L mol <sup>-1</sup> cm <sup>-1</sup> )	$\lambda_{\text{em max}}$ (nm)	$\phi_{\text{F}}$	$\tau_{\text{F}}$ (ns) <sup>h</sup>
dichloro- <i>s</i> -tetrazine <sup>a</sup> 	515	460	551, 567	0.14	58
 <b>101</b>	520	730	563 <sup>b</sup>	0.52	159
 <b>102</b>	528	660	576 <sup>c</sup>	0.14	39
chloro-methoxy- <i>s</i> -tetrazine <sup>a</sup> 	520	-	567	0.38	160
 <b>103</b>	526	520	576 <sup>d</sup>	0.21	45
 <b>96</b>	518	822	566 <sup>e</sup>	0.09	-
 <b>104</b>	525	540	572 <sup>f</sup>	0.37	112
 <b>112</b>	517	400	562 <sup>g</sup>	0.32	158
 <b>105</b>	526	180	572 <sup>d</sup>	0.18	59
 <b>106</b>	425 529	720 320	-	-	-

a: data taken from ref. 12; b:  $\lambda_{\text{ex}} = 520\text{nm}$ ; c:  $\lambda_{\text{ex}} = 528\text{nm}$ ; d:  $\lambda_{\text{ex}} = 526\text{nm}$ ; e: data taken from ref. 13; f:  $\lambda_{\text{ex}} = 525\text{nm}$ ; g: data taken from ref. 14; h:  $\lambda_{\text{ex}} = 520\text{nm}$ .

It was also true for *s*-tetrazines **96** and **98** presented in the previous paragraph. This is confirmed in the butyl series since **102** has similar fluorescent behavior to 3-chloro-6-methoxy-*s*-tetrazine while **102** or **103** are similar to dichloro or dimethoxy-*s*-tetrazines. The same trend is observed for compounds **96** and **104** (4 times increase of the fluorescence quantum yield) and **105** and **112** (1.7 times increase of the fluorescence quantum yield). These results are a valuable contribution for future design of highly fluorescent *s*-tetrazines.

Finally the special case of compound **105** has to be mentioned. It has been shown that *s*-tetrazines linked to aliphatic amines are weakly to non fluorescent because the non bonding orbital of the nitrogen is conjugated with the *s*-tetrazine  $\pi$  cloud<sup>3</sup>. In the previous paragraph, the same result was observed with compound **99** where *s*-tetrazine is directly linked to an electron withdrawing imide. Compound **105** is also weakly fluorescent and falls in the same category. Therefore, there is still no simple way to synthesize a fluorescent *s*-tetrazine substituted with a nitrogen atom.

### 3.2.4 Electrochemical studies

The electrochemical studies of these butyl-*s*-tetrazines have been performed, using cyclic voltammetry. Figure 3.9 shows the CV response of tetrazine **104**. The first reduction which corresponds to *s*-tetrazine is completely reversible as for 3-chloro-6-methoxy-*s*-tetrazine. This is the case for all *n*-butyl-*s*-tetrazines synthesized (Table 3.6). The potential of this reduction depends on the electron affinity of the substituent as already observed previously on other derivatives<sup>12</sup>. The reduction potential of all the *n*-butyl-*s*-tetrazines is shifted toward the more negative values when compared to their chloro-*s*-tetrazine equivalent. For example, the first redox potential for dichloro-*s*-tetrazine found at -0.68V shifts to -0.87V for 3-butyl-6-chloro-*s*-tetrazine **101** and -1.19V for dibutyl-*s*-tetrazine **102**. The same trend occurs when going from dichloro-*s*-tetrazine (-0.68V) to 3-chloro-6-methoxy-*s*-tetrazine (-0.99V) and to 3-butyl-6-methoxy-*s*-tetrazine (-1.19V).

It is possible to further reduce the aromatic moiety of butyl-*s*-tetrazines below approximately -2V (data not shown) but it is an electrochemically irreversible process as in most *s*-tetrazines studied to date. Compound **105** is a special case since the naphthalimide part can also be reduced. However, it is an irreversible process while in **112** it is partially reversible (*vide infra*).

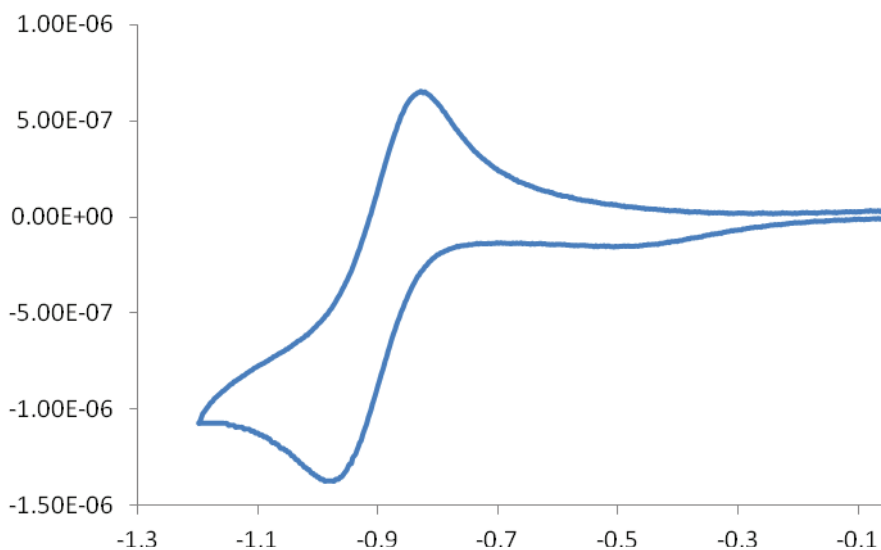


Figure 3.9. CV's of tetrazine **104** (Scan rate: 100mV s<sup>-1</sup>).

Table 3.6. Electrochemical data for butyl-*s*-tetrazines and corresponding chloro-*s*-tetrazines (pot. vs. Ag/10<sup>-1</sup> M Ag<sup>+</sup>).

compound	$E_{red}^{0}$ (V)	compound	$E_{red}^{0}$ (V)
	-0.87		-0.68
	-1.19		
	-1.19		-0.99
	-0.92		-0.63
	-1.63		-0.86
	-1.21		

In conclusion, a series of *n*-butyl-*s*-tetrazines have been prepared from an unexpected S<sub>N</sub>Ar reaction between *n*-butyl lithium and chloro-*s*-tetrazines. The reaction works with *s*-tetrazines substituted by electron withdrawing or donating groups and the yields are acceptable to good (16 to 52%). The introduction of this alkyl substituent on the *s*-tetrazine core has a similar effect as a methoxy on its photophysical and electrochemical properties.

However, the usefulness of this transformation is certain since it opens up a new way to synthesize unsymmetrical alkyl-*s*-tetrazines bearing a heteroatom, which would be difficult to obtain by other methods. One possible future interest for this transformation is that it could help extend the fields of application of *s*-tetrazines to water since it yields fluorescent and electroactive derivatives devoid of the hydrolysable chlorine.

### 3.3 Toward *s*-tetrazine based fluorescent dyads

#### 3.3.1 Molecular design

We have shown in the previous paragraphs that it is rather difficult to improve the fluorescence properties of *s*-tetrazine by simple modifications of its substituents. Indeed it seems that a maximum is reached when the two substituents are of opposite electron affinity. Furthermore, replacement of the oxygen by nitrogen atom quenches the fluorescence. It was then desirable to try to take advantage of the unique fluorescent properties of *s*-tetrazine to build fluorescent dyads. The main goal was to overcome the low absorption of the *s*-tetrazine visible band and use an energy donor with efficient absorption to improve the overall brightness of the molecule. The dyads comprise three moieties: an energy donor, a link and a fluorescent energy acceptor. The latter being the *s*-tetrazine, the two first should be compatible with it. In other words, it should not quench the fluorescence of *s*-tetrazine.

In the two following paragraphs, preliminary work toward the synthesis of these dyads will be presented. The emphasis will be on the choice of the energy donor and the link. The detailed studies of the working dyads will then be given in the next chapter.

*s*-Tetrazine is a strong electron acceptor. Hence, the energy donor should not be oxydazable or it will quench the fluorescence by an electron transfer process as seen with molecule **97** in the first paragraph. As a consequence, imides and benzimidazoles were chosen since they are weak electron acceptors and can not be oxidized. Many dyads have been design with various imides linked to *s*-tetrazine either by an alkyl

chain (Figure 3.10) or a phenyl one (Figure 3.11) to compare the effect of the nature of the link. Then the photophysical and electrochemical properties of the *s*-tetrazine in these dyads have been studied.

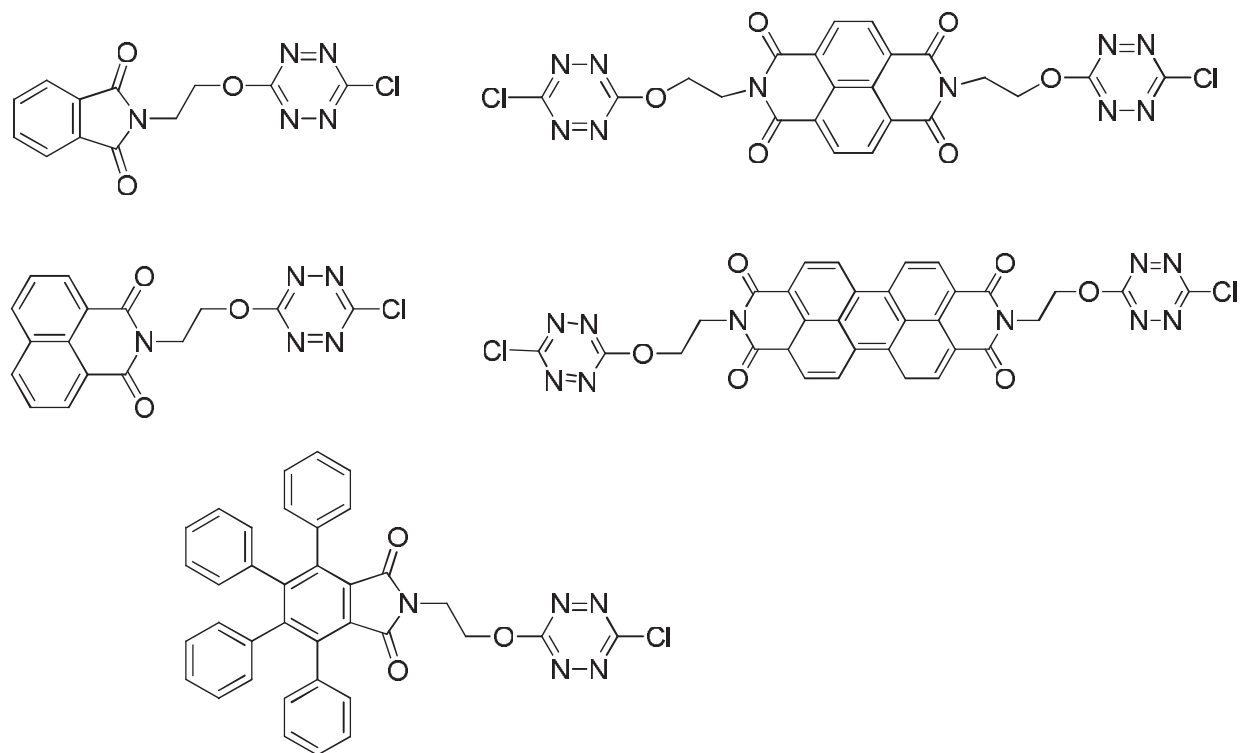


Figure 3.10. Targets with ethoxy link.

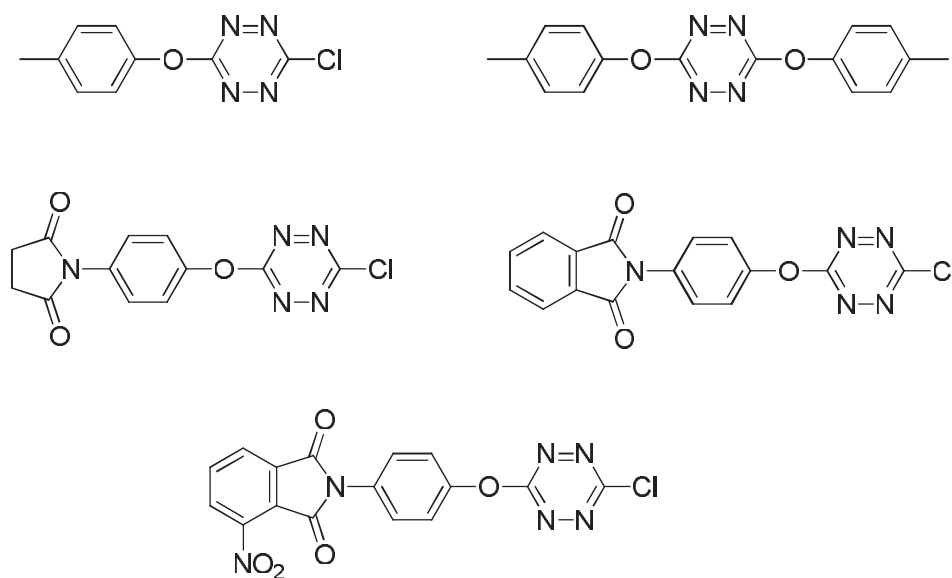


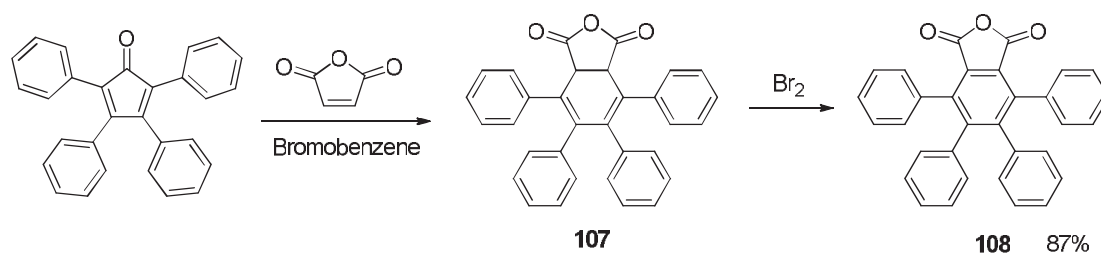
Figure 3.11. Targets with phenoxy link.

Work on the benzimidazoles will be presented in the next paragraph.

### 3.3.2 Synthesis

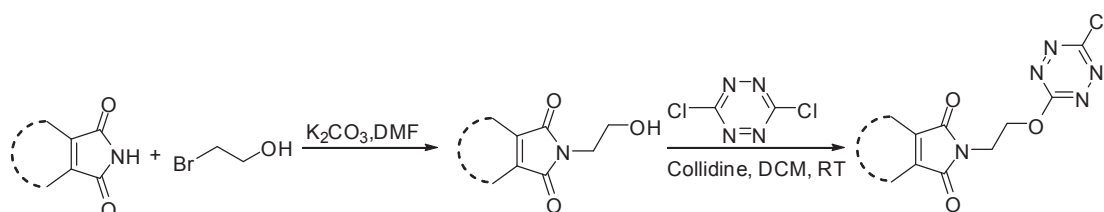
#### 3.3.2.1 Preparation of *s*-tetrazine-imides linked by an ethoxy

All starting imides are commercially available except tetraphenylphthalimide which was obtained from the corresponding anhydride. It was synthesized from tetraphenylcyclopentadienone<sup>8,9</sup> in two steps and 87% overall yield (Scheme 3.7).



Scheme 3.7. Preparation of tetraphenylphthalic anhydride **108**.

*N*-(2-hydroxyethyl)-imides were prepared according to published procedures mainly by reaction of the imide with 2-bromoethanol in the presence of potassium carbonate in refluxing DMF for several hours (Scheme 3.8) followed by column chromatography purification. *N*-(2-hydroxyethyl)-imide **113** was obtained by reaction between anhydride **108** and 2-aminoethanol. Subsequently, the corresponding *s*-tetrazines were synthesized by S<sub>N</sub>Ar reaction with dichloro-*s*-tetrazine following the standard protocol described in the first part of the chapter. Table 8 gathers the yields of the reactions.



Scheme 3.8. Preparation of *N*-(2-hydroxyethyl)-imides and corresponding *s*-tetrazines.

Table 8. Yields of *N*-(2-hydroxyethyl)-imides and corresponding *s*-tetrazine derivatives.

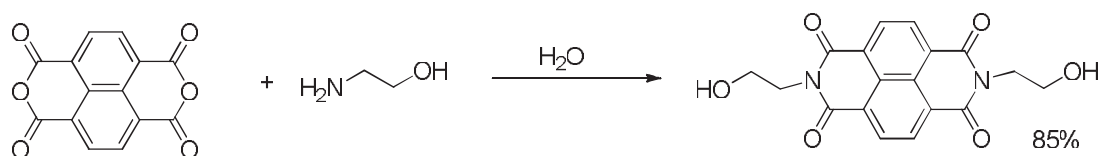
reactant	<i>N</i> -(2-hydroxyethyl)-imide	Yield	<i>s</i> -tetrazine	Yield
	 <b>109</b>	99% <sup>a</sup>	 <b>110</b>	70%



		74% <sup>b</sup>		56%
		50%		25%
		4%		- <sup>c</sup>

a: ref. 4; b: ref. 5; c: decomposition.

Compound **109**, **111** and **113** have been obtained in good yields, but the reaction yield for compound **115** is about 4% which is very low. Hence a different protocol was tested: 1,4,5,8-naphthalenetetracarboxylic dianhydride was reacted with ethanolamine in H<sub>2</sub>O (Scheme 3.9) and the yield increases to 85%. The difference is possibly due to the solvent. The product is not easy to extract from DMF while it precipitates in water and can be recovered by direct filtration in the second case.

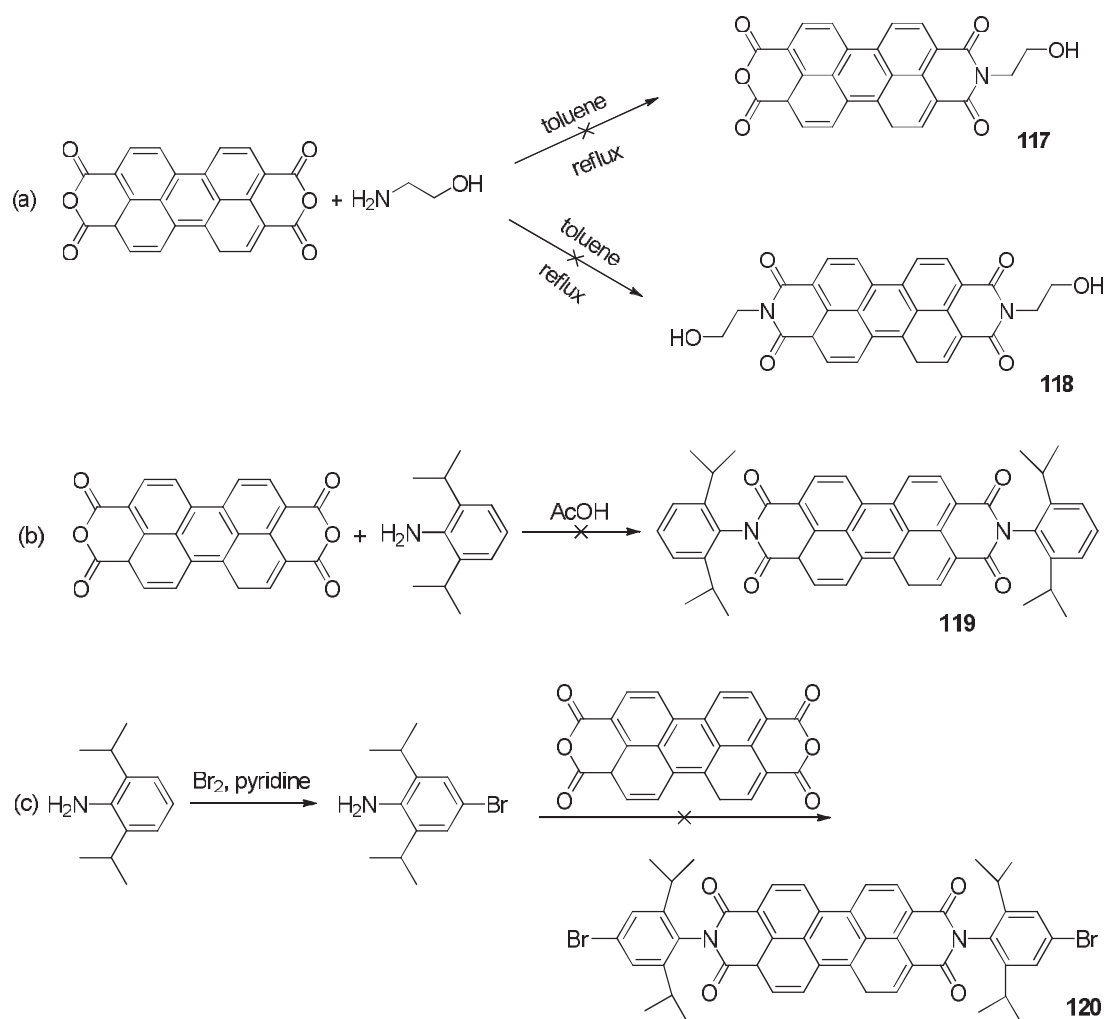


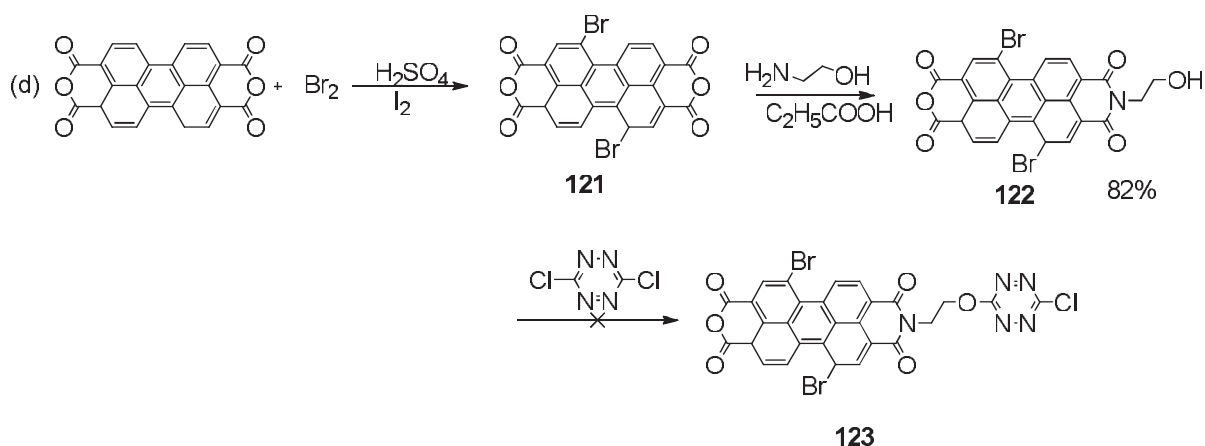
Scheme 3.9. Preparation of **115** from 1,4,5,8-naphthalenetetracarboxylic dianhydride.

However, the reaction of compound **115** with dichloro-*s*-tetrazine is blocked because of the low solubility of **115** in dry organic solvents. Although high temperature, pressure tube and larger quantity of solvent have been used to increase the quantity of **115** in solution, it does not give the expected *s*-tetrazine **116**. TLC analysis indicated that no new *s*-tetrazine is formed and that the dichloro-*s*-tetrazine decomposed under these conditions.

It was also tried to prepare an *s*-tetrazine–perylene bis-imide dyad. First, 3,4,9,10-perylenetetracarboxylic dianhydride was reacted with ethanolamine in refluxing toluene for 7h but none of the expected target compounds **117** or **118** were obtained (Scheme 3.10a). Considering that their solubility might be low in organic

solvents, **119** and **120** (Scheme 3.10b and c) were targeted since it has been demonstrated that introduction of a 2,6-diisopropylphenyl on perylene bis-imide improves its solubility<sup>10</sup>. Furthermore, it has been reported in the literature that it is possible to selectively hydrolyze one substituent and subsequently introduce another one such as ethanolamine<sup>10b</sup>. Unfortunately, in our hands, all attempts to obtain either **119** or **120** failed.





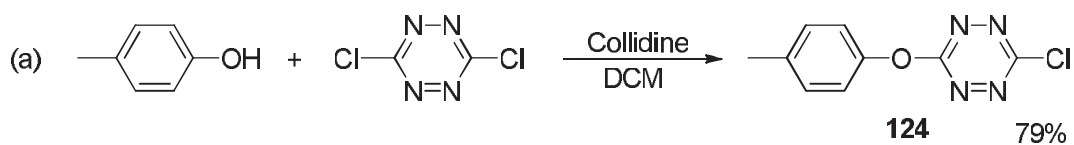
Scheme 3.10. Attempts to prepare perylene bis-imide – *s*-tetrazine dyads.

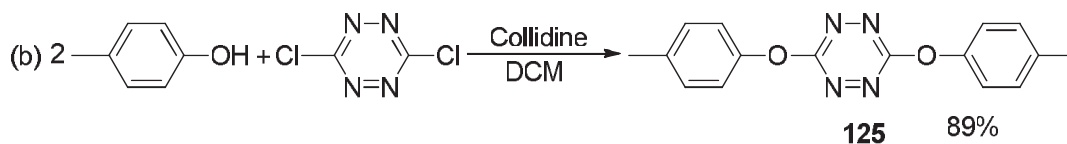
Another reported strategy to improve the solubility of perylene bis-imide is to introduce substituents in the so called bay area (positions 1, 6, 7 and 12) to distort the perylene. Bromine has been often used for this purpose. Additionally, it enhances the reactivity of the imides. Compound **121** was obtained (Scheme 3.10d) following reported procedures and used to form compound **122**. Mass spectrometry confirmed the expected product, but the extremely low solubility of **122** prevented the formation of **123**. Hence, it was decided not to pursue the synthetic efforts to get an *s*-tetrazine-perylene bis-imide dyad.

### 3.3.2.2 Preparation of *s*-tetrazines linked to a phenoxy

It has been demonstrated in paragraph 3.1 that linking an *s*-tetrazine directly to phthalimide (**99**) or pentachlorophenol (**96**) leads to a marked decrease of their fluorescence quantum yield. It was then decided to study in more depth the origin of this phenomenon by attaching a phenoxy or different imides-phenoxy substituents to *s*-tetrazine.

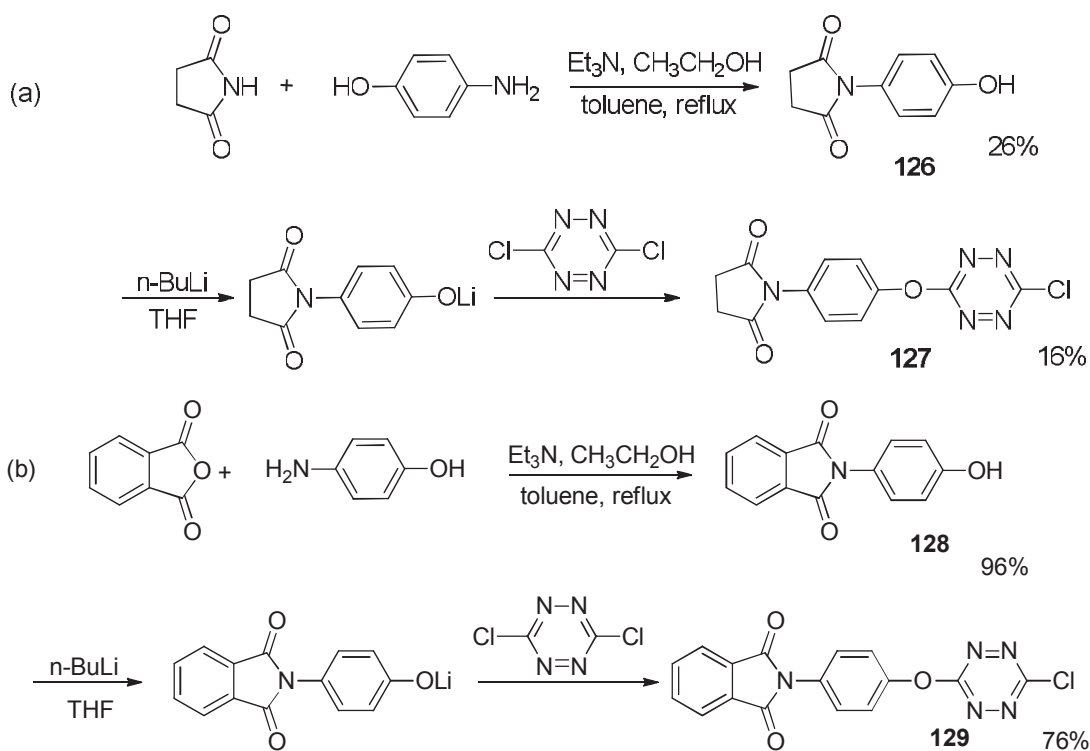
*s*-tetrazines **124** and **125** were obtained directly by  $S_NAr$  reaction between dichloro-*s*-tetrazine and *p*-cresol (Scheme 3.11). Introduction of one or two substituents can be controlled by the quantity of phenol used as already demonstrated<sup>11</sup>.

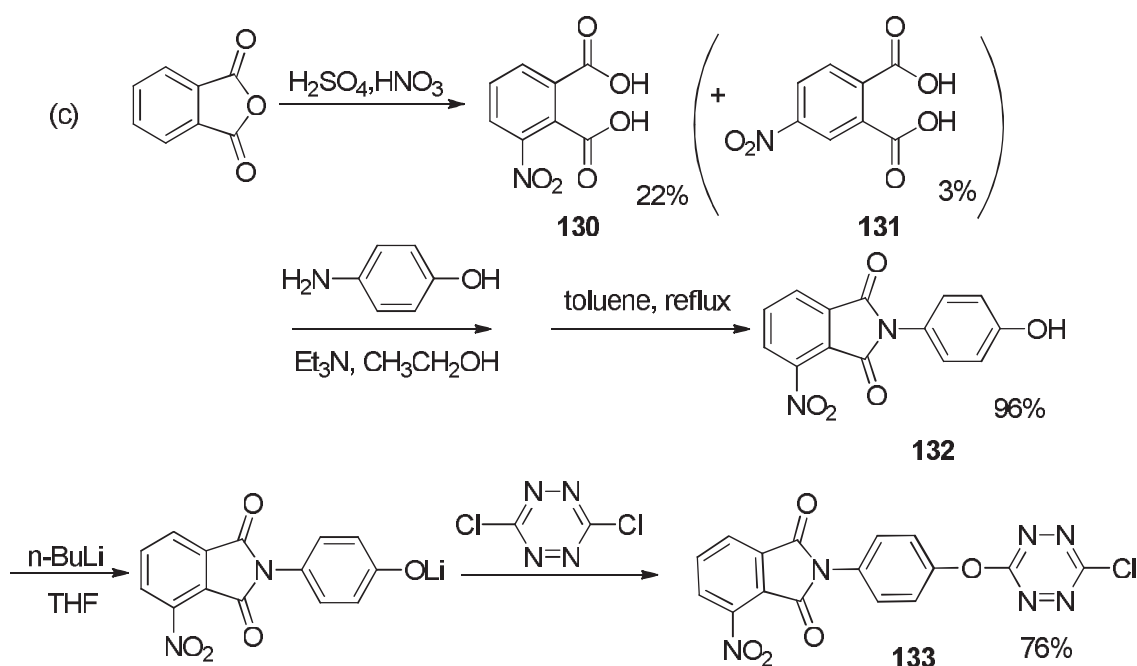




Scheme 3.11. Preparation of phenoxy substituted *s*-tetrazines.

The *p*-imidephenol derivatives have been synthesized according to published procedures<sup>12,13,14</sup> (Scheme 3.12). Their  $S_NAr$  reaction with dichloro-*s*-tetrazine has been done with the corresponding lithium phenolate, prepared by action of *n*-butyl lithium. Reaction yields are high for **129** and **133** (76%) and low for **127** (16%). This might be due to a lower stability of the anion of **128**.





Scheme 3.12. Preparation of *N*-(4-hydroxyphenyl)-imides and the corresponding *s*-tetrazine derivatives.

### 3.3.3 Spectroscopic studies

The absorption and fluorescence spectra of all obtained *s*-tetrazines have been recorded in solution in dichloromethane. The results have been compared to those of 3-(adamant-1-ylmethoxy)-6-chloro-*s*-tetrazine **93** chosen as reference since it does not bear a pendant optically active group.

Absorption spectra of the series of *s*-tetrazines are given in figure 3.12 and corresponding characteristics in table 9. All compounds display the usual visible band of the *s*-tetrazine attributed to its  $n\text{-}\pi^*$  transition. Absorption maxima for all mono substituted compounds are found around 520 nm. No effect of the nature of the link (alkyl or phenyl) is apparent. Absorption of compound **125** is bathochromically shifted by 10 nm compared to **124**, a usual feature on going from single to double substitution on the *s*-tetrazine.

The most striking differences in the absorption spectra are found in the UV region. On one hand 3-(adamant-1-ylmethoxy)-6-chloro-*s*-tetrazine displays the usual  $\pi\text{-}\pi^*$  transition of the tetrazine centered at 330nm. On the other hand, all the imide substituted tetrazines have more intense absorption bands in the same area. This is due to a  $\pi\text{-}\pi^*$  transition located on the substituent. It is noteworthy that compound **112** shows the greatest intensity, and we will discuss this compound in the next chapter. Finally the simple phenoxy mono substituted tetrazine **124** has a UV absorption band similar to **93** while in **125** it is red shifted. This is also a usual feature on going from

one to two oxygen substituents on the *s*-tetrazine since it has been demonstrated that its  $\pi$ - $\pi^*$  transition is highly influenced by the electron affinity of the substituents.

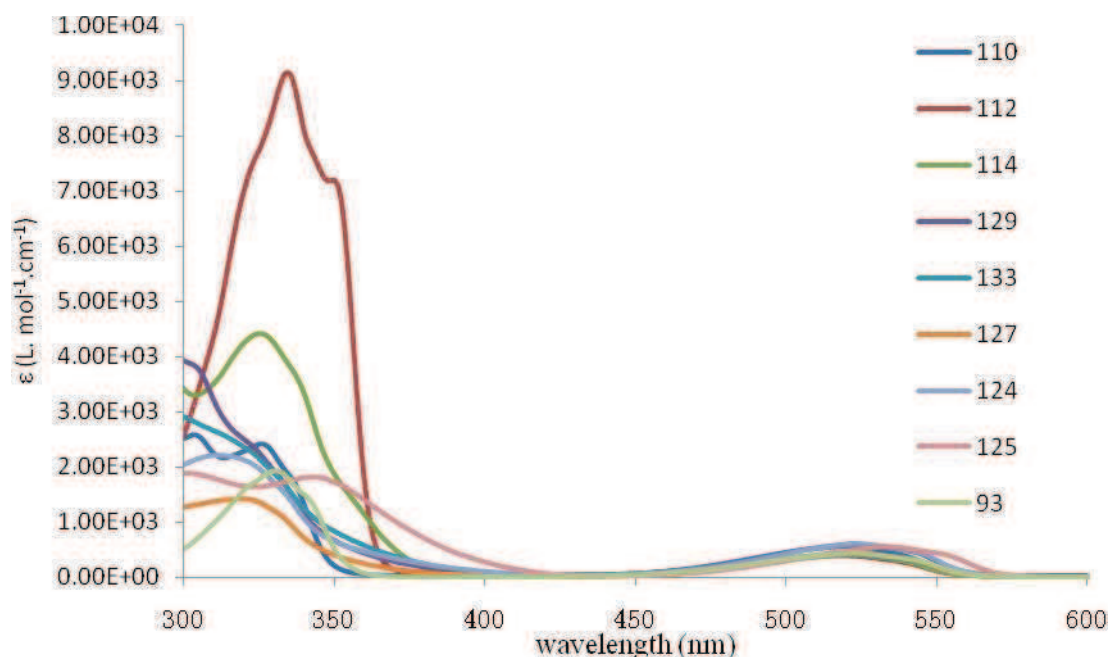


Figure 3.12. Absorption spectra of *s*-tetrazines in DCM.

We also investigated the fluorescence emission of these *s*-tetrazine compounds in solution in dichloromethane (Figure 3.13 and Table 3.9) upon excitation in their visible band. All monosubstituted compounds present a fluorescence band centered *ca.* 565 nm except **129** whose emission band peaks at an uncharacteristically low wavelength (549 nm) for no obvious reason. Similarly to the result of the absorption spectra, the fluorescence band of **125** is shifted by 10 nm to the red compared to **124** reflecting the strong donating properties of the phenoxy group.

Stokes shift of the derivatives substituted by an imidephenoxy are smaller than for the other compounds. This might be due to the more rigid structure in the case of phenyl compared to ethyl, where, in the latter case, the flexible character of the link may allow a stronger reorganization between the fundamental and excited states.

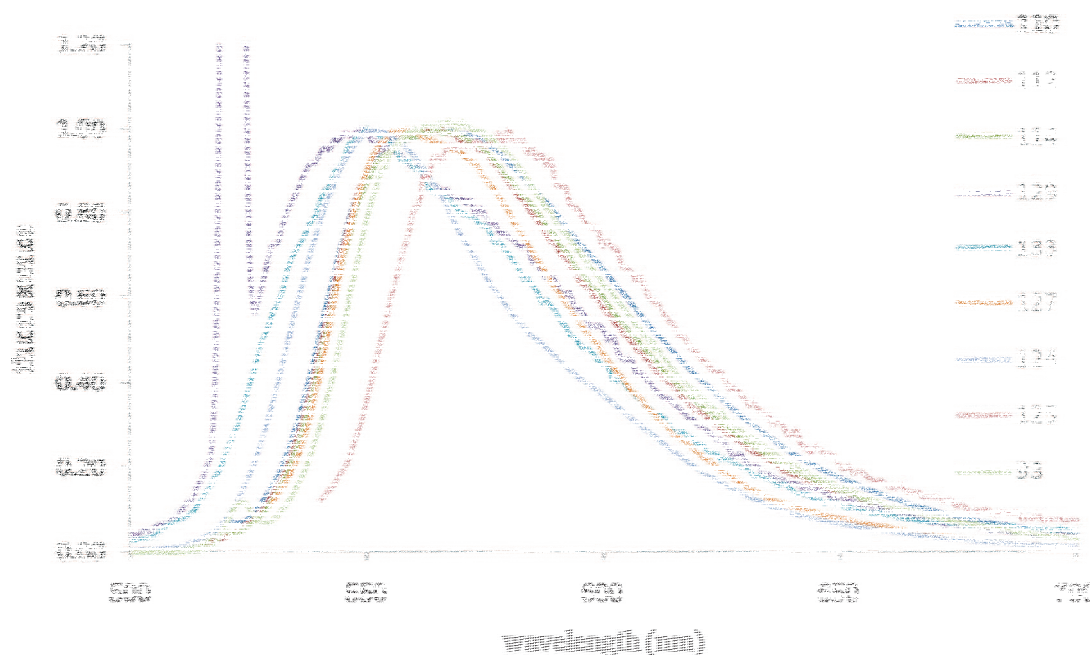


Figure 3.13. Normalized fluorescence spectra of *s*-tetrazines recorded in DCM ( $\lambda_{\text{ex}} = \lambda_{\text{abs,max}}$ )

However, the more striking differences are observed on the fluorescence quantum yields and lifetimes, which happen to be strongly linked to the nature of the spacer between the *s*-tetrazine and the imide group. When the spacer is a non conjugated ethyl group, the fluorescence of the *s*-tetrazine is practically unaffected. Fluorescence quantum yields for the three *s*-tetrazines **110**, **112** and **117** are about 0.3-0.4, and lifetimes are about 110-158ns. These values are comparable to those observed for *s*-tetrazine **93** or 3-chloro-6-methoxy-*s*-tetrazine. When *s*-tetrazine is connected to a phenol spacer, the fluorescence quantum yields drop considerably and the lifetimes become much shorter, with the appearance of multiexponential decays.

In addition, *s*-tetrazines **124** and **125** substituted by a cresol display the same features with the appearance of small fluorescence quantum yields and complex fluorescence decays. This allows us to conclude that fluorescence quenching likely occurs through photoinduced electron transfer from the electron-rich phenolic moiety to the *s*-tetrazine ring in its excited state.

Table 3.9. Spectroscopic characteristics of all compounds in this paragraph.

Molecule	$\lambda_{\text{abs}}^{\text{max}}$ (nm)	$\epsilon$ (L.mol <sup>-1</sup> .cm <sup>-1</sup> )	$\lambda_{\text{fluo}}^{\text{max}}$ (nm)	Stokes shift (cm <sup>-1</sup> )	$\Phi_{\text{fluo}}$	$\tau_{\text{fluo}}$ (ns) <sup>a</sup>
<b>93</b>	522	570	563	1395	0.4	160
<b>110</b>	519	550	565	1569	0.41	112
<b>112</b>	518	400	567	1668	0.48	158

<b>114</b>	519	800	565	1569	0.33	113
<b>127</b>	522	450	558	1236	0.03	2.3 (99.9%) 51.8 (0.1%) <sup>b</sup>
<b>129</b>	521	600	549	979	0.02	0.3 (98.5%) 1.7 (1.1%) 11.0 (0.4%) <sup>b</sup>
<b>133</b>	522	400	557	1204	0.01	2.0 (96.2%) 5.7 (3.8%) <sup>b</sup>
<b>124</b>	524	600	565	1385	0.001	0.1 (98.4%) 2.2 (1.4%) 21.0 (0.2%) <sup>b</sup>
<b>125</b>	534	550	580	1485	0.007	2.3 (99%) 20.5 (1%) <sup>b</sup>

a)  $\lambda_{\text{exc}} = 495\text{nm}$ ; b) multiexponential decays (the number in parenthesis are the normalized contribution of the lifetimes to the decay).

We have also checked the fluorescence of compounds **110**, **112**, **114**, **129** and **133** upon illumination at 300nm into the imide absorption band. Fluorescence of *s*-tetrazine is always observed, but because there is an overlap between the  $\pi\text{-}\pi^*$  band of the *s*-tetrazine and the  $\pi\text{-}\pi^*$  band of the imides and the absorption coefficients have comparable values, it is difficult to firmly conclude on the existence of an excited state energy transfer from the imide to the *s*-tetrazine. However, more detailed studies have been done with compound **112** which will be introduced in details in the next chapter.

### 3.3.4 Electrochemical studies

The electrochemical studies of all compounds have been performed, using cyclic voltammetry as a tool, to characterize not only the *s*-tetrazine electrochemistry, but also the reduction of the functional group, which also displays a reversible behavior in several cases.

Figure 3.14 shows the CV response of both compounds **114** and **133**, where the completely reversible behavior of the *s*-tetrazine first transfer is followed at lower potentials by another wave, completely or partially reversible. In the case of the nitrophthalimide **133**, the second wave is reversible because of the presence of the nitro group that both considerably raises the reduction potential and stabilizes the anion radical on the imide moiety. In the case of **114**, the imide reduction is also reversible for the same reason.



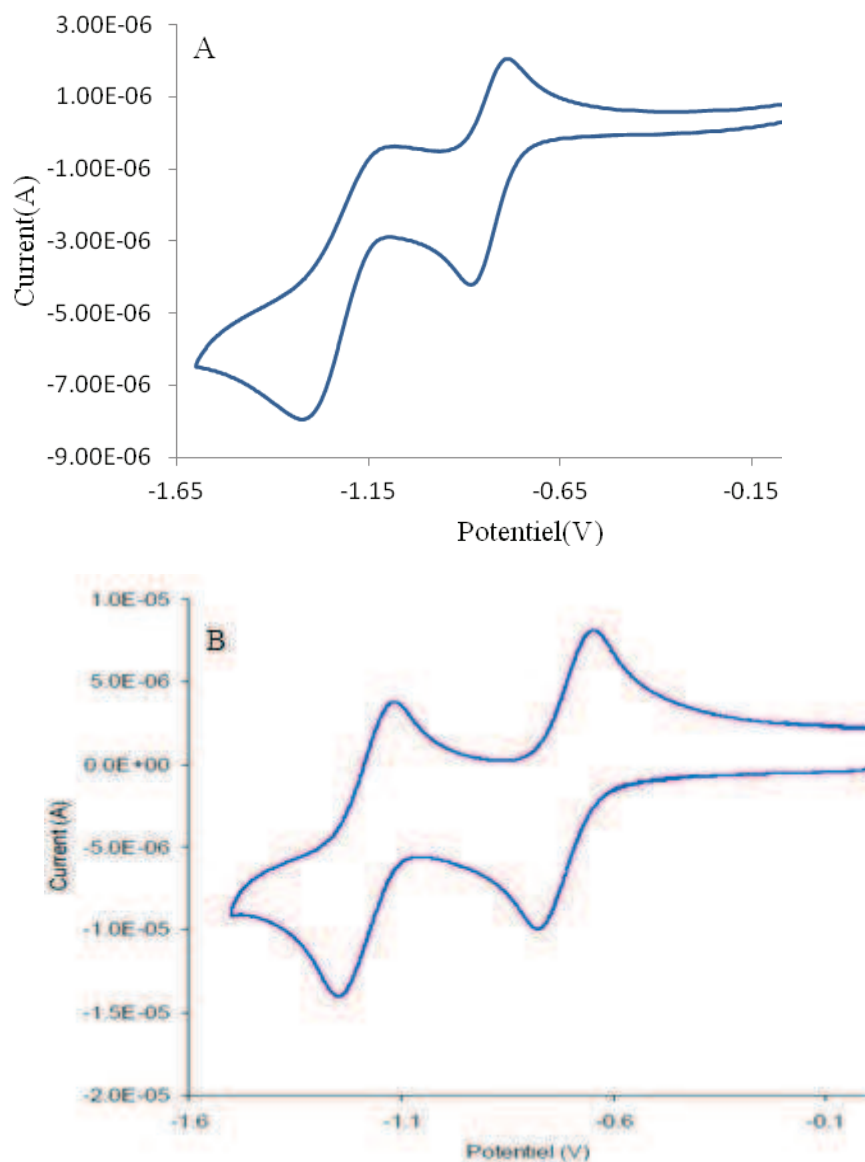


Figure 3.14. Cyclic voltammograms of (A) compound **114** and (B) compound **133** at 100mV/s in DCM/TBAFP (pot. vs. Ag/10<sup>-1</sup> M Ag<sup>+</sup>).

Therefore, it is noteworthy that it is possible to form two quite stable and independent anion-radicals on the same molecule, each displaying a perfectly electrochemically reversible behavior, a relatively rare occurrence in organic electrochemistry.

For other derivatives, for example **110**, the second system is less reversible, and there is a slight increase in the observed current (Figure 3.15). This is likely due to the existence of some overlap between the beginning of the second reduction of the *s*-tetrazine and the phthalimide reduction<sup>b</sup>.

<sup>b</sup> Detailed electrochemical studies of compound **112** will be introduced in the next chapter.

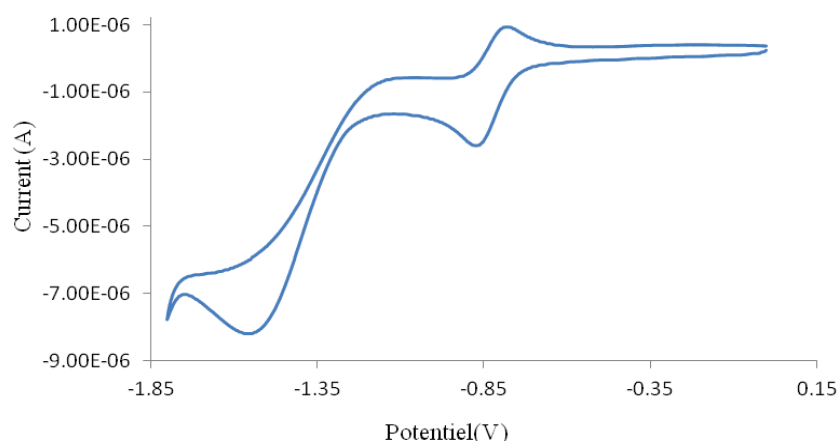


Figure 3.15. Cyclic voltammograms of compound **110** at 100mV/s in DCM/TBAFP (pot. vs.  $\text{Ag}/10^{-1} \text{ M Ag}^+$ ).

All the electrochemical data for *s*-tetrazines presented in this paragraph are listed in table 3.10. The first redox potential is ascribed to the *s*-tetrazine, whereas the second redox couple can always be assigned to the pendant group linked to the *s*-tetrazine. It can be noticed that a shift of 100mV toward more positive potentials occurs for the first redox couple when the substituent on the *s*-tetrazine changes from an alkoxy to a phenoxy. Both electroactive groups behave as independent redox sites in all compounds whatever the spacer.

In all cases, no additional wave has been observed below -2V, although an increase in the background current is sometimes noticeable after -1.9V and should probably be ascribed to the second reduction of *s*-tetrazine.

Table 3.10. Electrochemical data for *s*-tetrazines from this paragraph (pot. vs.  $\text{Ag}/10^{-1} \text{ M Ag}^+$ )

compound	<b>110</b>	<b>112</b>	<b>114</b>	<b>127</b>	<b>129</b>	<b>133</b>	<b>124</b>	<b>125</b>
$E_{red1}^0$ (V)	-0.84	-0.86	-0.84	-0.74	-0.74	-0.74	-0.79	-0.95
$E_{red2}^0$ (V)	-1.85	-1.70	-1.23	- <sup>a</sup>	-1.74	-1.19	- <sup>a</sup>	- <sup>a</sup>

a. No second wave observable before -2V, although an increase in the background current is sometimes noticeable after -1.9V and probably arising from the second tetrazine reduction.

In conclusion, new *s*-tetrazines-imides dyads linked either by a phenoxy or an ethoxy have been successfully prepared. The main synthetic difficulty encountered has been the solubility of the intermediate imide-alcohol. The  $\text{S}_{\text{N}}\text{Ar}$  reaction does not proceed when the reactant is too insoluble in organic solvents. If high temperature, pressure tube and/or longer time are used to try to force the reaction, the dichloro-*s*-

tetrazine decomposes. So the best choice, when possible, is to improve the solubility of the imide-alcohol.

Fluorescence and electrochemical studies confirmed our assumption: the nature of the link can play a crucial role on to the *s*-tetrazine properties. The most dramatic effects have been seen on the fluorescence quantum yields and lifetimes. Both of them are high with an ethoxy linker and drop with a phenoxy one. It is probable that a photoinduced electron transfer happens between the phenoxy moiety and the *s*-tetrazine in its excited state, which leads to a strong fluorescence quenching. Hence, the design of fluorescent dyads comprising *s*-tetrazine as the main emitter is possible but careful attention should be paid to the molecular design.

### 3.4 Tetrazines benzimidazole dyads

#### 3.4.1 Molecular design

Benzimidazole is an electron withdrawing group and a good UV absorber used in sunscreen. It is then possible to use as energy donor instead of imides for *s*-tetrazines. Two sites of the benzimidazole are easily amenable to functionalization: position 1 and 2 (Figure 3.16).

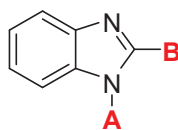


Figure 3.16. Sites selected for the functionalization of benzimidazole.

Based on the work on imides, it was decided to introduce the *s*-tetrazine in position A *via* an ethoxy link. Different functional groups were introduced in position B (Figure 3.17).

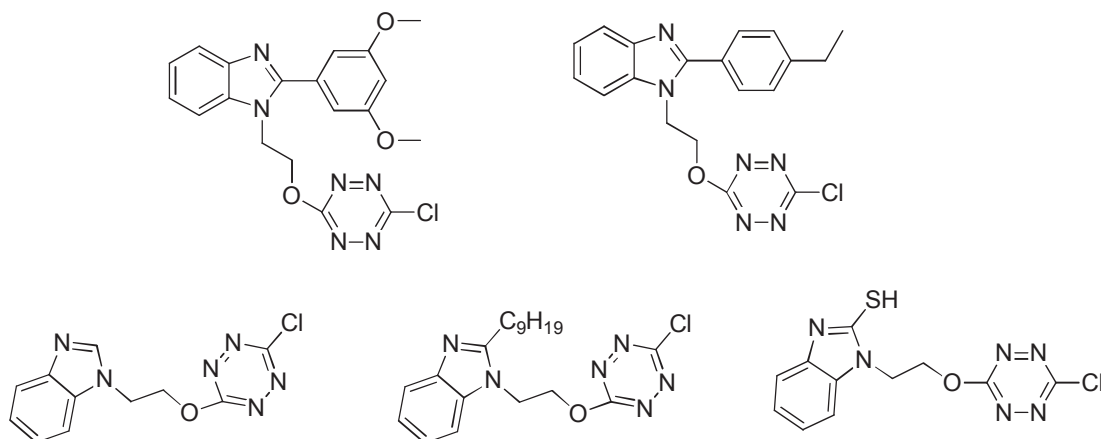
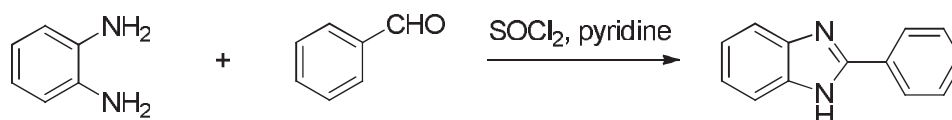


Figure 3.17. *s*-Tetrazine-benzimidazole dyads.

The main difference between the chosen groups is their electronic affinity since they can have an effect on the position of the absorption band of benzimidazole<sup>c</sup>.

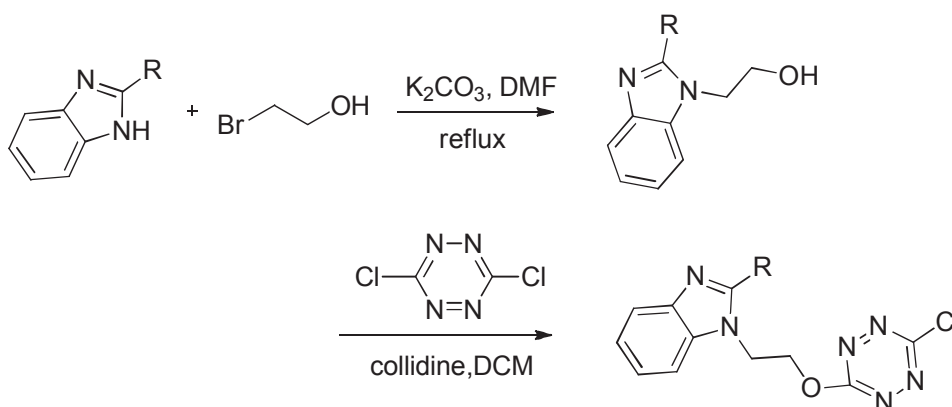
### 3.4.2 Synthesis

The synthetic strategy used to obtain the targets was based on our previous work on imide-tetrazine. The starting benzimidazoles were prepared from 1,2-diaminobenzene as followed(Scheme 3.13)<sup>15</sup>:



Scheme 3.13. Preparation of 1H-benzimidazoles.

The ethoxy link was introduced on the benzimidazole by reaction with 2-bromoethanol (Scheme 3.14) in the same way as for the imides previously shown. Then the synthesis of the dyad was carried out by classical S<sub>N</sub>Ar reaction with dichloro-*s*-tetrazine.



Scheme 3.14. Preparation of 1-(6-chloro-*s*-tetrazine-3-yloxy)ethyl-benzimidazole.

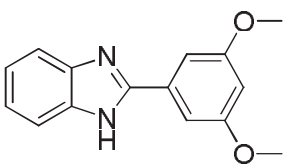
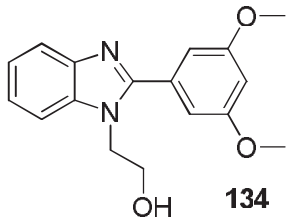
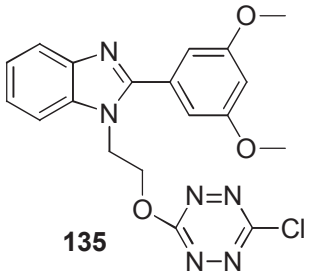
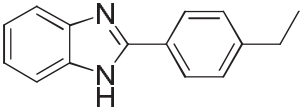
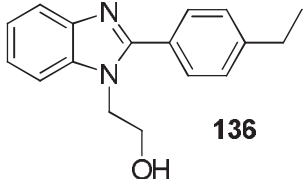
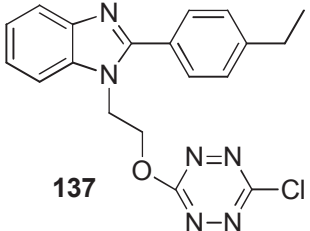
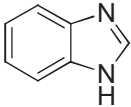
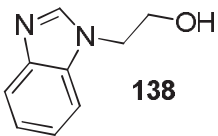
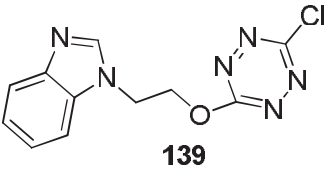
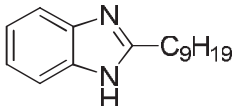
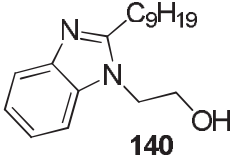
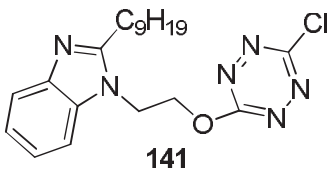
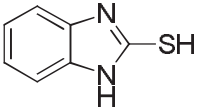
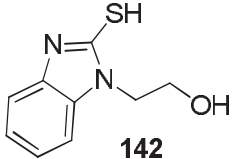
Table 3.10 lists the details the yields obtained for the synthesis of both hydroxyethylbenzimidazoles and the dyads. All *N*-(2-hydroxyethyl)-benzimidazoles were obtained in good yields except compound **142**, which has two possible reactive points and it was difficult to assign the structure of the product from NMR spectra.

<sup>c</sup> Benzimidazoles bearing electron withdrawing groups were also synthesized and will be presented in the next chapter.

Additionally, the crude compound was reacted with dichloro-*s*-tetrazine, but TLC analysis of the reaction indicated that the *s*-tetrazine decomposed and no new *s*-tetrazine derivative could be observed.

The expected dyads **135** and **137** could be obtained albeit in moderate yields. In the course of the synthesis of compound **139**, TLC analysis indicated that no new *s*-tetrazine product formed even after extended reaction time, while the dichloro-*s*-tetrazine decomposed. The lack of reactivity of *N*-(2-hydroxyethyl)-benzimidazole **138** can come from its poor solubility. Dyad **141** was obtained successfully, but it is unstable above 40°C. Consequently, it is hard to get the compound out of a solution.

Table 3.11. Synthetic yields of *N*-(2-hydroxyethyl)-benzimidazole and corresponding dyads.

reactant	<i>N</i> -(2-hydroxyethyl)-benzimidazole	yield	<i>s</i> -tetrazine	yield
	 <b>134</b>	65%	 <b>135</b>	23%
	 <b>136</b>	74%	 <b>137</b>	23%
	 <b>138</b>	65%	 <b>139</b>	- <sup>a</sup>
	 <b>140</b>	90%	 <b>141</b>	23% <sup>b</sup>
	 <b>142</b>	- <sup>c</sup>		

a: decomposed; b: decomposed at 40°C; c: NMR indicated the product is not the target

### 3.4.3 Spectroscopic studies

The absorption spectra of benzimidazole-tetrazines **135** and **137** were recorded in dichloromethane (Figure 3.18). Besides the typical absorption band of *s*-tetrazine in the visible corresponding to the  $n\text{-}\pi^*$  transition, the strong absorption of the benzimidazole moiety can be found in the UV region at approximately 300 nm. The UV absorption of *s*-tetrazine ( $\pi\text{-}\pi^*$  transition) can also be seen as a shoulder on the red edge of the benzimidazole band. The benzimidazole band arising from a  $\pi\text{-}\pi^*$  transition is similar in position and intensity for both compounds.

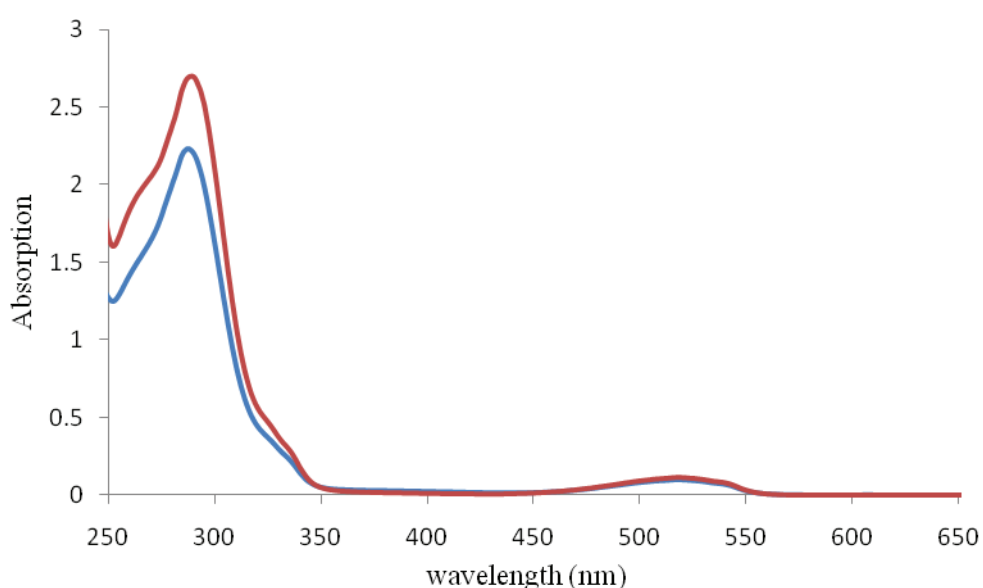


Figure 3.18. Absorption spectra of **135** (blue) and **137** (red) in dichloromethane.

The fluorescence properties of both compounds were also investigated (Figure 3.19) in dichloromethane upon excitation in the visible band of *s*-tetrazine.

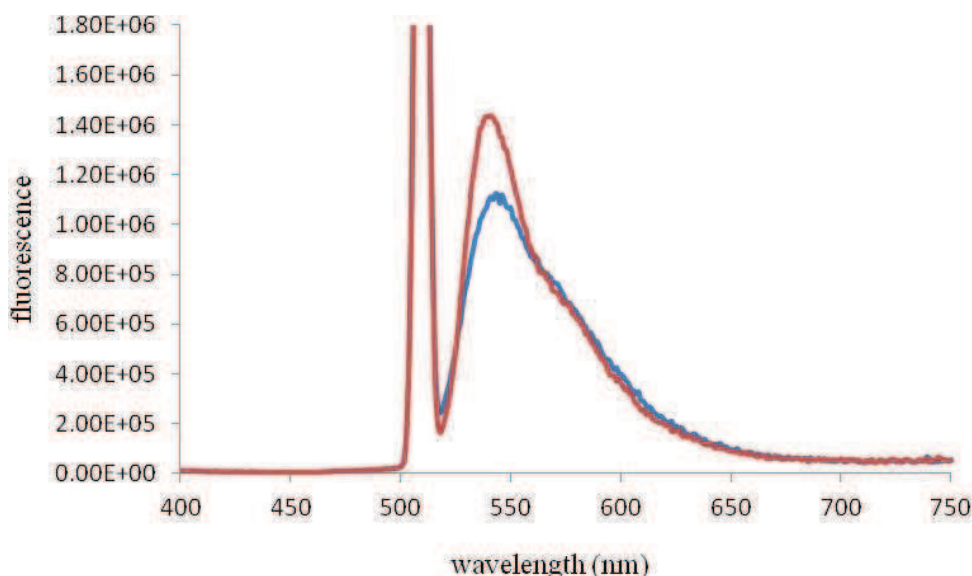


Figure 3.19. Fluorescence spectra of **135** (red) and **137** (blue) in dichloromethane ( $\lambda_{\text{ex}}=510\text{nm}$ ).

Table 3.12 gathers the spectroscopic characteristics of *s*-tetrazines **135**, **137**, and chloromethoxy-*s*-tetrazine as the reference. The position of the visible absorption band of **135** and **137** due to an  $n\text{-}\pi^*$  transition is similar to that of chloromethoxy-*s*-tetrazine and is found close to 520nm. On the contrary, the position of the fluorescence band of **135** and **137** is shifted by approximately by 25 nm to the blue compared to chloromethoxy-*s*-tetrazine. Hence, molecules **135** and **137** have a much smaller Stokes shift ( $\approx 850\text{ cm}^{-1}$ ) than chloromethoxy-*s*-tetrazine ( $\approx 1600\text{ cm}^{-1}$ ). These results are rather difficult to explain since unlike molecule **129** the link is not rigid and benzimidazole is not conjugated with the *s*-tetrazine moiety.

However, the most striking results can be seen on the fluorescence quantum yields and lifetimes which are considerably lower than those of chloromethoxy-*s*-tetrazine. In fact they have similar values to those of compounds **124**, **125** and **133** which are substituted by a phenoxy. This loss of fluorescence properties might be ascribed to the benzimidazole moiety, especially its substituent in the 2 position. They are electron donor phenyl groups and could be involved in a excited state electron transfer with *s*-tetrazine. Hence, the nature of the substituent on the benzimidazole is crucial to the design of fluorescent *s*-tetrazine-benzimidazole dyads and should not be oxydizable.

Table 3.12. Spectroscopic characteristics of **135**, **137** and chloromethoxy-*s*-tetrazine.

Molecule	$\lambda_{\text{abs}}^{\text{max}}$ (nm)	$\epsilon$ ( $\text{L}\cdot\text{mol}^{-1}\cdot\text{cm}^{-1}$ )	$\lambda_{\text{fluo}}^{\text{max}}$ (nm)	Stokes shift ( $\text{cm}^{-1}$ )	$\Phi_{\text{fluo}}^{\text{a}}$	$\tau_{\text{fluo}}^{\text{b}}$ (ns)
<b>135</b>	518	705	541	821	0.005	0.9

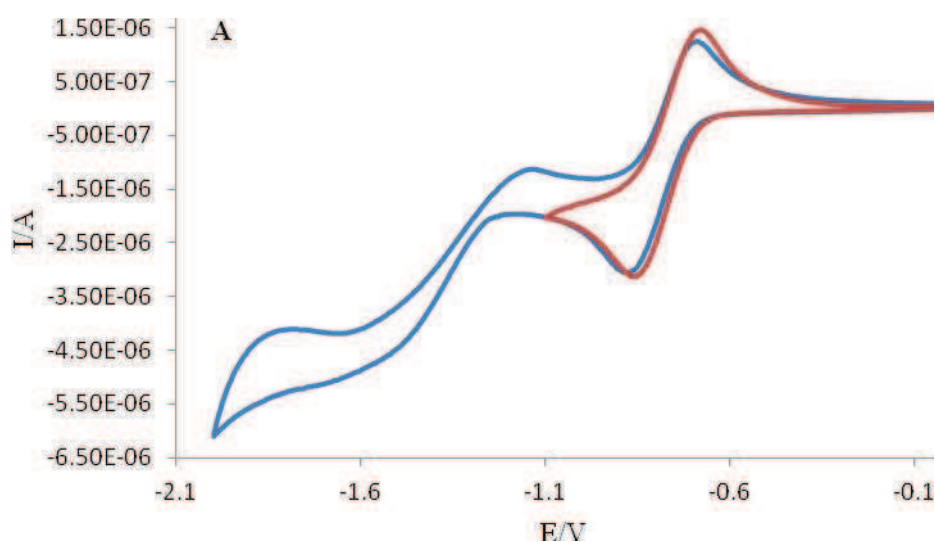
<b>137</b>	518	794	543	889	0.005	1.2
chloromethoxy- <i>s</i> -tetrazine	520		567	1594	0.38	160

a:  $\lambda_{\text{ex}}=510\text{nm}$ ; b:  $\lambda_{\text{ex}}=495\text{nm}$ .

### 3.4.4 Electrochemical studies

The electrochemical properties of **135** and **137** have been determined in dichloromethane using cyclic voltammetry (Figure 3.20). The first *s*-tetrazine reduction found at  $-0.77\text{V}$  for both compounds is completely reversible. Processes at lower potentials are irreversible. The reduction potential of benzimidazole is reported at about  $-1\text{V}$  in MeCN (*vs*  $\text{Ag}/\text{Ag}^+$ )<sup>16</sup>. The second electrochemical process can then be attributed to benzimidazole and the third one to the second reduction of *s*-tetrazine. It is interesting to note that even when the potential is lowered to  $-2\text{V}$ , the reoxydation of the anion radical of *s*-tetrazine is still reversible like in other derivatives already presented.

Additionally, the first redox potential for **135** and **137** found at  $-0.77\text{V}$  (*vs*  $\text{Ag}/\text{Ag}^+$ ) is shifted by  $+0.2\text{V}$  compared to chloromethoxy-*s*-tetrazine ( $-0.99\text{V}$ )<sup>2</sup>. It is rather difficult to explain this change which was not observed in dyads **110** or **112** of similar structures.





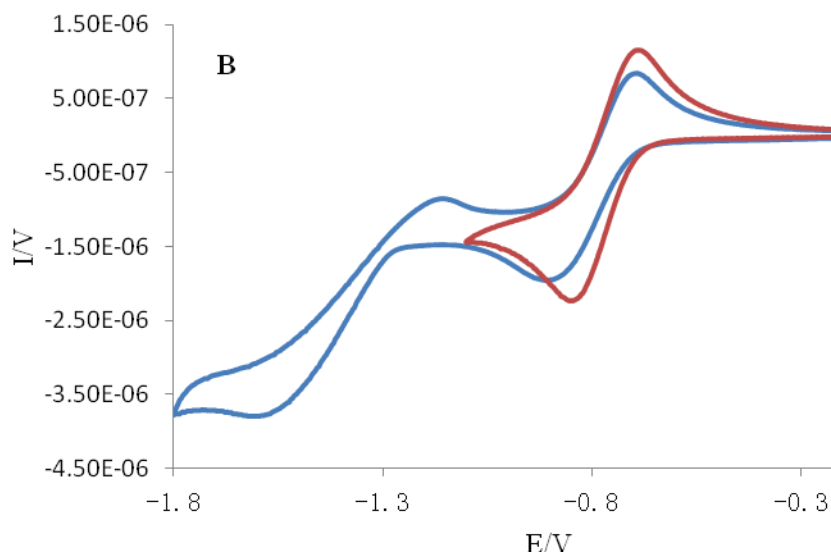


Figure 3.20. CV's of tetrazine **137** (A) and **135** (B) in dichloromethane at different potentials (scan rate:  $100\text{mV s}^{-1}$ ).

In conclusion, new *s*-tetrazines-benzimidazole dyads have been prepared. On one occasion (**141**) the product was too unstable to be studied. Photophysical studies showed that the nature of the 2-substituent on the benzimidazole is crucial since it can act as a fluorescence quencher when it is oxydazble. Hence the dyads **135** and **137** can not be considered for further study of the energy transfer but replacement of the electron rich substituent by an electron withdrawing one should lead to benzimidazoles suitable as energy donor for *s*-tetrazine.

### 3.5 Concluding remarks

In this chapter, different types of *s*-tetrazine derivatives have been synthesized and studied in order to gain better insight into their physico-chemical properties. It appears that the size of the substituent on *s*-tetrazine does not change its properties contrary to its electron affinity. It is clear that attachment of electron donor groups quenches the fluorescence of *s*-tetrazine (see *e.g.* derivatives **124** and **125**) even if they are not directly linked as seen in molecules **97** or **135** and **137**. However, this result could be used to design new fluorescent switches based on *s*-tetrazine where the emission can be externally controlled by a remote functional substituent. For example, the substituent could be electroactive and the fluorescence controlled by its redox state<sup>17</sup>. Another possibility is the design of off-on fluoroionophores for cations based on photoinduced electron transfer.

A new type of *s*-tetrazine derivatives have also been obtained through an unexpected reactivity of chloro-*s*-tetrazines. Indeed, it was demonstrated for the first time that these derivatives can undergo nucleophilic substitution with *n*-butyl lithium

to give unsymmetrical *s*-tetrazines bearing one heteroatom and one alkyl chain. Furthermore, these rather unique derivatives retain the usual properties of *s*-tetrazines (fluorescence, electroactivity). This reaction could find some applications in the development of non hydrolysable *s*-tetrazine for biolabeling.

Finally, exploratory work toward the design and synthesis of new fluorescent *s*-tetrazines dyads has been done. It results that naphthalimide and carefully selected benzimidazole can act as energy donors and that the link between the two should be an alkyl chain. In any way, to remain fluorescent, the dyads should never possess an electron donating group whatever its position. Further development of this research will be presented in the next chapter.

## Reference

1. Kim, Y.; Kim, E.; Clavier, G.; Audebert, P., New tetrazine-based fluoro-electrochromic window; modulation of the fluorescence through applied potential. *Chem Commun* **2006**, (34), 3612-3614.
2. Clavier, G.; Audebert, P., s-Tetrazines as Building Blocks for New Functional Molecules and Molecular Materials. *Chem Rev* **2010**, *110* (6), 3299-3314.
3. Gong, Y. H.; Miomandre, F.; Meallet-Renault, R.; Badre, S.; Galmiche, L.; Tang, J.; Audebert, P.; Clavier, G., Synthesis and Physical Chemistry of s-Tetrazines: Which Ones are Fluorescent and Why? *Eur J Org Chem* **2009**, (35), 6121-6128.
4. Audebert, P.; Miomandre, F.; Clavier, G.; Vernieres, M. C.; Badre, S.; Meallet-Renault, R., Synthesis and properties of new tetrazines substituted by heteroatoms: Towards the world's smallest organic fluorophores. *Chem-Eur J* **2005**, *11* (19), 5667-5673.
5. Gong, Y. H.; Audebert, P.; Tang, J.; Miomandre, F.; Clavier, G.; Badre, S.; Meallet-Renault, R.; Marrot, J., New tetrazines substituted by heteroatoms including the first tetrazine based cyclophane: Synthesis and electrochemical properties. *J Electroanal Chem* **2006**, *592* (2), 147-152.
6. Farago, J.; Novak, Z.; Schlosser, G.; Csampai, A.; Kotschy, A., The azaphilic addition of organometallic reagents on tetrazines: scope and limitations. *Tetrahedron* **2004**, *60* (9), 1991-1996.
7. Jun Yang, M. R. K., Weilong Li, Swagat Sahu, and Neal K. Devaraj, Metal-Catalyzed One-Pot Synthesis of Tetrazines Directly from Aliphatic Nitriles and Hydrazine. *Angew. Chem. Int. Ed.* **2012**, *51*, 1-5.
8. Newkome, G. R.; Islam, N. B.; Robinson, J. M., Chemistry of Heterocyclic-Compounds .21. Synthesis of Hexa(2-Pyridyl)Benzene and Related Phenyl(2-Pyridyl)Benzenes - Characterization of Corresponding Substituted Cyclopentenolone Intermediates. *J Org Chem* **1975**, *40* (24), 3514-3518.
9. Organic Syntheses, Vol. 23, p. 93 (1943); Coll. Vol. 3, p.807 (1955).
10. (a) Langhals, H., Control of the interactions in multichromophores: Novel concepts. Perylene bis-imides as components for larger functional units. *Helv Chim Acta* **2005**, *88* (6), 1309-1343; (b) Langhals, H.; Jaschke, H.; Bastani-Oskoui, H.; Speckbacher, M., Perylene dyes with high resistance to alkali. *Eur J Org Chem* **2005**, (20), 4313-4321.
11. Dumas-Verdes, C.; Miomandre, F.; Lepicier, E.; Galangau, O.; Vu, T. T.; Clavier, G.; Meallet-Renault, R.; Audebert, P., BODIPY-Tetrazine Multichromophoric Derivatives. *Eur J Org Chem* **2010**, (13), 2525-2535.
12. Trujillo-Ferrara, J.; Vazquez, I.; Espinosa, J.; Santillan, R.; Farfan, N.; Hopfl, H., Reversible and irreversible inhibitory activity of succinic and maleic acid derivatives on acetylcholinesterase. *Eur J Pharm Sci* **2003**, *18* (5), 313-322.
13. Flores-Sandoval, C. A.; Zaragoza, I. P.; Maranon-Ruiz, V. F.; Correa-Basurto, J.; Trujillo-Ferrara, J., Theoretical study of aryl succinic and maleic acid derivatives. *J Mol Struct-Theochem* **2005**, *713* (1-3), 127-134.
14. Jindal, D. P.; Singh, B.; Coumar, M. S.; Bruni, G.; Massarelli, P., Synthesis of 4-(1-oxo-isoindoline) and 4-(5,6-dimethoxy-1-oxo-isoindoline)-substituted phenoxypropanolamines and their beta(1), beta(2)-adrenergic receptor binding studies. *Bioorg Chem* **2005**, *33* (4), 310-324.
15. Van Gysel August, Maquestiau Andre, Vanden Eynde Jean-Jacques, Mayence Annie, Vanovervelt Jean-Claude, Process for the preparation of 1H-benzimidazoles, 1996, EP 0511187B1

16. Alberti, A.; Carloni, P.; Ebersson, L.; Greci, L.; Stipa, P., New insights into N-tert-butyl-alpha-phenylnitron (PBN) as a spin trap .2. the reactivity of PBN and 5,5-dimethyl-4,5-dihydropyrrole N-oxide (DMPO) toward N-heteroaromatic bases. *J Chem Soc Perk T 2* **1997**, (5), 887-892.
17. Quinton, C.; Alain-Rizzo, V.; Dumas-Verdes, C.; Clavier, G.; Miomandre, F.; Audebert, P., Design of New Tetrazine-Triphenylamine Bichromophores - Fluorescent Switching by Chemical Oxidation. *Eur J Org Chem* **2012**, (7), 1394-1403.



## Chapter 4 New brightly fluorescent *s*-tetrazines

We introduced several fluorescent and electroactive *s*-tetrazine compounds in chapters 2 and 3. The fluorescence properties of *s*-tetrazine are quite unusual (good fluorescence quantum yield  $\phi_F$  and long excited state lifetime  $\tau_F$ ) and have been used for the detection of electron donating molecules for example<sup>1</sup>. However, their visible absorption band comes from an  $n\text{-}\pi^*$  transition. This type of electronic transition is typically weak since the overlap between the  $n$  and  $\pi$  molecular orbitals is usually small. As a consequence,  $n\text{-}\pi^*$  transitions are characterized by a low molar absorption coefficient  $\epsilon$  which, in the case of *s*-tetrazines, is usually close to  $500 \text{ L}\cdot\text{mol}^{-1}\cdot\text{cm}^{-1}$ . As a consequence, brilliance, defined as the product  $\epsilon \times \phi_F$ , of *s*-tetrazines is low. This can be detrimental to the use of *s*-tetrazine as fluorescent biolabels or sensors. All attempts to improve the intrinsic photophysical properties of *s*-tetrazines presented before showed that they are maximized for derivatives comprising one chlorine and one alkoxy. So a different approach had to be pursued to improve the brightness.

A strategy to improve this property is to design a molecular dyad comprising a strongly absorbing moiety which can undergo excited state energy transfer (EET) with *s*-tetrazine (Figure 4.1). The overall brilliance would then be improved thanks to the combination of the large  $\epsilon$  of the energy donor and the good fluorescence properties of *s*-tetrazine.

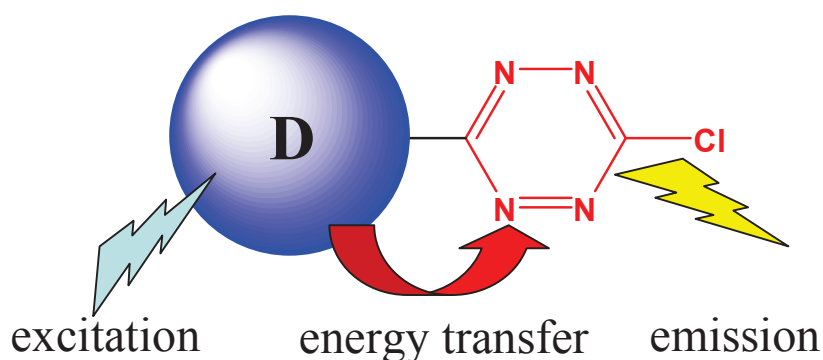


Figure 4.1. Design of molecular dyads based on *s*-tetrazine for energy transfer.

### 4.1 Resonant Energy transfer

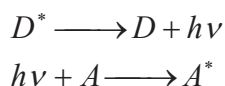
Energy transfer from an excited molecule (donor, D) to another that is chemically different (acceptor, A) according to



is called heterotransfer. This process is possible provided that the emission spectrum of the donor partially overlaps the absorption spectrum of the acceptor. There are two main types of energy transfer: radiative and non-radiative<sup>2</sup>.

It is important to distinguish between both processes since they have different effects on the photophysical properties of the partners. Their main characteristics are:

1. *Radiative transfer* is a two-step process where a photon  $h\nu$  emitted by a donor D is absorbed by an acceptor A



This process is observed when the average distance between D and A is larger than the wavelength. Such a transfer does not require any interaction between the partners, but it depends on the spectral overlap and on the concentration. Radiative transfer results in a decrease of the donor fluorescence intensity in the region of the spectral overlap. However, the donor fluorescence decay is unchanged.

2. *Non-radiative transfer* of excitation energy requires some interaction between a donor D and an acceptor A. It can occur if the emission spectrum of the donor overlaps the absorption spectrum of the acceptor, so that several vibronic transitions in the donor have practically the same energy as corresponding transitions in the acceptor (coupled transitions, figure 4.2). So non-radiative transfer occurs without emission of photons at distances less than the wavelength and results from short- or long-range interactions between molecules. Non-radiative transfer results in a homogeneous decrease of the donor fluorescence intensity over its entire spectrum and its fluorescence decay is shortened. If the acceptor is itself a fluorophore, increased fluorescence emission is observed.

In the case of molecular dyads, where the distance is short and more or less fixed, non-radiative energy transfer is favored. This transfer is often referred as *resonance energy transfer* (RET) since the in comes from the coupling of two resonant electronic transitions or *electronic energy transfer* (EET).

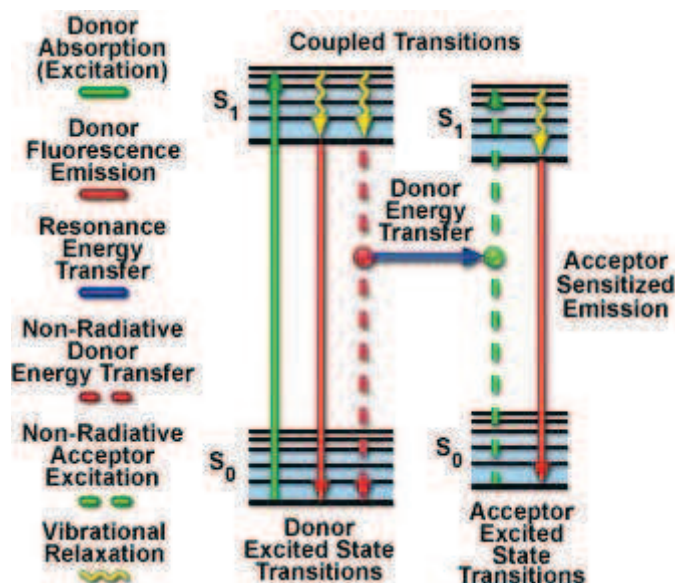


Figure 4.2. Non-radiative transfer of excitation energy depicted on a Perrin-Jablonski Diagram

RET can result from different interaction mechanisms. The interactions may be Coulombic and/ or due to intermolecular orbital overlap. The Coulombic interactions consist of long-range dipole-dipole interactions (Förster's mechanism) and short-range multi-polar interactions. The interactions due to intermolecular orbital overlap, which include electron exchange (Dexter's mechanism) and charge resonance interactions, are only short range (Figure 4.3).

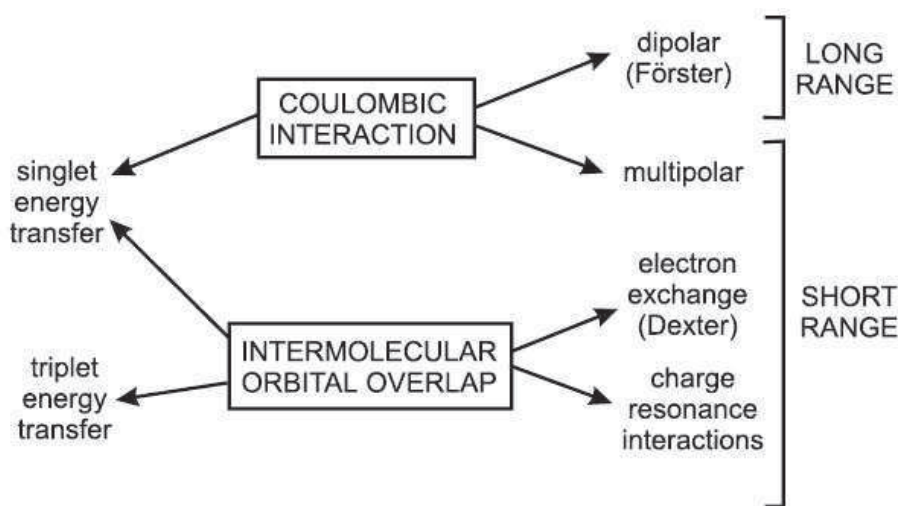


Figure 4.3. Types of interactions involved in non-radiative transfer mechanism.

The two main theories exist to study RET: Förster and Dexter. The Förster is based on long range dipole-dipole interactions. The energy transfer efficiency



between donor and acceptor molecules decrease as the sixth power of the distance separating the two. Consequently, the ability of the donor fluorophore to transfer its excitation energy to the acceptor by non-radiative interaction decreases sharply with increasing distance between the molecules, limiting the RET phenomenon to a maximum donor-acceptor separation radius of approximately 10 nanometers. At distances less than 1 nanometer, several other modes of energy and / or electron transfer are possible and Dexter theory should be considered. An additional requirement for resonance energy transfer is that the fluorescence lifetime of the donor molecule must be of sufficient duration to permit the event to occur. Both the rate and the efficiency of energy transfer are directly related to the lifetime of the donor fluorophore in the presence and absence of the acceptor.

According to Förster's theory, the rate of energy transfer is given by the equation:

$$K_T = \frac{1}{\tau_D^0} \left[ \frac{R_0}{r} \right]^6$$

where  $\tau_D^0$  is the donor lifetime in the absence of the acceptor,  $R_0$  is the Förster critical distance, and  $r$  is the distance separating the donor and the acceptor chromophores.  $R_0$  correspond to the distance at which transfer and spontaneous decay of the excited donor are equally probable. It can be determined from spectroscopic data since it is proportional to the fluorescence quantum yield of the donor in the absence of the acceptor, the spectral overlap between the fluorescence spectrum of the donor and the absorption spectrum of the acceptor. It also contains an orientation factor  $\kappa^2$  which depends on the relative orientation of the transition moments of the partners.

The transfer efficiency is defined as:

$$\Phi_T = \frac{K_T}{1/\tau_D^0 + K_T}$$

So the transfer efficiency can be related to the ratio  $r/R_0$ :

$$\Phi_T = \frac{1}{1 + (r/R_0)^6}$$

The Dexter theory or electron exchange is applicable at short distances since it requires overlap of molecular orbitals. The rate constant for the transfer becomes:

$$K_T = \frac{2\pi}{h} KJ' \exp\left(-\frac{2r}{L}\right)$$

where  $J'$  is an integral overlap between the fluorescence spectrum of the donor and the absorption spectrum of the acceptor (however of a different form from Förster

theory),  $L$  is the average Bohr radius and  $K$  a constant unrelated to any spectroscopic data. Hence in Dexter theory, the transfer rate  $K_T$  has an exponential dependence on distance but is difficult to determine experimentally. However, in both theories the transfer efficiency will depend on the spectral overlap of the donor and acceptor.

The energy transfer can be observed by exciting the donor with light of wavelengths corresponding to the absorption maximum of the donor fluorophore and detecting light emitted at wavelengths centered near the emission maximum of the acceptor. An alternative detection method is to measure the fluorescence lifetime of the donor fluorophore in the presence and absence of the acceptor. So the efficiency of energy transfer can be evaluated from steady state fluorescence spectra or fluorescence decays of the donor molecule and is given by:

$$\Phi_{ET} = 1 - \frac{\Phi_D}{\Phi_D^0} = 1 - \frac{\tau_D}{\tau_D^0}$$

where  $\Phi_D^0$  and  $\Phi_D$  are the donor fluorescence quantum yields in the absence and presence of acceptor, respectively and  $\tau_D^0$  and  $\tau_D$  are the decay time of the donor in the absence and presence of acceptor, respectively.

## 4.2 Molecular design and synthesis

### 4.2.1 Molecular design

From the theory developed above, the design of a molecular dyad for RET should meet several general criterions:

- overlap of the fluorescence spectrum of the energy donor and the absorption one of the acceptor

- the donor should have a reasonable fluorescence lifetime

- the two moieties should be kept at close distance but should not be conjugated

Furthermore, the special properties of *s*-tetrazine bring one major additional constraint: the energy donor should not be electron donating since it would otherwise quench the fluorescence of *s*-tetrazine by a photoinduced electron transfer (PET) process. It has been shown in the previous chapter that indeed any electron rich molecule in the vicinity of *s*-tetrazine plays a detrimental role on the fluorescence. It has also been shown that the link between the two moieties should be electronically innocent.

Two families of molecules have then been selected: benzimidazoles and imides which are known electron withdrawing fluorophores which can not be oxidized in organic solvents and have an intense absorption band in the UV range. The link will be an ethyl chain which allows short distance without electronic interference.

Preliminary studies have demonstrated that even if benzimidazole is an electron withdrawing group, the substituent R in the 2 position (figure 3.18) has to be chosen carefully since it can either lead to unstable molecules (alkyl chain) or quenching of the fluorescence of *s*-tetrazine (electron rich phenyl rings). Thus, the target benzimidazole donors selected are 2-trifluoromethyl- and 2-pentafluorophenyl-benzimidazoles (Figure 4.4).

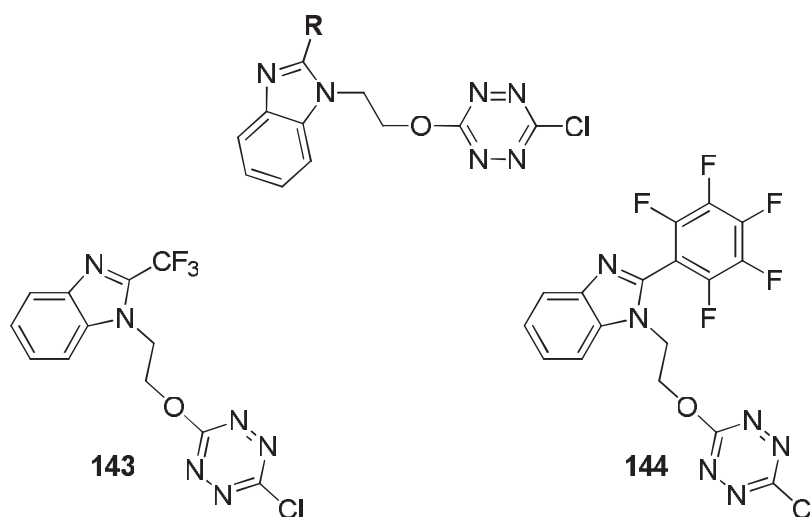


Figure 4.4. Dyads benzimidazole - *s*-tetrazine synthetic targets.

Work on the imide family has shown that all dyads synthesized were still fluorescent when an ethyl linker is used (Figure 4.5). However, phthalimide or its derivatives do not absorb light as efficiently as 1,8-naphthalimide. So the dyad nicknamed **NITZ** (112) was selected to study RET but not molecules **110** and **114**.

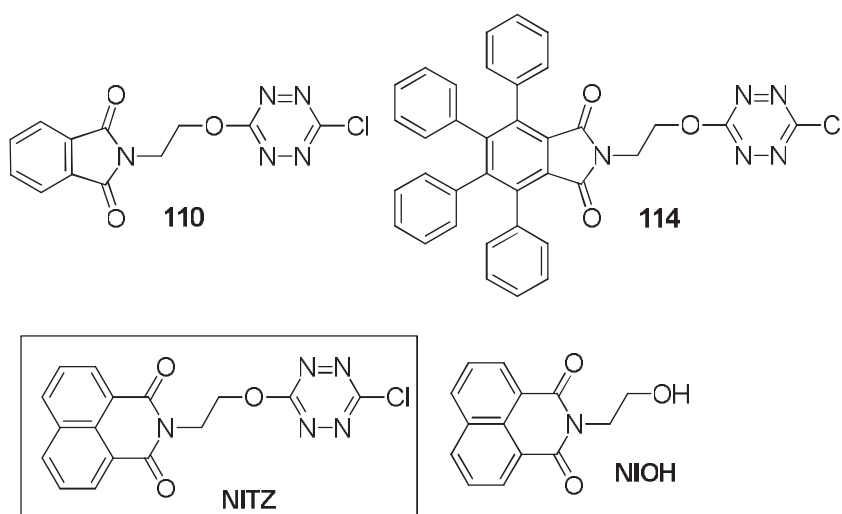


Figure 4.5. Structure of imide - *s*-tetrazines fluorescent dyads and *N*-(2-hydroxyethyl)-1,8-naphthalimide.

It was also reasoned that a reasonable approach to increase the absorption of the ensemble would be to introduce more than one energy donor moiety in a single molecule. Naphthalimide was selected for this purpose because of its intrinsic good absorption as well for its reliable chemistry. Hence two “n-ads” (n=3 or 4) comprising two or three naphthalimides have been designed (Figure 4.6) based on the available starting materials.

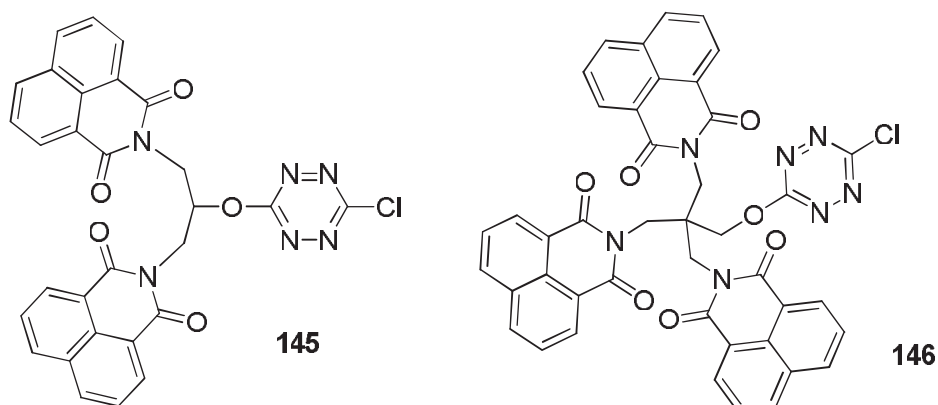
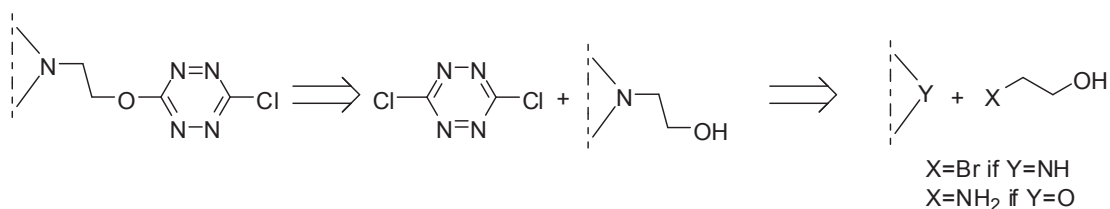


Figure 4.6. Imide - *s*-tetrazines “n-ads”.

#### 4.2.2 Preparation of the novel *s*-tetrazines n-ads

Based on previous synthetic work, the retrosynthetic scheme adopted for all dyads places as the last step the introduction of *s*-tetrazine through a  $S_NAr$  reaction between dichloro-*s*-tetrazine and a hydroxyl appended benzimidazole or naphthalimide (Scheme 4.1). Thus, the first step will be the preparation of the alcohol. The synthesis of NITZ following this scheme has already been presented in chapter 3 (molecule **112**).

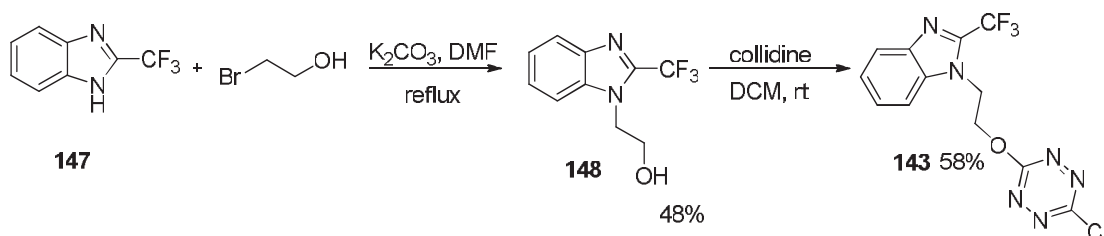


Scheme 4.1. Retrosynthetic scheme for the dyads.

The synthesis of molecules **145** and **146** will adopt a similar strategy: first an *n*-mer alcohol of the naphthalimide will be prepared followed by introduction of *s*-tetrazine.

#### 4.2.2.1 Preparation of compound **143**

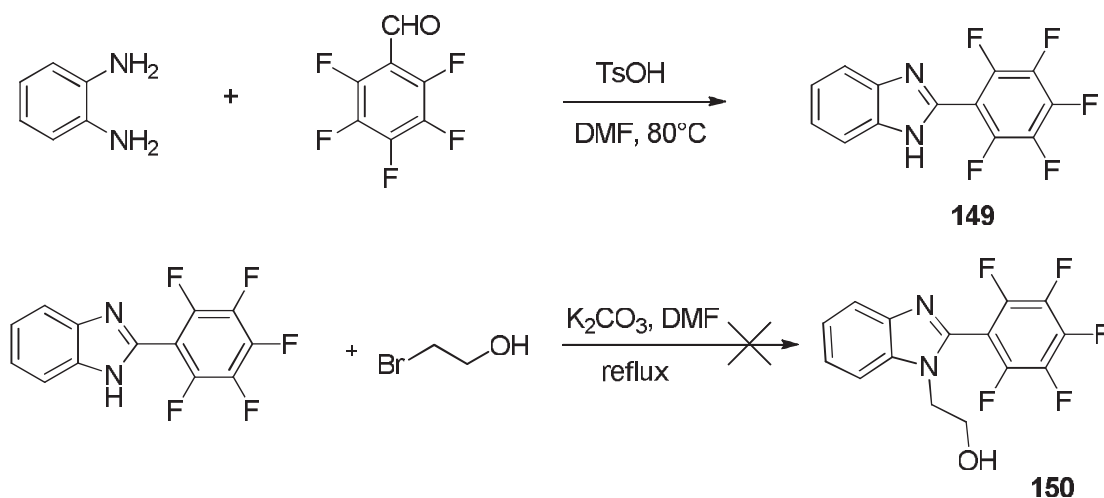
*N*-(2-hydroxyethyl)-2-trifluoromethyl-benzimidazole was synthesized by the reaction of 2-bromoethanol and 2-trifluoromethyl-1H-benzimidazole which is commercial. Two procedures were compared. First benzimidazole and 2-bromoethanol were refluxed for 18 hours in *N,N*-dimethylformamide in the presence of potassium carbonate (Scheme 4.2). Product **6** was obtained in 48% yield. Second, microwave activation was applied instead of temperature. The reaction gave the same outcome (similar yield) but in a shorter time (1.5+1.5h). Subsequently alcohol **148** and dichloro-*s*-tetrazine were coupled using the usual  $S_NAr$  conditions and compound **143** was obtained with 58% yield.



Scheme 4.2. Preparation of **143**

#### 4.2.2.2 Preparation of compound **144**

*N*-(2-hydroxyethyl)-2-pentafluorophenyl-benzimidazole **149** was prepared according to a reported synthetic procedure<sup>3</sup> by acid catalyzed condensation of pentafluorobenzaldehyde with *o*-phenylenediamine in 25% yield (Scheme 4.3). Unfortunately, the nucleophilic substitution reaction of **149** on 2-bromoethanol failed as indicated by NMR analysis of the crude product.

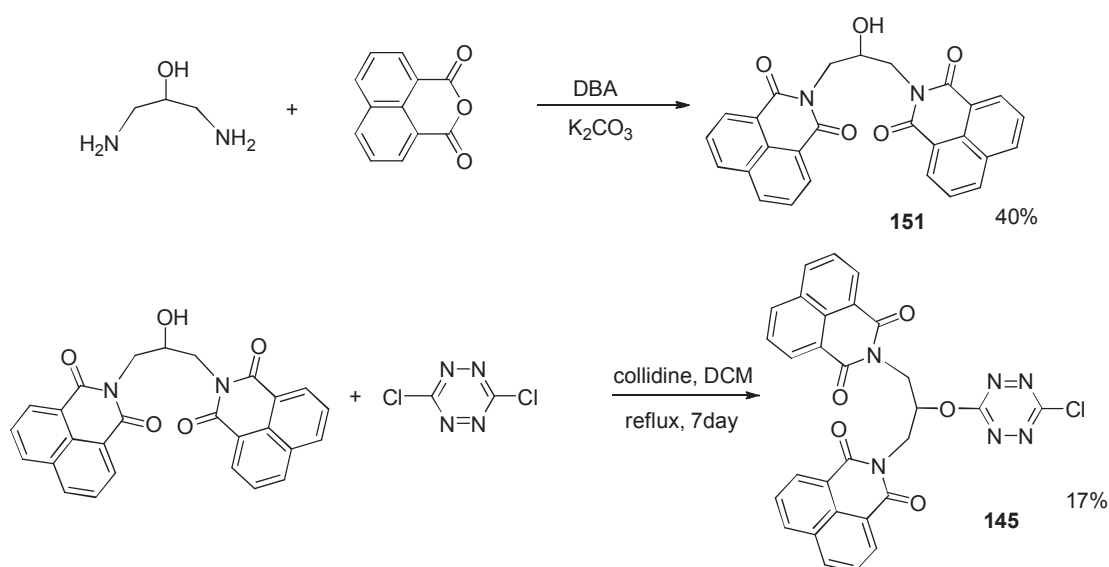


Scheme 4.3. Attempt to prepare benzimidazole **150**.

Perfluorinated phenyl rings are known to be susceptible to nucleophilic substitution reactions primarily with primary amines and thiols in organic solvents<sup>4</sup>. Despite the absence of one of those nucleophiles in the medium, it is possible that under the quite forcing conditions used (DMF, reflux), a weaker one like an alcohol could react in the same manner and failed to give the expected product. This shortage prevented us to get the target benzimidazole dyad **144**.

#### 4.2.2.3 Preparation of compound **145**

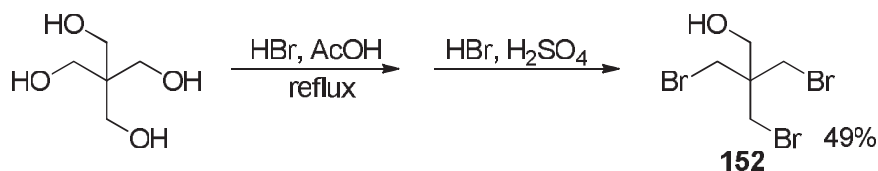
The intermediate bis-naphthalimide alcohol **151** was conveniently prepared from the commercially available 1,3-diamino-2-propanol and 1,8-naphthalic anhydride (scheme4). The reaction was carried out in *N,N*-dimethylacetamide (DMA) at 100°C and gave **151** in 40% yield. However, introduction of *s*-tetrazine was not so successful. No target *s*-tetrazine **145** could be obtained when the standard S<sub>N</sub>Ar conditions were applied (dichloro-*s*-tetrazine, collidine in DCM at room temperature) even after long reaction time. Thus, stronger conditions had to be applied: excess dichloro-*s*-tetrazine at 70°C for 7 days, to obtain **145** with 17% yield. This result again confirmed the weaker reactivity of secondary alcohols toward the S<sub>N</sub>Ar reaction on dichloro-*s*-tetrazine.



Scheme 4.4. Synthesis of **145**.

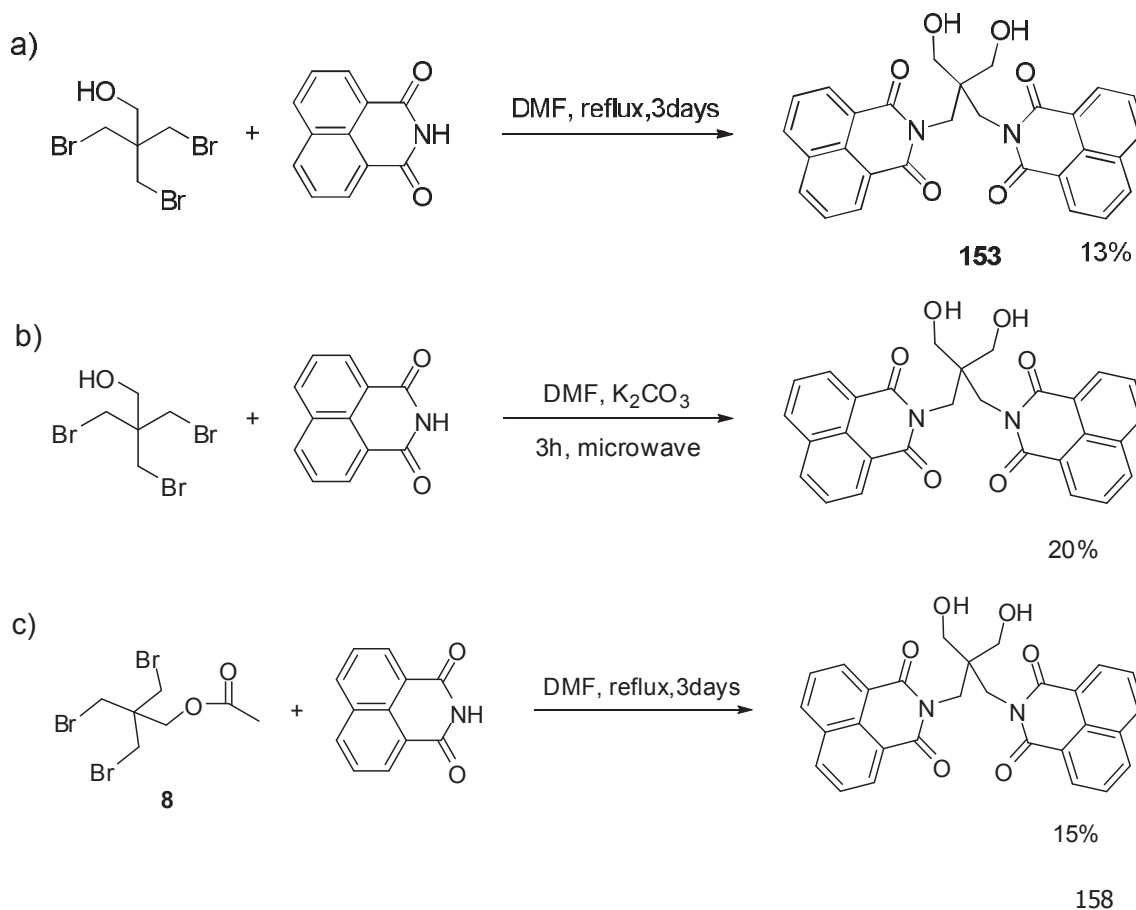
#### 4.2.2.4 Preparation of compound **146**

The synthesis of compound **146** first necessitates the preparation of a tribromo alcohol which is not commercial. Pentaerythritol was selected as the starting compound and three of its hydroxyl groups could be substituted by bromine cleanly using bromic acid to give **152** (Scheme 4.5)<sup>5</sup>.



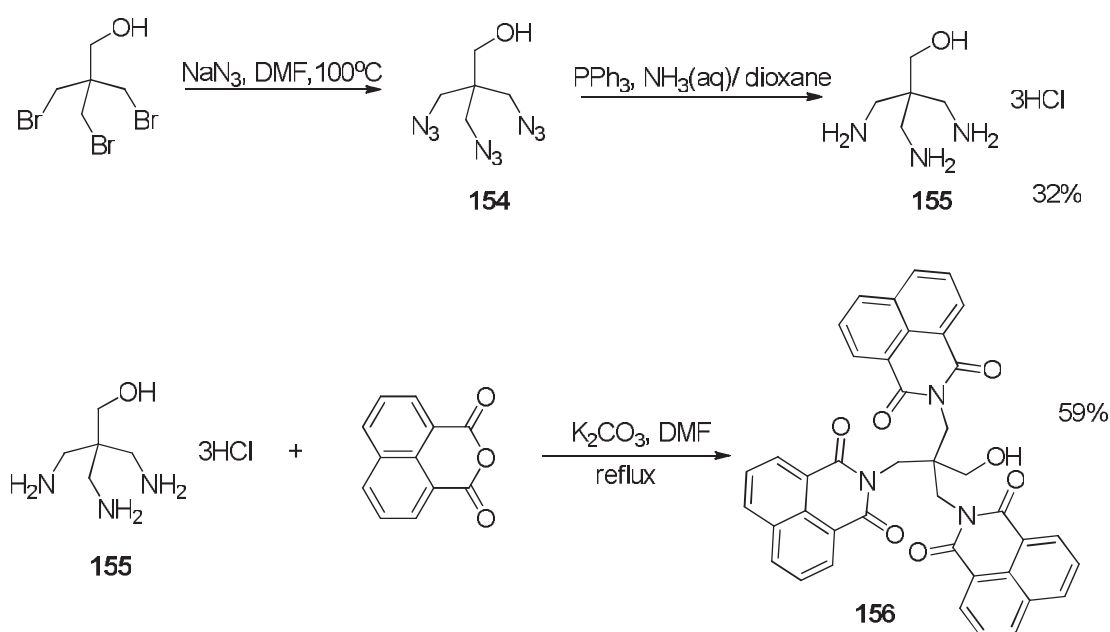
Scheme 4.5. Preparation of the tribromo alcohol **152**

Compound **152** was then directly reacted with naphthalimide in refluxing DMF but failed to give the expected product. A bis-naphthalimide product was obtained instead (Scheme 4.6a). NMR analysis of the product revealed that one bromide has been lost in the course of the reaction and was replaced by a hydroxyl to give compound **153** probably because of traces of water in the media. However, addition of a drying agent (potassium carbonate, Scheme 4.6b) or modification of the starting tribromo alcohol into its O-acetyl form (Scheme 4.6c) gave the same results. The hydrolysis of one bromide during the course of the reaction seems to be unavoidable so the starting alcohol had to be further modified.



Scheme 4.6. Different approaches attempted to prepare a tris-naphthalimide from 1,8-naphthalimide.

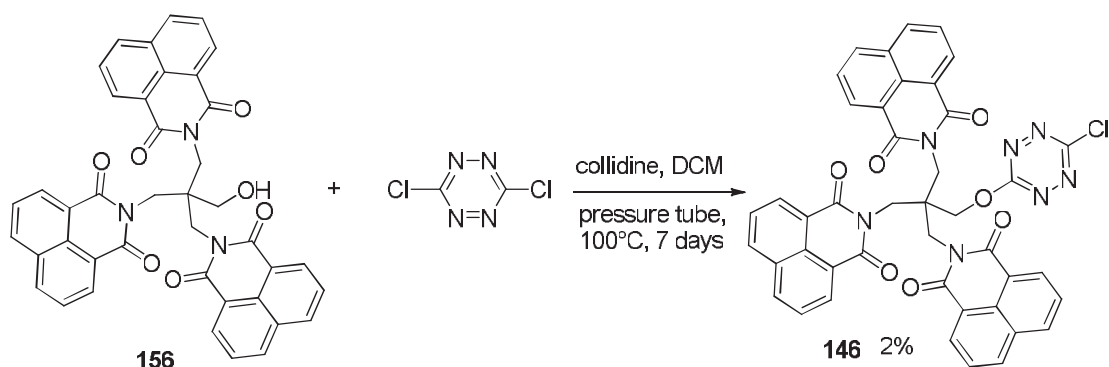
Since introduction of the naphthalimide can also be done by reaction of an amine with naphthalic anhydride, molecule **152** was further converted in two steps in the triamino alcohol **155** (refmolec10) which does not have any hydrolysable group (Scheme 4.7). First, bromines are converted to azides to give compound **154** which is then converted to **155** by a Staudinger reaction. Reaction of **155** with 1,8-naphthalic anhydride using similar conditions to the synthesis of **151**, gave the tris-naphthalimide **156** in good yield ( $\approx 60\%$ ).



Scheme 4.7. Preparation of the triamino alcohol **154** and tris-naphthalimide **156**.

Compound **156** and dichloro-*s*-tetrazine were then reacted under the usual conditions (collidine in DCM at room temperature) but no new product could be detected. Various alternative reaction conditions have been tested: reflux, long reaction time or excess dichloro-*s*-tetrazine but failed to give the expected product. Microwave activation only led to decomposition of dichloro-*s*-tetrazine. Finally compound **146** could be obtained in low yield by running the reaction in a pressure tube for 7 days (Scheme 4.8).





Scheme 4.8. Preparation of **146**.

Four “n-ads” containing *s*-tetrazines have been synthesized: compounds **143**, **112**, **145** and **146** and their physico-chemical properties have been examined giving particular care to the study of energy transfer.

### 4.3 Spectroscopic studies of *N*-(2-(6-chloro-*s*-tetrazine-3-yloxy)ethyl)-2-trifluoromethylbenzimidazole **143**

#### 4.3.1 Electrochemical study

The electrochemical study of *N*-(2-(6-chloro-*s*-tetrazine-3-yloxy)ethyl)-2-trifluoromethyl-benzimidazole **143** has been performed, using cyclic voltammetry to characterize not only the *s*-tetrazine electrochemistry but also the reduction of the benzimidazole. Figure 4.7 shows the CV response of *N*-(2-(6-chloro-*s*-tetrazine-3-yloxy)ethyl)-2-trifluoromethyl-benzimidazole, where the completely reversible first reduction of the *s*-tetrazine is followed, at lower potentials, by another wave. The reduction potential of *s*-tetrazine is found at -0.83V, which is close to the standard reduction potential of chloro-methoxy-*s*-tetrazine. Thus, *s*-tetrazine in dyad **143** is not electronically coupled to the benzimidazole. The second system is irreversible, and there is a slight increase in the observed current. This is likely due to the existence of some overlap between the beginning of the second (sluggish and irreversible) reduction of the tetrazine and the benzimidazole reduction, which occur at comparable potentials.

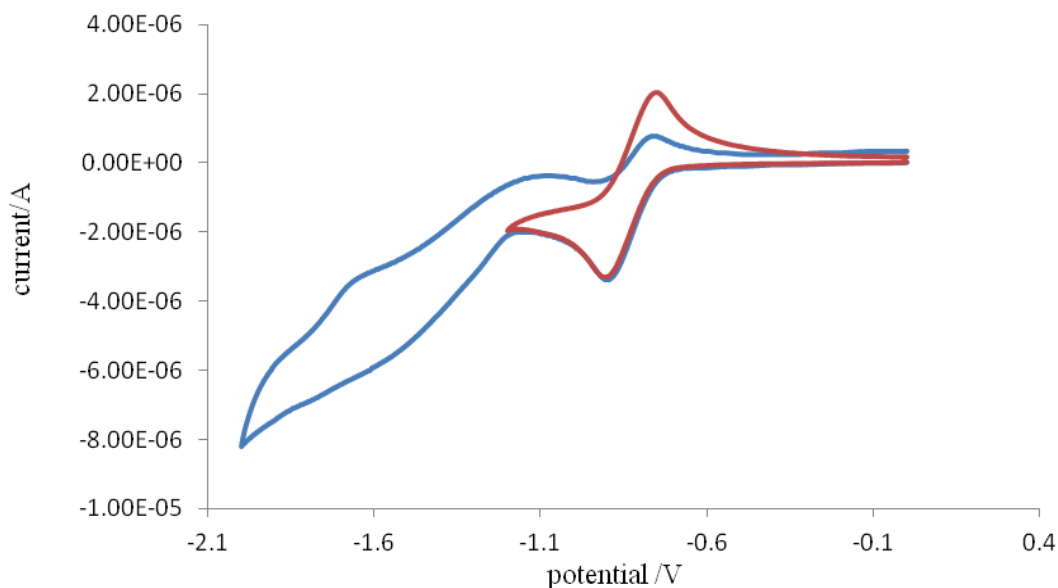


Figure 4.7: Cyclic voltammogram of *N*-(2-(6-chloro-*s*-tetrazine-3-yloxy)ethyl)-2-trifluoromethyl-benzimidazole **143** (1mm diameter Pt electrode, 100 mV/s, DCM/TBAFP, potentials vs. Ag/  $10^{-2}$  M Ag<sup>+</sup>).

### 4.3.2 Absorption and fluorescence studies

The UV-vis absorption spectra of *N*-(2-hydroxyethyl)-2-trifluoromethyl-benzimidazole **148** and *N*-(2-(6-chloro-*s*-tetrazine-3-yloxy)ethyl)-2-trifluoromethyl-benzimidazole **143** recorded in solution in dichloromethane are shown in figure 4.8. As other *s*-tetrazines, *N*-(2-(6-chloro-*s*-tetrazine-3-yloxy)ethyl)-2-trifluoromethyl-benzimidazole have two absorption bands: one at 314nm and one at 511nm respectively corresponding to the  $\pi$ - $\pi^*$  transition and n- $\pi^*$  transition of *s*-tetrazine. However, compared to the simple chloromethoxy-*s*-tetrazine, it has one more intense absorption band below 300 nm. The exact same band can be seen on the spectra of *N*-(2-hydroxyethyl)-2-trifluoromethyl-benzimidazole and can then be attributed to the  $\pi$ - $\pi^*$  transition of benzimidazole. Thus, the two moieties of the dyad retain their own individual spectroscopic features and behave as independent chromophores. It is also noteworthy that the UV absorption of benzimidazole is stronger than that of *s*-tetrazine and both transitions has a very small overlap.

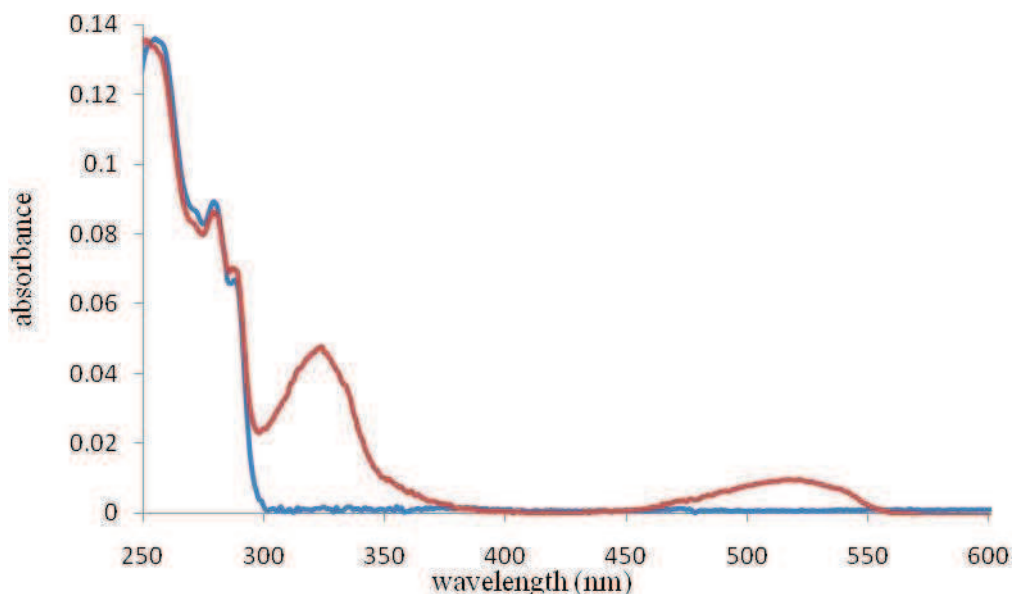


Figure 4.8. Absorption spectra of *N*-(2-(6-chloro-*s*-tetrazine-3-yloxy)ethyl)-2-trifluoromethyl-benzimidazole **143** (red) and *N*-(2-hydroxyethyl)-2-trifluoromethyl-benzimidazole **148** (blue) recorded in DCM at the same concentration.

Regarding fluorescence properties, *N*-(2-hydroxyethyl)-2-trifluoromethyl-benzimidazole **148** behaves like a classic benzimidazole<sup>6</sup> (Figure 4.9). Its maximum emission is found at 320nm and its fluorescence quantum yield is  $\Phi_F=0.28$ . Comparison of this spectrum with the absorption one of compound **143** shows that they partially overlap. It is important to note that this overlap is greater in the UV region than the visible one.

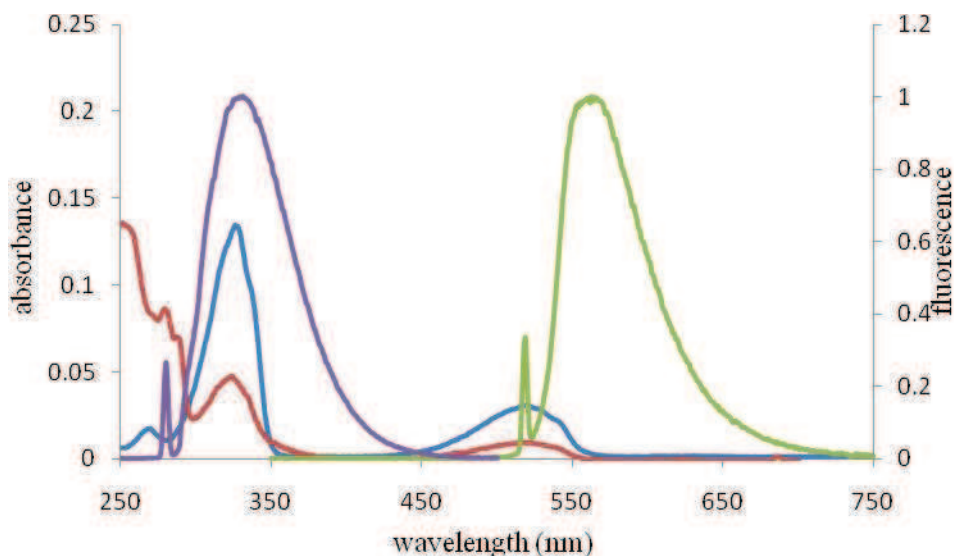


Figure 4.9. Absorption spectrum of *N*-(2-(6-chloro-*s*-tetrazine-3-yloxy)ethyl)-2-trifluoromethyl-benzimidazole **143** (red) and chloromethoxy-*s*-tetrazine (blue); fluorescence spectrum of *N*-(2-hydroxyethyl)-2-trifluoromethyl-benzimidazole **148** (purple) ( $\lambda_{\text{ex}}=280\text{nm}$ ) and (green) ( $\lambda_{\text{ex}}=518\text{nm}$ ).

In summary, it is important to note that the two chromophores behaves independently in the dyad, the *s*-tetrazine moiety is still fluorescent, the benzimidazole moiety has an intense absorption band below 300nm, and the emission spectrum of **148** overlaps the  $\pi$ - $\pi^*$  absorption band of *s*-tetrazine. So it is possible to have an energy transfer process between the  $S_1$  state of benzimidazole and the  $S_2$  state *s*-tetrazine.

### 4.3.3 Study of the energy transfer in 143

Fluorescence spectra of **143** were recorded upon excitation of the benzimidazole moiety ( $\lambda_{\text{ex}}=280\text{nm}$ ) and *s*-tetrazine moiety ( $\lambda_{\text{ex}}=518\text{nm}$ ), and compared to the fluorescence spectra of **148** excited at  $\lambda_{\text{ex}}=280\text{nm}$  (Figure 4.10).

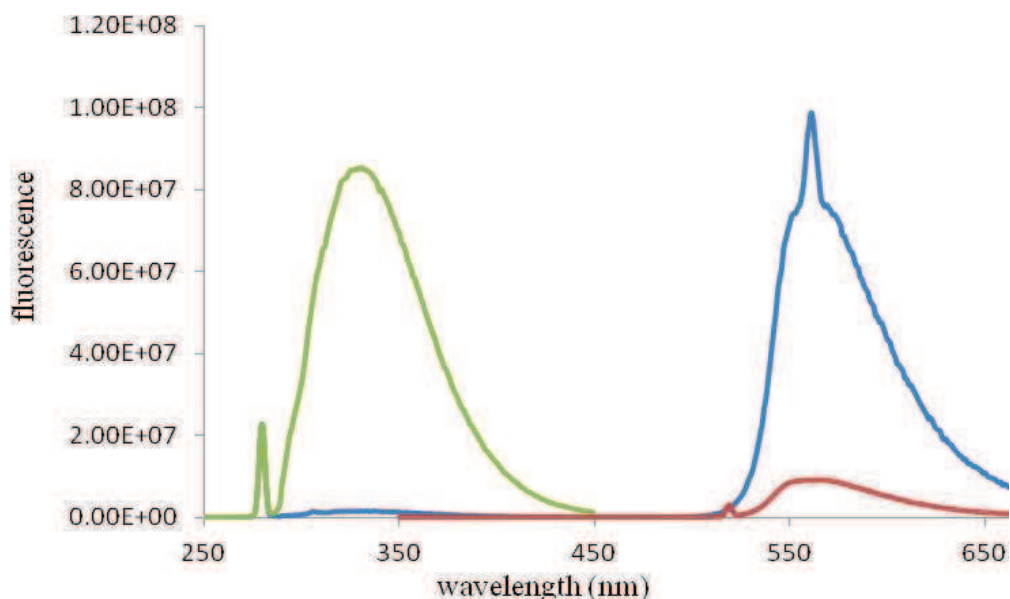


Figure 4.10. Fluorescence spectra of **148** (green) and **143** (blue) at  $\lambda_{\text{ex}}=280\text{nm}$  (normalization the range 280nm-480nm) and **143** at  $\lambda_{\text{ex}}=518\text{nm}$  (red), recorded at the same concentration in dichloromethane. The peak at 560nm in the blue spectrum corresponds to the second harmonic of the excitation wavelength.

The fluorescence spectrum of *N*-(2-(6-chloro-*s*-tetrazine-3-yloxy)ethyl)-2-trifluoromethyl-benzimidazole **143** upon excitation at 280nm has two bands: one from

the benzimidazole moiety and one from the *s*-tetrazine moiety. The first band has the same maximum as **148** (320nm) but its intensity is considerably smaller. It indicates that there is a highly efficient energy transfer in this molecule between the donor and the acceptor. In addition, almost all the recorded fluorescence is emitted by the *s*-tetrazine core, with an 8.5 increased intensity compared to that observed upon excitation of *s*-tetrazine in its  $n-\pi^*$  absorption band. So the study of fluorescence of **143** evidences the occurrence of an energy transfer between the two chromophores.

Measurement of the fluorescence lifetimes of the donor fluorophore in the presence and absence of the acceptor is an alternative detection method of energy transfer. It also can explain the mechanism underlying the energy transfer. So the fluorescence decays of the benzimidazole moiety of **148** and **143** were recorded after excitation at  $\lambda_{\text{ex}}=290\text{nm}$  (Figure 4.11). The decays could be fitted by a single exponential function and the fluorescence lifetimes for the benzimidazoles are 16.6ns in the first case and 17.7ns in the second one. Hence similar values for both benzimidazoles are obtained. This is a quite surprising result that points out to a non radiative energy transfer process. *s*-Tetrazine fluorescence decays have also been recorded after excitation at 290nm (Figure 4.12) and at 495nm (Figure 4.13). They could also be fitted by a single exponential function and the fluorescence lifetimes are in both cases equal to 160ns which is a typical value for *s*-tetrazine. The decay profile of **143** does not display any rising time as could be expected from a non radiative energy transfer. However, this could come from the instrumental resolution which is in the order of a few nanoseconds with the set-up used.

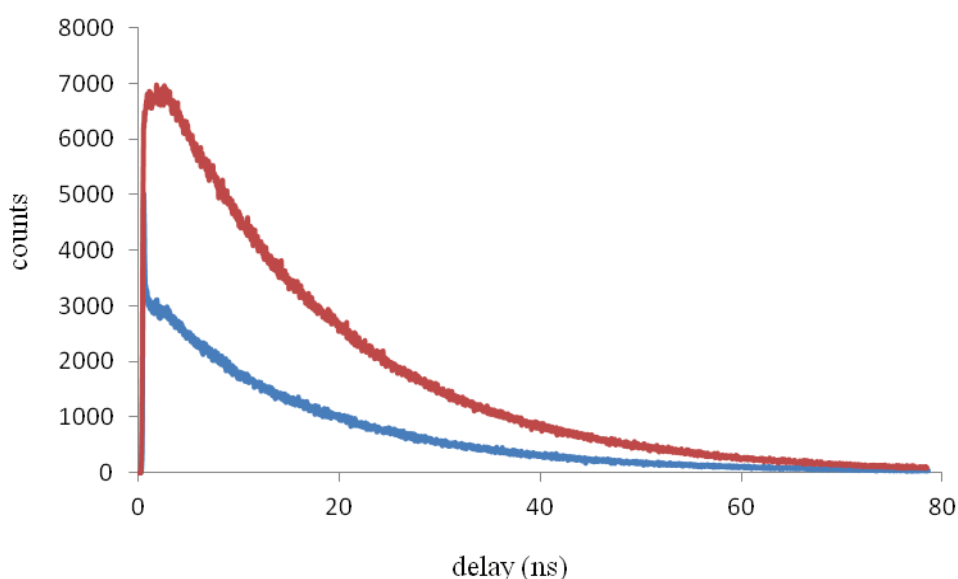


Figure 4.11. Fluorescence decay profiles of *N*-(2-(6-chloro-s-tetrazine-3-yloxy)ethyl)-2-trifluoromethyl-benzimidazole **143** (blue) and *N*-(2-hydroxyethyl)-2-trifluoromethyl-benzimidazole **148** (red) recorded at  $\lambda_{em}=350\text{nm}$  after excitation at 290nm.

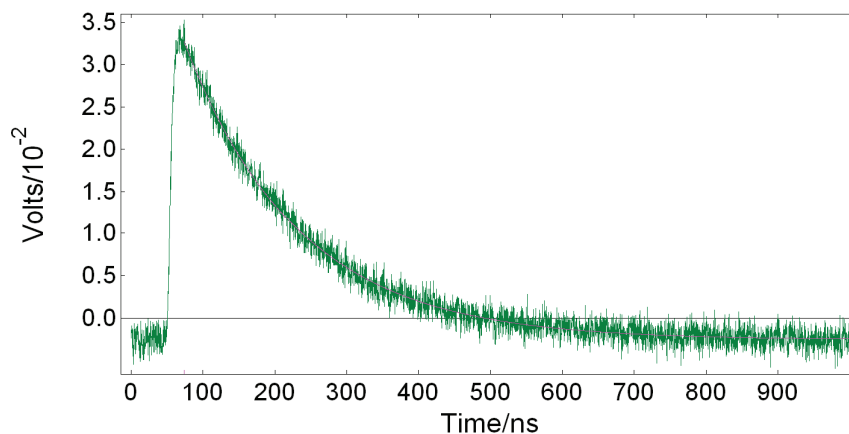


Figure 4.12. Fluorescence decay profiles of **143** recorded at  $\lambda_{em}=575\text{nm}$  after excitation at  $\lambda_{ex}=290\text{nm}$ . The red line corresponds to the monoexponential fit.

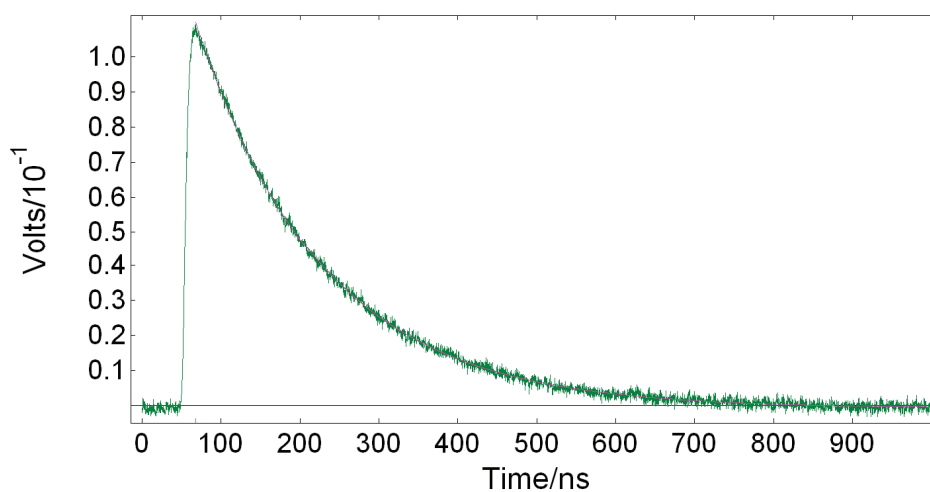


Figure 4.13. Fluorescence decay profiles of **143** recorded at  $\lambda_{em}=575\text{nm}$  after excitation at  $\lambda_{ex}=495\text{nm}$ . The red line corresponds to the monoexponential fit.

The spectroscopic data relevant to the energy transfer are reported in table 4.1.

Table 4.1. Detailed Spectroscopic data for **143** and **148**.

Molecule/	$\lambda_{abs}$ (nm)	$\epsilon$ ( $\text{L}\cdot\text{mol}^{-1}\cdot\text{cm}^{-1}$ )	$\lambda_{em}$ (nm)	$\Phi_{fluo}$	$\epsilon_{(\lambda_{ex})}\times\Phi_{fluo}$	$\tau_{fluo}$ (ns)
-----------	-------------------------	---	------------------------	---------------	--	-----------------------

	253					
<b>148</b>	280	3600 (280)	320 <sup>a</sup>	0.28 <sup>a</sup>	1008	17.7 <sup>c</sup>
	287					
<b>143</b> (tetrazine data)	518	580	555 <sup>b</sup>	0.36 <sup>b</sup>	209 (1548 <sup>a</sup> )	159 <sup>c</sup> , 161 <sup>d</sup>
<b>143</b> (imide data)	280	4300	320 <sup>a</sup>	0.005 <sup>a</sup>	22	16.6 <sup>c</sup>

<sup>a</sup>  $\lambda_{\text{ex}}=280$  nm; <sup>b</sup>  $\lambda_{\text{ex}}=518$  nm; <sup>c</sup>  $\lambda_{\text{ex}}=290$  nm; <sup>d</sup>  $\lambda_{\text{ex}}=495$  nm

On the assumption that all the fluorescence lost by the donor is transferred to the acceptor, the efficiency of the energy transfer is given by:

$$\Phi_{ET} = 1 - \frac{\Phi_D}{\Phi_D^0} = 1 - \frac{0.005}{0.28} = 0.98$$

This value shows that the energy transfer is quite efficient. Additionally, the brightness of *s*-tetrazine in the dyad **143** is increased 7.4 times upon changing the excitation from 518nm to 280nm.

In conclusion, comparison of the steady state fluorescence spectra of dyad **143** and **148** proves that there is an efficient energy transfer (98%) from the benzimidazole donor to the *s*-tetrazine acceptor. Surprisingly, the fluorescence lifetimes of benzimidazole are similar in the presence and absence of the acceptor (*i.e.* in **143** and **148** respectively) and no rising time could be detected in the fluorescence decay of *s*-tetrazine in **143** after excitation of benzimidazole. These results fit the expectations for a radiative energy transfer. This is quite unusual for a molecular dyad where both partners are close to each other and further studies should be done to confirm this result.

## 4.4 Spectroscopic and electrochemical studies of NITZ

### 4.4.1 Electrochemistry

Cyclic voltammetry of NITZ has been performed to characterize the electrochemical behavior of *s*-tetrazine and 1,8-naphthalimide, which are both electroactive. Figure 4.14 shows the CV response of NITZ, where the completely reversible first reduction wave of *s*-tetrazine is followed at lower potentials by another wave which is only partially reversible. This second system also displays a slight

increase in the observed current. This is likely to be due to the existence of some overlap between the beginning of the second (sluggish and irreversible) reduction of *s*-tetrazine and the reduction of naphthalimide which occur at comparable potentials. Cyclic voltammetry of *N*-(2-hydroxyethyl)-1,8-naphthalimide (NIOH, table 4.2) confirms that naphthalimide is reduced at the same potential (-1.70V) in both molecules. Thus, the two electroactive components of NITZ are electrochemically independent and are not electronically coupled.

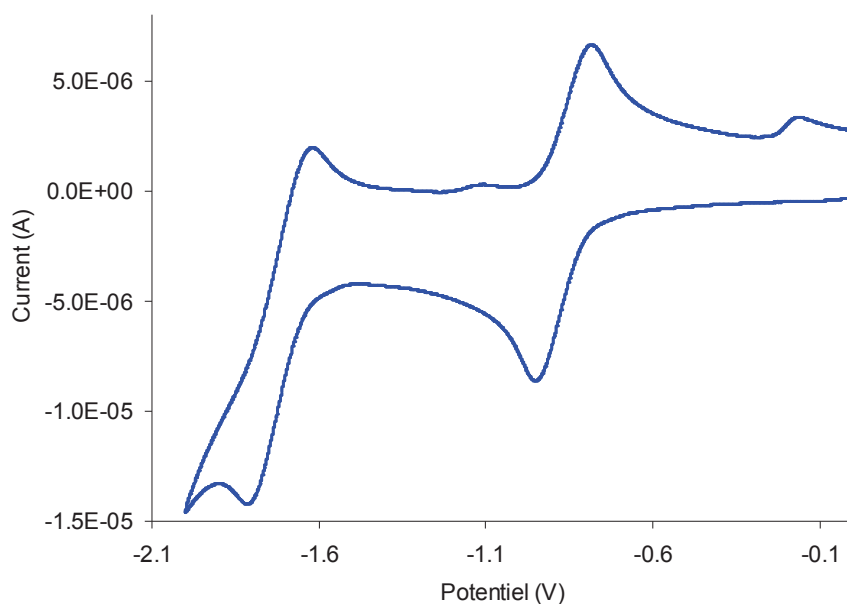


Figure 4.14. Cyclic voltammogram of **NITZ** (1 mm diameter pt) electrode, 100 mV/s, DCM/TBAFP, potentials vs. Ag/ 10<sup>-2</sup> M Ag<sup>+</sup>).

Table 4.2. Electrochemical data for **NIOH** and **NITZ**.

compound	<b>NIOH</b>	<b>NITZ</b> (tetrazine data)	<b>NITZ</b> (imide data)
$E_{red}^0/V$	-1.70	-0.86	-1.70

#### 4.4.2 Absorption and fluorescence studies

The UV-vis. absorption spectrum of **NITZ** has two main bands (Figure 4.15). The less intense one in the visible is centered at 517 nm and is typical of the  $n-\pi^*$  transition of *s*-tetrazine. The band in the UV centered at 330nm is much more intense than the typical  $\pi-\pi^*$  transition of *s*-tetrazine located in the same range as seen in figure 15a by comparison with the absorption spectrum of chloromethoxy-*s*-tetrazine. Absorption spectra of **NIOH** (Figure 4.15b) present the same intense band centered at



330nm which can safely be attributed to the first  $\pi$ - $\pi^*$  transition of 1,8-naphthalimide<sup>7</sup>. So the UV band of NITZ comes from an overlap of the  $\pi$ - $\pi^*$  transitions of *s*-tetrazine and 1,8-naphthalimide. Comparison of the absorption spectrum of NITZ and the sum of the spectra of its individual components (Figure 4.15b) shows that they are very similar which means that *s*-tetrazine and 1,8-naphthalimide moieties are independent chromophores in the dyad.

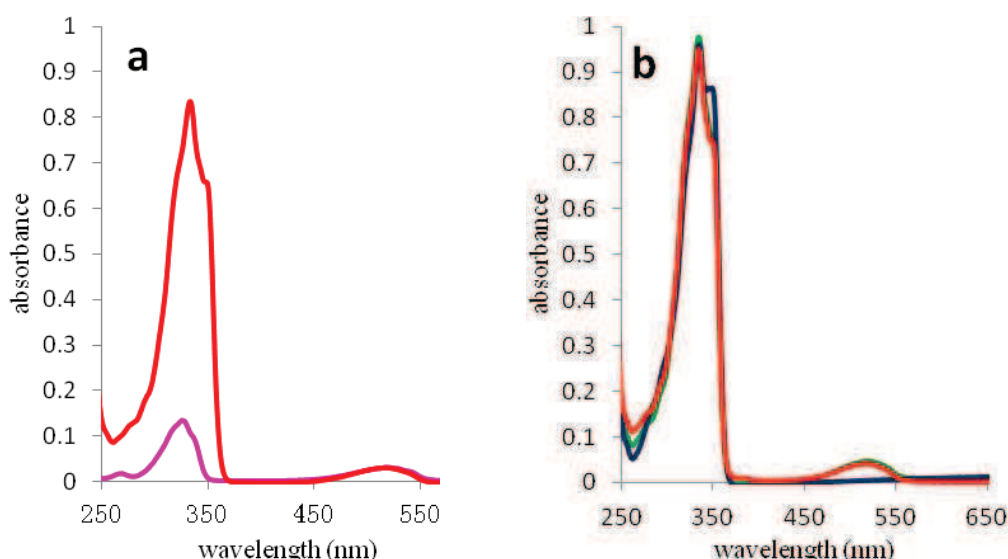


Figure 4.15. (a) Absorption spectra of NITZ (red) and chloromethoxy-*s*-tetrazine (pink); (b) Absorption spectra of NITZ (red), NIOH (blue), the sum of NIOH and chloromethoxy-*s*-tetrazine (green).

Fluorescence spectrum of NITZ excited in the visible band of *s*-tetrazine ( $\lambda_{\text{ex}}=518$  nm) have been shown in chapter 3 and it presents the usual features of the chromophore. Fluorescence spectrum of NIOH (Figure 4.16) shows that it behaves as a standard naphthalimide<sup>7</sup>. It should be noted that the fluorescence quantum yields are usually not very high with this type of compounds and is 0.06 for NIOH (Table 4.2). More interestingly, the emission spectrum of NIOH has a small overlap with the visible absorption band of NITZ. So it is possible to have energy transfer between the two moieties.

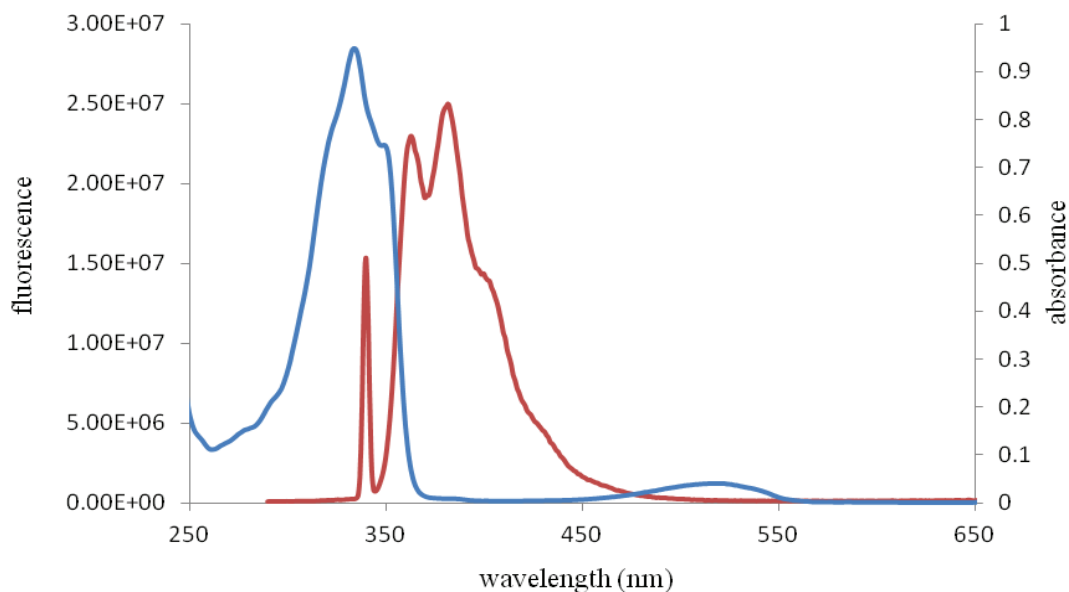


Figure 4.16. Absorption spectrum of **NITZ** (blue) and fluorescence spectrum of **NIOH** (red,  $\lambda_{\text{ex}}=340\text{nm}$ )

#### 4.4.3 Study of energy transfer

Then in order to investigate whether the energy transfer exists or not between the imide and the tetrazine, fluorescence spectra of **NITZ** were recorded upon excitation of the naphthalimide moiety ( $\lambda_{\text{ex}}=355\text{nm}$ ) and *s*-tetrazine moiety ( $\lambda_{\text{ex}}=518\text{nm}$ ), and they were compared to the emission spectrum of **NIOH** recorded for  $\lambda_{\text{ex}}=355\text{nm}$  (Figure 4.17). It is important to note that the 355 nm excitation wavelength was selected after careful examination of the absorption spectra of **NIOH** and chloromethoxy-*s*-tetrazine to ensure selective excitation of the naphthalimide<sup>a</sup>.

<sup>a</sup> It has also been verified that chloromethoxy-*s*-tetrazine excited at 355nm does not emit light.

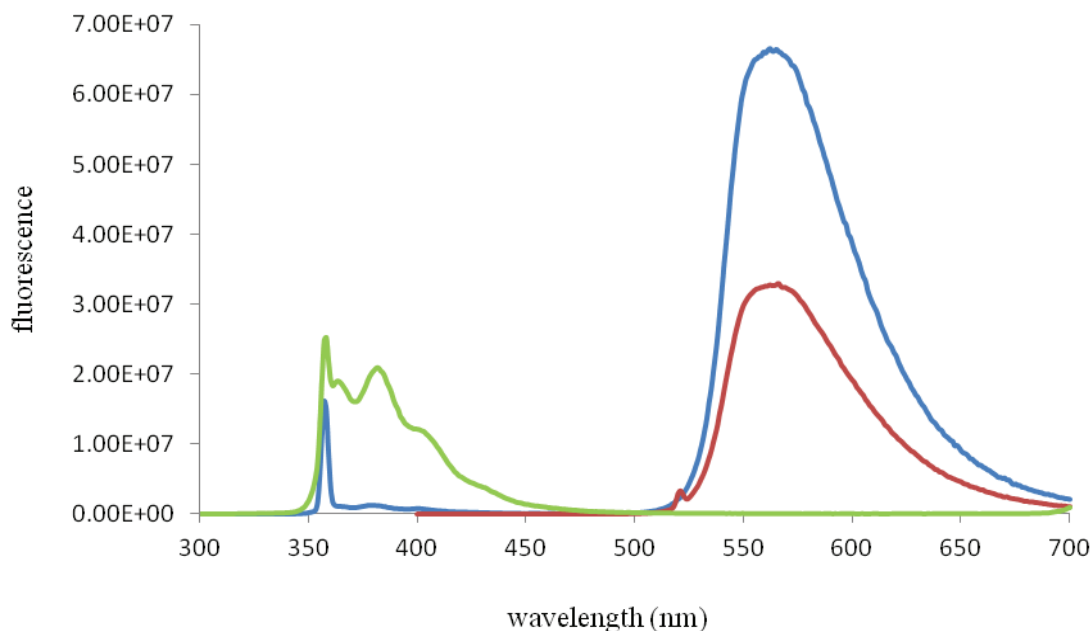


Figure 4.17. Fluorescence spectra of **NIOH** (green), **NITZ** with  $\lambda_{\text{ex}}=355\text{nm}$  (blue) and **NITZ** with  $\lambda_{\text{ex}}=518\text{nm}$  (red). All the solutions are at the same concentration.

There are two bands in the emission spectra of **NITZ** when excited at 355nm: one is due to the naphthalimide moiety and the other is corresponding to *s*-tetrazine. The first band has a similar shape to the one of **NIOH** but is considerably less intense. In addition, almost all the recorded fluorescence is emitted by the *s*-tetrazine core, with an increased intensity compared to that observed upon excitation of *s*-tetrazine in its  $n-\pi^*$  absorption band. This result evidences the occurrence of an energy transfer between the two chromophores.

Fluorescence lifetimes have also been determined to confirm the occurrence of energy transfer. The fluorescence decays of naphthalimide in **NIOH** and **NITZ** with  $\lambda_{\text{ex}}=355\text{nm}$  were recorded (Figure 4.18). Both decays could be fitted by a single exponential and the results give a fluorescence lifetime for the naphthalimide of 0.37ns in **NIOH** case and 0.03ns in **NITZ**. On the other hand, the tetrazine fluorescence decay after excitation at the same wavelength is more complex and displays a rising time. The decay could be fitted by a bi-exponential function giving a rising time of 0.06ns similar to the fluorescence lifetime of the naphthalimide in **NITZ** and a decay one of 158ns typical of the *s*-tetrazine.

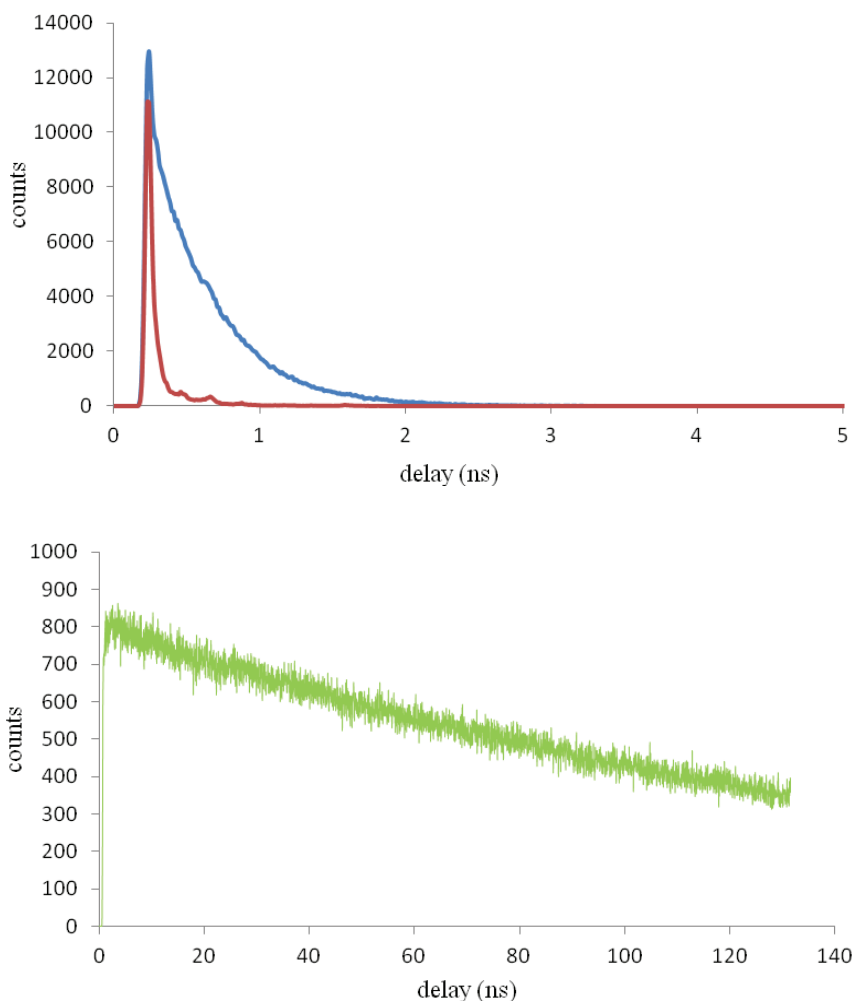


Figure 4.18. Fluorescence decay profiles upon excitation at 355nm. Top: **NIOH** (blue) and **NITZ** (red) for  $\lambda_{em}=365nm$ ; bottom: **NITZ** (green) for  $\lambda_{em}=562nm$ .

The results of the time resolved fluorescence prove that there is resonant energy transfer from the naphthalimide to the *s*-tetrazine. Furthermore, the shortening of the fluorescence lifetime of the naphthalimide in **NITZ** compared to the one in **NIOH** and the presence of a rising time in the decay of *s*-tetrazine prove that it is a non radiative process.

Further quantification and elucidation of the mechanism of the energy transfer has been done. The spectroscopic data of **NIOH** and **NITZ** relevant to the energy transfer are reported in table 4.3.

Table 4.3. Detailed Spectroscopic data for **NITZ** and **NIOH**.

Molecule/data	$\lambda_{abs}$ (nm)	$\epsilon$ (L.mol <sup>-1</sup> .cm <sup>-1</sup> )	$\lambda_{em}$ (nm)	$\Phi_{fluo}$	$\epsilon_{(\lambda_{ex})} \times \Phi_{fluo}$	$\tau_{fluo}$ (ns)
---------------	-------------------------	--	------------------------	---------------	--	-----------------------

<b>NIOH</b>	335	8700	363, 382, 402 <sup>a</sup>	0.061 <sup>a</sup>	522	0.37 <sup>c</sup>
<b>NITZ</b> ( <i>s</i> -tetrazine data)	517	400	562 <sup>b</sup>	0.32 <sup>b</sup> (0.3 <sup>c</sup> )	200 (1509)	158 <sup>c,d</sup>
<b>NITZ</b> (imide data)	334	9100	378 400 <sup>c</sup>	0.003 <sup>c</sup>	15	0.03 <sup>c</sup>

<sup>a</sup>  $\lambda_{\text{ex}}=350$  nm; <sup>b</sup>  $\lambda_{\text{ex}}=517$  nm; <sup>c</sup>  $\lambda_{\text{ex}}=355$  nm; <sup>d</sup>  $\lambda_{\text{ex}}=495$  nm

The efficiency of energy transfer can be determined using either the variation of fluorescence quantum yield or the change in fluorescence lifetimes of the naphthalimide in the presence and absence of the *s*-tetrazine acceptor. Hence, on the assumption that all the fluorescence lost by the donor is transferred to the acceptor, the efficiency of the energy transfer is given by the two following expressions.

$$\Phi_{ET} = 1 - \frac{\Phi_D}{\Phi_D^0} = 1 - \frac{0.003}{0.061} = 0.95$$

$$\Phi_{ET} = 1 - \frac{\tau_D}{\tau_D^0} = 1 - \frac{0.03}{0.37} = 0.92$$

It is noteworthy that the two calculated values of efficiency are in good agreement.

The rate associated with the transfer is:

$$K_T = \frac{1}{\tau_D} - \frac{1}{\tau_D^0} = \frac{1}{0.03} - \frac{1}{0.37} = 3.08 \times 10^{10} \text{ s}^{-1}$$

This is two orders of magnitude higher than the radiative rate of the **NIOH** ( $k_R = \Phi_{\text{fluor}}/\tau_{\text{fluor}} 1.65 \times 10^8 \text{ s}^{-1}$ ). The rate of formation of the excited state of *s*-tetrazine determined from the measured rising time is  $1.67 \times 10^{10} \text{ s}^{-1}$ . This value is in good agreement with  $K_T$  given the uncertainty on the determination of the value of the rising time which is short in front of the decay time.

The calculated transfer efficiency is quite high. According to Förster theory, the efficiency of the transfer can be obtained from the spectroscopic data. The critical Förster radius for the dyad **NITZ** was calculated from the spectral overlap and is:  $R^0 = 9.3 \text{ \AA}$  taking  $\kappa^2 = 2/3$  (isotropic dynamic average). The theoretical RET efficiency can be obtained from  $R^0$  and the distance  $r$  between the two chromophores. An estimation of the value of  $r$  was obtained by quantum mechanic geometry optimization of **NITZ**. The distance between the imide donor and the *s*-tetrazine ring acceptor mass centers

were found at  $r=8.5\text{\AA}$ . Therefore, the efficiency of the energy transfer of NITZ according to Förster theory is

$$\Phi_T = \frac{1}{1 + (r/R_0)^6} = \frac{1}{1 + (8.5/9.3)^6} = 0.63$$

The discrepancy between the calculated and the experimental values incline us to think that the energy transfer mechanism would rather be of the Dexter type or a mixed one.

The main goal of the synthesis of the dyad NITZ was to improve the overall brightness of *s*-tetrazine. It is clear from the data in table 3 that it is reached since a 7.5 times increase is obtained upon excitation of the naphthalimide instead of the *s*-tetrazine. We also made an evaluation of the improved brilliance of the molecule by simply visually comparing the brilliance of a  $5 \times 10^{-6}$  M solution of NITZ and the one of a solution of 3-(adamant-1-ylmethoxy)-6-chloro-*s*-tetrazine, which owns the same tetrazine emitter but without the presence of the imide donor. At these concentrations, both solutions are almost colorless (only the *s*-tetrazine is colored, but its absorption is low; Figure 4.19A). Figure 19B shows the fluorescence of both dilute solutions (3-(adamant-1-ylmethoxy)-6-chloro-*s*-tetrazine (left) and NITZ (right)) excited with a laboratory UV lamp peaking at 365nm. It is clear that because of the efficiency of the imide absorbance and the energy transfer, the brightness of the solution of NITZ is much higher than the one of the standard *s*-tetrazine.

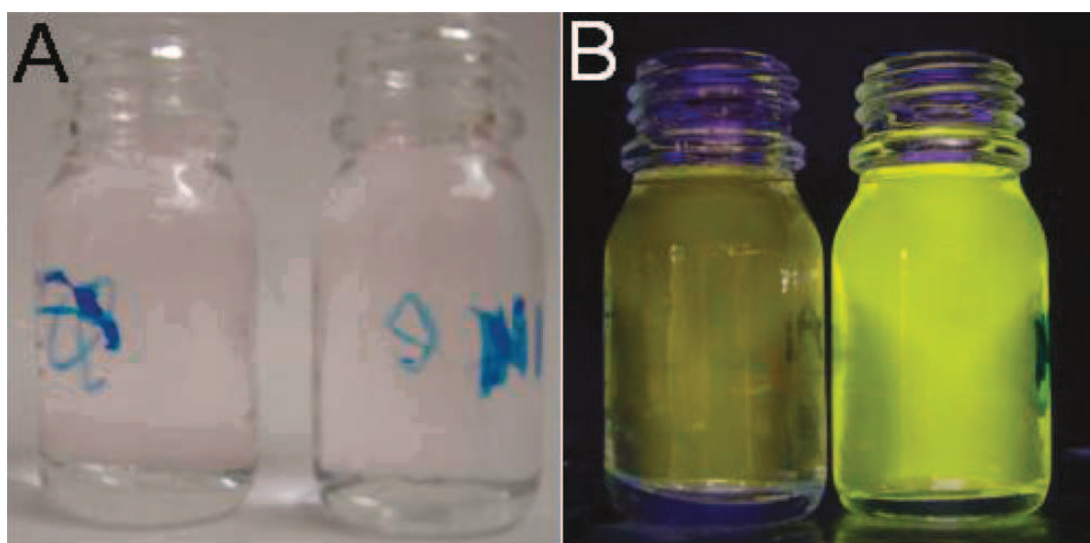


Figure 4.19. Picture of two  $5 \times 10^{-6}$  M solutions of: left, 3-(adamant-1-ylmethoxy)-6-chloro-*s*-tetrazine and right, NITZ, both in standard white light (A) and UV light (B).

It should be emphasized that this situation is solely due to the proximity of the two chromophores in the dyad molecule. Upon irradiation of a mixed solution of concentrated **NIOH** ( $c \approx 10^{-3}$  M) and diluted 3-(adamant-1-ylmethoxy)-6-chloro-*s*-tetrazine ( $c = 5 \times 10^{-6}$  M) under UV, no energy transfer occurs, and only the weak individual fluorescence of both compounds can be observed (Figure 4.20).



Figure 4.20. Picture of, left, a solution containing a mixture of concentrated **NIOH** ( $10^{-3}$  M) and diluted 3-(adamant-1-ylmethoxy)-6-chloro-*s*-tetrazine ( $5 \times 10^{-6}$  M) and, right, a diluted solution of **NITZ** ( $5 \times 10^{-6}$  M), under UV light irradiation (peak at 365nm).

All *s*-tetrazines, including **NITZ** are soluble in most organic polymers because of their moderate molecular weight. Figure 4.21 shows the pictures of a block of polystyrene into which **NITZ** has been dispersed at a  $10^{-5}$  M concentration. Such a low amount of dye gives a perfectly transparent object under ambient light while it exhibits a nice yellow fluorescence when exposed to UV light. In addition, the picture has been taken three weeks after the object fabrication, which demonstrates that the fluorophore does not degrade in normal condition.

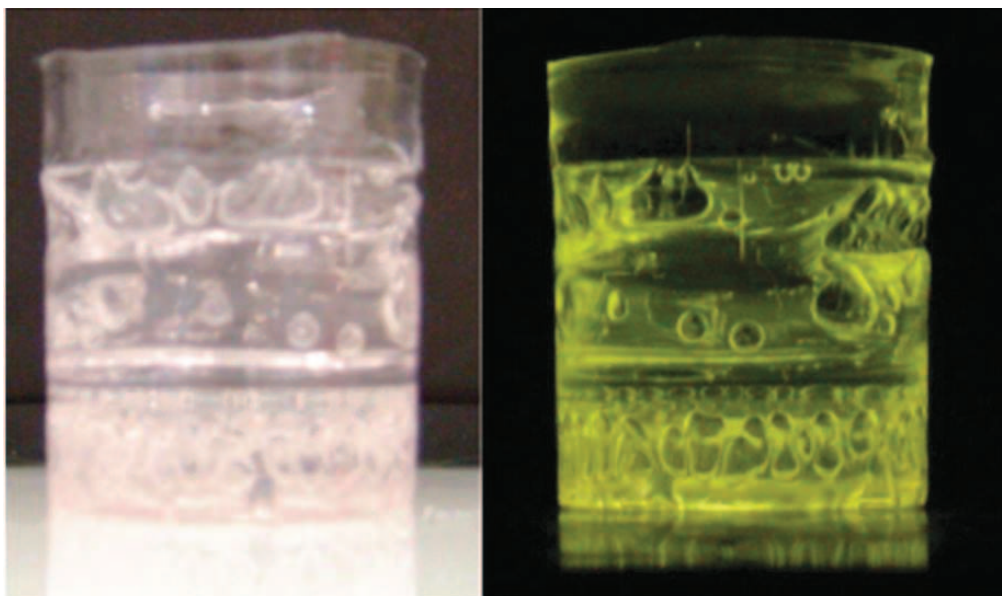


Figure 4.21. Picture of a block of polystyrene incorporating **NITZ** under white (left) and UV (right) light. The dye concentration in the polymer was *ca.*  $10^{-5}$  M.

In conclusion, a naphthalimide - *s*-tetrazine dyad has been synthesized. It contains two independent electroactive units and presents a very bright yellow fluorescence thanks to an efficient resonant energy transfer without modification of the intrinsic fluorescent properties of *s*-tetrazine. It is an extremely important progress in the improvement of fluorescence properties of *s*-tetrazine and this compound could be used as multi-color fluorescent materials. An example of application of this molecule in an electrofluorochromic cell will be presented in the last paragraph of the chapter.

## 4.5 Spectroscopic studies of **145**

### 4.5.1 Absorption and fluorescence studies

Since **NITZ** showed very good properties it was then interesting to develop the concept further up. For this purpose triad **145** (also nicknamed **2NITZ**), containing two naphthalimides and one *s*-tetrazine, was prepared (Scheme 4.4) and studied. The absorption spectrum of **2NITZ** (Figure 4.22) has the characteristic absorption visible band of *s*-tetrazine at 518nm due to its  $n-\pi^*$  transition. In addition, it presents a very intense UV band at 330nm characteristic of naphthalimide. A comparison of the spectra of **2NITZ**, **NITZ**, and chloromethoxy-*s*-tetrazine at the same concentration has also been done. The intensity of the  $n-\pi^*$  transition is almost unchanged whatever the molecule. This means that the substituent doesn't change the characteristics of this



absorption. However the major variations can be seen in the UV region. As seen before, chloromethoxy-*s*-tetrazine has a small  $\pi$ - $\pi^*$  transition, and **NITZ** a more intense one overlapping the *s*-tetrazine transition. Very interestingly for the aimed application, **2NITZ** have a band with the same shape and position than **NITZ** but is twice more intense. Thus, the chromophores are independent and the absorption of the two naphthalimides adds up in **2NITZ**.

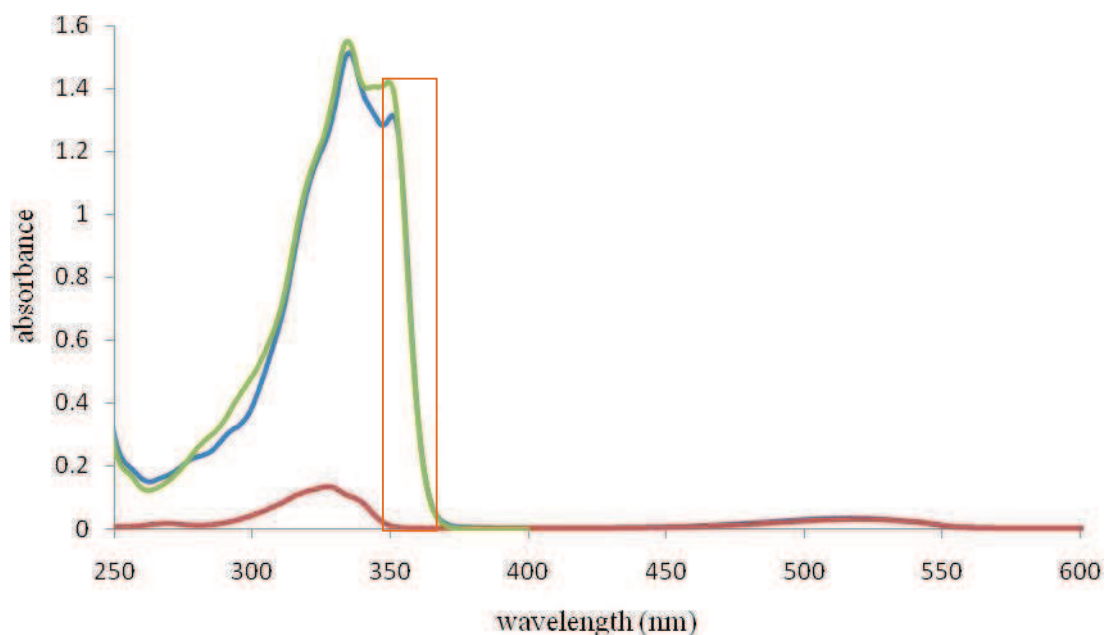


Figure 4.22. Absorption spectra of chloromethoxy-*s*-tetrazine (red), **NITZ** (green) and **2NITZ** (blue) recorded at the same concentration.

It is also clear that despite the overlap between naphthalimide and *s*-tetrazine bands, the absorption between 350 and 365 nm completely belongs to the  $\pi$ - $\pi^*$  transition of naphthalimide. The same situation was found with **NITZ**, but the molar absorption coefficient of **2NITZ** is much higher at 355 nm ( $17827 \text{ L}\cdot\text{mol}^{-1}\cdot\text{cm}^{-1}$ ).

Prior to investigation of the energy transfer between the two naphthalimides and *s*-tetrazine, the fluorescence spectrum of **151** ( $\lambda_{\text{ex}}=364\text{nm}$ ) and the absorption one of **2NITZ** were compared (Figure 4.23). It shows first that the emission spectrum of **151** has a different shape from the one of the simple naphthalimide **NIOH** since, in addition to the normal structured emission band of naphthalimide with a maximum at 379 nm, it also has a broad band from 450 to 600 nm. This emission band could come from the formation of an excimer between the two naphthalimides of **151** since such excimer formation has already been reported for other naphthalimide dyads<sup>8,9</sup>. Proof of the excimeric nature of this band could be gained from fluorescence decay measurements. However, whatever its nature, this extended emission is beneficial for

the energy transfer since it increases the spectral overlap between the emission of naphthalimide and the absorption of *s*-tetrazine.

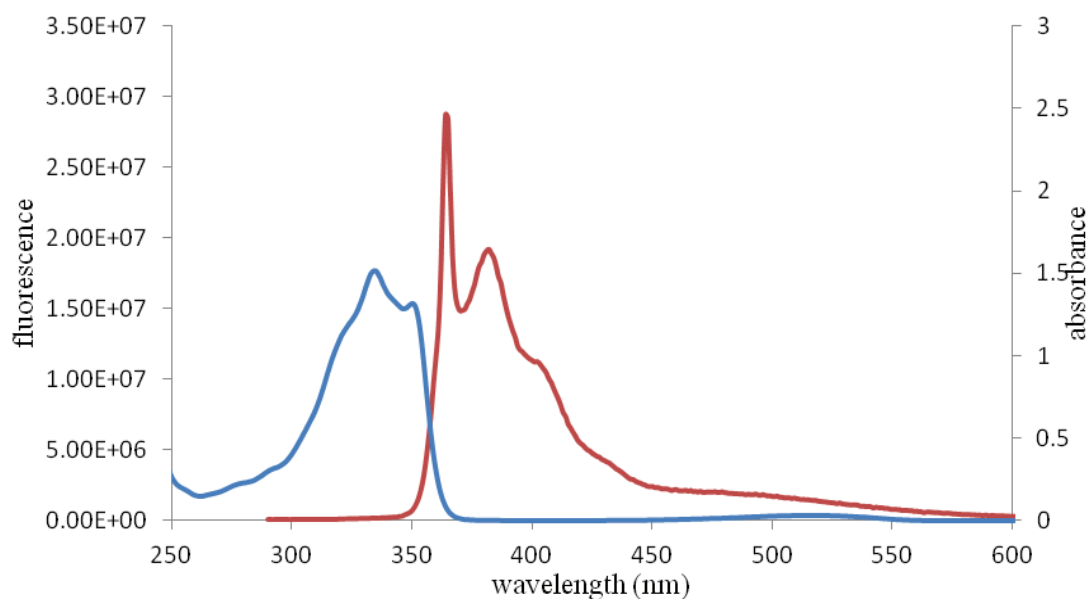


Figure 4.23. Absorption spectra of **2NITZ** (blue) and fluorescence spectra of **151** (red) with  $\lambda_{\text{ex}}=364\text{nm}$ .

#### 4.5.2 Energy transfer study

From the above, two important points have to be emphasized: first the naphthalimide absorption band overlaps the  $\pi$ - $\pi^*$  band of the *s*-tetrazine; second, the emission spectrum of **151** overlaps the absorption spectrum of the **2NITZ**. So it is expected to have an energy transfer process similar to the one in **NITZ** between the two imides and *s*-tetrazine in **2NITZ**.

The fluorescence spectra of **2NITZ** were recorded upon excitation of the naphthalimide moiety ( $\lambda_{\text{ex}}=355\text{nm}$ ) and *s*-tetrazine moiety ( $\lambda_{\text{ex}}=516\text{nm}$ ), and they were compared to the emission spectrum of **151** recorded for  $\lambda_{\text{ex}}=355\text{nm}$  (Figure 4.24). There are two bands in the emission spectra of **2NITZ** when excited at 355nm: one is due to the naphthalimide moiety and the other is corresponding to *s*-tetrazine. The first band has a similar shape to the one of **151** but is considerably less intense. In addition, almost all the recorded fluorescence is emitted by the *s*-tetrazine core, with an increased intensity compared to that observed upon direct excitation of *s*-tetrazine in its  $n$ - $\pi^*$  absorption band. These results evidence the occurrence of an energy transfer from the two naphthalimides to *s*-tetrazine.

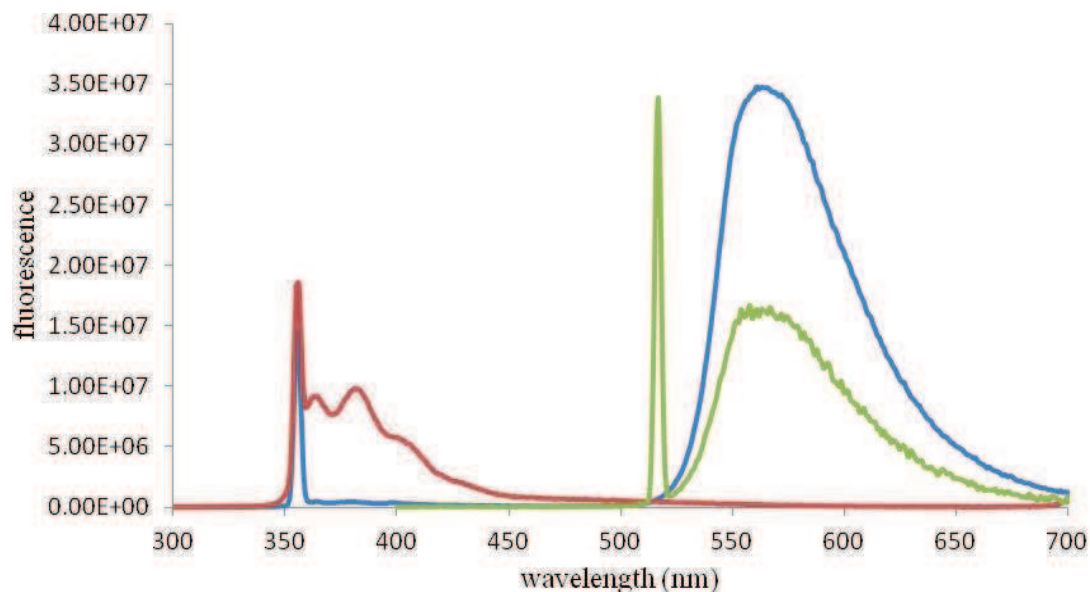
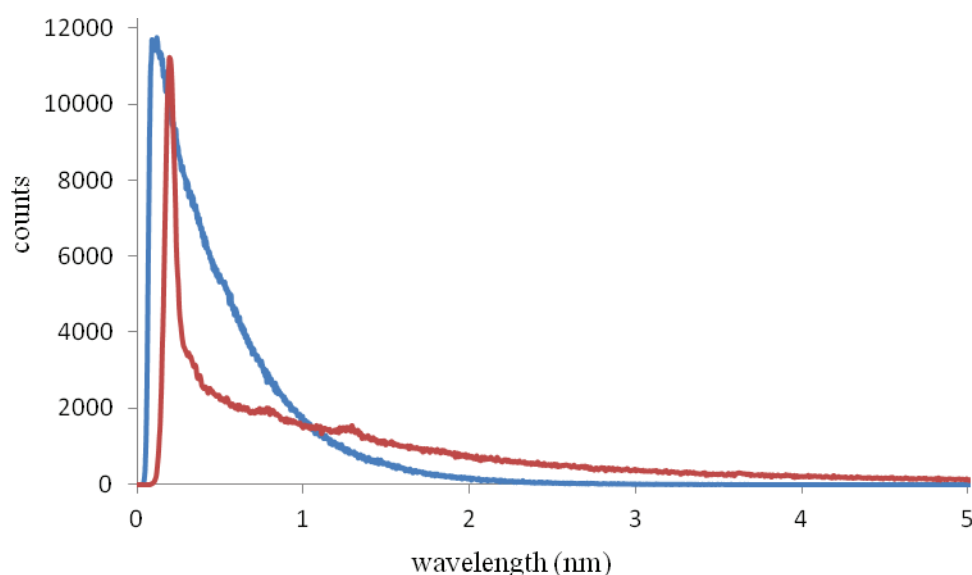


Figure 4.24. Fluorescence spectra of **151** (red), **2NITZ** with  $\lambda_{\text{ex}}=355\text{nm}$  (blue) and **2NITZ** with  $\lambda_{\text{ex}}=518\text{nm}$  (green). The two solutions have the same concentration.

Additionally, the fluorescence decays of **151** and **2NITZ** were measured (Figure 4.25). Both decays recorded at 380nm could be fitted by a single exponential and the results give a fluorescence lifetime for the naphthalimide of 0.39ns in **151** and 0.007ns in **2NITZ**. In addition, the lifetimes of *s*-tetrazine are  $\tau_{\text{F}}=160\text{ns}$  following excitation at 355nm and  $\tau_{\text{F}}=162\text{ns}$  following excitation at 516nm.



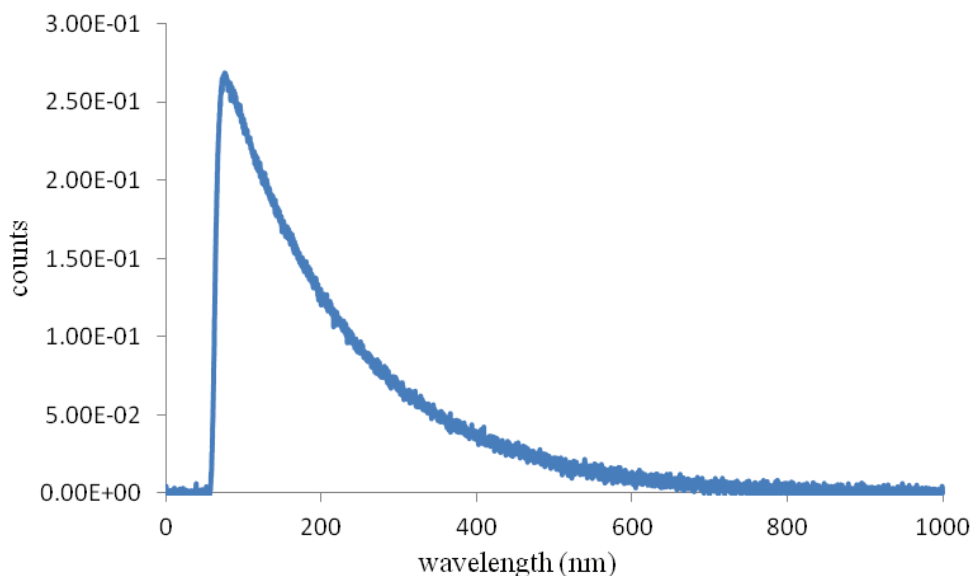


Figure 4.25. Fluorescence decay profiles following excitation at 355nm. Up: **151** (blue) and **2NITZ** (red) for  $\lambda_{em}=380\text{nm}$ ; down: **2NITZ** for  $\lambda_{em}=565\text{nm}$

The shortening of the fluorescence lifetime on going from **151** to **2NITZ** proves that there is a non radiative energy transfer between the naphthalimides and *s*-tetrazine. The fluorescence decay of *s*-tetrazine in NITZ after excitation at 355nm has no apparent rising time (Figure 4.25 down). However, the set-up used to measure this decay has an instrumental resolution of a few nanoseconds and the rising time should be of the same order as  $\tau_{\text{fluo}}$  of naphthalimide in NITZ (0.007ns). This two time ranges are then incompatible and it is not possible to see such rapid event on the set-up used. Detailed spectroscopic data for **151** and **2NITZ** were reported in table 4.4.

Table 4.4. Detailed Spectroscopic Data for **2NITZ** and **151**

Molecule/data	$\lambda_{\text{abs}}$ (nm)	$\epsilon$ (L.mol <sup>-1</sup> .cm <sup>-1</sup> )	$\lambda_{\text{em}}$ (nm)	$\Phi_{\text{fluo}}$	$\epsilon_{(\lambda_{\text{ex}})} \times \Phi_{\text{fluo}}$	$\tau_{\text{fluo}}$ (ns)
<b>151</b>	335	16200	362,	0.09 <sup>a</sup>	1455	0.39 <sup>c</sup>
			379, 397 <sup>a</sup>			
<b>2NITZ</b> (tetrazine data)	516	600	558 <sup>b</sup>	0.33 <sup>b</sup>	200	160 <sup>c</sup>
				(0.29 <sup>c</sup> )	(5170 <sup>c</sup> )	162 <sup>b</sup>
<b>2NITZ</b> (imide data)	335	17800	363	0.004 <sup>c</sup>	71	0.007 <sup>c</sup>
			379 397 <sup>c</sup>			

<sup>a</sup>  $\lambda_{\text{ex}}=350$  nm; <sup>b</sup>  $\lambda_{\text{ex}}=516$  nm; <sup>c</sup>  $\lambda_{\text{ex}}=355$  nm;

From these data, the efficiency of the energy transfer is:

$$\Phi_{ET} = 1 - \frac{\Phi_D}{\Phi_D^0} = 1 - \frac{0.004}{0.09} = 0.96$$

$$\Phi_{ET} = 1 - \frac{\tau_D}{\tau_D^0} = 1 - \frac{0.007}{0.39} = 0.98$$

It is noteworthy that the two calculated values are in good agreement. The rate associated with the transfer is:

$$K_T = \frac{1}{\tau_D} - \frac{1}{\tau_D^0} = \frac{1}{0.007} - \frac{1}{0.39} = 1.4 \times 10^{11} \text{ s}^{-1}$$

which is three orders of magnitude faster than the radiative rate of **151** ( $k_R=2.31 \times 10^8 \text{ s}^{-1}$ ).

The calculated transfer efficiency is very high. The critical Förster radius for the dyad **2NITZ** was calculated from the spectral overlap and is:  $R^0=11.3 \text{ \AA}$  taking  $\kappa^2=2/3$  (isotropic dynamic average). The theoretical RET efficiency can be obtained from  $R^0$  and the distance  $r$  between the two chromophores. An estimation of the value of  $r$  was obtained by quantum mechanic geometry optimization of **2NITZ**. The shortest distance between the imide donor and the *s*-tetrazine ring acceptor mass centers were found at  $r=8.25 \text{ \AA}$ . Therefore, the efficiency of the energy transfer of **2NITZ** according to Förster theory is

$$\Phi_T = \frac{1}{1 + (r/R_0)^6} = \frac{1}{1 + (8.25/11.3)^6} = 0.89$$

Similarly to **NITZ** the calculated and the experimental values show a discrepancy which points out to an energy transfer mechanism of the Dexter type or a mixed Dexter-Förster.

The measured efficiency of energy transfer for **2NITZ** is similar to the one found for **NITZ**. Nevertheless, the large absorbance from the two imides has an important impact on brightness. The quantitative evaluation of the brilliance (Table 4.4) shows that it is 25.8 times higher when **2NITZ** is excited at 355nm (selective of the imide moiety) rather than 516nm (selective of the tetrazine moiety). Even more,

the combination of two naphthalimides and an efficient energy transfer impart a much higher brilliance to **2NITZ** than to **NITZ** (5100 and 1600 respectively at  $\lambda_{\text{ex}}=355\text{nm}$ ).

In order to compare the brightness of chloromethoxy-*s*-tetrazine, **NITZ** and **2NITZ** absorption and fluorescence spectra were observed at the same concentration. Figure 4.22 presents the overlaid absorption spectra of these three *s*-tetrazines. The intensity of the  $n-\pi^*$  transition is completely identical whatever the molecule. However, **2NITZ** show the most intense absorption in the UV, since the band corresponds to the absorption of both naphthalimide and *s*-tetrazine.

Then the fluorescence spectra were recorded on the same solutions, with excitation wavelengths specific of *s*-tetrazine (516nm) or of naphthalimide (364nm). In the first case (excitation at 516nm, Figure 4.26), spectra with roughly the same intensity are obtained. This again proves that the fluorescence properties of *s*-tetrazine are independent of its local environment.

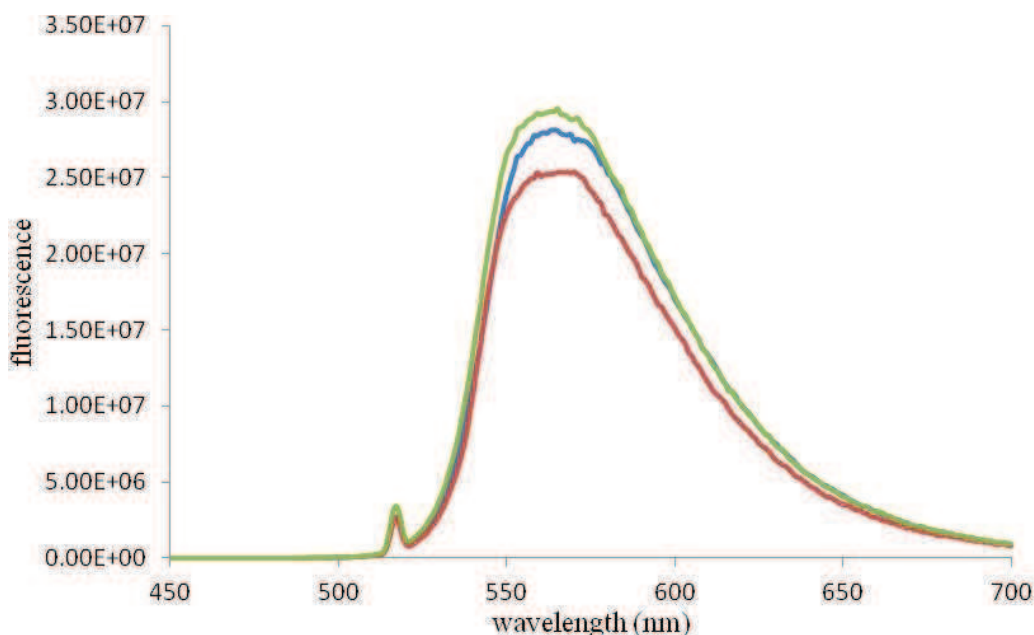


Figure 4.26. Fluorescence spectra of chloromethoxy-*s*-tetrazine (red), **NITZ** (green) and **2NITZ** (blue) with  $\lambda_{\text{ex}}=516\text{nm}$ . All solutions are at the same concentration.

In the second case (excitation at 364nm Figure 4.27), entirely different fluorescence spectra are recorded. Chloromethoxy-*s*-tetrazine displays no emission of photons at all. For **NITZ**, the emission of naphthalimide is almost quenched and the emission of *s*-tetrazine is intense because of the energy transfer. **2NITZ** with two naphthalimide shows weak emission from the naphthalimides and an *s*-tetrazine emission which is more than two times stronger than its emission in **NITZ**.

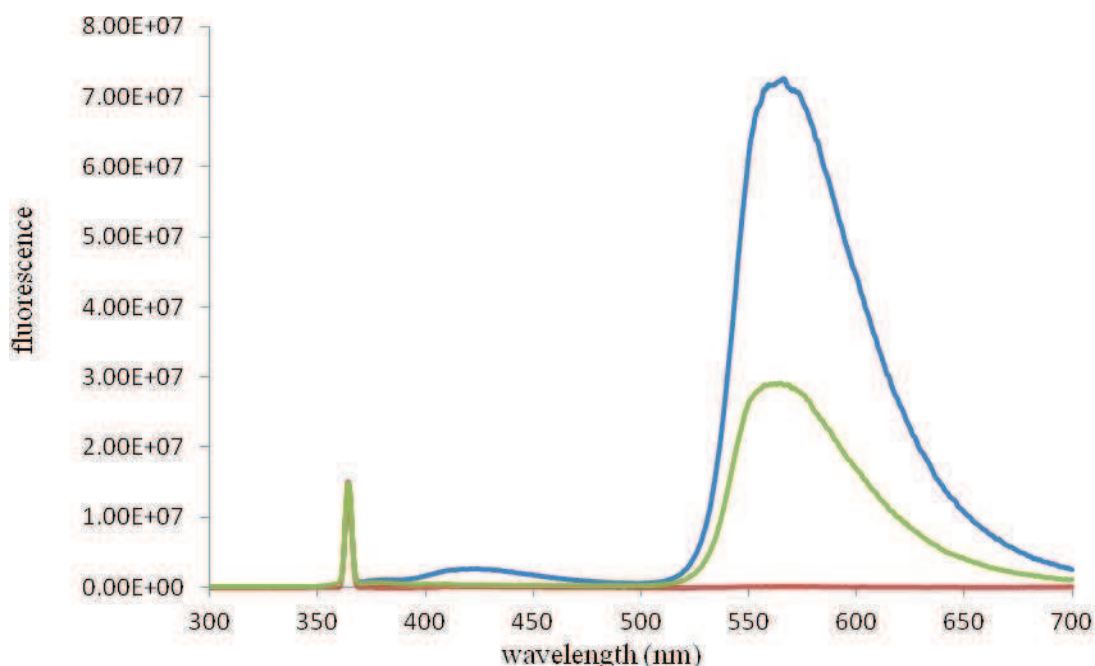


Figure 4.27. Fluorescence spectra of chloromethoxy-*s*-tetrazine (red), **NITZ** (green) and **2NITZ** (blue) with  $\lambda_{\text{ex}}=364\text{nm}$ . All solutions are at the same concentration.

In addition, we made a visual demonstration of the evolution of the brilliance by simply comparing  $5 \times 10^{-6}$  M solutions of chloromethoxy-*s*-tetrazine, **NITZ**, **2NITZ** and **151** (Figure 4.28). The illumination is provided by a laboratory UV lamp peaking at 365nm but both naphthalimide and *s*-tetrazine are excited. First of all, emission of the bis-naphthalimide **151** is barely detectable by the eye at this concentration and fluorescence of the simple chloromethoxy-*s*-tetrazine is faint. On the contrary, both “n-ads” display an intense yellow fluorescence thanks to the efficiency of the naphthalimide absorbance and of the energy transfer. Furthermore, **2NITZ** comprising two energy donor moieties visually shows a more intense fluorescence than **NITZ**. Thus it can be seen visually that although both molecules have an almost equally efficient energy transfer, the brightness of **2NITZ** is indeed improved thanks to the two naphthalimide groups.

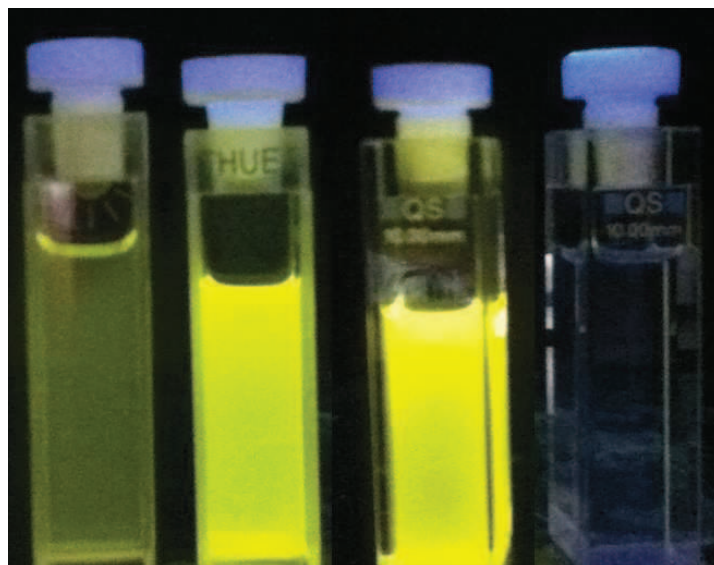


Figure 4.28. Picture of  $5 \times 10^{-6}$  M solutions of (left to right), chloromethoxy-*s*-tetrazine, **NITZ**, **2NITZ** and **151** under UV light (365nm).

### 4.5.3 Color analysis of 2NITZ fluorescence

Considering that **2NITZ** has two types of chromophore, each emitting light although in a very different ration, it was interesting to determine the true emitted color by using the CIE 1931 xy chromaticity diagram<sup>10</sup>. The coordinates of the overall emission are  $x=0.484$  and  $y = 0.522$  which correspond to a yellow-orange color (Figure 4.29). Hence **NITZ** shows pretty much only the yellow emission of *s*-tetrazine.

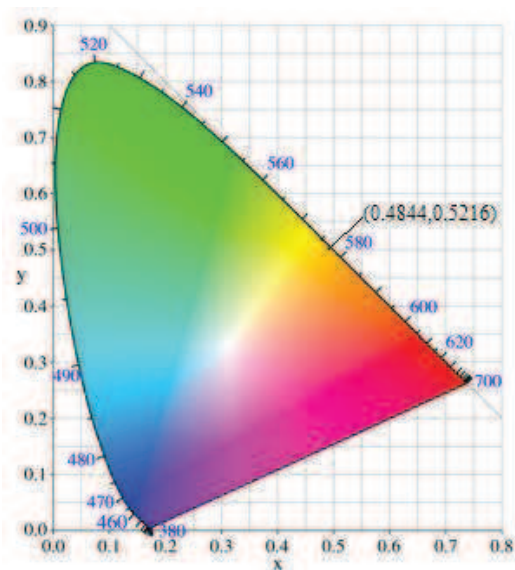


Figure 4.29. Coordinates of the emission of **2NITZ** excited at 355nm on the CIE 1931 chromaticity diagram.



In conclusion, we have demonstrated that **2NITZ** undergo an efficient intramolecular resonant energy transfer like **NITZ** but is brighter thanks to the introduction of a second naphthalimide. Let us now examine the case molecule **146** containing one more.

## 4.6 Spectroscopic studies for **146**

### 4.6.1 Absorption and fluorescence studies

Elaborating further on the concept of multichromophoric molecules tetrad **146** (also nicknamed **3NITZ**), containing three naphthalimides and one *s*-tetrazine, was prepared (Scheme 4.7) albeit in poor yield and studied. The absorption spectrum of **3NITZ** (Figure 4.30) has the characteristic absorption visible band of *s*-tetrazine at 518nm due to its  $n-\pi^*$  transition. In addition, it presents a highly intense UV band at 330nm characteristic of naphthalimide. The difference of intensity between the two bands is so important that the visible absorption of *s*-tetrazine is barely visible on the same scale. Thus, similarly to **2NITZ**, the absorption of the three naphthalimides adds up in **3NITZ**.

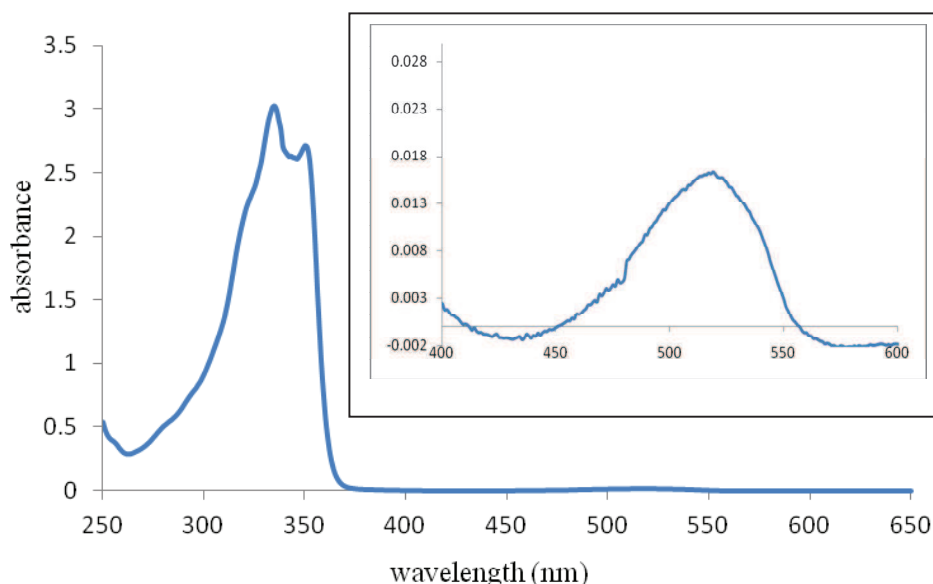


Figure 4.30. Absorption spectrum of **3NITZ** in DCM.

Prior to investigation of the energy transfer between the three naphthalimides and *s*-tetrazine, the fluorescence spectrum of the tris-naphthalimide **156** ( $\lambda_{\text{ex}}=355\text{nm}$ ) and the absorption one of **3NITZ** were compared (Figure 4.31). It has to be noted first

that the emission spectrum of **156** has a similar shape to the one of the simple naphthalimide **NIOH**. Hence, unlike the bis-naphthalimide **151**, molecule **156** does not have an apparent emission band coming from the formation of an excimer between two naphthalimides. This could come from the more congested geometry of **156** which might not allow the necessary free volume for the intramolecular reorganization leading to the formation of the excimer. The fluorescence quantum yield of **156** is 0.07 a similar value to **NIOH** and **151**. The emission spectrum of **156** also partially overlaps the absorption spectrum of **3NITZ** like in the two previous cases. So it is possible to have energy transfer between naphthalimides and *s*-tetrazine.

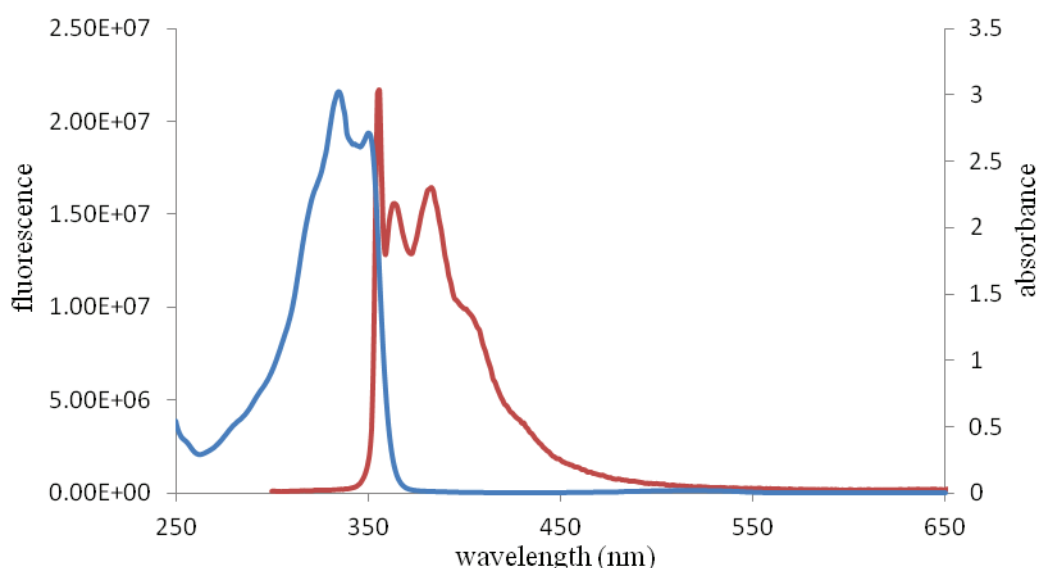


Figure 4.31. Absorption spectrum of **3NITZ** (blue) and fluorescence spectrum of **3NIOH** (red) with  $\lambda_{\text{ex}}=355\text{nm}$

#### 4.6.2 Energy transfer studies for **3NITZ**

The same methodology as for **NITZ** and **2NITZ** was applied to **3NITZ** to investigate the energy transfer between the three naphthalimides and *s*-tetrazine. The fluorescence spectra of **3NITZ** and **156** were recorded upon excitation of the naphthalimide moiety ( $\lambda_{\text{ex}}=355\text{nm}$ ; Figure 4.32). There are two bands in the emission spectra of **3NITZ**: one is due to the naphthalimide moieties and the other corresponds to *s*-tetrazine. The first band has a similar shape to the one of **156** but is less intense. However, the relative decrease of fluorescence intensity for **3NITZ** vs. **156** is not as pronounced as for **NITZ** or **2NITZ**.

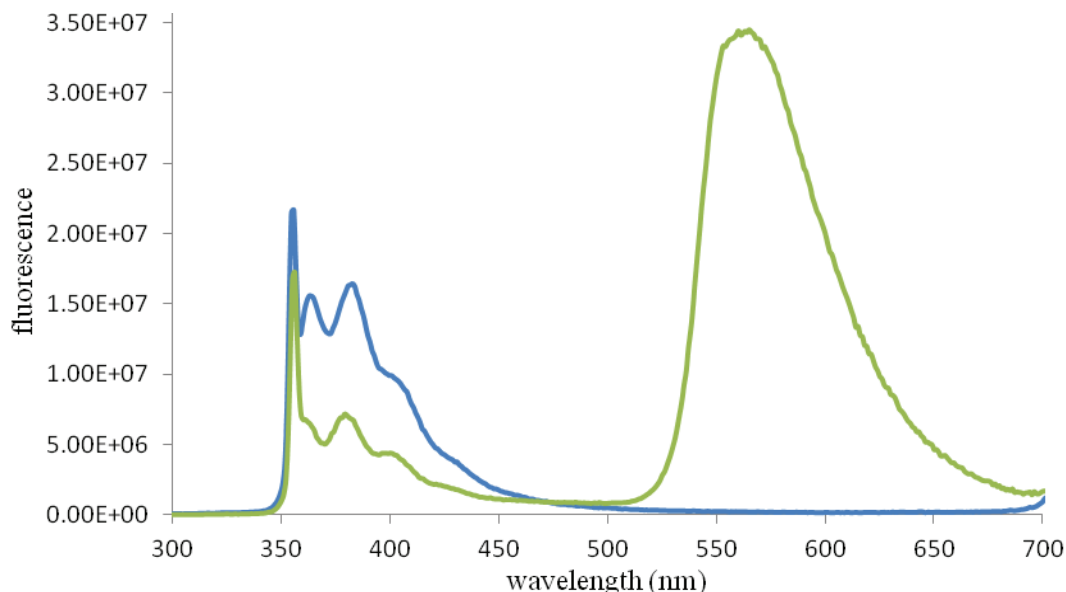


Figure 4.32. Fluorescence spectra of **3NITZ** (green) and **14** (blue) with  $\lambda_{\text{ex}}=355\text{nm}$  in DCM.

These results confirm the occurrence of an energy transfer between the three naphthalimides and *s*-tetrazine. From the data table 4.5, the efficiency of the energy transfer is:

$$\Phi_{ET} = 1 - \frac{\Phi_D}{\Phi_D^0} = 1 - \frac{0.033}{0.071} = 0.54$$

The efficiency is lower than for the other naphthalimide-*s*-tetrazine “n-ads”. Half of the excited naphthalimides transfer their energy to *s*-tetrazine and half emit blue light. So the fluorescence color of whole molecule is a mixture of naphthalimide’s blue and *s*-tetrazine’s yellow. It is then possible to consider the preparation of a white fluorescent compound or material by combining these two chromophores in the appropriate amount. In addition, the recorded fluorescence emitted by the *s*-tetrazine core after energy transfer is  $\approx 40$  times more intense than upon direct excitation of *s*-tetrazine in its  $n-\pi^*$  absorption band (Figure 4.33).

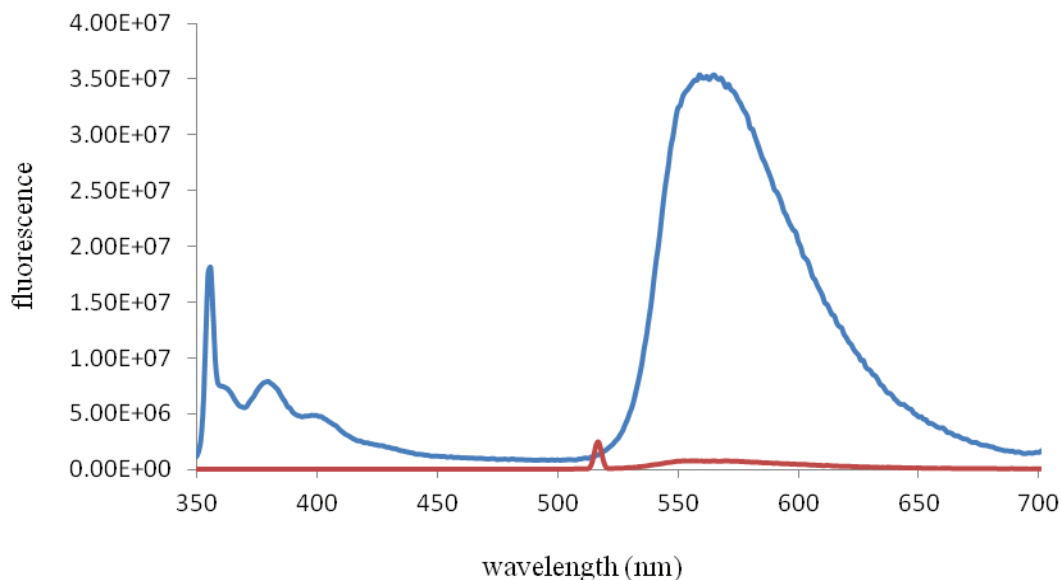


Figure 4.33. Fluorescence spectra of **3NITZ** with  $\lambda_{\text{ex}}=355\text{nm}$  (blue) and  $\lambda_{\text{ex}}=516\text{nm}$  (red).

The fluorescence decays of **156** and **3NITZ** were also measured (Figure 4.34). All decays could be fitted by a single exponential. The decays recorded at 383nm give a fluorescence lifetime for the naphthalimide of 0.30ns and 0.25ns in **156** and **3NITZ** respectively. The shortening of the fluorescence lifetime of naphthalimides in **3NITZ** proves that there is a non radiative energy transfer between the naphthalimides and *s*-tetrazine. The energy transfer efficiency calculated from these lifetimes is:

$$\Phi_{ET} = 1 - \frac{\tau_D}{\tau_D^0} = 1 - \frac{0.25}{0.30} = 0.17$$

which is inexplicably much lower than the one obtained from the fluorescence quantum yields. The lifetimes of *s*-tetrazine are  $\tau_F=153\text{ns}$  following excitation at 355nm and  $\tau_F=158\text{ns}$  following excitation at 516nm (data not shown). These values are typical for *s*-tetrazines. Similarly to **2NITZ**, no rising time could be detected on the decay of tetrazine (Figure 4.34 down) because of set-up limitations.

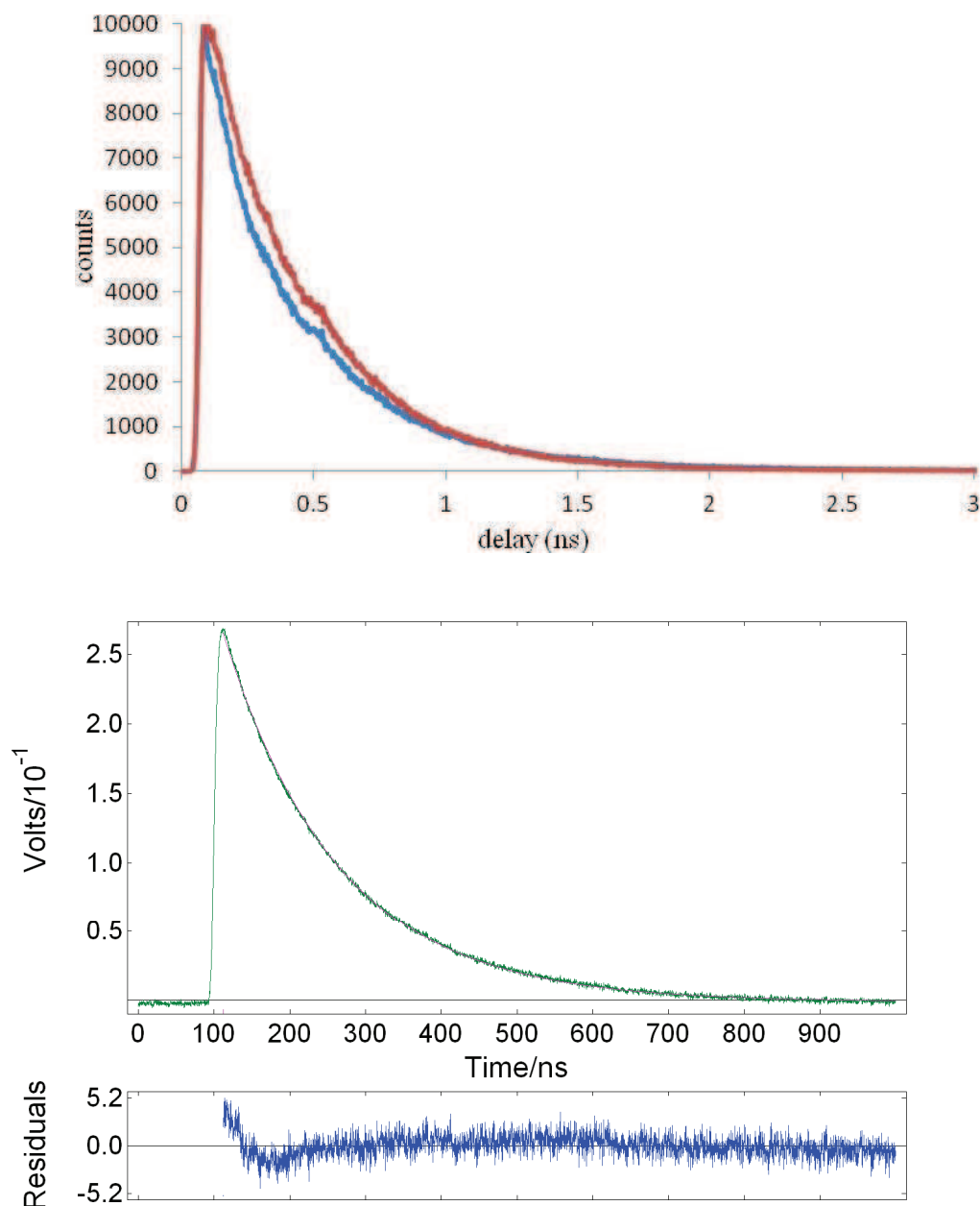


Figure 4.34. Fluorescence decay profiles upon excitation at 355nm. Up: **156** (red) and **3NITZ** (blue) for  $\lambda_{em}=383\text{nm}$ ; Down: **3NITZ** for  $\lambda_{em}=565\text{nm}$

So a non radiative energy transfer in **3NITZ** between the naphthalimides and *s*-tetrazine is apparent from the fluorescence spectra and decays. However, the efficiency of the transfer is lower than for **NITZ** or **2NITZ**, but this could lead to obtain multi-colored fluorescent compounds and even white emissive molecules. Despite the lesser efficiency of the RET, the brightness of **3NITZ** is about 7800 (table 4.5) which is greater than for **2NITZ** or **NITZ**, because of the increased number of naphthalimides in the molecule.

Table 4.5. Detailed spectroscopic data for **3NITZ** and **156**

Molecule/data	$\lambda_{\text{abs}}$ (nm)	$\epsilon$ (L.mol <sup>-1</sup> .cm <sup>-1</sup> )	$\lambda_{\text{em}}$ (nm)	$\Phi_{\text{fluo}}$	$\epsilon_{(\lambda_{\text{ex}})} \times \Phi_{\text{fluo}}$	$\tau_{\text{fluo}}$ (ns)
<b>156</b>	335	24259	364, 383, 397 <sup>a</sup>	0.071 <sup>a</sup>	1722	0.30 <sup>a</sup>
<b>3NITZ</b> (tetrazine data)	516	623	558 <sup>b</sup>	0.43 <sup>b</sup> (0.29 <sup>a</sup> )	268 (7754 <sup>a</sup> )	153 <sup>a</sup> 158 <sup>b</sup>
<b>3NITZ</b> (imide data)	335	26740	363 379 396 <sup>a</sup>	0.033 <sup>a</sup>	882	0.25 <sup>a</sup>

<sup>a</sup>  $\lambda_{\text{ex}}=355$  nm; <sup>b</sup>  $\lambda_{\text{ex}}=516$  nm.

## 4.7 Application of NITZ: three colors electrofluorochromic cell

Compound **NITZ** has two remarkable characters. One is the energy transfer from naphthalimide to *s*-tetrazine to activate fluorescence of the latter; the other is that two quite stable and independent anion-radicals can be formed on the molecule, and both of them display (quasi)reversible electrochemical behavior. It has also been previously demonstrated in the laboratory and in collaboration with Pr. Eunkyong Kim of Yonsei University (Seoul, Korea), that inclusion of chloromethoxy-*s*-tetrazine and other derivatives in a solid state electrochemical cell gives a reversible on-off fluorescent device as a function of the redox state of *s*-tetrazine<sup>11,12</sup>. Thus, it was interesting to test **NITZ** in such a device to check whether it could act as a multicolor electrofluorescent switch.

The cell including **NITZ** is a sandwiched device made of two layers packed between two transparent ITO (Indium tin oxide) electrodes. The first layer, a layer of a viscous polymer electrolyte solution was coated on an ITO plate by spin coating and then photo-cured so that it became a stiff solid polymer electrolyte film. Then a layer of the polymer electrolyte solution containing 1 wt% of **NITZ** was coated on the other ITO plate. The two plates were then contacted and sealed with a reference electrode in a 3-electrodes system. The redox potentials of **NITZ** in solid polymer electrolyte

media in 3-electrodes system were observed at -0.67 V and -1.58 V, corresponding to the reduction wave of the *s*-tetrazine and the naphthalimide units, respectively (Figure 4.35). These potentials match well those found in solution (Table 4.2). These two reduction waves were reversible and reproduced by multiple measurements.

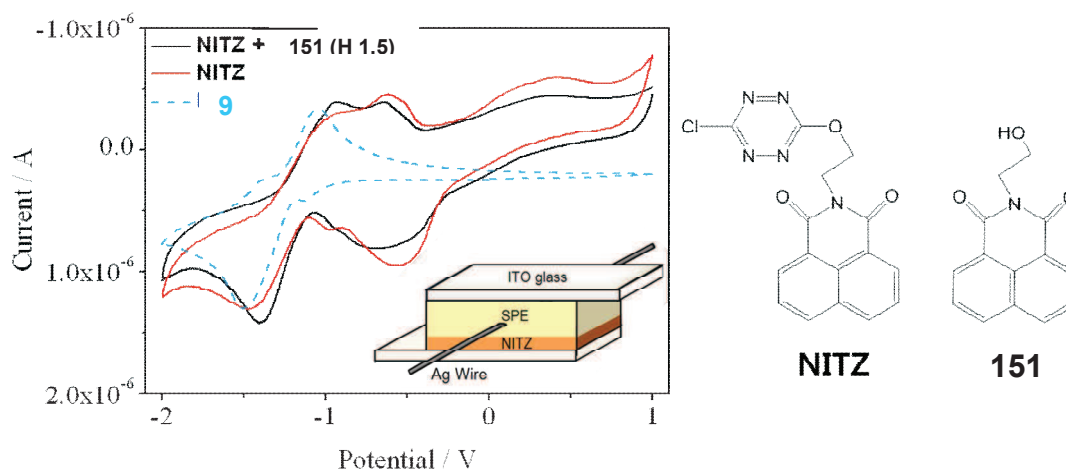


Figure 4.35. Cyclic voltammogram of **NITZ** (red line), **NITZ** blended with **151** (black), and **151** (blue dashed line) in solid polymer electrolyte, recorded at a scan rate of 20 mV/s in a 3-electrodes switching cell with an Ag wire reference. Inset: structure of the three-electrode device with a thin **NITZ** layer, a silver wire, and a solid polymer electrolyte (SPE) layer.

The electrofluorochromic switching of **NITZ** was examined by monitoring the photoluminescent properties at different applied potentials (Figure 4.36) in the three-electrode switching device. The cell showed vivid yellow fluorescence before application of potential or when the applied potential to the cell was positive. Noteworthy, the minimum content of **NITZ** to observe the fluorescence was much lower than that of chloromethoxy-*s*-tetrazine thanks to the improved brightness of the dyad. Upon application of a negative potential below zero, the fluorescence was quenched and the cell was significantly extinguished to dark when the applied potential was beyond -1.0V and then almost completely extinguished after -1.4 V. The fluorescence intensity change occurred without a shift of the spectral band with the potential change, indicating that the fluorescence quenching originated from the electrochemical reduction of the neutral fluorophore *s*-tetrazine to its anion-radical form, without the production of side products.

Additionally, the fluorescence intensity of *s*-tetrazine decreased when the applied potential was in between the reduction potential of *s*-tetrazine that of naphthalimide (-0.6 ~ -1.2 V), where the former unit should be reduced but not the latter. Moreover, the blue fluorescence from naphthalimide was not observed in any stage of reduction even after *s*-tetrazine units were completely reduced (> -1.0 V).

After -1.0 V, although very weak, the fluorescence from the cell was still observed as dark yellow, indicating the occurrence of energy transfer from naphthalimide to *s*-tetrazine, similarly to the neutral state. The yellow emission from the energy transferred state of **NITZ** was almost completely extinguished only after -1.4 V, beyond which the cell was dark as shown in the photographs of Figure 4.36.

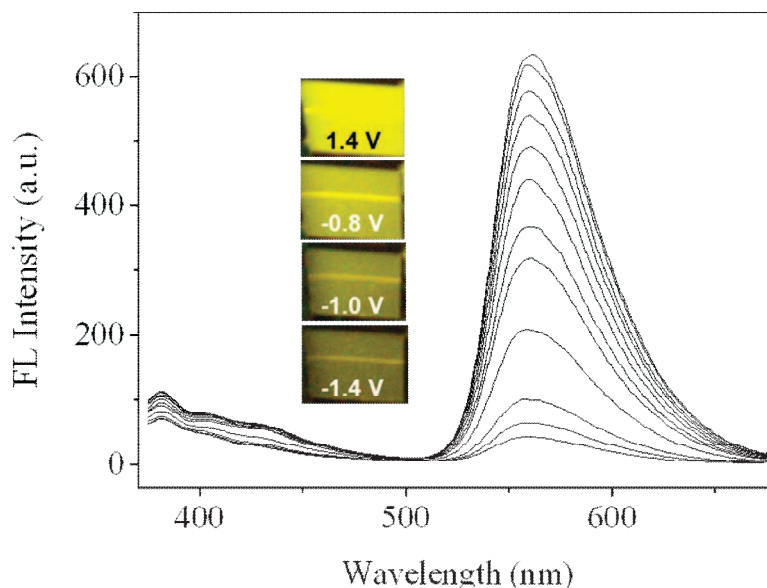


Figure 4.36. Fluorescence changes of a three-electrode switching cell containing **NITZ** at different applied potentials from +1.4 V to -1.4 V with 0.2 V decrease at each step. Each spectrum was obtained after applying the target potential for 60 s to obtain the fluorescence spectrum at saturated state (excitation at 355 nm). Inset: Fluorescence switching image of the **NITZ** at +1.4 V, -0.8 V, -1.0 V and -1.4 V.

Hence electrofluorescent switching of **NITZ** only allows a yellow to black alternation (Figure 4.37, picture **NITZ** (H0)). The fluorescence of the naphthalimide could never be detected when the applied potential was sufficient to reduce *s*-tetrazine and keep the naphthalimide in its neutral state. This is probably coming from the poor fluorescence quantum yield of naphthalimide and the high dilution of **NITZ** in the device. Indeed and as was demonstrated with bis-naphthalimide **151** (Figure 4.28) when this fluorophore is too diluted, no emission can be detected visually.

Thus a three color display was developed through an alternative approach consisting in blending **NITZ** with **151** in the device. It was first verified that electrochemical properties of naphthalimide **151** and the blend in the solid electrochemical cell remained unchanged (Figure 4.35). The cell containing **151** displays blue fluorescence at low potentials and is dark when a sufficiently negative



potential is applied (Figure 4.37, picture 151). The reversibility of the process was also verified.

In the next step, variation of the ratio of the two molecules in the blend gave an optimum for 1 **NITZ** for 1.5 **151** since this mixture has the perfect blue and yellow colors balance to give white fluorescence (Figure 4.37, picture H1.5). The white emission was dimmed away and blue emission was observed when the applied potential was in the intermediate range (-0.6 V ~ -1.2 V) and then the fluorescence was completely extinguished to dark when the potential was beyond -1.4 V. These results can be understood easily based on the redox reaction of each molecules discussed above. As the *s*-tetrazine unit is reduced, its yellow contribution disappeared and only blue emission of **151** remained in the intermediate potential range. Then at the extreme case, where naphthalimide reduction occurs at -1.4 V or lower potentials, emission from this unit is quenched to extinguish fluorescence of the cell. Thus when the **151** content was smaller (H0.5), the cell showed pale yellow as the color mixing to reach white emission was incomplete. Importantly the fluorescence from the cell is reasonably switchable at each state, to achieve a multicolor switching electrofluorochromic device (Figure 4.37 right). However, the electrofluorochromic response of the naphthalimide part is less reversible than the *s*-tetrazine one.

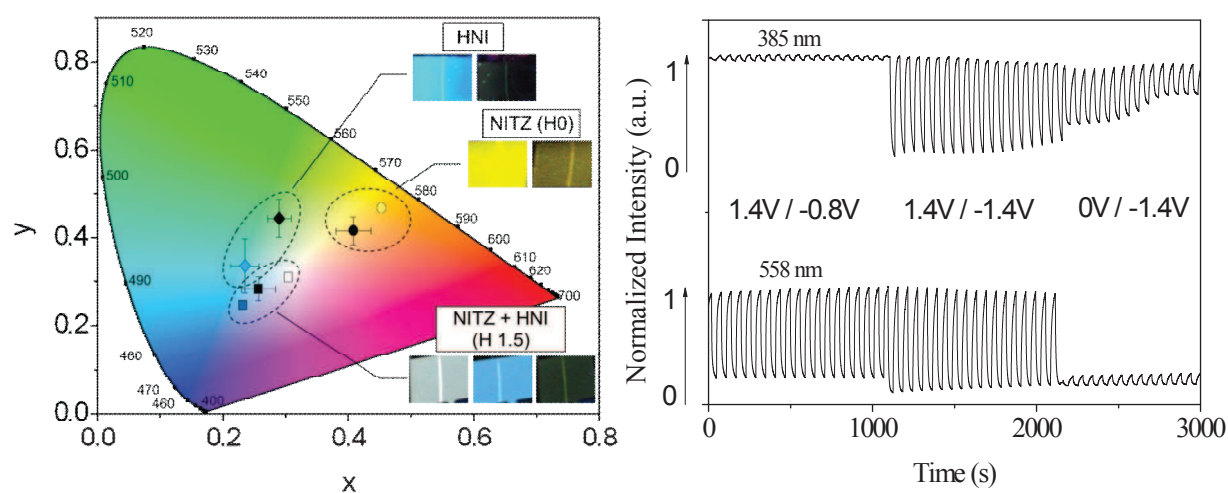


Figure 4.37. (left) The reversible emission color change of the cell with **NITZ** blend (H1.5) in chromaticity diagram as compared to the cell of **NITZ** (H0) and **151** (called **HNI**), measured at different potentials. Photographs are the image of the reversible fluorescence switching cells, at given potential. The white bar in the photograph corresponds to a silver wire (1cm) reference. (right) Fluorescence switching of the blended device (H1.0) between multi-color states. The relative intensity was calculated by dividing fluorescence intensity at a given potential by initial intensity.

The combination of the **NITZ** dyad with **151** for electrofluorochromic cell opens a new method to control fluorescence color.

## 4.8 Conclusion

The brightness of *s*-tetrazine has been improved by the synthesis of several dyads and higher equivalents. Two families of fluorophores have been appended to *s*-tetrazine: naphthalimide and benzimidazole. For both families, dyads were prepared (**NITZ** and **143** respectively) and an efficient intramolecular energy transfer was detected. The behavior of molecule **143** containing 2-trifluoromethylbenzimidazole as the energy donor is puzzling since photophysical studies indicated that the energy transfer seems to be radiative. Additional experiments and synthesis of new dyads with other benzimidazole derivatives would be needed to confirm this result.

The naphthalimide fluorophore proved to be very attractive since it gave a very efficient RET with *s*-tetrazine in **NITZ**. Furthermore, it could be used to synthesize a triad (**2NITZ**) and a tetrad (**3NITZ**) displaying even higher brightness. Energy transfer in **3NITZ** is incomplete (efficiency of  $\approx 50\%$ ). This is limiting for the goal pursued but could be useful to design molecules with multi fluorescence emission and even more interesting, white fluorescent molecules.

Finally, dyad **NITZ** was successfully incorporated in an electrofluorochromic cell and its yellow fluorescence was reversibly switched off and on. Furthermore, a blend of **NITZ** and **151** was also tested. The cell can be alternated between three different states: it goes from white to blue to dark when starting from a neutral potential (all species in their neutral state) to an intermediate negative one (*s*-tetrazine is reduced) to a very negative one (all species are reduced). This multicolor switching electrofluorochromic device opens up new and interesting opportunities for the development of multicolor passive displays.

## Reference

1. Allain C., Galmiche L., Audebert P., Pansu R., Riou-Kerangal (née Leray) I., « 1,2,4,5-tétrazines 3,6 fonctionnalisées, procédé de préparation, compositions en comportant et utilisation à la détection de polluants organiques », PCT/FR2011/053157
2. Valeur, B., *Molecular fluorescence : principles and applications*. Wiley-VCH: Weinheim ; New York, 2002; p xiv, 387 p.
3. Han, X. M.; Ma, H. Q.; Wang, Y. L., P-TsOH catalyzed synthesis of 2-arylsubstituted benzimidazoles. *Arkivoc* **2007**, 150-154.
4. Becer, C. R.; Hoogenboom, R.; Schubert, U. S., Click Chemistry beyond Metal-Catalyzed Cycloaddition. *Angew Chem Int Edit* **2009**, *48* (27), 4900-4908.
5. Davis, B. G.; Khumtaveeporn, K.; Bott, R. R.; Jones, J. B., Altering the specificity of subtilisin *Bacillus lentus* through the introduction of positive charge at single amino acid sites. *Bioorgan Med Chem* **1999**, *7*(11), 2303-2311.
6. Sinha, H. K.; Dogra, S. K., Absorptiometric and Fluorometric Study of Solvent Dependence and Prototropism of 2-Substituted Benzimidazole Derivatives. *J Chem Soc Perk T 2* **1987**, (10), 1465-1472.
7. Ramachandram, B.; Saroja, G.; Sankaran, N. B.; Samanta, A., Unusually high fluorescence enhancement of some 1,8-naphthalimide derivatives induced by transition metal salts. *J Phys Chem B* **2000**, *104* (49), 11824-11832.
8. Ferreira, R.; Baleizao, C.; Munoz-Molina, J. M.; Berberan-Santos, M. N.; Pischel, U., Photophysical Study of Bis(naphthalimide)-Amine Conjugates: Toward Molecular Design of Excimer Emission Switching. *J Phys Chem A* **2011**, *115* (6), 1092-1099.
9. Shelton, A. H.; Sazanovich, I. V.; Weinstein, J. A.; Ward, M. D., Controllable three-component luminescence from a 1,8-naphthalimide/Eu(III) complex: white light emission from a single molecule. *Chem Commun* **2012**, *48* (22), 2749-2751.
10. Smith, Thomas; Guild, John (1931–32). "The C.I.E. colorimetric standards and their use". *Transactions of the Optical Society* *33* (3): 73–134.
11. Kim, Y.; Kim, E.; Clavier, G.; Audebert, P., New tetrazine-based fluoro-electrochromic window; modulation of the fluorescence through applied potential. *Chem Commun* **2006**, (34), 3612-3614.
12. Kim, Y.; Do, J.; Kim, E.; Clavier, G.; Galmiche, L.; Audebert, P., Tetrazine-based electrofluoro-chromic windows: Modulation of the fluorescence through applied potential. *J Electroanal Chem* **2009**, *632* (1-2), 201-205.

## General conclusion and perspectives:

In conclusion, in this work we have been interested in various research topics pertaining *s*-tetrazine chemistry, electrochemistry and photophysics. I would like in this conclusion to outline the main points that we can draw from the results exposed.

The design of special supramolecular *s*-tetrazines was definitively a very promising idea, the results, although effective, did not fully match our hopes in this direction. *s*-Tetrazines, despite the assertions of previous theoretical works, will probably not find applications in anion sensing and detection, since complexation is followed by a photoinduced reaction. However, this situation could open up new perspectives in the development of new *s*-tetrazine derivatives for the photo-degradation of pollutants.

Similarly, the introduction of bulky groups onto the *s*-tetrazine ring, that was initially expected to have a sizable influence on the electrochemical behavior, and possibly the fluorescence, was finally found to lead only to small differences compared to the generic *s*-tetrazines having methyl or ethyl substituents. Although introducing adamantanyl group had indeed a crystallogenic effect, and also lead to compounds easier to manipulate (higher temperatures of melting and sublimation, increase of the actual mass of chemical per *s*-tetrazine ring) the overall influence on the fundamental properties of *s*-tetrazines was quite moderate. It was also disappointing to find out that direct attachment of electron withdrawing groups on *s*-tetrazine degraded its photophysical properties.

The discovery that it was possible to prepare chloroalkyl, alkoxyalkyl and even dialkyl *s*-tetrazines, through a simple synthetic procedure, was indeed an interesting result that could be advantageous for future synthesis of water resistant fluorescent *s*-tetrazine.

Lastly, we were able to find an efficient photoactive antenna, the naphthalimide, which is able to transfer almost quantitatively its energy to *s*-tetrazine, and make it much brighter, without affecting neither the stability of the dyad or bringing along large synthetic difficulties. As seen from the many trials shown, it was not quite certain to be able to obtain such a result when the work was started. Actually this molecule is now being patented, and we are now at the edge of finding real life applications for it (for example for anti-fraud labeling). This research area is still active in the group and other efficient antennas are actively looked after.

We hope we have made the demonstration that *s*-tetrazines are indeed fascinating molecules, and their development, for spectroscopic and analytical applications is only starting now after a long period of disinterest among the chemists community. It is very likely that many compounds and materials with remarkable properties featuring this unique little ring will be discovered in the coming years.

# Chapter 5 Experimental Section

## General procedures

### Synthesis

Commercial reagents were purchased from Sigma-Aldrich or Acros Chemical and used as received. All solvents for synthesis were synthetic grade and purchased from Carlo-Erba. Anhydrous solvents were freshly distilled before use according to published procedures. Microwave synthesis reactor was monowave 300 from Anton Paar Company. All column chromatographies (CC) were performed on silica gel 60 (0.040-0.063mm), silica gel SDS (Société de Documentation et Synthèse, Peypin, Bouches du Rhone). Analytical thin layer chromatographies (TLC) were performed on silica gel 60F254 (60A/15 $\mu$ m) coated on aluminum plates (SDS), and detected by UV (254nm or 365nm). The deuterated solvents were purchased from SDS. NMR spectra were recorded on a JEOL ECS-400 spectrometer. Chemical shifts are given in ppm related to the protonated solvent as internal reference ( $^1\text{H}$ :  $\text{CHCl}_3$  in  $\text{CDCl}_3$ , 7.26ppm;  $\text{CHD}_2\text{SOCD}_3$  in  $\text{CD}_3\text{SOCD}_3$ , 2.49ppm;  $\text{CHD}_2\text{CN}$  in  $\text{CD}_3\text{CN}$ , 1.94ppm;  $^{13}\text{C}$ :  $^{13}\text{CDCl}_3$  in  $\text{CDCl}_3$ , 77.14ppm;  $^{13}\text{CD}_3\text{SOCD}_3$  in  $\text{CD}_3\text{SOCD}_3$ , 39.6ppm;  $^{13}\text{CD}_3\text{CN}$  in  $\text{CD}_3\text{CN}$ , 1.3ppm, 118.3ppm). Coupling constants (J) are given in Hz. Mass spectrometry was performed on a MS Spectrometer (LC)ESI/TOF (LCT Waters, 2001), in the CNRS laboratory “imagif” (Gif sur Yvette). Melting points were measured with a Kofler melting point apparatus.

### Absorption and fluorescence spectroscopies

All solvents were of spectroscopic grade.

#### *Steady-state spectroscopy*

All spectroscopic experiments were carried out in DCM (spectroscopic grade from SDS) and at concentrations *ca.* 10  $\mu\text{mol.L}^{-1}$  for absorption spectra and *ca.* 1  $\mu\text{mol.L}^{-1}$  for fluorescence spectra where only dilute solutions with an absorbance below 0.1 at the excitation wavelength  $\lambda_{\text{ex}}$  were used. UV/vis absorption spectra were recorded on a Varian Cary 500 spectrophotometer. Fluorescence emission and excitation spectra were measured on a SPEX fluorolog-3 (Horiba Jobin-Yvon). For

emission fluorescence spectra, the excitation wavelengths were usually set equal to the maximum of the corresponding absorption spectra. Sulforhodamine 101 in ethanol ( $\Phi_F = 0.9$ ) was used for the determination of the relative fluorescence quantum yields.

### *Time-resolved spectroscopy*

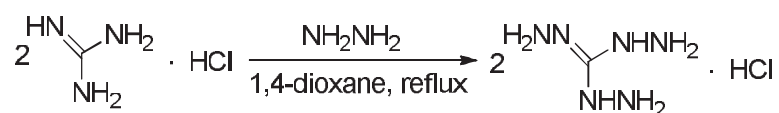
The fluorescence decay curves were obtained with a time-correlated single-photon-counting (TSPC) method using a titanium-sapphire laser (1015 nm, 82 MHz, repetition rate lowered to 0.8 MHz thanks to a pulse peaker, 1 ps pulse width) pumped by an argon ion laser. A doubling or tripler crystal is used to reach 495 and 355 nm excitations. Data were analyzed by a nonlinear least-squares method (Levenberg-Marquardt algorithm) with the aid of Globals software (Globals Unlimited, University of Illinois at Urbana-Champaign, Laboratory of Fluorescence Dynamics). Pulse deconvolution was performed from the time profile of the exciting pulse recorded under the same conditions by using a Ludox solution. To estimate the quality of the fit, the weighted residuals were calculated. In the case of single photon counting, they are defined as the residuals, that is, the difference between the measured value and the fit, divided by the square root of the fit.  $\chi^2$  is equal to the variance of the weighted residuals. A fit was said to be appropriate for  $\chi^2$  values between 0.8 and 1.2.

### **Electrochemistry**

Electrochemical studies were performed using dichloromethane (DCM) (SDS, anhydrous for analysis) as a solvent, with *N,N,N,N*-tetrabutylammonium hexafluorophosphate (TBAP) (Fluka, puriss.) as the supporting electrolyte. The substrate concentration was *ca.* 5 mmol.L<sup>-1</sup>. A homemade 1 mm diameter Pt or glassy carbon electrode was used as the working electrode, along with an Ag<sup>+</sup>/Ag (10<sup>-2</sup> M) reference electrode and a Pt wire counter electrode. The cell was connected to a CH Instruments 600B potentiostat monitored by a PC computer. The reference electrode was checked versus ferrocene as recommended by IUPAC. In our case, E°(Fc<sup>+</sup>/Fc) = 0.097 V. All solutions were degassed by argon bubbling prior to each experiment.

#### 5.1 Preparation of 3,6-dichoro-1,2,4,5-tetrazine

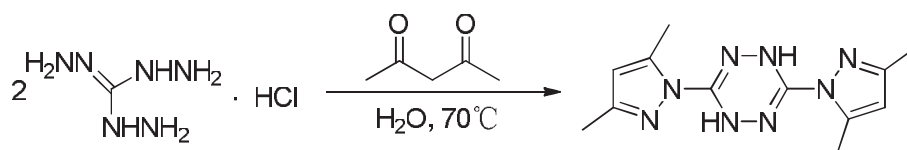
##### 5.1.1 Preparation of triaminoguanidine monohydrochloride.



To a slurry of guanidine hydrochloride (19.1g, 0.20mol) in 1,4-dioxane (100ml) was added hydrazine monohydrate (34.1g, 0.68mol) with stirring. The mixture was heated under reflux for 2 hours. After the mixture cooled to ambient temperature, the product was collected by filtration, washed with 1, 4-dioxane, and dried to give 27.7g (98%) of pure triaminoguanidine monohydrochloride.

$^{13}\text{C}$  NMR (100MHz,  $\text{D}_2\text{O}$ ):  $\delta$  160.8 ppm.

### 5.1.2 Preparation of 3,6-bis (3,5-dimethylpyrazol-1-yl)-1,2-dihydro-1,2,4,5-tetrazine

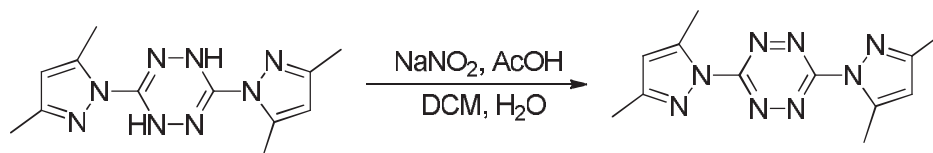


To a solution of triaminoguanidine monohydrochloride (7.03g, 0.05mol) in water (50ml) was added 2,4-pentanedione (10.26ml, 0.1mol) dropwise with stirring at  $25^\circ\text{C}$  for 0.5h. It was heated at  $70^\circ\text{C}$  for 4h, during which time solid precipitated from solution. The product was filtered from the cooled mixture, washed with water, and dried to yield 5.77g (85%) of pure 3,6-bis-(3,5-dimethylpyrazol-1-yl)-1,2-dihydro-*s*-tetrazine.

$^1\text{H}$  NMR (400MHz,  $\text{CDCl}_3$ )  $\delta$ : 2.21 (s, 6H), 2.47 (s, 6H), 5.95 (s, 2H), 8.09 (bs, 2H) ppm.

$^{13}\text{C}$  NMR (100MHz,  $\text{CDCl}_3$ ):  $\delta$  13.4, 13.7, 109.8, 142.3, 145.8, 149.9 ppm.

### 5.1.3 Preparation of 3, 6-bis (3,5-dimethylpyrazol-1-yl)-1,2,4,5-tetrazine



In a 1L two necked round bottom flask, a solution of sodium nitrite (26.2g, 0.38mol) in 588ml of water was prepared and 60ml of DCM was added. The temperature was lowered at  $0^\circ\text{C}$  and 3, 6-bis (3, 5-dimethylpyrazol-1-yl)-1,2-dihydro-*s*-tetrazine (37g, 0.136mol) was introduced. Acetic acid (18.67ml, 0.326mol) was added dropwise. After gas evolution stopped, the organic layer was separated and the aqueous layer was extracted with DCM (3\*100ml). The organic layer are reunited,

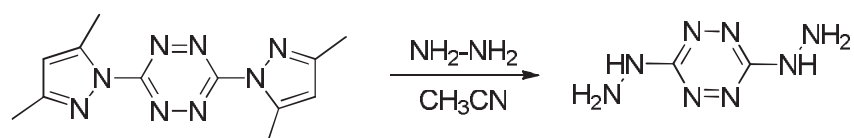


washed to neutrality with 5% aqueous solution of  $K_2CO_3$ , dried over calcium chloride and filtered. The crude product is obtained by evaporation of the solvent under reduced pressure. The dark red solid obtained is washed several times with diethyl ether to give 33.45g (91%) of pure 3,6-bis(3,5-dimethyl-1H-pyrazol-1-yl)-*s*-tetrazine.

$^1H$  NMR (400MHz,  $CDCl_3$ ):  $\delta$  2.39 (s, 6H), 2.72 (s, 6H), 6.20 (s, 2H) ppm;

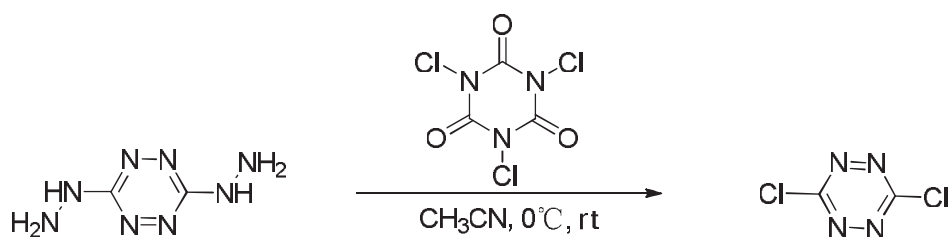
$^{13}C$  NMR (100MHz,  $CDCl_3$ ):  $\delta$  13.9, 14.7, 111.9, 143.8, 154.5, 159.3 ppm.

#### 5.1.4 Preparation of 3, 6-dihydrazino-1, 2, 4, 5-tetrazine



To a slurry of 3,6-bis(3,5-dimethyl-1H-pyrazol-1-yl)-*s*-tetrazine (23.8g, 0.09mol) in acetonitrile (150ml), was added hydrazine monohydrate (9.4ml, 0.19mol) dropwise at the ambient temperature. After the addition was complete, the mixture was refluxed for 20min. the mixture was cooled to room temperature, filtered, and washed with acetonitrile to provide 3,6-dihydrazinyl-*s*-tetrazine in quantitative yield.

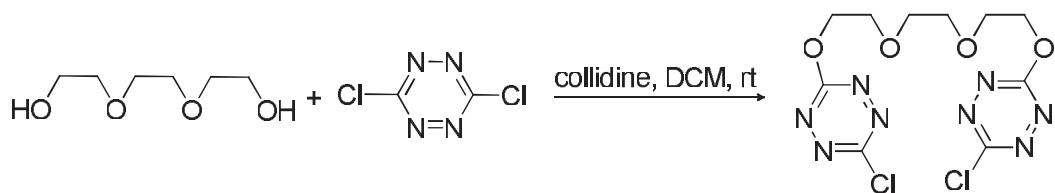
#### 5.1.5 Preparation of 3, 6-dichloro-1,2,4,5-tetrazine



To a slurry of 3,6-dihydrazinyl-*s*-tetrazine (12.5g, 0.088mol) in acetonitrile (350ml) at  $0^\circ C$  was added dropwise over 30 min a solution of trichloroisocyanuric acid (40.8g, 0.18mol) in acetonitrile (250ml). After the addition was finished, the reaction vessel was allowed to warm to room temperature and stirred for 20min. The white insoluble precipitate was removed by filtration and the volatiles removed in vacuo to give crude 3,6-dichloro-*s*-tetrazine which was passed through a short column chromatography to afford 10.75g (81%) of pure product as an orange powder.

$^{13}C$  NMR (100MHz,  $CDCl_3$ ):  $\delta$  168.1 ppm.

#### 5.2 Preparation of 1,6-bis (6-chloro-1,2,4,5-tetrazine-3-yloxy) triethylene glycane



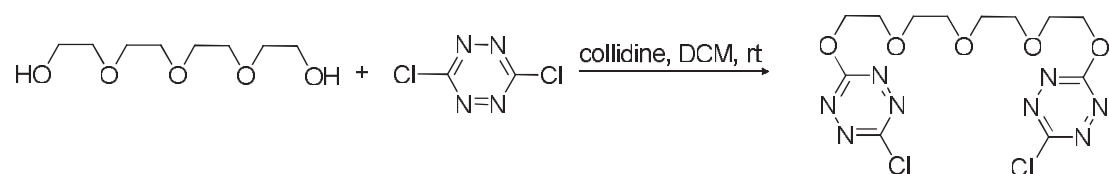
In a 50ml flacon, 0.15g (1mmol) triethylene glycol was dissolved in 20ml dry DCM, 0.35 g (2.32mmol) 3, 6-dichloro-1,2,4,5-tetrazine was added, then 0.15ml collidine was dropped under argon. The reaction was keep at room temperature for 3h, and then the solvent was removed in vacuo. The mixture was purified by column (PE: DCM =5:1), 0.35g (yield is 92%) product was obtained.

$^1\text{H}$  NMR (400MHz,  $\text{CDCl}_3$ ):  $\delta$  3.74 (m, 4H), 3.98 ( m, 4H ), 4.81 ( m, 4H ) ppm ;

$^{13}\text{C}$  NMR (100MHz,  $\text{CDCl}_3$ ):  $\delta$  68.7, 69.7, 70.9, 164.4, 166.7 ppm.

Mass: (M+Na) $^+$ : 401.0272.

### 5.3 Preparation of 1,6-bis (6-chloro-1,2,4,5-tetrazine-3-yloxy) tetraethylene glycane



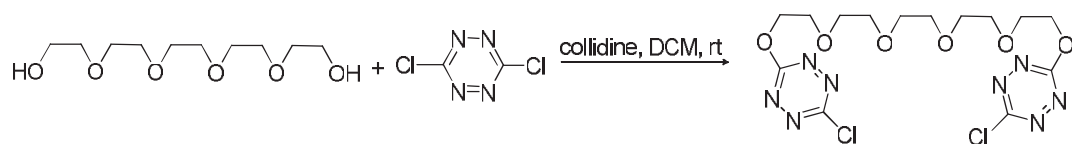
In a 50ml flacon, 0.338g (1.74mmol) tetraethylene glycol was dissolved in 20ml dry DCM, 0.663g (4.39mmol) 3, 6-dichloro-1,2,4,5-tetrazine was added, then 0.58ml collidine was dropped under argon. The reaction was keep at room temperature for 3h, and then the solvent was removed in vacuo. The mixture was purified by column (PE: DCM =5:1), 0.6g (yield is 80%) product was obtained.

$^1\text{H}$  NMR (400MHz,  $\text{CDCl}_3$ ):  $\delta$  3.65 (m, 4H), 3.72 ( m, 4H ), 3.99 ( m, 4H ), 4.83 (m, 4H) ppm.

$^{13}\text{C}$  NMR (100MHz,  $\text{CDCl}_3$ ):  $\delta$  68.6, 69.7, 70.5, 70.7, 164.2, 166.6 ppm.

Mass: (M+Na) $^+$ : 445.0513

### 5.4 Preparation of 1,6-bis (6-chloro-1,2,4,5-tetrazine-3-yloxy) pentaethylene glycane



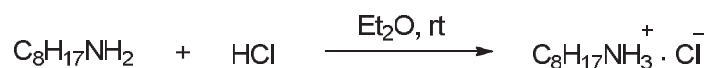
In a 100ml flacon, 0.30g (1.3mmol) pentaethylene glycol was dissolved in 50ml dry DCM, 0.5g (3.3mmol) 3, 6-dichloro-1,2,4,5-tetrazine was added, then 0.43ml collidine was dropped under argon. The reaction was kept at room temperature for 3h, and then the solvent was removed in vacuo. The mixture was purified by column (PE: DCM =5:1), 0.28g (yield is 46%) product was obtained.

$^1\text{H}$  NMR (400MHz,  $\text{CDCl}_3$ ):  $\delta$  3.61 (m, 4H), 3.67 (m, 4H), 3.94 (m, 4H), 4.07 (m, 4H), 4.78 (m, 4H) ppm.

$^{13}\text{C}$  NMR (100MHz,  $\text{CDCl}_3$ ):  $\delta$  60.5, 68.7, 69.9, 70.7, 71.0, 164.4, 166.8 ppm.

Mass:  $(\text{M}+\text{Na})^+$ : 489.0780

### 5.5 Preparation of *n*-octylammonium chloride



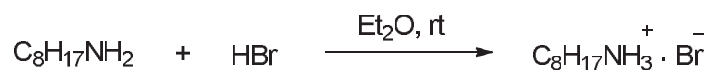
An excess of aqueous 36% HCl (3ml) was added to a solution of octylamide (2ml, 12.1 mmol) in  $\text{Et}_2\text{O}$  (20ml). The resulting mixture was stirred at room temperature for 30min. The solvent was removed under reduced pressure and the product recrystallized from  $\text{Et}_2\text{O}$  at  $0^\circ\text{C}$ . 1.5g (yield is 75%) white crystals was obtained.

$^1\text{H}$  NMR (400MHz,  $\text{CDCl}_3$ ):  $\delta$  0.87 (t, 3H,  $\text{CH}_3$ ), 1.37-1.27 (m, 10H,  $(\text{CH}_2)_5\text{CH}_2\text{CH}_2\text{NH}_3$ ), 1.77 (m, 2H,  $\text{CH}_2\text{CH}_2\text{NH}_3$ ), 2.98 (m, 2H,  $\text{CH}_2\text{NH}_3$ ), 8.28 (brs, 3H;  $\text{NH}_3$ ) ppm

$^{13}\text{C}$  NMR (100MHz,  $\text{CDCl}_3$ ):  $\delta$ : 14.1, 22.6, 26.5, 27.7, 28.9, 29.1, 31.7, 40.1 ppm.

m.p.:  $204\text{-}205^\circ\text{C}$

### 5.6 Preparation of *n*-octylammonium bromide



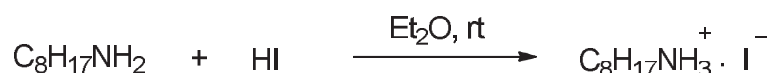
An excess of aqueous 48% HBr (6ml) was added to a solution of octylamide (4ml, 24.2 mmol) in  $\text{Et}_2\text{O}$  (40ml). The resulting mixture was stirred at room temperature for 1h. The solvent was removed in vacuo and the product recrystallized from acetone at  $0^\circ\text{C}$ . 2.15g (yield is 43%) light yellow crystals was obtained.

$^1\text{H}$  NMR (400MHz,  $\text{CDCl}_3$ ):  $\delta$  0.88 (t, 3H,  $\text{CH}_3$ ,  $J=6.6\text{Hz}$ ), 1.40-1.27 (m, 10H,  $(\text{CH}_2)_5\text{CH}_2\text{CH}_2\text{NH}_3$ ), 1.81 (m, 2H,  $\text{CH}_2\text{CH}_2\text{NH}_3$ ), 3.04 (m, 2H,  $\text{CH}_2\text{NH}_3$ ), 7.93 (brs, 3H;  $\text{NH}_3$ ) ppm.

$^{13}\text{C}$  NMR (100MHz,  $\text{CDCl}_3$ ):  $\delta$  14.3, 22.8, 26.7, 27.7, 29.1, 29.2, 31.9, 40.2 ppm.

m.p.: 207-208°C.

### 5.6 Preparation of *n*-octylammonium iodide



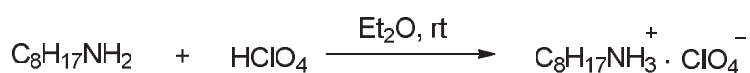
An excess of aqueous 57% HI (3ml) was added to a solution of octylamide (3ml, 12.1 mmol) in  $\text{Et}_2\text{O}$  (20ml). The resulting mixture was stirred at room temperature for 1h. The solvent was removed in vacuo and the product recrystallized from petroleum ether at 0°C. 1.5g (yield is 48%) yellow crystals was obtained.

$^1\text{H}$  NMR (400MHz,  $\text{CDCl}_3$ ):  $\delta$  0.88 (t, 3H,  $\text{CH}_3$ ), 1.42-1.27 (m, 10H,  $(\text{CH}_2)_5\text{CH}_2\text{CH}_2\text{NH}_3$ ), 1.86 (m, 2H,  $\text{CH}_2\text{CH}_2\text{NH}_3$ ), 3.14(m, 2H,  $\text{CH}_2\text{NH}_3$ ), 7.52 (brs, 3H;  $\text{NH}_3$ ) ppm.

$^{13}\text{C}$  NMR (100MHz,  $\text{CDCl}_3$ ):  $\delta$  14.3, 22.8, 26.8, 27.5, 29.1, 29.2, 31.9, 40.7 ppm.

m.p.: 205-206°C

### 5.7 Preparation of *n*-octylammonium perchlorate

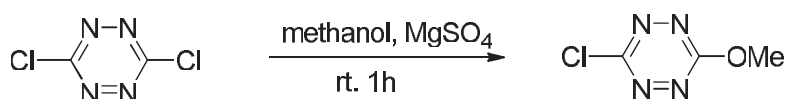


An excess of aqueous 60%  $\text{HClO}_4$  (0.3ml) was added to a solution of octylamide (0.42ml, 1.7 mmol) in  $\text{Et}_2\text{O}$  (10ml). The resulting mixture was stirred at room temperature for 1h. The solvent was removed in vacuo and the product recrystallized from petroleum ether at 0°C. 0.38g (yield is 99%) white crystals was obtained.

$^1\text{H}$  NMR (400MHz,  $\text{CDCl}_3$ ):  $\delta$  0.88 (t, 3H,  $\text{CH}_3$ ), 1.37-1.27 (m, 10H,  $(\text{CH}_2)_5\text{CH}_2\text{CH}_2\text{NH}_3$ ), 1.73 (m, 2H,  $\text{CH}_2\text{CH}_2\text{NH}_3$ ), 3.14(m, 2H,  $\text{CH}_2\text{NH}_3$ ), 7.17 (brs, 3H;  $\text{NH}_3$ ) ppm.

$^{13}\text{C}$  NMR (100MHz,  $\text{CDCl}_3$ ):  $\delta$  14.3, 22.8, 26.4, 27.4, 29.1, 29.2, 31.9, 41.5 ppm.

### 5.8 Preparation of 3-choro-6-methoxy-1,2,4,5-tetrazine

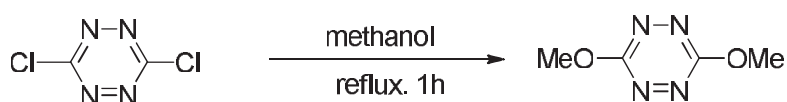


To a solution of dichloro-*s*-tetrazine (1.0g, 6.62mmol) in 100ml of methanol was added 0.5g MgSO<sub>4</sub>. The mixture was stirred at room temperature for 1h. The solids were filtered and washed with twice DM, and the filtrate was evaporated. After a short column chromatography (PE: EA= 8:1), a red fluorescent solid was obtained which is easy to sublimate (0.5g, 50%).

<sup>1</sup>H NMR (400MHz, CDCl<sub>3</sub>): δ 4.33 (s, 3H) ppm.

<sup>13</sup>C NMR (100MHz, CDCl<sub>3</sub>): δ 57.5, 164.6, 167.1 ppm.

### 5.9 Preparation of 3,6-dimethoxy-1,2,4,5-tetrazine

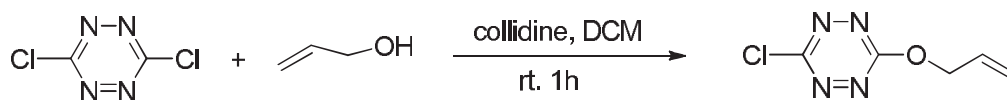


To a solution of dichloro-*s*-tetrazine (1.0g, 6.62mmol) in 100ml of methanol was added 0.5g MgSO<sub>4</sub>. The mixture was stirred at room temperature for 1h. The solids were filtered and washed with twice DM, and the filtrate was evaporated. After a short column chromatography (PE: EA= 8:1), a red fluorescent solid was obtained which is easy to sublimate (0.1g, 10.6%).

<sup>1</sup>H NMR (400MHz, CDCl<sub>3</sub>): δ 4.23 (s, 3H) ppm.

<sup>13</sup>C NMR (100MHz, CDCl<sub>3</sub>): δ 56.8, 165.6 ppm.

### 5.10 Preparation of 3-(allyloxy)-6-chloro-1,2,4,5-tetrazine

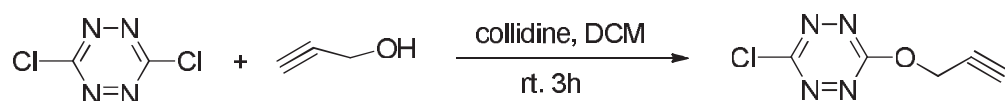


In a 150ml flacon, 0.40g (6.90mmol) allyl alcohol was added in 100ml dry DCM, 1.05g (6.95mmol) 3, 6-dichloro-1,2,4,5-tetrazine was added, then 0.91ml collidine was dropped under argon. The reaction was kept at room temperature for 1h,

and then the solvent was removed in vacuo. The mixture was purified by column (PE: EA =4:1), 0.51g (yield is 43%) was obtained.

$^1\text{H}$  NMR (400MHz,  $\text{CDCl}_3$ ):  $\delta$  5.17 (d,  $J=5.96\text{Hz}$ , 2H), 5.43 (m, 1H), 5.55 (m, 1H), 6.13 (m, 2H) ppm.

#### 5.11 Preparation of 3-chloro-6-(prop-2-ynoxy)-1,2,4,5-tetrazine

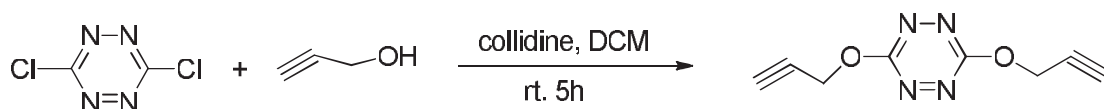


In a 150ml flacon, 0.39ml (6.60mmol) propargyl alcohol was added in 100ml dry DCM, 1.0g (6.62mmol) 3, 6-dichloro-1,2,4,5-tetrazine was added, then 0.90ml collidine was dropped under argon. The reaction was keep at room temperature for 3h, and then the solvent was removed in vacuo. The mixture was purified by column (PE: EA =2:1), 0.50g (yield is 44.6%) was obtained.

$^1\text{H}$  NMR (400MHz,  $\text{CDCl}_3$ ):  $\delta$  2.63 (t,  $J=2.28\text{Hz}$ , 1H), 5.30 (d,  $J=2.76\text{Hz}$ , 2H) ppm.

$^{13}\text{C}$  NMR (100MHz,  $\text{CDCl}_3$ ):  $\delta$  57.8, 75.7, 77.5, 165.2, 166.1 ppm.

#### 5.12 Preparation of 3,6-bi(prop-2-ynoxy)-1,2,4,5-tetrazine

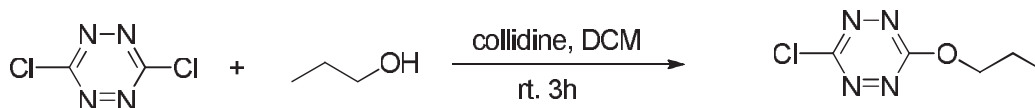


In a 150ml round bottom flask, 0.39ml (6.60mmol) propargyl alcohol was added in 100ml dry DCM, 1.0g (6.62mmol) 3, 6-dichloro-1,2,4,5-tetrazine was added, then 0.90ml collidine was dropped under argon. The reaction was keep at room temperature for 5h, and then the solvent was removed in vacuo. The mixture was purified by column (PE: EA =2:1), 0.40g (yield is 63.7%) red compound was obtained.

$^1\text{H}$  NMR (400MHz,  $\text{CDCl}_3$ ):  $\delta$  2.59 (t,  $J=2.28\text{Hz}$ , 2H), 5.23 (d,  $J=2.28\text{Hz}$ , 4H) ppm.

$^{13}\text{C}$  NMR (100MHz,  $\text{CDCl}_3$ ):  $\delta$  57.2, 76.5, 76.8, 165.7 ppm.

#### 5.13 Preparation of 3-chloro-6-propanoxy-1,2,4,5-tetrazine

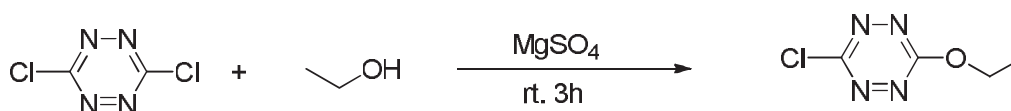


To a solution of dichloro-*s*-tetrazine (0.5g, 3.31mmol) in 50ml of dry DM was added 1-propanol (0.25ml, 3.30mmol) and 0.45ml collidine under N<sub>2</sub>. The mixture was stirred at room temperature for 5h. Then the solvent was removed in vacuo, after a short column chromatography (PE: EA= 2:1), the pure compound was obtained (0.42g, 73%).

<sup>1</sup>H NMR (400MHz, CDCl<sub>3</sub>): δ 1.12 (t, *J*=7.56Hz, 3H), 1.18 (m, 2H), 4.62 (t, *J*=6.42Hz, 2H) ppm.

<sup>13</sup>C NMR (100MHz, CDCl<sub>3</sub>): δ 5.9, 17.6, 68.1, 159.8, 162.4 ppm.

#### 5.14 Preparation of 3-chloro-6-ethoxy-1,2,4,5-tetrazine

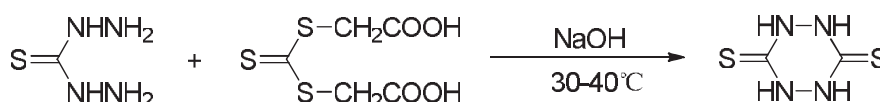


To a solution of dichloro-*s*-tetrazine (0.8g, 0.53mmol) in 30ml of ethanol was added 1.48g MgSO<sub>4</sub>. The mixture was stirred at room temperature for 3h. The solids were filtered and washed with twice DM, and the filtrate was evaporated. After a short column chromatography (PE: EA= 2:1), the pure compound was obtained (0.5g, 58.8%).

<sup>1</sup>H NMR (400MHz, CDCl<sub>3</sub>): δ 1.59 (t, *J*=7.32Hz, 3H), 4.73 (dd, *J*<sub>1</sub>=7.32Hz, *J*<sub>2</sub>=14.2Hz, 2H) ppm.

<sup>13</sup>C NMR (100MHz, CDCl<sub>3</sub>): δ 14.3, 67.1, 164.4, 166.7 ppm.

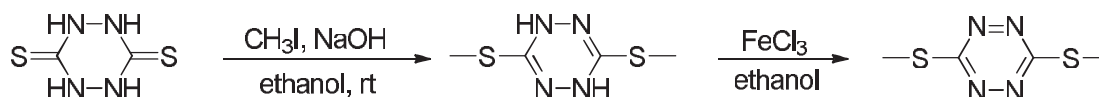
#### 5.15 Preparation of 1,4-dihydro-1,2,4,5-tetrazinane-3,6-dithiol



The thiocarbohydrazide (5.3g, 0.05mol) was dissolved in 75ml of water and heated to 40°C. To this solution was added dropwise a solution of dicarboxymethyl-trithiocarbonate (11.3g, 0.05mol) in 100ml of 1N NaOH. The mixture was stirred at 40°C for another 20min and at room temperature for 30min, then cooled to 0°C. The

slightly yellow solids were filtered out, washed with water, and dried in vacuum (3.16g, 43%).

#### 5.16 Preparation of 3,6-bis (methylthio)-1,2,4,5-tetrazine



Dithio-*p*-urazine (3.16g, 0.021mol) was dissolved in 1N aq. NaOH (1.76g, 0.042mol) and degassed with Ar. A solution of CH<sub>3</sub>I (2.7ml, 0.021mol) in 20ml of ethanol was added dropwise through a dropping funnel, during which time a pale yellow solid precipitated. The mixture was stirred for another 2 hours and the solids were filtered, washed with water and dried in vacuum to give 3,6-bis(methylthio)-1,4-dihydro-*s*-tetrazine (0.7g, 20%).

<sup>1</sup>H NMR (400MHz, CDCl<sub>3</sub>): δ 2.41 (s, 6H), 6.54 (br, 2H) ppm.

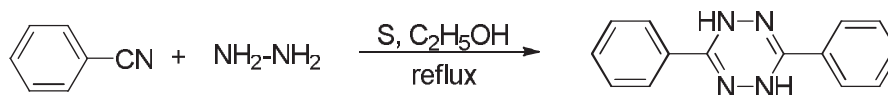
<sup>13</sup>C NMR (100MHz, CDCl<sub>3</sub>): δ 14.1, 150.9 ppm.

An aqueous 2N solution of ferric chloride (1.37g, 8.2mmol) was added dropwise to the solution of 3,6-bis(methylthio)-1,4-dihydro-*s*-tetrazine (0.72g, 4.1mmol) in ethanol at room temperature. The mixture was stirred for 30min and extracted with ether. The ether layer was dried with MgSO<sub>4</sub>, and the ether was removed by evaporation. After a short column chromatography (silica, PE:EA=5:1) 0.22g (yield is 31%) of 3,6-bis(methylthio)-*s*-tetrazine was obtained as a red solid.

<sup>1</sup>H NMR (400MHz, CDCl<sub>3</sub>): δ 2.71 (s, 6H) ppm.

<sup>13</sup>C NMR (100MHz, CDCl<sub>3</sub>): δ 13.4, 172.8 ppm.

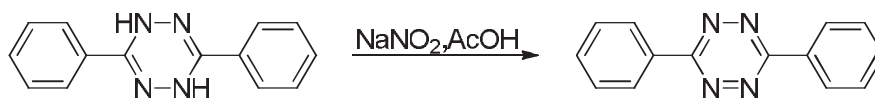
#### 5.17 Preparation of 1, 4-dihydro-3, 6-diphenyl-1,2,4,5-tetrazinane



Treatment of a solution of benzonitrile (5.16g, 0.05mole) in ethanol (15ml) with hydrazine hydrate (10ml), followed by the addition of flowers of sulphur (1g) and heating the mixture at reflux for 2 hours afforded yellow powder 8.3g 1,4-dihydro-3,6-diphenyl-1,2,4,5-dihydrotetrazine, the yield is 70%.

#### 5.18 Preparation of 3, 6-diphenyl-1,2,4,5-tetrazinane



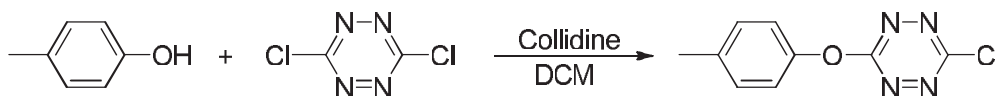


In a 250ml round bottom flask, a solution of sodium nitrite (3.38g, 0.05mol) in 76ml of water was prepared and 8ml of DCM was added. The temperature was lowered at 0 °C and 1,2-dihydro-3,6-diphenyl-1,2,4,5-dihydro-tetrazine (4.15g, 0.018mol) was introduced. Acetic acid (2.41ml, 0.042mol) was added dropwise. After gas evolution stopped, the organic layer was separated and the aqueous layer was extracted with DCM (3x25ml). The organic layer are reunited, washed to neutrality with 5% aqueous solution of K<sub>2</sub>CO<sub>3</sub>, dried over calcium chloride and filtered. The crude product is obtained by evaporation of the solvent under reduced pressure. The dark red solid obtained is washed several times with diethyl ether to give 3.6g of pure 3, 6- diphenyl- *s*-tetrazine, yield is 85%.

<sup>1</sup>H NMR (400MHz, CDCl<sub>3</sub>): δ 7.76 (m, 6H), 8.67 (m, 4H) ppm.

<sup>13</sup>C NMR (100MHz, CDCl<sub>3</sub>): δ 128.1, 129.3, 131.8, 132.7, 164.1 ppm.

#### 5.20 Preparation of 3-chloro-6-(*p*-tolylloxy)-1,2,4,5-tetrazine



*p*-cresol (0.37g, 3.4mmol) and 3,6-dichloro tetrazine (0.56g, 3.7mmol) were dissolved in dry 50ml dry dichloromethane, 2,4,6-collidine (0.50ml, 3.6mmol) was added at room temperature under N<sub>2</sub>. After stirring 2h, the solvent was removed under reduced pressure, and purified by column chromatography (PE: DCM=1:1). 0.60g product is obtained, yield is 79%.

<sup>1</sup>H NMR (400MHz, CDCl<sub>3</sub>): δ 2.41 (s, 3H), 7.14 (d, 2H, *J*=8.2Hz), 7.28 (d, 2H, *J*=7.8Hz) ppm.

<sup>13</sup>C NMR (100MHz, CDCl<sub>3</sub>): δ 21.1, 120.4, 130.7, 136.9, 149.5, 165.1, 167.7 ppm.

#### 5.21 Preparation of 3,6-di(*p*-tolylloxy)-1,2,4,5-tetrazine



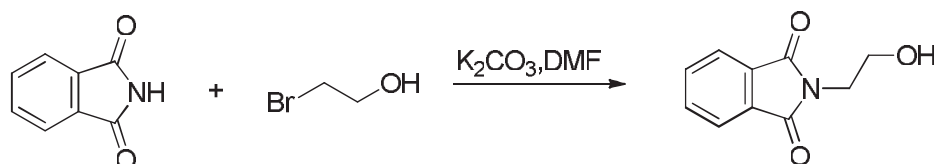
*p*-cresol (0.5g, 4.6mmol) and 3,6-dichloro tetrazine (0.3g, 2.0mmol) were dissolved in dry 30ml dry dichloromethane, 2,4,6-collidine (0.60ml, 4.1mmol) was added at room temperature under N<sub>2</sub>. After refluxing 2h, the solvent was removed

under reduced pressure, and purified by column chromatography (PE: DCM=1:1). 0.50g product is obtained, yield is 89%.

$^1\text{H}$  NMR ( $\text{CDCl}_3$ ):  $\delta$  2.38 (s, 6H), 7.13 (d, 4H,  $J=8.2\text{Hz}$ ), 7.23 (d, 4H,  $J=8.2\text{Hz}$ ) ppm.

$^{13}\text{C}$  NMR ( $\text{CDCl}_3$ ):  $\delta$  20.9, 120.5, 130.5, 136.2, 150.2, 167.4 ppm.

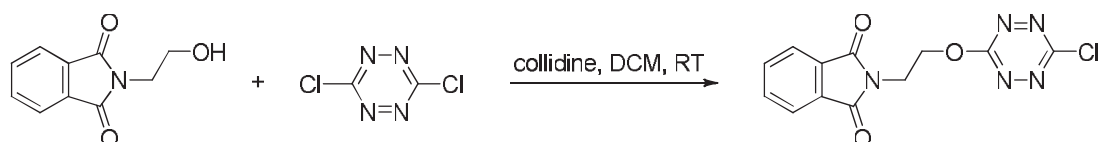
### 5.22 Preparation of N-(2-hydroxyethyl)-phthalimide



2-Bromoethanol (0.125g, 1mmol) was dissolved in 15ml DMF. To the solution potassium carbonate (0.138g, 1mmol) and phthalimide (0.147g, 1mmol) were added and then refluxed for 10h. After cooled to room temperature, the mixture was extract by ethyl acetate. The product was obtained, 0.19g, yield is 99%.

$^1\text{H}$  NMR (400MHz,  $\text{CDCl}_3$ ):  $\delta$  2.80 (s, 1H, OH), 3.87 (s, 4H, NCH<sub>2</sub>, CH<sub>2</sub>O), 7.71 (dd, 2H,  $J_1=3.0\text{Hz}$ ,  $J_2=5.4\text{Hz}$ , H-6, H-7), 7.83 (dd, 2H,  $J_1=3.0\text{Hz}$ ,  $J_2=5.4\text{Hz}$ , H-5, H-8) ppm.

### 5.23 Preparation of N-(2-(6-chloro-s-tetrazine-3-yloxy) ethyl)-phthalimide



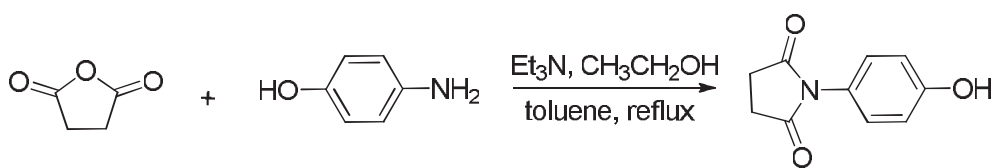
N-ethanol-phthalimide (0.191g, 1mmol) and 3,6-dichloro tetrazine (0.20g, 1.32mmol) were dissolved in dry 15ml dichloromethane, 2,4,6-collidine (0.14ml, 1mmol) was added at room temperature under N<sub>2</sub>. After stirring 2h, the solvent was removed under reduced pressure, and purified by column chromatography (PE: DCM=1:1). 0.214g product is obtained, yield is 70%.

$^1\text{H}$  NMR (400MHz,  $\text{CDCl}_3$ ):  $\delta$  4.23 (t, 2H,  $J=5.5\text{Hz}$ ), 4.91 (t, 2H,  $J=5.5\text{Hz}$ ), 7.71 (m, 2H), 7.82 (m, 2H) ppm.

$^{13}\text{C}$  NMR (100MHz,  $\text{CDCl}_3$ ):  $\delta$  36.0, 67.2, 123.5, 131.8, 134.3, 164.6, 166.3, 168.1 ppm.

m.p.: 95°C

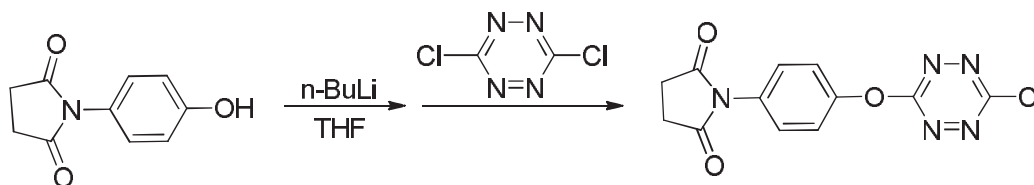
### 5.24 Preparation of N-(4-hydroxyphenyl)-2,5-pyrrolidine



4-Aminophenol (7.45g, 50mmol) and triethylamine (2ml) were added to a solution of succinimide (6.2g, 60mmol) in ethanol (100ml) and the reaction mixture was stirred at room temperature for 4h. The solvent was removed under reduced pressure and the solid residue was dried in vacuum desiccators for 24h. The residue obtained was refluxed in distilled dry toluene (20ml) for 6h using Dean and Stark apparatus to affect cyclization. The solvent was removed under reduced pressure and the solid was washed with ether. The residue was refluxed in distilled water for 0.5h to remove unreacted materials. The solid obtained was crystallized from methanol to afford (4.7g, 25.6%).

$^1\text{H}$  NMR (400MHz, DMSO- $d_6$ ):  $\delta$  2.73(4H, s), 6.82 (2H, d,  $J=8.6$  Hz ), 7.01 (2H, d,  $J=8.6$  Hz ) ppm.

#### 5.25 Preparation of N-(2-(6-chloro-*s*-tetrazine-3-yloxy) phenyl)-pyrrolidine



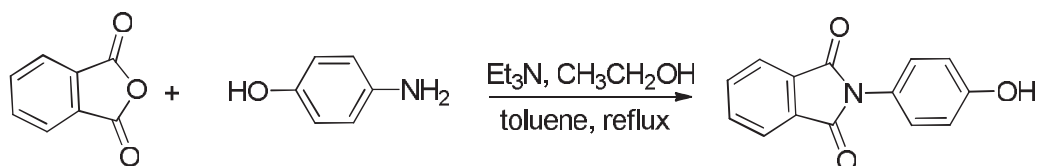
N-(4-hydroxyphenyl)-2,5-pyrrolidine (0.231g, 1mmol) was dissolved in 15ml dry THF, n-Butyllithium (0.625ml, 1mmol) was dropped under  $\text{N}_2$ . Then the solution of 3,6-dichloro-*s*-tetrazine in THF (1.0mmol/10ml) added quickly. After 1h at room temperature, the solvent was removed under reduced pressure, and purified by column chromatography. Yield is 0.05g, 16.4%.

$^1\text{H}$  NMR (400MHz,  $\text{CDCl}_3$ ):  $\delta$  2.93(4H, m), 7.39 (2H, d,  $J=8.0$ Hz), 7.47 (2H, d,  $J=8.0$  Hz ) ppm.

$^{13}\text{C}$  NMR (100MHz,  $\text{CDCl}_3$ ):  $\delta$  28.5, 115.3, 121.1, 128.9, 130.4, 152.0, 166.9, 177.0 ppm.

Mass ( $\text{M}^+$ ): 305

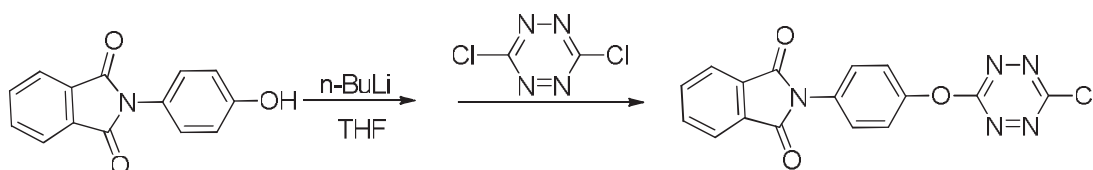
#### 5.26 Preparation of N-(2-hydroxyphenyl)-phthalimide



4-Aminophenol (2.0g, 18mmol) and triethylamine (2ml) were added to a solution of phthalic anhydride (3.0g, 20mmol) in ethanol (100ml) and the reaction mixture was stirred at room temperature for 4h. The solvent was removed under reduced pressure and the solid residue was dried in a vacuum desiccators for 24h. The residue obtained was refluxed in distilled dry toluene (20ml) for 6h using Dean and Stark apparatus to effect cyclization. The solvent was removed under reduced pressure and the solid was washed with ether. The residue was refluxed in distilled water for 0.5h to remove unreacted materials. The solid obtained was crystallized from methanol to afford (4.2g, 96%).

$^1\text{H}$  NMR (400MHz, DMSO- $d_6$ ):  $\delta$  6.80 (2H, d,  $J=9.0\text{Hz}$ ), 6.26 (2H, d,  $J=9.0\text{Hz}$ ), 7.92 (4H, m), 9.70 (1H, brs) ppm.

#### 5.27 Preparation of *N*-(2-(6-chloro-*s*-tetrazine-3-yloxy)-phenyl)-phthalimide



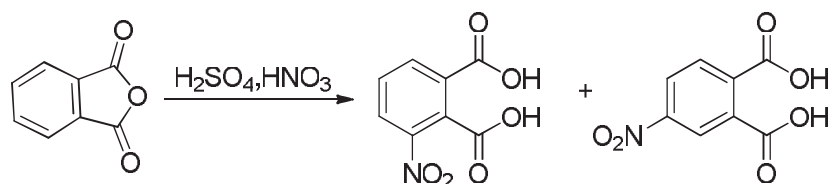
*N*-(4'-hydroxy-phenyl)phthalimide (0.239g, 1mmol) was dissolved in 15ml dry THF, *n*-Butyllithium (0.625ml, 1mmol) was dropped under  $\text{N}_2$ . Then the solution of 3,6-dichloro-*s*-tetrazine in THF (1.0mmol/10ml) added quickly. After 1h at room temperature, the solvent was removed under reduced pressure, and purified by column chromatography. Yield is 0.32g, 76.2%.

$^1\text{H}$  NMR (400MHz,  $\text{CDCl}_3$ ):  $\delta$  7.43(2H, d,  $J=6.0\text{Hz}$ ), 7.62 (2H, d,  $J=6.0\text{Hz}$ ), 7.82 (2H, m), 7.99(2H, m) ppm.

$^{13}\text{C}$  NMR (100MHz,  $\text{CDCl}_3$ ):  $\delta$  121.4, 123.5, 129.3, 130.1, 131.6, 134.8, 151.2, 164.0, 166.9, 167.3 ppm.

Mass ( $\text{M}^+$ ): 353

#### 5.28 Preparations of 3-nitrophthalic acid and 4-nitrophthalic acid

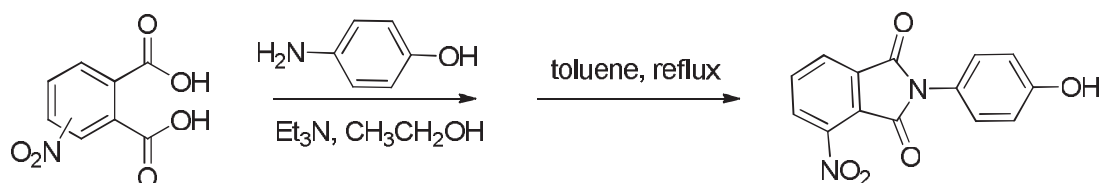


In the beaker are placed 5ml of commercial sulfuric acid cooled to 0°C and 12.5g of technical phthalic anhydride is added, the mixture is stirred by mechanical stirrer. After drop slowly the solution of sulfuric acid and nitric acid (17:20.8ml), keep the mixture reaches 80°C for 3h. Then 200ml of water poured into the crock. After cooling, the solid mixture of 3- and 4-nitrophthalic acids is filtered by suction through a Buchner funnel. The wet cake is returned to the crock and stirred thoroughly with 50ml of water, which dissolves a large amount of the 4-nitrophthalic acid. The mixture is again filtered and air-dried. The yield is 4.5g (3-:4- = 6:1).

3-nitrophthalic acid  $^1\text{H}$  NMR (400MHz, DMSO-d<sub>6</sub>):  $\delta$  7.80 (1H, t,  $J=8.0\text{Hz}$ ), 8.23 (1H, d,  $J=8.0\text{Hz}$ ), 8.33 (1H, d,  $J=8.0\text{Hz}$ ) ppm.

4-nitrophthalic acid  $^1\text{H}$  NMR (100MHz, DMSO-d<sub>6</sub>):  $\delta$  7.90 (1H, t,  $J=8.0\text{Hz}$ ), 8.42 (1H, d,  $J=8.0\text{Hz}$ ), 8.46 (1H, d,  $J=8.0\text{Hz}$ ) ppm.

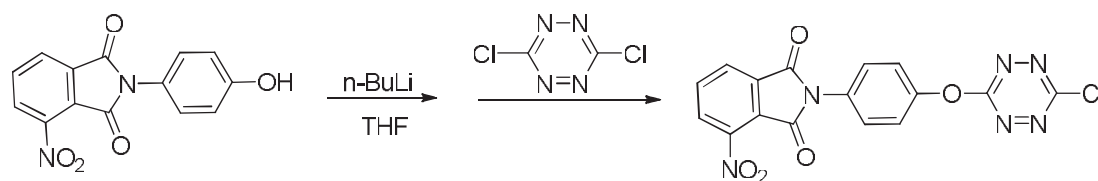
#### 5.29 Preparation of N-(2-hydroxyphenyl)-3-nitrophthalimide



4-aminophenol (3.7g, 25mmol) and triethylamine (1ml) were added to a solution of 3- and 4-nitrophthalic acid (4.5g, 20mmol) in ethanol (100ml) and the reaction mixture was stirred at room temperature for 4h. The solvent was removed under reduced pressure and the solid residue was dried in vacuum desiccators for 24h. The residue obtained was refluxed in distilled dry toluene (20ml) for 6h using Dean and Stark apparatus to effect cyclization. The solvent was removed under reduced pressure and the solid was washed with ether. The residue was refluxed in distilled water for 0.5h to remove unreacted materials. The solid obtained was crystallized from methanol to afford 0.56g N-(4'-hydroxyphenyl)-3-nitrophthalimide.

$^1\text{H}$  NMR (400MHz, DMSO-d<sub>6</sub>):  $\delta$  6.87(2H, d,  $J=8.0\text{Hz}$ ), 7.20 (2H, d,  $J=8.0\text{Hz}$ ), 8.10 (1H, m), 8.22 (1H, d,  $J=8.0\text{Hz}$ ), 8.31 (1H, d,  $J=8.0\text{Hz}$ ), 9.81(1H, br) ppm.

### 5.30 Preparation of N-(2-(6-chloro-s-tetrazine-3-yloxy) phenyl) -3-nitrophthalimide



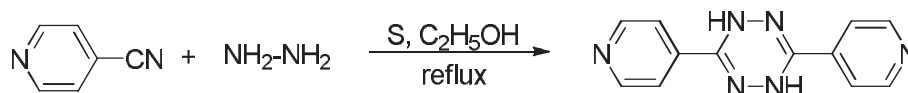
N-(4'-hydroxyphenyl)-3-nitrophthalimide (0.231g, 1mmol) was dissolved in 15ml THF, n-Butyllithium (0.625ml, 1mmol) was dropped under N<sub>2</sub>. Then the solution of 3,6-dichloro-s-tetrazine in THF (1.0mmol/10ml) added quickly. After 1h at room temperature, the solvent was removed under reduced pressure, and purified by column chromatography. Yield is 0.32g, 76.2%.

<sup>1</sup>H NMR (400MHz, CDCl<sub>3</sub>): δ 7.45(2H, d, J=8.0Hz), 7.61 (2H, d, J=8.0Hz), 8.02 (1H, m), 8.19 (1H, d, J=8.0Hz), 8.25 (1H, d, J=8.0Hz) ppm.

<sup>13</sup>C NMR (100MHz, DMSO-d<sub>6</sub>): δ 121.2, 122.6, 126.9, 128.3, 128.4, 129.1, 133.1, 136.0, 144.6, 151.1, 161.8, 164.1, 164.4, 167.1 ppm.

Mass (M<sup>+</sup>): 398

### 5.31 Preparation of 3,6-di(pyridin-4-yl)-1,4-dihydro-1,2,4,5-tetrazine

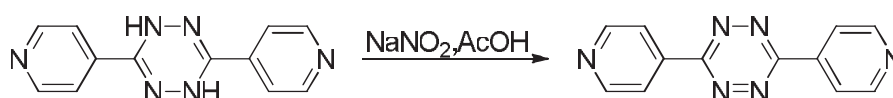


Treatment of a solution of cyanopyridine (5.2g, 0.05mole) in ethanol (20ml) with hydrazine hydrate (10ml), followed by the addition of flowers of sulphur (1g) and heating the mixture at reflux for 2 hours afforded yellow powder 8.33g 1,2-dihydro-3,6-dipyridine-1,2,4,5-dihydrotetrazine, the yield is 70%.

<sup>1</sup>H NMR (400MHz, CDCl<sub>3</sub>): δ 1.70 (s, 2H), 8.52 (d, 4H, J=6.0Hz), 8.96 (d, 4H, J=6.0Hz) ppm.

<sup>13</sup>C NMR (100MHz, CDCl<sub>3</sub>): δ 121.4, 138.7, 151.3, 163.8 ppm.

### 5.32 Preparation of 3,6-di(pyridin-4-yl)-1,2,4,5-tetrazine



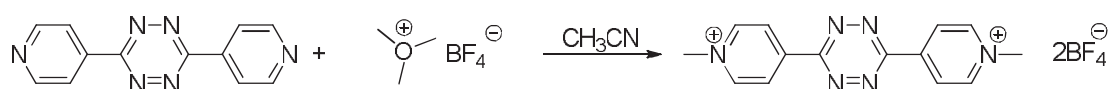
In a 250ml round bottom flask, a solution of sodium nitrite (3.45g, 0.05mol) in 76ml of water was prepared and 8ml of DCM was added. The temperature was

lowered at 0°C and 3,6-di(pyridin-4-yl)-1,4-dihydro-1,2,4,5-tetrazine (10g, 0.042mol) was introduced. Acetic acid (2.41ml, 0.042mol) was added dropwise. After gas evolution stopped, the organic layer was separated and the aqueous layer was extracted with DCM (3x25ml). The organic layer are reunited, washed to neutrality with 5% aqueous solution of K<sub>2</sub>CO<sub>3</sub>, dried over calcium chloride and filtered. The crude product is obtained by evaporation of the solvent under reduced pressure. The dark red solid obtained is washed several times with diethyl ether to give 7.9g 3,6-dipyridine-*s*-tetrazine, yield is 80%.

<sup>1</sup>H NMR (400MHz, CDCl<sub>3</sub>): δ 8.52 (d, 4H, *J*=6.0Hz), 8.96 (d, 4H, *J*=6.0Hz) ppm.

<sup>13</sup>C NMR (100MHz, CDCl<sub>3</sub>): δ 121.4, 138.6, 151.3, 163.8 ppm.

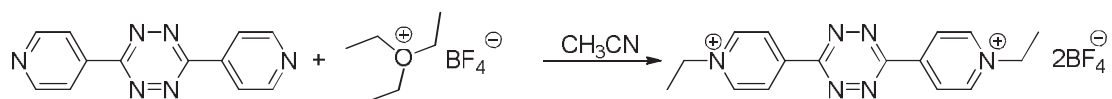
### 5.33 Preparation of 3,6-di(1-methyl-pyridin-4-yl)-1,2,4,5-tetrazine tetrafluoroborate



A mixture of 0.38g (1.6mmol) 3,6-dipyridine-*s*-tetrazine and 0.532g (3.6mmol) Me<sub>3</sub>OBF<sub>4</sub> was heated to reflux in 100ml acetonitrile for 18h. After reducing the volume to 3ml, amount of 10ml dichloroethane was added and put it in fridge(-20°C) overnight. 0.7g (yield is 99%) was obtained by filtration.

<sup>1</sup>H NMR (400MHz, CD<sub>3</sub>CN): δ 4.46 (s, 6H), 8.97 (d, 4H, *J*=6.4Hz), 9.12 (d, 4H, *J*=6.4Hz) ppm.

### 5.34 Preparation of 3,6-di(1-ethyl-pyridin-4-yl)-1,2,4,5-tetrazine tetrafluoroborate

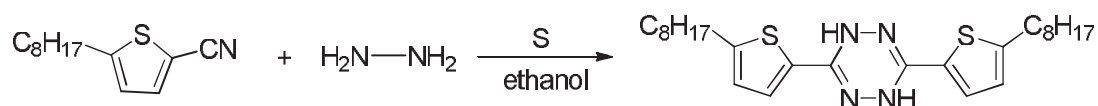


A mixture of 0.38g (1.6mmol) 3,6-dipyridine-*s*-tetrazine and 0.684g (3.6mmol) Et<sub>3</sub>OBF<sub>4</sub> was heated to reflux in 100ml acetonitrile for 18h. After reducing the volume to 3ml, amount of 10ml dichloroethane was added and put it in fridge(-20°C) overnight. 0.5g (yield is 67%) was obtained by filtration.

<sup>1</sup>H NMR (400MHz, CD<sub>3</sub>CN): δ 1.69 (t, 6H, *J*=7.3Hz), 4.75 (q, 4H), 9.04 (m, 4H), 9.20 (m, 4H) ppm.

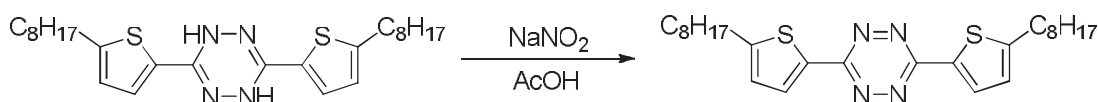
<sup>13</sup>C NMR (100MHz, CD<sub>3</sub>CN): δ 16.6, 59.0, 127.4, 127.6, 147.0, 162.8 ppm.

### 5.35 Preparation of 3,6-bis(5-octylthiophen-2-yl)-1,4-dihydro-1,2,4,5-tetrazine



Treatment of a solution of 5-octylthiophene-2-carbonitrile (1.654g, 0.07mole) in ethanol (5ml) with hydrazine hydrate (1.49ml), followed by the addition of flowers of sulphur (0.15g) and heating the mixture at reflux for 2 hours afforded yellow powder 0.34g 3,6-bis(5-octylthiophen-2-yl)-1,4-dihydro-s-tetrazine, the yield is 1%.

### 5.36 Preparation of 3,6-bis(5-octylthiophen-2-yl)-1,2,4,5-tetrazine

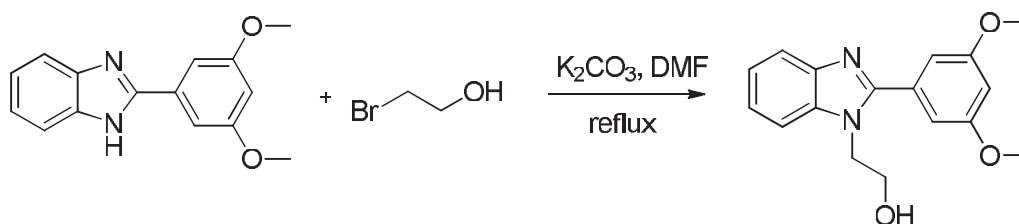


In a 50ml round bottom flask, a solution of sodium nitrite (0.128g, 0.0018mol) in 5ml of water was prepared and 2ml of DCM was added. The temperature was lowered at 0 °C and 3,6-bis(5-octylthiophen-2-yl)-1,4-dihydro-s-tetrazine (0.34g, 0.0007mol) was introduced. Acetic acid (0.09ml, 0.0016mol) was added dropwise. After gas evolution stopped, the organic layer was separated and the aqueous layer was extracted with DCM (3x25ml). The organic layer are reunited, washed to neutrality with 5% aqueous solution of K<sub>2</sub>CO<sub>3</sub>, dried over calcium chloride and filtered. The crude product is obtained by evaporation of the solvent under reduced pressure. The dark red solid obtained is washed several times with diethyl ether to give 0.2g of pure 3,6-bis(5-octylthiophen-2-yl)-s-tetrazine, yield is 60%.

<sup>1</sup>H NMR (400MHz, CDCl<sub>3</sub>): δ 0.88(t, *J*=6.88Hz, 6H), 1.28 (m, 20H), 1.75 (m, 4H), 2.90 (t, *J*=7.56Hz, 4H), 6.93 (d, *J*=3.68Hz, 2H), 8.07 (d, *J*=3.68Hz, 2H) ppm.

<sup>13</sup>C NMR (100MHz, CDCl<sub>3</sub>): δ 14.1, 22.7, 29.1, 29.2, 29.3, 30.6, 31.5, 31.8, 126.4, 130.9, 133.2, 154.3, 161.1 ppm.

### 5.37 Preparation of 2-(3,5-dimethoxyphenyl)-1-(2-hydroxyethyl)-benzimidazole





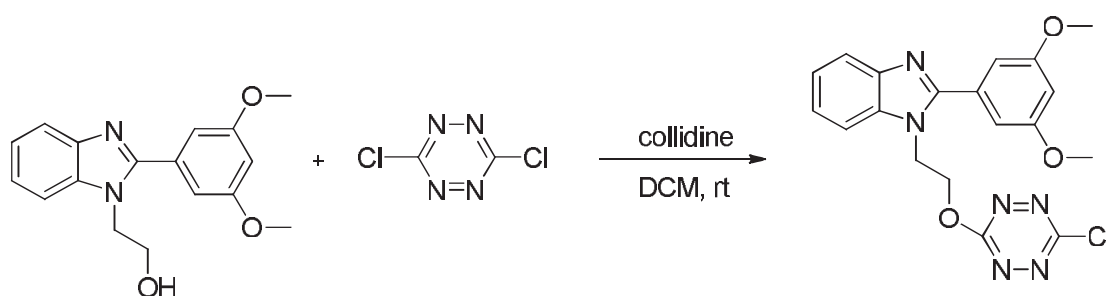
2-Bromoethanol (0.281g, 2.2mmol) was dissolved in 15 ml DMF. To the solution Potassium carbonate (0.359g, 2.6mmol) and 2-(3,5-dimethoxyphenyl)-1H-benzimidazole (0.5g, 2.0mmol) were added and then refluxed for 18h. After cooled to room temperature, the mixture was extract by ethyl acetate and washed with water. The pure product was obtained after column (PE:EA=1:1). Yield 0.38g (65%).

<sup>1</sup>H NMR (400MHz, DMSO-d<sub>6</sub>): δ 3.81 (m, 8H, 2OCH<sub>3</sub>, CH<sub>2</sub>OH), 4.34 (t, 2H, *J*=5.5Hz, NCH<sub>2</sub>), 5.07(t, 1H, *J*=5.5Hz, OH), 6.67(t, 1H, *J*=5.5Hz), 7.05(d, 2H, *J*=2.7Hz), 7.26(m, 2H), 7.67(m, 2H) ppm.

Mass: (M+H)<sup>+</sup> 299.1408

m.p.: 60-62°C

### 5.38 Preparation of 2-(3,5-dimethoxyphenyl)-1-(2-(6-chloro-*s*-tetrazine-3-yloxy)ethyl)-benzimidazole



2-(3,5-dimethoxyphenyl)-1- hydroxyethyl-benzimidazole (0.032g, 0.1mmol) and 3,6-dichloro tetrazine(0.035g, 0.2mmol) were dissolved in dry 20ml dichloromethane, 2,4,6-collidine (0.05ml, 0.3mmol) was added at room temperature under N<sub>2</sub>. After stirring 4h, the solvent was removed under reduced pressure, and purified by column chromatography (PE: EA=2:1). Yield 0.01g, 23%.

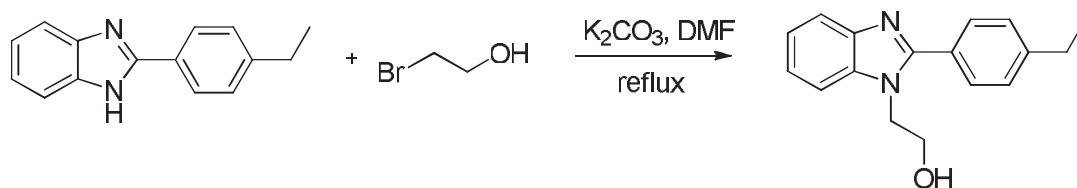
<sup>1</sup>H NMR (400MHz,CDCl<sub>3</sub>): δ 3.83 (s, 6H, 2-OCH<sub>3</sub>), 4.85 (t, 2H, *J*=4.6Hz), 4.91(t, 2H, *J*=4.6Hz), 6.48 (t, 1H, *J*=2.3Hz), 6.74 (d, 2H, *J*=2.3Hz), 7.34(m, 2H), 7.47(m, 1H), 7.81(m, 1H) ppm.

<sup>13</sup>C NMR (100MHz,CDCl<sub>3</sub>): δ42.7, 55.7, 67.8, 102.0, 107.6, 109.7, 120.5, 123.1, 123.5, 131.6, 135.0, 143.1, 154.1, 160.9, 164.7, 166.1 ppm.

Mass (M+H)<sup>+</sup>: 413.1134 (M+1)

m.p.: 160-166°C

### 5.39 Preparation of 2-(4-ethylphenyl)-1- hydroxyethyl-benzimidazole



2-Bromoethanol (0.267g, 2.2mmol) was dissolved in 15 ml DMF. To the solution Potassium carbonate (0.30g, 2.2mmol) and 2-(4-ethylphenyl)-1H-benzimidazole (0.454g, 2mmol) were added and then refluxed for 18h. After cooled to room temperature, the mixture was extract by ethyl acetate and washed with water. The pure product was obtained after column (PE: EA=2:1). Yield 0.4g (74%).

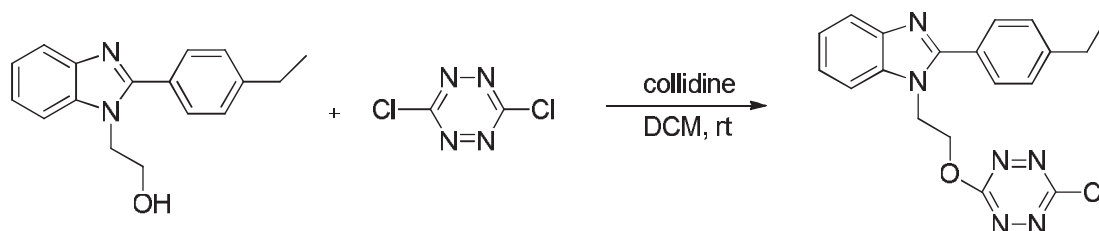
$^1\text{H}$  NMR (400MHz,  $\text{CDCl}_3$ ):  $\delta$  1.17 (m, 3H), 2.61 (q, 2H), 3.94 (t, 1H,  $J=6.6\text{Hz}$ ), 4.02 (q, 2H), 4.26 (t, 2H,  $J=5.7\text{Hz}$ ), 7.64(d, 2H,  $J=4.1\text{Hz}$ ), 7.60 (m, 1H), 7.37 (m, 1H), 7.20(d, 2H,  $J=7.8\text{Hz}$ ), 7.14 (m, 2H) ppm.

$^{13}\text{C}$  NMR (100MHz,  $\text{CDCl}_3$ ):  $\delta$  15.3, 28.7, 47.1, 60.5, 110.4, 119.4, 122.2, 122.4, 127.5, 128.0, 129.7, 135.8, 142.7, 145.8, 154.3 ppm.

Mass ( $\text{M}+\text{H}$ ) $^+$ : 267.1492

m.p.: 126-128 $^\circ\text{C}$

#### 5.40 Preparation of 2-(4-ethylphenyl)-1-(2-(6-chloro-s-tetrazine-3-yloxy) ethyl)-benzimidazole



2-(4-ethylphenyl)-1- hydroxyethyl-benzimidazole (0.032g, 0.1mmol) and 3,6-dichloro tetrazine(0.035g, 0.2mmol) were dissolved in dry 20ml dichloromethane, 2,4,6-collidine (0.05ml, 0.3mmol) was added at room temperature under  $\text{N}_2$ . After stirring 4h, the solvent was removed under reduced pressure, and purified by column chromatography (PE: EA=2:1). Yield 0.01g, 23%.

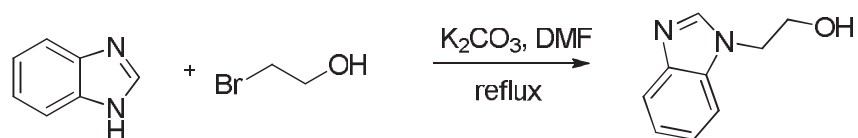
$^1\text{H}$  NMR (400MHz,  $\text{CDCl}_3$ ):  $\delta$  1.27 (t, 3H,  $J=7.3\text{Hz}$ ), 2.70 (q, 2H,  $J=7.3\text{Hz}$ ), 4.81 (d, 2H,  $J=5.0\text{Hz}$ ), 4.92 (d, 2H,  $J=5.0\text{Hz}$ ), 7.28 (m, 2H), 7.32(m, 2H), 7.50(m, 1H), 7.57(m, 2H), 7.80(m, 1H) ppm.

$^{13}\text{C}$  NMR (100MHz,  $\text{CDCl}_3$ ):  $\delta$  15.3, 28.8, 42.8, 67.8, 109.7, 120.4, 123.0, 123.3, 127.2, 128.4, 129.6, 135.2, 143.2, 146.5, 154.4, 164.6, 166.1 ppm.

Mass (M+H)<sup>+</sup>: 381.1224

m.p.: 158-160°C

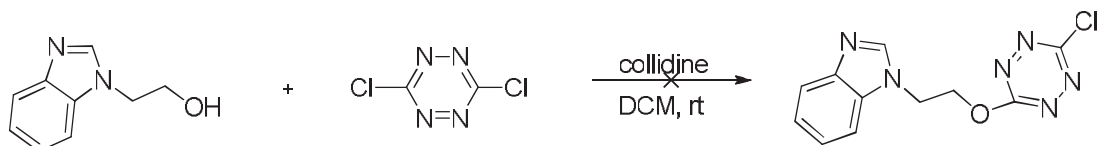
#### 5.41 Preparation of N-(2-hydroxyethyl)-benzimidazole



2-Bromoethanol (0.265g, 2.2mmol) was dissolved in 15 ml DMF. To the solution Potassium carbonate (0.36g, 2.6mmol) and benzimidazole (0.223g, 1.9mmol) were added and then refluxed for 18h. After cooled to room temperature, the mixture was extract by ethyl acetate and washed with water. The pure product was obtained after column (PE:EA=2:1). Yield 0.2g (65%).

<sup>1</sup>H NMR (400MHz, DMSO-d<sub>6</sub>): δ 3.73 (m, 2H), 4.27 (t, 2H, *J*=5.3Hz), 4.97 (t, *J*=5.3Hz, 1H, -OH), 7.20 (m, 2H), 7.62(m, 2H), 8.15(s, 1H) ppm.

#### 5.42 Preparation of N-(2-(6-chloro-*s*-tetrazine-3-yloxy) ethyl)-benzimidazole

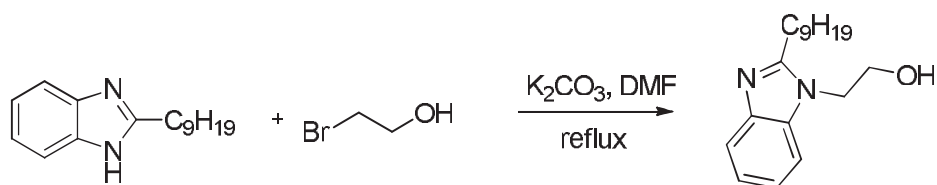


(1). N-(2-hydroxyethyl)-benzimidazole (0.030g, 0.19mmol) and 3,6-dichloro tetrazine(0.056g, 0.37mmol) were dissolved in dry 20ml dichloromethane, 2,4,6-collidine (0.05ml, 0.3mmol) was added at room temperature under N<sub>2</sub>. After stirring 4h, the TLC indicated no reaction.

(2). N-(2-hydroxyethyl)-benzimidazole (0.030g, 0.19mmol) and 3,6-dichloro tetrazine(0.056g, 0.37mmol) were dissolved in dry 20ml dichloromethane, 2,4,6-collidine (0.05ml, 0.3mmol) was added at room temperature under N<sub>2</sub>. After stirring overnight, the TLC indicated no reaction.

(3). N-(2-hydroxyethyl)-benzimidazole (0.030g, 0.19mmol) and 3,6-dichloro tetrazine(0.056g, 0.37mmol) were dissolved in dry 10ml dichloromethane, 2,4,6-collidine (0.05ml, 0.3mmol) was added at room temperature under N<sub>2</sub>. After reacted in pressure tube at 40°C for 4h, the TLC indicated no reaction.

#### 5.43 Preparation of N-(2-hydroxyethyl)-2-nonyl-benzimidazole



2-Bromoethanol (0.164g, 1.3mmol) was dissolved in 15 ml DMF. To the solution Potassium carbonate (0.25g, 1.8mmol) and 2-nonylbenzimidazole (0.25g, 1.0mmol) were added and then refluxed for 1day. After cooled to room temperature, the mixture was extract by ethyl acetate and washed with water. The pure product was obtained after column (PE:EA=1:1). Yield 0.26g (90%).

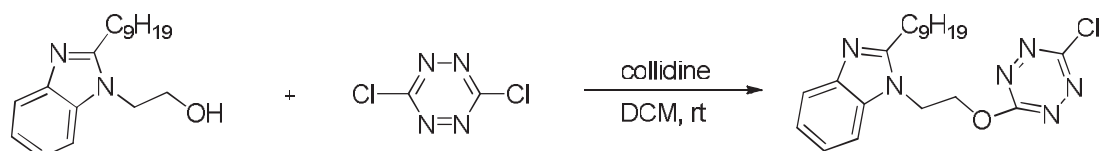
$^1\text{H}$  NMR (400MHz, DMSO- $d_6$ ):  $\delta$  0.88 (t,  $J=6.9\text{Hz}$ , 3H), 1.27 (m, 12H), 1.75 (m, 2H), 2.85 (t,  $J=6.9\text{Hz}$ , 2H), 3.67 (q, 2H), 4.20 (t,  $J=5.5\text{Hz}$ , 2H), 4.93 (t,  $J=5.5\text{Hz}$ , 1H, -OH), 7.11 (m, 2H), 7.49 (m, 2H) ppm.

$^{13}\text{C}$  NMR (100MHz, DMSO- $d_6$ ):  $\delta$  14.0, 22.1, 26.5, 26.9, 28.7, 28.9, 29.0, 31.3, 45.6, 59.6, 110.0, 118.2, 121.0, 121.2, 135.2, 142.4, 155.6 ppm.

Mass (M+H) $^+$ : 298.2301

m.p.: 94-96°C

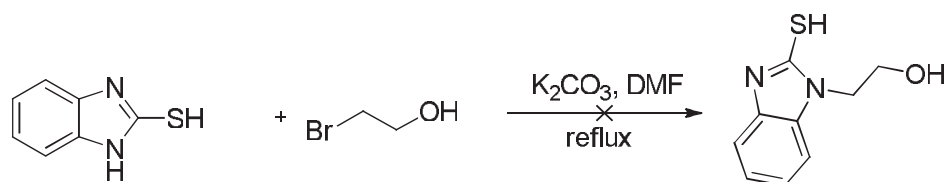
#### 5.44 Preparation of N-(2-(6-chloro-*s*-tetrazine-3-yloxy)ethyl)-2-nonyl-benzimidazole



N-(2-hydroxyethyl)-2-nonyl-benzimidazole (0.032g, 0.11mmol) and 3,6-dichloro tetrazine(0.034g, 0.22mmol) were dissolved in dry 20ml dichloromethane, 2,4,6-collidine (0.03ml, 0.22mmol) was added at room temperature under  $\text{N}_2$ . After stirring 5h, the solvent was removed under reduced pressure, and purified by column chromatography (PE: EA=2:1). Yield 0.01g, 23%.

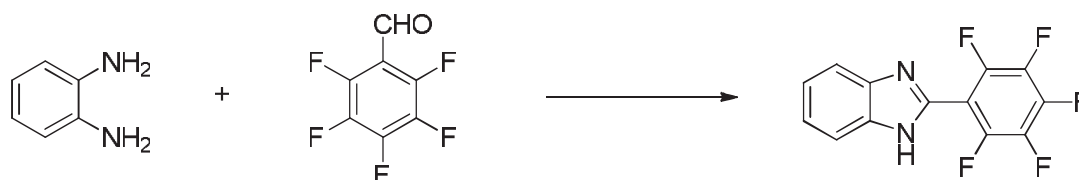
$^1\text{H}$  NMR (400MHz,  $\text{CDCl}_3$ ):  $\delta$  0.88 (m, 3H), 1.28 (m, 14H), 3.01 (t, 2H,  $J=8.0\text{Hz}$ ), 4.71 (t, 2H,  $J=5.7\text{Hz}$ ), 4.98 (t, 2H,  $J=5.3\text{Hz}$ ), 7.40 (m, 2H), 7.73(m, 2H) ppm.

#### 5.45 Preparation of N-(2-hydroxyethyl)-2- sulfhydryl-benzimidazole



2-Bromoethanol (1.38g, 11.2mmol) was dissolved in 15 ml DMF. To the solution Potassium carbonate (1.9g, 13.7mmol) and 2-sulfhydryl-benzimidazole (1.49g, 9.9mmol) were added and then refluxed for 1day. After cooled to room temperature, the mixture was extract by ethyl acetate and washed with water. The product is not the target compound as we expected by NMR.

#### 5.46 Preparation of 2-perfluorophenyl-benzimidazole



(1). 2,3,4,5,6-pentafluorobenzaldehyde (0.36g, 1.8mmol) and *o*-phenylenediamine (0.2g, 1.8mmol) were thoroughly mixed in DMF (5ml), then *p*-TsOH (0.07g, 0.37mmol) was added, and the solution heated and stirred at 80°C for 2h. When the reaction was finished, the solution was cooled to room temperature. The reaction mixture was added dropwise with vigorous stirring into a mixture of Na<sub>2</sub>CO<sub>3</sub> (0.37mmol) and water (10ml). And the product was extracted into EtOAc, the organic phase was washed with water and dried by Na<sub>2</sub>SO<sub>4</sub>. Evaporation of solvent gave the crude product, and purified by column chromatography over the silica gel to afford a pure compound 0.13g.

<sup>1</sup>H NMR (400MHz, CDCl<sub>3</sub>): δ 7.31 (m, 2H), 7.68 (m, 2H), 8.11 (s, 1H) ppm.

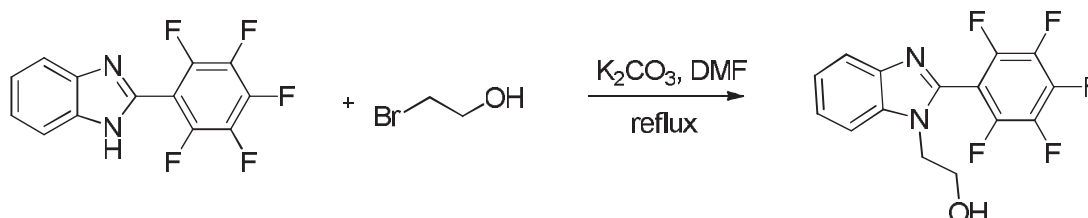
Mass (M+H)<sup>+</sup>: 285.0446

(2). In 10ml dry dichloromethane with 0.1ml thionyl chloride solution, 0.1ml pyridine and 2,3,4,5,6-pentafluorobenzaldehyde (0.2g, 1mmol) were added under argon, and the temperature was keeping at 5-10 °C. After stirring 1 hour, *o*-phenylenediamine (0.2g, 1mmol) was added, and then 1ml Sodium acetate (0.082g, 2mmol) aqueous solution was dropped. Then keep stirring at room temperature for 8h, and filter, washed with water. The crude compound was dried, and purified by column chromatography over the silica gel to afford 0.02g of the pure compound

<sup>1</sup>H NMR (400MHz, CDCl<sub>3</sub>): δ 7.31 (m, 2H), 7.68 (m, 2H), 8.11 (s, 1H) ppm.

Mass (M+H)<sup>+</sup>: 285.0446

#### 5.47 Preparation of N-(2-hydroxyethyl)- 2-perfluorophenyl-benzimidazole



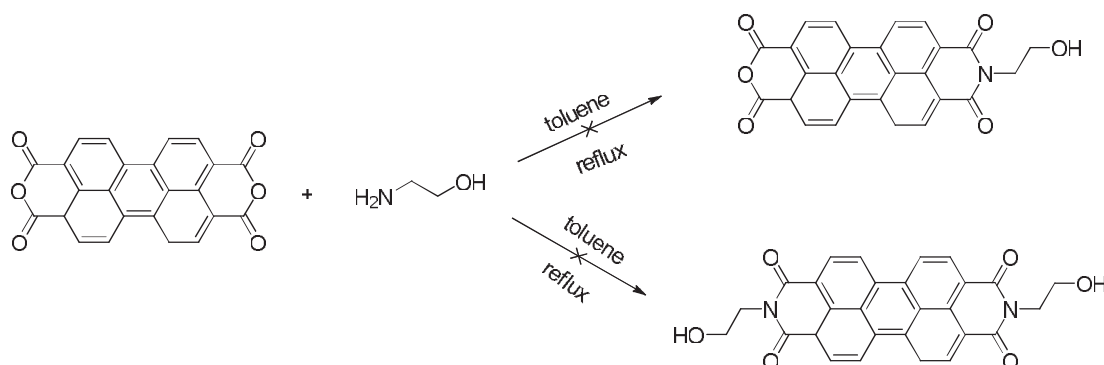
(1) 2-Bromoethanol (0.26g, 2.08mmol) was dissolved in 15 ml DMF. To the solution Potassium carbonate (0.7g, 5.1mmol) and 2-perfluorophenyl-benzimidazole (0.5g, 1.76mmol) were added and then refluxed for 10h. After cooled to room temperature, the mixture was extract by ethyl acetate. 0.2g product was obtained after the coloum. But the NMR shows it is not the compound we expected.

(2) 2-Bromoethanol (0.26g, 2.08mmol) was dissolved in 10 ml DMF. To the solution Potassium carbonate (0.7g, 5.1mmol) and 2-perfluorophenyl-benzimidazole (0.5g, 1.76mmol) were added and then put it into the microwave (130°C, 2h), then the mixture was extract by ethyl acetate. 0.15g product was obtained after the coloum.

<sup>1</sup>H NMR (400MHz, CDCl<sub>3</sub>): δ 3.89 (m, 2H), 4.12 (t, *J*=5.0Hz, 2H), 7.03 (t, *J*=7.8Hz, 1H), 7.13 (t, *J*=7.6Hz, 1H), 7.25 (d, *J*=8.2Hz, 1H), 7.31 (d, *J*=8.2Hz, 1H), 7.49 (s, 1H) ppm.

<sup>13</sup>C NMR (100MHz, CDCl<sub>3</sub>): 48.0, 60.0, 109.7, 119.3, 122.2, 122.9, 133.3, 142.6, 143.3 ppm.

#### 5.48 Preparation of N-ethoxy-3,4,9,10-Perylenetetracarboxylic dianhydride

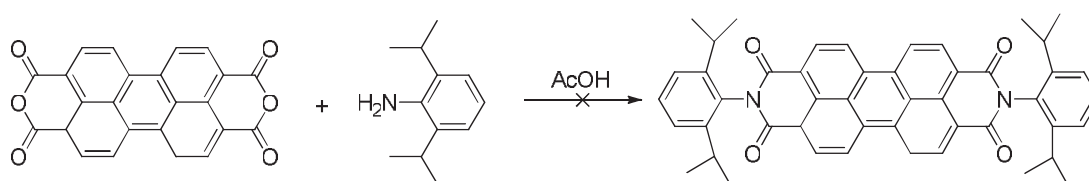


(1) Ethanolamine (0.6g, 9.8mmol) was dissolved in 15 ml toluene. To the solution Potassium carbonate (0.3g, 2.2mmol) and 3,4,9,10-Perylenetetracarboxylic dianhydride (0.84g, 2.14mmol) were added and then refluxed for 7h. After cooling to

room temperature, the solvent removed in vacuum, and the mixture are insoluble in any solvent.

(2) Ethanolamine (1.17g, 15mmol) was dissolved in 70 ml ethanol. To the solution 3,4,9,10-Perylenetetracarboxylic dianhydride (1g, 2.5mmol) were added and then refluxed for 2.5h, then 130ml H<sub>2</sub>O was added under N<sub>2</sub>, refluxed overnight. After cooling to room temperature, added KOH, stirring overnight. Then the residuum washed with water after filter, but the mixture are insoluble in any solvent.

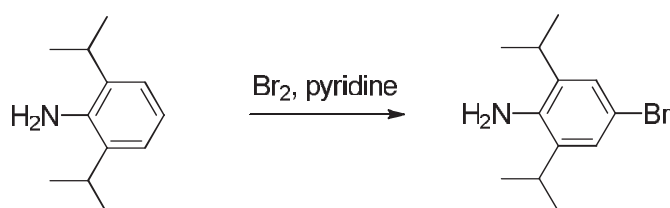
#### 5.49 Preparation of N-(2,6-diisopropylaniline)- 3,4,9,10-Perylenetetracarboxylic dianhydride



(1). 3,4,9,10-Perylenetetracarboxylic dianhydride (1.176g, 2.96mmol) was suspended in acetic acid (40ml) and heated at reflux, then 2,6-diisopropylaniline (3.75ml, 20mmol) was added into this mixture. The mixture was kept at reflux at 120°C for 3h, and in fact 3,4,9,10-Perylenetetracarboxylic dianhydride can't dissolve in the solution, and after usual work-up procedure TLC (at low concentration) indicated most of the dianhydride remained.

(2). Prepare a suspension of 3,4,9,10-Perylenetetracarboxylic dianhydride (0.784g, 2mmol) in 40ml propionic acid, then 2,6-diisopropylaniline (1.87ml, 10mmol) was added. The mixture refluxed under N<sub>2</sub> for 26h. Filter quickly (keep the mixture is hot) after stop the reaction, then put the filtrate in fridge for 2h. Then extracted by DCM, and washed with water. The NMR indicated the product is a mixture.

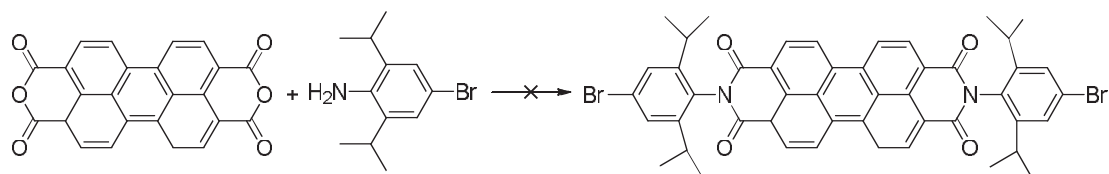
#### 5.49 Preparation of 4-bromo-2,6-di-2-propylaniline



Bromine (16.08g, 100.6mmol) was dissolved in small portions in 30ml of cooled (-10°C) pyridine. The red solution was added dropwise to a cooled (-10°C) mixture of 2,6-di-2,2-propylaniline (17.0g, 95.8mmol) in 20ml of pyridine. The reaction mixture was stirred for 30min at 0°C and for a further 1.5h at room temperature. Next, it was treated with an exceed of sodium carbonate in water and extracted with diethyl ether. All volatiles were evaporated. Vacuum distillation afforded of the product, which was crystallized from n-pentane; yield: 17.01 g (66.40mol, 69%).

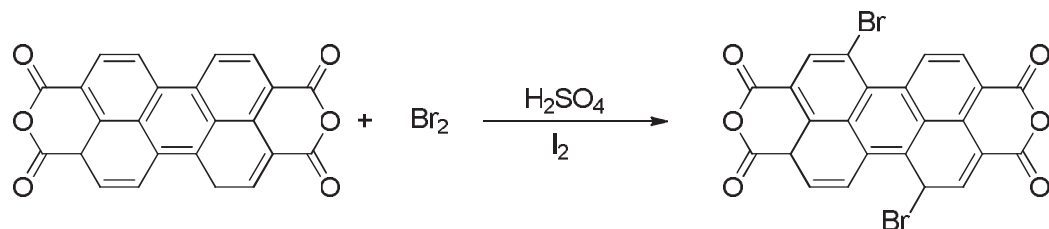
<sup>1</sup>H NMR (400MHz, CDCl<sub>3</sub>): δ 1.0 (d, J= 6.9 Hz, 12H, CH<sub>3</sub>), 2.4 (q, 2H, CH), 3.1 (s, 2H, NH<sub>2</sub>), 7.3 (s, 2H, H-Ar) ppm.

#### 5.50 Preparation of N-(4-bromo-2,6-di-2-propylaniline)- 3,4,9,10-Perylenetetracarboxylic dianhydride



3,4,9,10-Perylenetetracarboxylic dianhydride (0.784g, 2mmol) was suspended in acetic acid (5ml) and heated at reflux, then 4-bromo-2,6-di-2-propylaniline (0.512g, 2mmol) was added into this mixture. The mixture was kept at reflux at 120°C for 3h, and in fact 3,4,9,10-Perylenetetracarboxylic dianhydride can't solve in the solution, and after usual work-up procedure TLC (at low concentration) indicated most of the dianhydride remained.

#### 5.51 Preparation of 1,7-Dibromoperylene-3,4:9,10-tetracarboxylic acid dianhydride

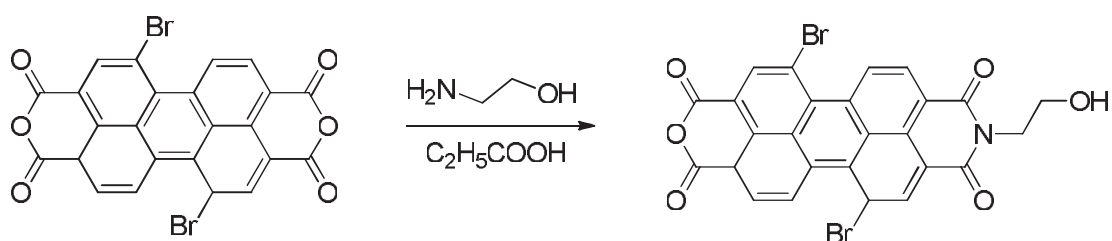


3,4,9,10-Perylenetetracarboxylic acid dianhydride (1 g, 2.55 mmol) was added to 150 mL of concentrated sulfuric acid and stirred at 55 °C for 18 h. Iodine (0.024 g, 0.095 mmol) was added to the reaction mixture, and stirring was continued for 5 h at 55°C. Bromine (0.2928 ml, 5.7 mmol) was added dropwise, and stirring was



continued at 85°C for another 48 h. The reaction mixture was cooled to room temperature, and excess bromine was expelled by purging with argon. The mixture was cooled in an ice bath, and 2.4 mL of water were added dropwise to precipitate the product. The precipitate was separated by centrifugation, and washed with 7.5 mL of 86 % H<sub>2</sub>SO<sub>4</sub>, followed by several washings with water. The crude product was dried for 3 days at 50 °C under vacuum to afford 3.14 g of a red solid. The crude product was used without further purification in the next step.

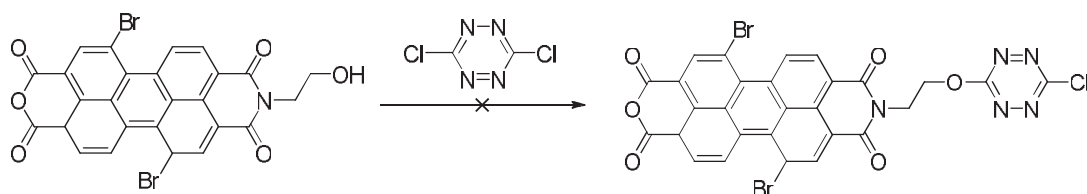
#### 5.52 Preparation of N-(2-hydroxyethyl)-1,7-dibromoperylene-3,4:9,10-tetracarboxydiimide



1,7-Dibromoperylene-3,4:9,10-tetracarboxylic dianhydride (0.21 g, 0.38 mmol) and ethanolamine (0.25mg, 4.2 mmol) were added to 10 mL of propionic acid, and purged with argon. The reaction mixture was refluxed at 155 °C for 3 days under an argon atmosphere. To the cold reaction mixture 10 mL of methanol were added. The precipitated product was isolated by filtration, and washed with methanol until the filtrate was colorless. The crude product was dried for 3 days at 50°C under vacuum to afford 0.20 g of a red solid (82 % yield). The crude product was used without further purification in the next reaction step.

Mass (M-H)<sup>+</sup>: 591.5008.

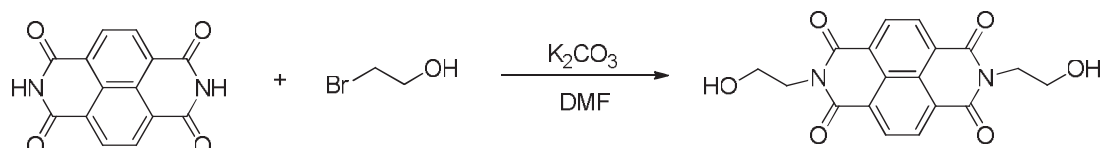
#### 5.53 Preparation of N-(2-(6-chloro-s-tetrazine-3-yloxy) ethyl)-1,7-dibromoperylene-3,4:9,10-tetracarboxydiimide



N-(2-hydroxyethyl)-1,7-dibromoperylene-3,4:9,10-tetracarboxydiimide (0.100g, 0.17mmol) and 3,6-dichloro tetrazine (0.11g, 0.73mmol) were suspension in dry 50ml

dichloromethane, 2,4,6-collidine (0.14ml, 1mmol) was added at room temperature under N<sub>2</sub>. After stirring overnight, TLC indicated no new compound, and the tetracarboxydiimide can't dissolve in DCM, while the 3,6-dichlorotetrazine decomposed.

#### 5.54 Preparation of N,N-Di(2-hydroxyethyl)- 1,4,5,8-Naphthalenetetracarbondiimide (1)

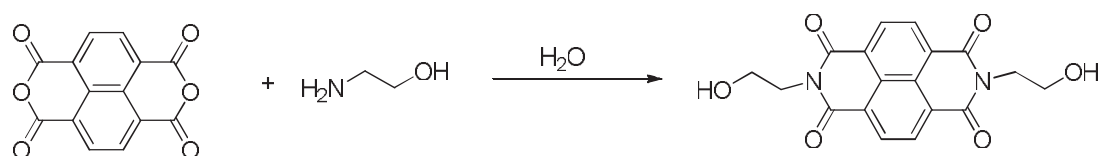


2-Bromoethanol (0.4g, 3.2mmol) was dissolved in 20 ml DMF. To the solution Potassium carbonate (0.4g, 2.9mmol) and 1,4,5,8-Naphthalenetetracarbondiimide (0.4g, 1.5mmol) were added and then refluxed for 10h. After cooled to room temperature, the mixture was extract by ethyl acetate, and recrystallization after the coloum (DCM: PE= 3:1). The product was purified by coloum, Yield 0.02g (4%).

<sup>1</sup>H NMR (400MHz, DMSO-d<sub>6</sub>): δ: 3.65 (M, 4H), 4.16 (t, *J* = 6.0 Hz, 4H), 4.85 (t, *J* = 6.2 Hz, 2H), 8.63 (m, 4H) ppm.

<sup>13</sup>C NMR (100MHz, DMSO-d<sub>6</sub>): δ: 42.2, 57.7, 126.2, 129.6, 130.3, 162.7 ppm.

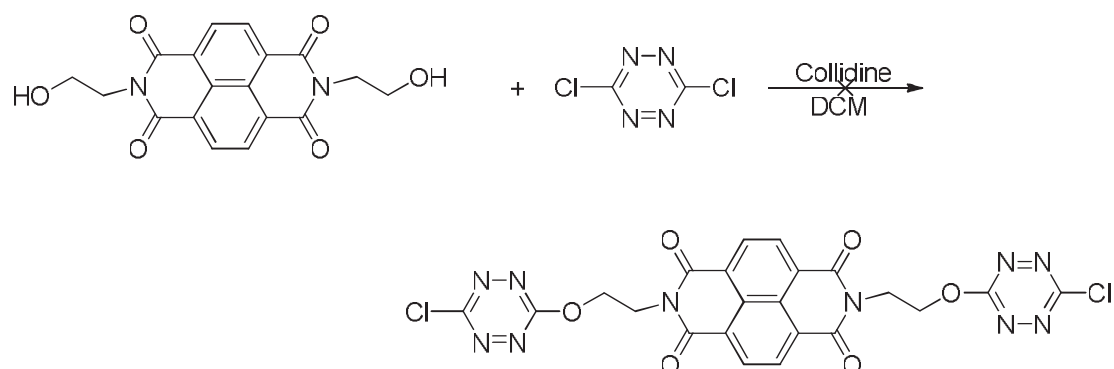
#### 5.55 Preparation of N,N-bi(2-hydroxyethyl)- 1,4,5,8-Naphthalenetetracarbondiimide (2)



Ethanolamine (2ml, 40mmol) was dissolved in 50 ml H<sub>2</sub>O. To the solution 1,4,5,8-Naphthalenetetracarboxylic dianhydride (2.68g, 10mmol) were added and then heated at 80°C for 18h. After cooled to room temperature, the mixture filter and washed with acetone, then recrystallization after the coloum (DCM:PE= 3:1). The product was purified by coloum, Yield 3.0 g (85%).

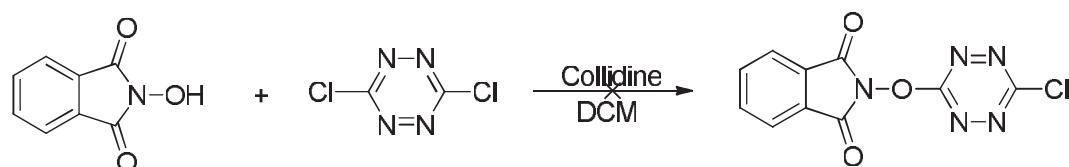
The NMR result is the same as the method 1.

5.56 Preparation of N,N-bis(2-(6-chloro-s-tetrazine-3-yloxy)ethyl)-1,4,5,8-Naphthalenetetracarbondiimide



N,N-bis(2-hydroxyethyl)- 1,4,5,8-Naphthalenetetracarbondiimide (0.177g, 0.5mmol) and 3,6-dichloro tetrazine (0.20g, 1.32mmol) were dissolved in dry 50ml dichloromethane, 2,4,6-collidine (0.14ml, 1mmol) was added at room temperature under N<sub>2</sub>. After stirring overnight, TLC indicated no new compound, while the 3,6-dichlorotetrazine decomposed.

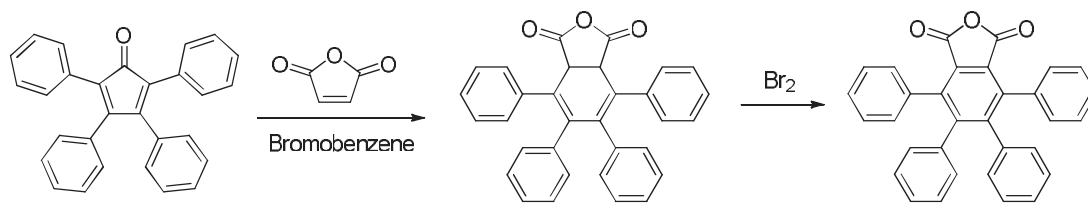
5.57 Preparation of N-(6-chloro-s-tetrazine-3-yloxy)-phthalimide



(1). N-hydroxyphthalimide (0.163g, 1mmol), 3,6-dichloro tetrazine (0.20g, 1.32mmol) were mixed in dry 20ml dichloromethane, 2,4,6-collidine (0.14ml, 1mmol) was added at room temperature under N<sub>2</sub>. But N-hydroxyphthalimide can't dissolve in dichloromethane, so after stirring overnight at 50°C, TLC indicated no new compound, while the 3,6-dichlorotetrazine decomposed.

(2). N-hydroxyphthalimide (0.32g, 2mmol) was added in 20ml dry THF, and n-BuLi (0.88ml, 2.2mmol) dropwise to the suspension at 0°C. 10min after, 3,6-dichloro tetrazine (0.30g, 2mmol) was added, and stirring at room temperature. But the TLC indicated no new compound as expected, while the 3,6-dichlorotetrazine decomposed.

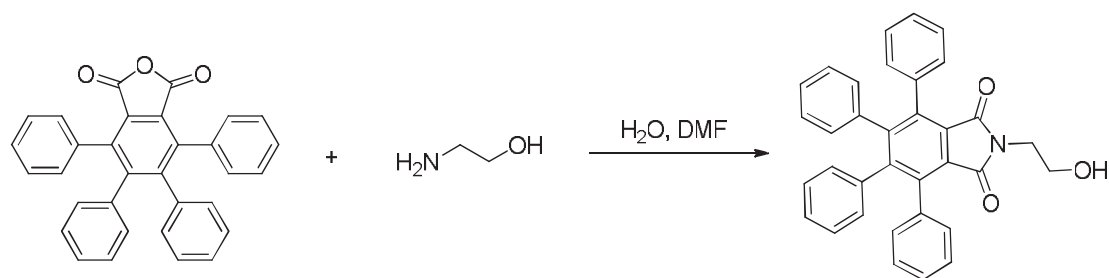
5.58 Preparation of tetraphenylphthalic anhydride



An intimate mixture of tetraphenylcyclopentadienone (3.5g, 0.94mol) and maleic anhydride (0.93g, 0.95mol) is placed in a 50ml. round-bottomed flask, and to it is added 5ml of bromobenzene. After the mixture has been refluxed gently for 3.5 hours, it is cooled, a solution of 0.7 ml. of bromine in 5 ml. of bromobenzene is added through the condenser, and the flask is shaken until the reagents are thoroughly mixed. After the first exothermic reaction has subsided, the mixture is refluxed gently for 3 hours. The flask is then immersed in a cooling bath and the temperature of the mixture is held at 0–10° for 2–3 hours. The mixture is filtered with suction, and the crystalline product is washed three times with 10ml. portions of petroleum ether (b.p. 60–68°). After the product has been dried in the air, it weighs 3.7g. (yield is 87%) and melts at 289–290°. It is light brown, but when pulverized it is almost colorless. The filtrate, when diluted with an equal volume of petroleum ether and cooled to 0–10°, yields an additional 2–3 g. of a less pure product which melts at 285–288°. The impure material may be purified by recrystallization from benzene, using 8–9 ml. of benzene per gram of solid.

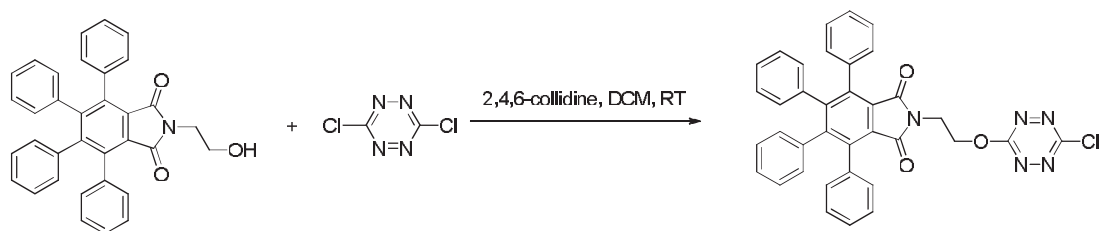
<sup>1</sup>H NMR (400MHz, CDCl<sub>3</sub>): δ 6.7 (m, 4H), 6.91 (m, 6H), 7.11 (m, 4H), 7.24 (m, 6H) ppm.

#### 5.59 Preparation of N-(2-hydroxyethyl)-tetraphenylphthalimide



Ethanolamine (0.125g, 1mmol) was dissolved in 15 ml DMF and 10ml H<sub>2</sub>O. To the solution 2,3,4,5-tetraphenylphthalic anhydride (0.2g, 1mmol) were added and then refluxed for 10h. After cooled to room temperature, the product was precipitated as gray solid, and not pure, Yield is about 50%.

### 5.60 Preparation of N-(2-(6-chloro-s-tetrazine-3-yloxy)ethyl)- tetraphenylphthalimide



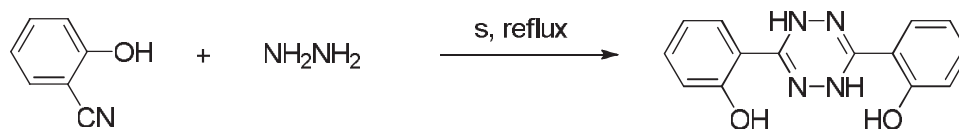
N-ethanol-2,3,4,5-tetraphenylphthalimide (0.50g, 1mmol) and 3,6-dichloro tetrazine(0.20g, 1.32mmol) were dissolved in dry 15ml dichloromethane, 2,4,6-collidine (0.14ml, 1mmol) was added at room temperature under  $N_2$ . After stirring 6h, the solvent was removed under reduced pressure and purified by column chromatography. Yield 0.15g (24.6%).

$^1H$  NMR (400MHz,  $CDCl_3$ ):  $\delta$  4.12 (t, 2H), 4.88 (t, 2H), 6.91 (m, 10H), 7.22 (m, 10H) ppm.

$^{13}C$  NMR (100MHz,  $CDCl_3$ ):  $\delta$  35.8, 66.9, 126.4, 127.1, 127.4, 127.5, 127.9, 129.9, 130.7, 135.4, 137.9, 139.7, 148.1, 164.5, 166.3, 167.1 ppm.

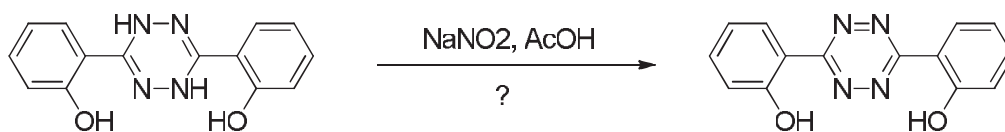
Mass ( $M^+$ ): 632.1516

### 5.61 Preparation of 3, 6-bis (2,2-diphenol)-1,2-dihydro-s-tetrazine



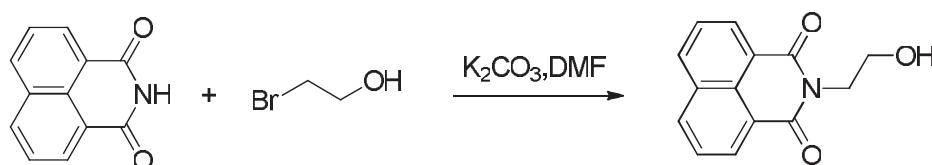
Treatment of solution of 2-hydroxybenzonitrile (5.95g, 0.05mol) in 15ml ethanol with hydrazine hydrates (10ml), followed by addition of flowers of sulphur (1g), and heating the mixture at reflux for 2h. Then filter, washed with water, dried. Because 3, 6-bis (2,2-diphenol)-1,2-dihydro-s-tetrazine can be oxidized by  $O_2$ , the mixture change to red in the air. So 5.2g product was obtained, but not pure.

### 5.62 Preparation of 3, 6-bis (2,2-diphenol)-s-tetrazine



In a 1L two necked round bottom flask, a solution of sodium nitrite (3.45g, 0.05mol) in 80ml of water was prepared and 10ml of DCM was added. The temperature was lowered at 0°C and 3, 6-bis (2,2-diphenol)-1,2-dihydro-s-tetrazine (4.96g ,0.0185mol) was introduced. Acetic acid (2.86ml) was added dropwise. After gas evolution stopped, the organic layer was separated and the aqueous layer was extracted with DCM (3x100ml). The organic layer are reunited, washed to neutrality with 5% aqueous solution of K<sub>2</sub>CO<sub>3</sub>, dried over calcium chloride and filtered. The crude product is obtained by evaporation of the solvent under reduced pressure. The dark red solid obtained is washed several times with diethyl ether, but it is still mixture after the column.

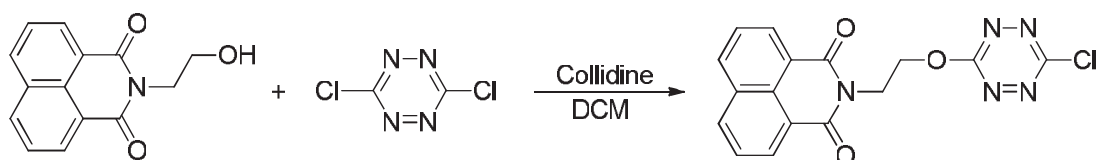
### 5.63 Preparation of N-(2-hydroxyethyl)-1,8-naphthalimide



2-Bromoethanol (0.125g, 1mmol) was dissolved in 15 ml DMF. To the solution Potassium carbonate (0.138g, 1mmol) and naphthalimide (0.2g, 1mmol) were added and then refluxed for 10h. After cooled to room temperature, the mixture was extract by ethyl acetate. The product was purified by coloum, Yield 0.18g (73.7%).

<sup>1</sup>H NMR (400MHz, CDCl<sub>3</sub>): δ 3.60 (t, *J*= 6.4 Hz, 2H, CH<sub>2</sub>), 4.12 (t, *J*= 6.4 Hz, 2H, CH<sub>2</sub>), 4.78 (t, *J*= 6.0 Hz, 1H, OH), 7.84 (t, *J*= 7.4 Hz, 2H, napht), 8.45 (dd, *J*= 7.3 Hz, 4H, napht) ppm.

### 5.64 Preparation of N-(2-(6-chloro-s-tetrazine-3-yloxy)ethyl)-1,8-naphthalimide



N-ethanol-naphtalimide (0.24g, 1mmol) and 3,6-dichloro tetrazine (0.20g, 1.32mmol) were dissolved in dry 15ml dichloromethane, 2,4,6-collidine (0.14ml, 1mmol) was added at room temperature under N<sub>2</sub>. After stirring 2h, the solvent was

removed under reduced pressure, and purified by column chromatography (PE: DCM=1:1). 0.20g product is obtained, yield is 56%.

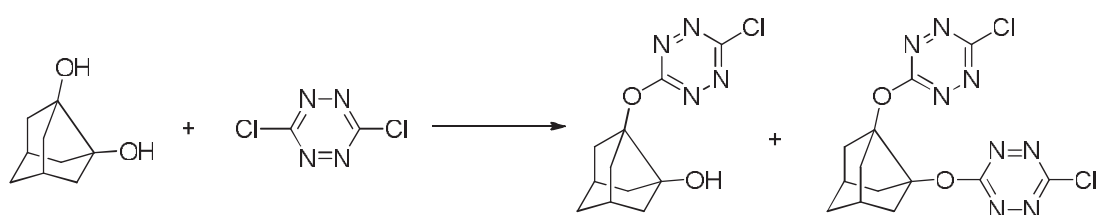
$^1\text{H}$  NMR (400MHz,  $\text{CDCl}_3$ ):  $\delta$  4.75 (t, 2H,  $J=5\text{Hz}$ ), 5.06 (t, 2H,  $J=5\text{Hz}$ ), 7.75 (t, 2H,  $J=7.5\text{Hz}$ ), 8.23 (d, 2H,  $J=7.5\text{Hz}$ ), 8.56 (d, 2H,  $J=7.5\text{Hz}$ ) ppm.

$^{13}\text{C}$  NMR (100MHz,  $\text{CDCl}_3$ ):  $\delta$  166.7, 164.5, 163.6, 134.5, 132.2, 131.7, 128.9, 127.1, 122.3, 67.7, 38.1 ppm.

m.p.: 157-158 $^\circ\text{C}$

Mass ( $\text{M}^+$ ): 355

### 5.65 Preparation of (2,3,5,6)-octahydro-2,5-methanopentalene-3,6-tetrazine

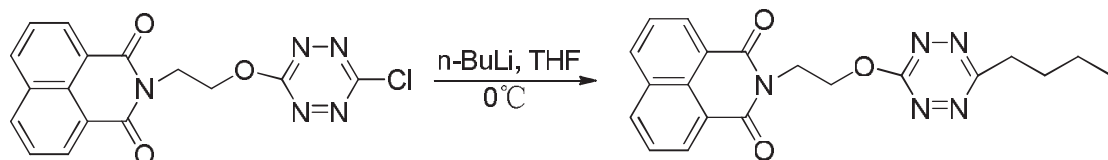


(2,3,5,6)-Octahydro-2,5-methanopentalene-3,6-diol (0.05g, 0.32mmol) and 3,6-dichloro tetrazine (0.11g, 0.72mmol) were dissolved in dry 15ml dichloromethane, 2,4,6-collidine (0.10ml, 0.72mmol) was added at room temperature under  $\text{N}_2$ . After stirring overnight, the solvent was removed under reduced pressure, and purified by column chromatography (PE: DCM=1:1). 0.001g (2,3,5,6)-octahydro-2,5-methanopentalene-3-ol-6-tetrazine was obtained, yield is 1.2%; 0.001g (2,3,5,6)-octahydro-2,5-methanopentalene-3,6-tetrazine was obtained, yield is 0.8%.

(2,3,5,6)-octahydro-2,5-methanopentalene-3-ol-6-tetrazine  $^1\text{H}$  NMR (400MHz,  $\text{CDCl}_3$ ):  $\delta$  0.83 (m, 4H), 1.24 (m, 6H) ppm.

(2,3,5,6)-octahydro-2,5-methanopentalene-3,6-tetrazine  $^1\text{H}$  NMR (400MHz,  $\text{CDCl}_3$ ):  $\delta$  0.83 (m, 5H), 1.24 (m, 5H) ppm.

### 5.66 Preparation of butyl-naphtalimideethoxy-s-tetrazine



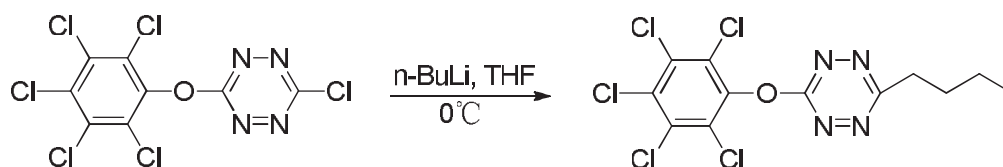
Chloro-naphtalimideethoxy-s-tetrazine (0.053g, 0.15mmol) was dissolved in 15ml dry THF. The solution was cooled to 0 $^\circ\text{C}$  by ice-bath for 10 min, then *n*-BuLi

(0.01g, 0.18mmol) was dropped under 0°C. The mixture was stirring 30min at room temperature. The solvent was removed under reduced pressure, then purified by column (PE: DCM=1:1). 0.01g butyl-naphthalimideethoxy-*s*-tetrazine was obtained, yield is 18%.

<sup>1</sup>H NMR (400MHz, CDCl<sub>3</sub>): δ 1.0 (t, *J*=7.3Hz, 3H), 1.55 (m, 4H), 4.57 (t, *J*=6.7Hz, 2H), 4.75 (t, *J*=5.3Hz, 2H), 4.97 (t, *J*=5.5Hz, 2H), 7.76 (t, *J*=7.8Hz, 2H), 8.23 (d, *J*=8.2Hz, 2H), 8.58 (d, *J*=7.3Hz, 2H) ppm.

<sup>13</sup>C NMR (100MHz, CDCl<sub>3</sub>): δ: 13.9, 19.1, 30.8, 38.4, 66.6, 69.9, 122.5, 127.1, 128.4, 131.7, 134.4, 164.5, 165.9, 166.3 ppm.

#### 5.67 Preparation of *n*-butyl-pentachlorophenoxy-*s*-tetrazine

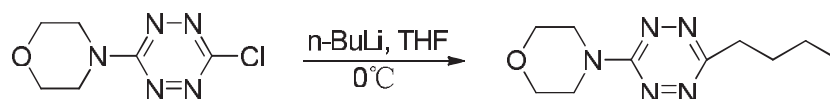


Chloro-pentachlorophenoxy-*s*-tetrazine (0.1g, 0.26mmol) was dissolved in 15ml dry THF. The solution was cooled to 0°C by ice-bath for 10 min, then *n*-BuLi (0.02g, 0.31mmol) was dropped under 0°C. The mixture was stirring 30min at room temperature. The solvent was removed under reduced pressure, then purified by column (PE:DCM=1:1). 0.03g *n*-butyl-pentachlorophenoxy-*s*-tetrazine was obtained, yield is 30%.

<sup>1</sup>H NMR (400MHz, CDCl<sub>3</sub>): δ 4.61 (2H, t, *J*=6.84Hz), 1.91 (m, 2H), 1.56 (m, 2H), 1.00 (t, *J*=7.32Hz, 3H,) ppm.

<sup>13</sup>C NMR (100MHz, CDCl<sub>3</sub>): δ 13.8, 19.1, 30.7, 70.7, 127.8, 132.7, 145.2, 165.1, 167.4 ppm.

#### 5.68 Preparation of *n*-butyl-morpholine-*s*-tetrazine



Chloro-morpholine-*s*-tetrazine (0.1g, 0.5mmol) was dissolved in 15ml dry THF. The solution was cooled to 0°C by ice-bath for 10 min, then *n*-BuLi (0.032g,

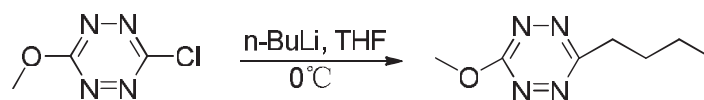


0.5mmol) was dropped under 0°C. The mixture was stirring 30min at room temperature. The solvent was removed under reduced pressure, then purified by column (PE: DCM=1:1). 0.05g *n*-butyl-morpholine-*s*-tetrazine was obtained, yield is 45%.

<sup>1</sup>H NMR (400MHz, CDCl<sub>3</sub>): δ 0.92 (t, *J*=7.32Hz, 3H), 1.45 (2H, m), 1.80 (2H, m), 3.80 (8H, m), 4.42 (2H, t, *J*=6.4Hz) ppm.

<sup>13</sup>C NMR (100MHz, CDCl<sub>3</sub>): δ 13.9, 19.1, 30.9, 44.4, 66.5, 69.0, 161.5, 164.5 ppm.

#### 5.69 Preparation of *n*-butyl-methoxy-*s*-tetrazine

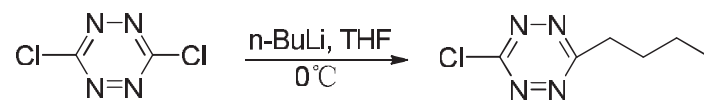


Chloromethoxy-*s*-tetrazine (0.15g, 1.03mmol) was dissolved in 15ml dry THF. The solution was cooled to 0°C by ice-bath for 10 min, then *n*-BuLi (0.08g, 1.24mmol) was dropped under 0°C. The mixture was stirring 30min at room temperature. The solvent was removed under reduced pressure, then purified by column (PE: DCM=1:1). 0.09g *n*-butyl-methoxy-*s*-tetrazine was obtained, yield is 52%.

<sup>1</sup>H NMR (400MHz, CDCl<sub>3</sub>): δ 0.99 (t, *J*=7.32Hz, 3H), 1.55 (m, 2H), 1.89 (m, 2H), 4.23 (s, 3H), 4.55 (t, *J*=6.44Hz, 2H,) ppm.

<sup>13</sup>C NMR (100MHz, CDCl<sub>3</sub>): δ 13.8, 19.1, 30.7, 56.8, 69.8, 166.4 ppm.

#### 5.70 Preparation of *n*-Butyl-chloro-*s*-tetrazine



Dichloro-*s*-tetrazine (0.1g, 0.66mmol) was dissolved in 10ml dry THF. The solution was cooled to 0°C by ice-bath for 10 min, then *n*-BuLi (0.05g, 0.78mmol) was dropped under 0°C. The mixture was stirring 30min at room temperature. The solvent was removed under reduced pressure, then purified by column (PE: DCM=1:1). 0.04g *n*-Butyl-chloro-*s*-tetrazine was obtained, yield is 35%.

<sup>1</sup>H NMR (400MHz, CDCl<sub>3</sub>): δ 1.01(t, *J*=7.32Hz, 3H), 1.56(m, 2H), 1.93(m, 2H), 4.66(t, *J*=6.88Hz, 2H) ppm.

$^{13}\text{C}$  NMR (100MHz,  $\text{CDCl}_3$ ):  $\delta$  13.8, 19.1, 30.6, 71.0, 164.3, 166.9 ppm.

### 5.71 Preparation of dibutyl-*s*-tetrazine

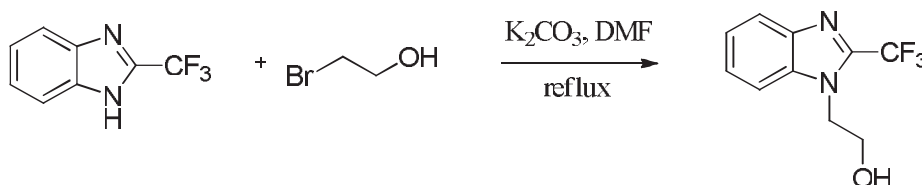


Dichlorotetrazine (0.1g, 0.66mmol) was dissolved in 10ml dry THF. The solution was cooled to 0°C for by ice-bath 10 min, then *n*-BuLi (0.10g, 1.56mmol) was dropped under 0°C. The mixture was stirring 30min at room temperature. The solvent was removed under reduced pressure, then purified by column (PE: DCM=1:1). 0.02g dibutyl-*s*-tetrazine was obtained, yield is 15.6%.

$^1\text{H}$  NMR ( $\text{CDCl}_3$ ):  $\delta$  1.01(t,  $J=7.32\text{Hz}$ , 3H), 1.48(m, 2H), 1.83(m, 2H), 4.48 (t,  $J=6.4\text{Hz}$ , 2H) ppm.

$^{13}\text{C}$  NMR ( $\text{CDCl}_3$ ):  $\delta$  13.8, 19.1, 30.8, 69.8, 166.2 ppm.

### 5.72 Preparation of N-(2-hydroxyethyl)-2-trifluoromethyl-benzimidazole



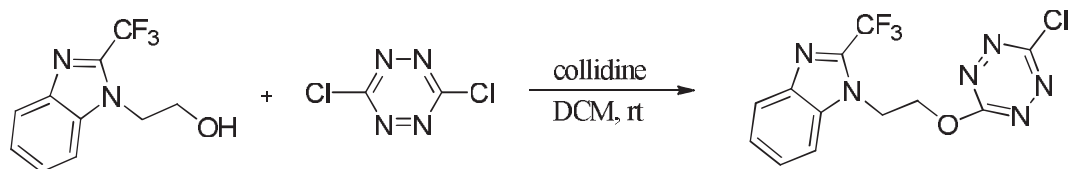
2-Bromoethanol (0.148g, 1.2mmol) was dissolved in 15 ml DMF. To the solution Potassium carbonate (0.13g, 1mmol) and 2-trifluoromethyl-1H-benzimidazole (0.169g, 1mmol) were added and then refluxed for 18h. After cooled to room temperature, the mixture was extract by ethyl acetate and washed with water. The pure product was obtained after column (PE: EA=1:1). Yield is 0.1g (48%)

$^1\text{H}$  NMR (400MHz,  $\text{DMSO-d}_6$ ):  $\delta$  3.77 (m, 2H), 4.45 (m, 2H), 5.0 (t, 1H), 7.35 (m, 1H), 7.45 (m, 1H), 7.80 (m, 2H) ppm.

Mass ( $\text{M}+\text{H}$ ) $^+$ : 231.0740

m.p.:90-92°C

### 5.73 Preparation of N-(2-(6-chloro-*s*-tetrazine-3-yloxy)ethyl)-2-trifluoromethyl-benzimidazole



N-ethanol- benzimidazole (0.023g, 0.1mmol) and 3,6-dichloro tetrazine(0.02g, 0.13mmol) were dissolved in dry 20ml dichloromethane, 2,4,6-collidine (0.02ml, 0.1mmol) was added at room temperature under N<sub>2</sub>. After stirring 4h, the solvent was removed under reduced pressure, and purified by column chromatography (PE: EA=2:1). Yield 0.02g, 58%.

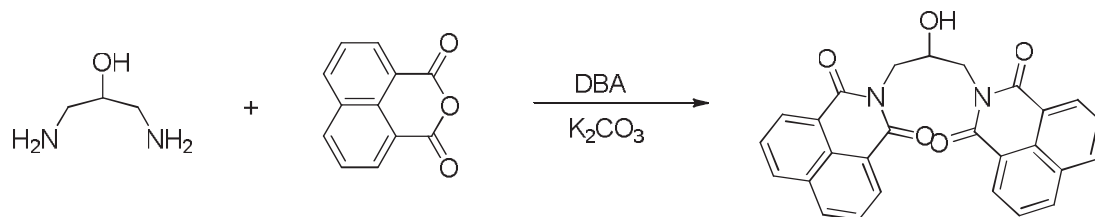
<sup>1</sup>H NMR (400MHz, CDCl<sub>3</sub>): δ 4.88 (t, 2H, J=5.2Hz), 5.03 (t, 2H, J=5.2Hz), 7.39 (m, 1H), 7.49 (m, 1H), 7.64 (m, 1H), 7.86 (m, 1H) ppm.

<sup>13</sup>C NMR (100MHz, CDCl<sub>3</sub>): δ 43.5, 68.2, 110.7, 117.8, 120.5, 121.9, 124.3, 126.2, 135.6, 141.0, 165.1, 166.2 ppm.

Mass (M<sup>+</sup>): 344.0

m.p.: 125-126°C

#### 5.74 Preparation of 2NIOH



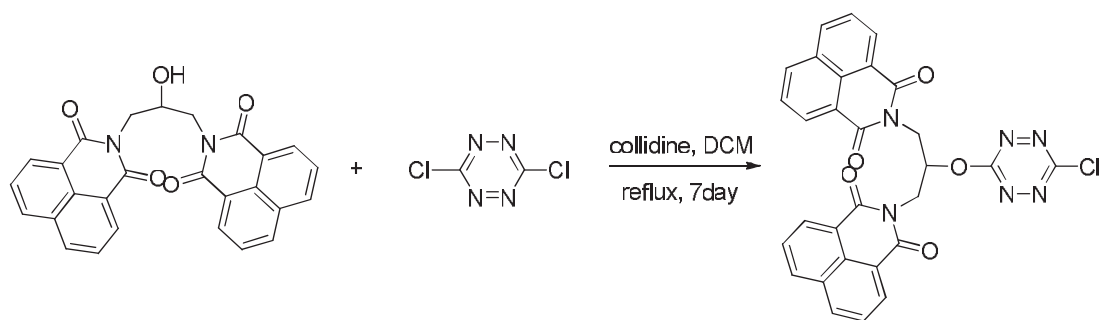
1,8-naphthalic anhydride (1g, 5.05mmol) was suspended in 10ml of N,N-dimethylacetamide (DMA). 1,3-Diamino-2-propanol (0.2g, 2.2mmol) was added to the suspension. The mixture was stirred at 100 °C for 12h. After removal of the solvent on a rotary evaporator, water (5ml) was added to the residue. The resulting white precipitate was filtered and dried, 0.2g (yield is 40%) pure product was obtained after the column (PE: EA=1:1).

<sup>1</sup>H NMR (400MHz, CDCl<sub>3</sub>): δ 4.52 (m, 5H), 7.75 (t, 4H, J=7.8Hz), 8.22 (d, 4H, J=8.2Hz), 8.59 (d, 4H, J=7.3Hz) ppm.

<sup>13</sup>C NMR (100MHz, CDCl<sub>3</sub>): δ 44.7, 69.7, 122.6, 127.1, 128.4, 131.7, 134.3, 165.1 ppm.

m.p.: >264°C

#### 5.75 Preparation of 2NITZ



2NIOH (0.1g, 0.22mmol) and 3,6-dichloro tetrazine(0.05g, 0.33mmol) were dissolved in dry 20ml dichloromethane, 2,4,6-collidine (0.05ml, 0.25mmol) was added at room temperature under  $N_2$ . After reflux 7 days, the solvent was removed under reduced pressure, and purified by column chromatography (PE: EA: DCM=1:1:2). Then 0.022g (yield is 17%) pure 2NITZ was obtained.

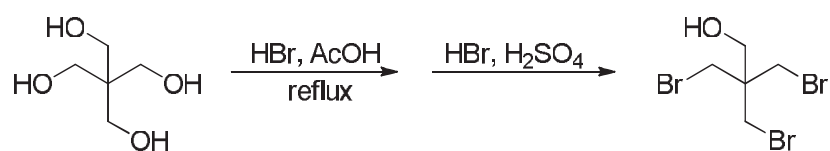
$^1H$  NMR (400MHz,  $CDCl_3$ ):  $\delta$  4.83 (m, 2H), 4.96 (m, 2H), 6.20 (m, 1H), 7.73 (t, 4H,  $J=7.8$ Hz), 8.21 (d, 4H,  $J=8.2$ Hz), 8.51 (d, 4H,  $J=7.3$ Hz) ppm.

$^{13}C$  NMR (100MHz,  $CDCl_3$ ):  $\delta$  40.9, 60.5, 122.3, 127.1, 128.3, 131.7, 131.8, 134.5, 164.6 ppm.

Mass ( $M+Na$ ) $^+$ : 587.0836

m.p.: 140°C

#### 5.76 Preparation of 2,2-bis(bromomethyl)-3-bromo-propan-1-ol

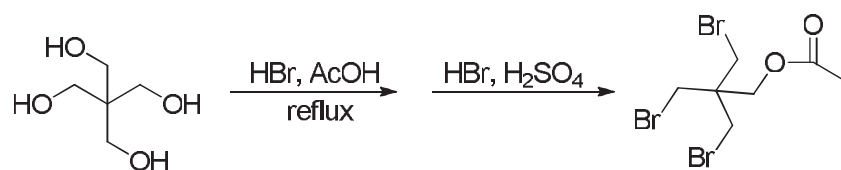


Pentaerythritol (12.8g, 94mmol) was dissolved in glacial AcOH: 48%HBr (aq) (1:4.2 v/v, 52ml) and heated under reflux. After 24h 48% HBr (aq) (42ml) and c.  $H_2SO_4$  (23ml) were added and the resulting solution heated under reflux. After a further 24h the reaction mixture was cooled. The lower liquid layer from the resulting mixture was separated and dissolved in  $CHCl_3$  (50ml), washed with water (20ml), dried (anhyd.  $K_2CO_3$ ), filtered and the solvent removed. The residue was purified by flash chromatography (EA:PE=1:9) to give 2,2-bis(bromomethyl)-3-bromo-propan-1-ol (15.1g, 49%) as a white crystalline solid.

$^1H$  NMR (400MHz,  $CDCl_3$ ):  $\delta$  3.75 (d, 2H,  $J=5.5$ Hz,  $-CH_2OH$ ), 3.53 (s, 6H,  $-CH_2Br$ ), 1.70 (br s, 1H, OH) ppm.

$^{13}C$  NMR (100MHz,  $CDCl_3$ ):  $\delta$  34.5, 62.5 ppm.

### 5.77 Preparation of 3-bromo-2,2-bis(bromomethyl)propyl acetate



Pentaerythritol (6.4g, 47mmol) was dissolved in glacial AcOH: 48% HBr (aq) (1:4.2 v/v, 30ml) and heated under reflux. After 24h 48% HBr (aq) (21ml) and c. H<sub>2</sub>SO<sub>4</sub> (12ml) were added and the resulting solution heated under reflux. After a further 24h the reaction mixture was cooled. The lower liquid layer from the resulting mixture was separated and dissolved in CHCl<sub>3</sub> (50ml), washed with water (20ml), dried (anhyd. K<sub>2</sub>CO<sub>3</sub>), filtered and the solvent removed. The residue was purified by flash chromatography (EA:PE=1:9) to give 3-bromo-2,2-bis(bromomethyl)propyl acetate (7g, 41%) as a white crystalline solid.

<sup>1</sup>H NMR (400MHz, CDCl<sub>3</sub>): δ 1.99 (s, 3H), 3.44 (s, 6H, -CH<sub>2</sub>Br), 4.07 (s, 2H ppm.

<sup>13</sup>C NMR (100MHz, CDCl<sub>3</sub>): δ 20.9, 34.3, 42.7, 63.6, 169.8 ppm.

### 5.78 Preparation of 2NI2OH (1)

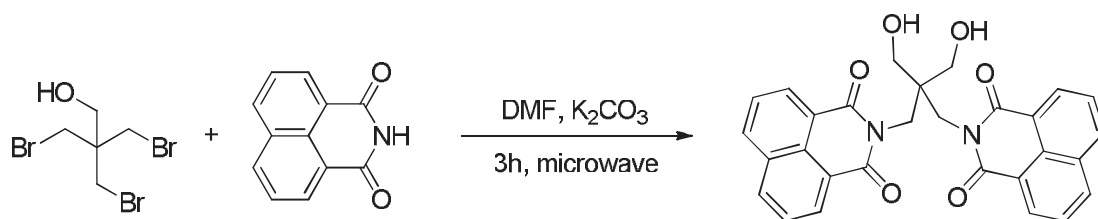


2,2-bis(bromomethyl)-3-bromo-1-propanol (0.05g, 0.15mmol) was dissolved in 10 ml DMF. To the solution Potassium carbonate (0.02g, 0.15mmol) and naphthalimide (0.3g, 1.5mmol) were added and then refluxed for 3 days. After cooled to room temperature, the mixture was extracted by ethyl acetate. The product was purified by column, Yield 0.01g (13%).

<sup>1</sup>H NMR (400MHz, CDCl<sub>3</sub>): δ 3.52 (t, *J* = 7.8 Hz, 4H, -CH<sub>2</sub>OH), 4.12 (t, *J* = 7.8 Hz, 2H, -OH), 4.54 (s, 4H), 7.78 (t, *J* = 7.8 Hz, 4H), 8.25 (d, *J* = 8.2 Hz, 4H), 8.60 (d, *J* = 7.3 Hz, 4H) ppm.

<sup>13</sup>C NMR (100MHz, CDCl<sub>3</sub>): δ 41.6, 48.8, 63.7, 122.2, 127.3, 128.3, 131.7, 132.2, 134.7, 166.0 ppm.

### Preparation of 2NI2OH (2)



2,2-bis(bromomethyl)-3-bromo-1-propanol (0.05g, 0.15mmol) was dissolved in 7 ml DMF. To the solution Potassium carbonate (0.02g, 0.15mmol) and naphthalimide (0.3g, 1.5mmol) were added and then with microwave (130°C, 3h). After cooled to room temperature, the mixture was extract by ethyl acetate. The product was purified by column, Yield 0.015g (20%) and gave the same NMR spectra as in the previous method.

### Preparation of 2N12OH (3)

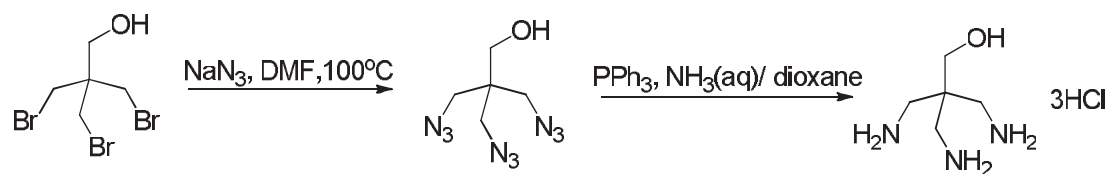


3-bromo-2,2-bis(bromomethyl)propyl acetate (0.05g, 0.13mmol) was dissolved in 10 ml DMF. To the solution Potassium carbonate (0.02g, 0.15mmol) and naphthalimide (0.3g, 1.5mmol) were added and then refluxed for 3 days. After cooled to room temperature, the mixture was extract by ethyl acetate. The product was purified by coloum, Yield 0.01g (15%).

$^1\text{H}$  NMR (400MHz,  $\text{CDCl}_3$ ):  $\delta$  3.52 (t,  $J = 7.8$  Hz, 4H,  $-\text{CH}_2\text{OH}$ ), 4.12 (t,  $J = 7.8$  Hz, 2H,  $-\text{OH}$ ), 4.54 (s, 4H), 7.78 (t,  $J = 7.8$  Hz, 4H), 8.25 (d,  $J = 8.2$  Hz, 4H), 8.60 (d,  $J = 7.3$  Hz, 4H) ppm.

$^{13}\text{C}$  NMR (100MHz,  $\text{CDCl}_3$ ):  $\delta$  41.6, 48.8, 63.7, 122.2, 127.3, 128.3, 131.7, 132.2, 134.7, 166.0 ppm.

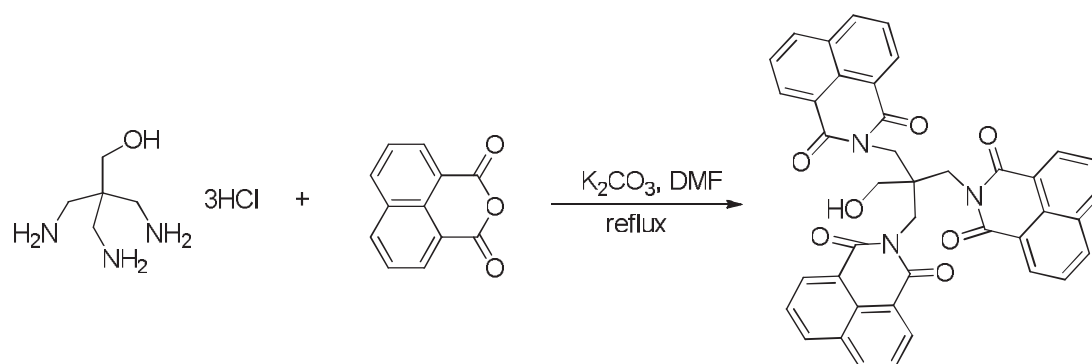
### 5.79 Preparation of 2,2-bis(aminomethyl)-3-amino-1-propanol trihydrochloride



NaN<sub>3</sub> (1.57g, 24.15mmol) was added to a solution of 2,2-bis(bromomethyl)-3-bromo-propan-1-ol (0.66g, 20.3mmol) in DMF (12ml) under N<sub>2</sub> and the resulting mixture warmed to 100°C. After 28h the solution formed was cooled, poured into water (100ml) and extracted with Et<sub>2</sub>O (250ml). The organic fractions were combined, dried with MgSO<sub>4</sub>, filtered and the volume of solvent reduced to 10ml. *P*-dioxane (20ml) was added and the volume of solvent reduced again to 10ml. *P*-dioxane(25ml), PPh<sub>3</sub> (2.66g, 10.14mmol) and NH<sub>3</sub>(aq, 30%, 10ml) were added with stirring. After 19h the solvent was removed, the residue suspended in CHCl<sub>3</sub> (100ml) and extracted with HCl (aq, 2.5M, 50ml). The aqueous fractions were combined, washed with CHCl<sub>3</sub> (20ml x 4) and concentrated to a volume of 50ml. c. HCl (aq, 2ml) was added and the solution cooled to 4°C. The white solid that crystallized from solution was filtered, washed with cold c. HCl (aq, 2ml), EtOH (3ml), Et<sub>2</sub>O (5 x 5) and dried under vacuum to give 2,2-bis(aminomethyl)-3-amino-propan-1-ol trihydrochloride (0.16g, 32%) as a white crystalline solid.

<sup>1</sup>H NMR (400MHz, D<sub>2</sub>O): δ 3.28 (s, 6H, -CH<sub>2</sub>N), 3.83 (s, 2H, -CH<sub>2</sub>OH) ppm.

#### 5.80 Preparation of 3NIOH



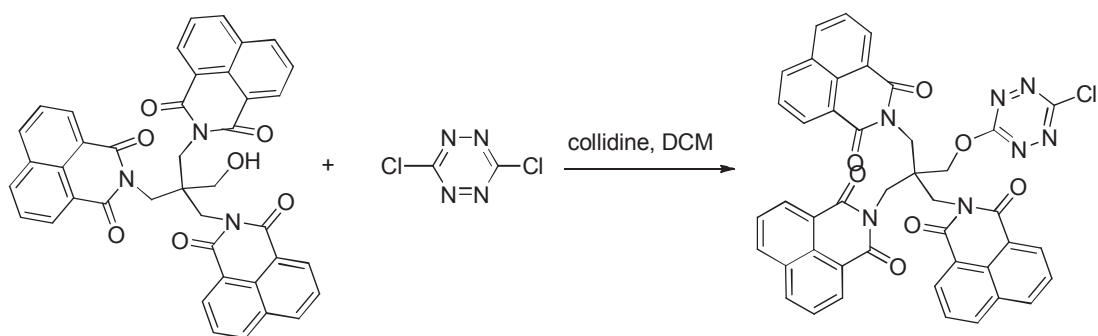
1,8-naphthalic anhydride (0.4g, 2mmol) was suspended in 15ml of dry DMF. 2,2-bis(aminomethyl)-3-amino-propan-1-ol trihydrochloride (0.1g, 0.4mmol) was added to the suspension. The mixture was heated to reflux for 12h. After removal of the solvent on a rotary evaporator, water was added to the residue. The resulting white precipitate was filtered and dried, and purified by column (PE:EA=1:1). 0.16g 2,2-bis(naphthalic -methyl)-3- naphthalic -propan-1-ol was obtained, yield is 59%.

<sup>1</sup>H NMR (CDCl<sub>3</sub>): δ 3.72 (d, 2H, *J*=7.3Hz, -CH<sub>2</sub>OH), 4.27 (t, 1H, *J*=7.8Hz, -OH), 4.66 (s, 6H, -CH<sub>2</sub>N), 7.72 (t, 6H, *J*=8.2Hz), 8.20 (d, 6H, *J*=8.7Hz), 8.55 (d, 6H, *J*=7.3Hz) ppm.

<sup>13</sup>C NMR (CDCl<sub>3</sub>): δ 44.3, 49.8, 64.2, 122.7, 127.1, 128.3, 131.7, 134.1, 165.6 ppm.

Mass (M+Na)<sup>+</sup>: 696.1741

### 5.81 Preparation of 3NITZ

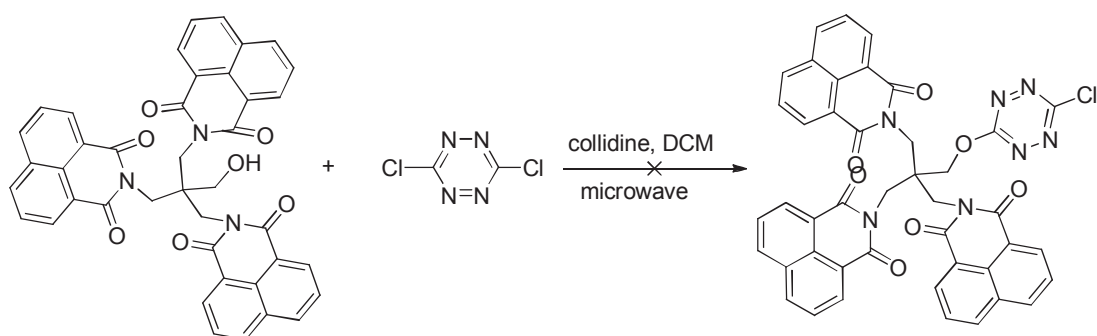


3NIOH (0.05g, 0.07mmol) and 3,6-dichloro tetrazine(0.112g, 0.74mmol) were dissolved in dry 10ml dichloromethane, 2,4,6-collidine (0.25ml, 0.12mmol) was added at room temperature under  $N_2$ . After heated at  $100^\circ C$  for 7 days in the pressure tube, the solvent was removed under reduced pressure, and purified by column chromatography (PE: EA: DCM=1:1:2). Then 0.01g (yield is 2%) pure 3NITZ was obtained.

$^1H$  NMR ( $CDCl_3$ ):  $\delta$  4.88 (m, 6H), 7.73 (m, 6H), 8.21 (m, 6H), 8.50 (m, 6H) ppm.

$^{13}C$  NMR ( $CDCl_3$ ):  $\delta$  44.1, 45.0, 51.1, 122.5, 127.0, 128.3, 131.6, 134.0, 165.4, 165.5 ppm.

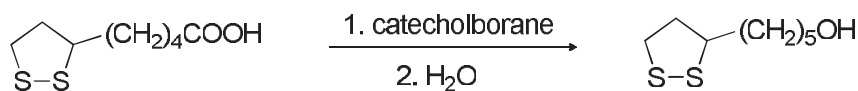
### 5.82 Preparation of 3NITZ by microwave



3NIOH (0.05g, 0.07mmol) and 3,6-dichloro tetrazine(0.112g, 0.74mmol) were dissolved in dry 10ml dichloromethane, 2,4,6-collidine (0.25ml, 0.12mmol) was added at room temperature under  $N_2$ . After reacted in microwave ( $130^\circ C$ , 10min), there are no compound expected obtained from the TLC.

### 5.83 Preparation of 1,2-dithiolane-3-pentanol





Lipoic acid (2.06 g, 10 mmol) was placed in a flame-dried 250 mL flask fitted with a stirrer and dropping funnel and connected to an oil bubbler to maintain a nitrogen atmosphere. Anhydrous chloroform (70 mL) was added followed by 1.0 M catecholborane, in tetrahydrofuran (50 mL, 50 mmol), dropwise. The mixture was refluxed (70-80 °C) for about 6 h. Cold water (20 mL) was then added dropwise and the organic solvent evaporated in vacuo. Dichloromethane (50 mL) was added and the mixture extracted with one 25 mL aliquot of water followed by six 25 mL aliquots of 1.0 M NaOH to remove the catechol. The organic portion was dried with sodium sulfate and filtered and solvent evaporated in vacuo. The crude product was purified by column chromatography (silica gel, CH<sub>2</sub>Cl<sub>2</sub>/ethyl acetate, 4:1). Yield: yellow oil, 88.5%.

<sup>1</sup>H NMR (CDCl<sub>3</sub>): δ 1.5 (broad, 8H, alkyl), 2.4 (quintet, 2H, ring CH<sub>2</sub>), 3.15 (t, 2H, CH<sub>2</sub>S), 3.6 (m, 3H, CHRS and CH<sub>2</sub>O) ppm.

<sup>13</sup>C NMR (CDCl<sub>3</sub>): δ 25.6, 29.2, 32.6, 35.0, 38.5, 40.4, 56.7, 62.8 ppm.

#### 5.84 Preparation of 3-chloro-6-(1,2-dithiolane-3-pentanoxy)-1,2,4,5-tetrazine



1,2-dithiolane-3-pentanol (0.19g, 1mmol) and 3,6-dichloro tetrazine (0.20g, 1.32mmol) were dissolved in dry 15ml dichloromethane, 2,4,6-collidine (0.14ml, 1mmol) was added at room temperature under N<sub>2</sub>. After stirring 2h, the solvent was removed under reduced pressure, and purified by column chromatography (PE: DCM=1:1). 0.25g product is obtained, yield is 82%.

<sup>1</sup>H NMR (400MHz, CDCl<sub>3</sub>): δ 1.53 (m, 8H), 2.41 (m, 1H), 3.09 (m, 2H), 3.51 (m, 1H), 4.60 (t, 2H, *J*=6.42Hz) ppm.

<sup>13</sup>C NMR (100MHz, CDCl<sub>3</sub>): δ 25.5, 28.3, 28.8, 34.7, 38.4, 40.2, 56.4, 70.7, 164.0, 166.6 ppm.



Contents lists available at ScienceDirect

## Journal of Electroanalytical Chemistry

journal homepage: [www.elsevier.com/locate/jelechem](http://www.elsevier.com/locate/jelechem)

## Tetrazines with hindered or electron withdrawing substituents: Synthesis, electrochemical and fluorescence properties

Zhou Qing<sup>a</sup>, Pierre Audebert<sup>a,b,\*</sup>, Gilles Clavier<sup>a</sup>, Fabien Miomandre<sup>a</sup>, Jie Tang<sup>b,\*</sup>,  
 Thanh T. Vu<sup>a</sup>, Rachel Méallet-Renault<sup>a</sup>

<sup>a</sup> PPSM, UMR 8531, PRES UniverSud, Ecole Normale Supérieure de Cachan, 61 Av. du P<sup>e</sup> Wilson, 94235 Cachan, France

<sup>b</sup> East China Normal University, Department of Chemistry, Shanghai 200062, China

## ARTICLE INFO

## Article history:

Received 16 October 2008

Received in revised form 25 March 2009

Accepted 26 March 2009

Available online 5 April 2009

## Keywords:

Tetrazine  
 Electrochemistry  
 Fluorescence  
 Synthesis  
 Electron transfer

## ABSTRACT

Several new *s*-tetrazines have been prepared with hindered, electron-withdrawing or electron-rich substituents. This is the first time that tetrazine bearing interactive functional groups other than ligands are described... Their electrochemical and spectroscopic properties have been investigated, especially concerning the electron transfer rate in the case of three selected compounds. Fluorescence occurs as expected as soon as the substituent linked to the tetrazine core is electron withdrawing enough. The existence of the tetrazine fluorescence with imide substituents might open the way to the preparation of bichromophoric fluorophores.

© 2009 Elsevier B.V. All rights reserved.

### 1. Introduction

*s*-Tetrazine chemistry has been known for more than one century [1], and their photophysical [2] and electrochemical [3] properties have been briefly recognized. However, only recently did these very original properties started to be fully investigated. With regards to the recently developed supramolecular chemistry [4], the *s*-tetrazine building block appears a very promising and fascinating one. *s*-Tetrazines are electroactive heterocycles, having a very high electron affinity which make them reducible at high to very high potentials. Since pentazine and hexazine are unknown and probably not stable [5], they are actually the electron poorest class of aromatic neutral C–N heterocycles. In addition, they have a low lying  $\pi^*$  orbital, with as consequence a low energy  $n\text{--}\pi^*$  transition in the visible range, which makes them highly colored. The chemistry of *s*-tetrazines has been recently reviewed [5], enlightening especially their interest in explosives synthesis [6] and coordination chemistry [7].

We, and others, have remarked that *s*-tetrazines substituted with heteroatoms display interesting fluorescence properties [8–11] that can be electrochemically monitored [12,13]. Actually, all these compounds are fluorescent on TLC as well as in the crystalline

state, which place them amongst the smallest organic fluorophores in the visible range ever prepared. This makes them especially attracting in view of sensing applications. Our first studies had shown indeed that chloromethoxy-*s*-tetrazine was among the best compounds, because the combination of a chlorine and an alkoxy substituent on a *s*-tetrazine appeared to lead to the maximum fluorescence yield ( $\phi_F = 0.38$ ) in dichloromethane [10]. However, this compound easily sublimates even at room temperature, and layers are not stable over days. An attracting development to overcome this drawback is thus to prepare chlorotetrazines with other alkoxy substituents, and especially hindered ones. Since tetrazines are electroactive, their electrochemistry is also interesting, especially as far as the electron transfer rate can be dependant on the substituents size and nature. We wished also to check how the fluorescence was dependant on the substituent nature. A point of interest was therefore to investigate the replacement of alkoxy substituents by more electron withdrawing substituents, and the imide group appeared especially interesting. In addition, it could open the possibility to prepare bichromophoric compounds.

In this article we report the synthesis of several new *s*-tetrazines featuring bulky alkoxy substituents, like adamantane related groups. We also report their electrochemical and fluorescence properties in solution. In addition, we also report the preparation and a few properties of tetrazines substituted by electron-attracting groups, namely the phthalimidochlorotetrazine, as well as the perchlorophenoxychlorotetrazine, with their electrochemical and spectroscopic characteristics.

\* Corresponding authors. Address: PPSM, UMR 8531, PRES UniverSud, Ecole Normale Supérieure de Cachan, 61 Av. du P<sup>e</sup> Wilson, 94235 Cachan, France. Tel.: +33 1 47 40 53 39; fax: +33 1 47 40 24 54 (P. Audebert).

E-mail addresses: [audebert@ppsm.ens-cachan.fr](mailto:audebert@ppsm.ens-cachan.fr), [Pieere.Audebert@ppsm.ens-cachan.fr](mailto:Pieere.Audebert@ppsm.ens-cachan.fr) (P. Audebert).

## 2. Experimental

### 2.1. Syntheses

All the reported alcohols were reacted using the same operating mode: a mixture of dichlorotetrazine (150 mg,  $10^{-3}$  moles) and alcohol (1.5 eq.) is dissolved into dry dichloromethane (DCM), degassed (about 20 ml), and added 2.5 eq (about 0.30 ml) of dry sym. collidine. The solution is stirred for about 2 h, then concentrated and purified on a silica gel column (usually DCM: Pet. Ether 1:1). Yields are in the 60–80% range for primary alcohols, and 10–20% for secondary alcohols.

Imides were purchased as their potassium salts and reacted as such, in acetonitrile (the salts are not soluble in DCM) for about 2 h. Then acetonitrile is completely taken off in vacuum, and the products are purified by chromatography similarly to above described.

Characterizations of the compounds (NMR data) are provided as Supplementary material.

### 2.2. Electrochemical studies

Electrochemical studies were performed using dichloromethane (DCM) (SDS, anhydrous for analysis) as a solvent, with *n*-tetrabutylammonium hexafluorophosphate (TBAFP) (Fluka, puriss.) as the supporting electrolyte (0.1 M), except for the kinetic studies where an acetonitrile/DCM mixture was used to improve the conductivity. The substrate concentration was *ca.* 5 mM. A 1 mm diameter Pt or glassy carbon electrode was used as the working electrode, along with a  $\text{Ag}^+/\text{Ag}$  ( $10^{-2}$  M) reference electrode and a Pt wire counter electrode. The cell was connected to a CH Instruments 600B potentiostat monitored by a PC computer. The reference electrode ( $\text{Ag}/10^{-2}$  M  $\text{Ag}^+$ ) was checked vs. ferrocene as recommended by IUPAC. In our case,  $E^\circ(\text{Fc}^+/\text{Fc}) = 0.097$  V. All solutions were degassed by argon bubbling prior to each experiment.

For kinetic studies, the ohmic drop was carefully compensated as detailed before [15]. The  $k^\circ$  value was determined according to the classical formula where the letters have the following meaning:

$$k^\circ = \sqrt{\frac{F}{RT}} \alpha D v_t$$

$v_t$  is the transition scan rate (crossing point in the  $E_p$  vs.  $\log v$  asymptots),  $\alpha$  the transfer coefficient (determined from the slopes of the  $E_p$  vs.  $\log v$  at high scan rate),  $D$  the diffusion coefficient of the electroactive species (neutral and reduced forms are assumed to have the same value of  $D$ ) and  $F$ ,  $R$ ,  $T$  have their usual meanings.

### 2.3. Fluorescence measurements

All solvents were of spectroscopic grade.

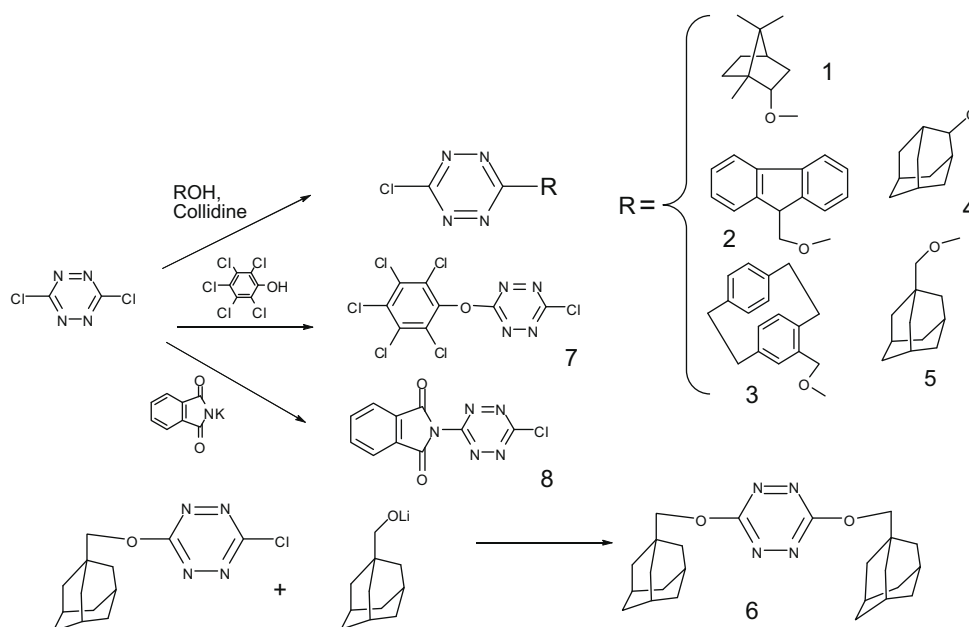
#### 2.3.1. Steady-state spectroscopy

A UV-Vis. Varian CARY 500 spectrophotometer was used. Excitation and emission spectra were measured on a SPEX Fluorolog-3 (Jobin-Yvon). A right-angle configuration was used. Optical density of the samples was checked to be less than 0.1 to avoid reabsorption artifacts. A rhodamine 6G standard (95% yield in ethanol) was used as reference.

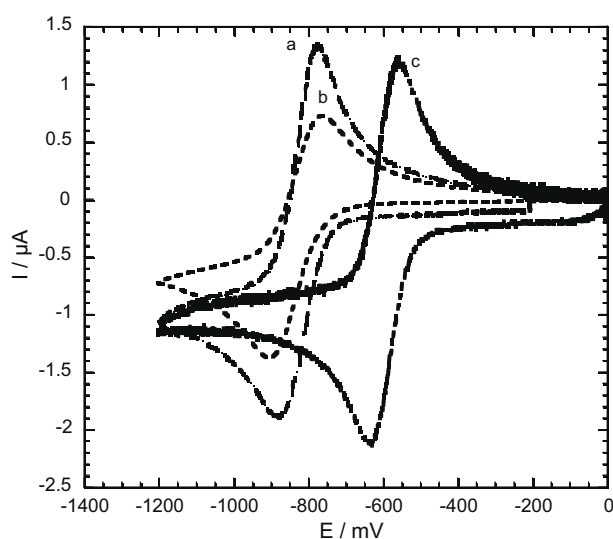
### 2.4. Theoretical modeling

All the geometry optimizations and scan were performed in vacuo on a Nec TX7 with 32 processors Itanium 2 of the Meso center at ENS Cachan.

Geometry optimizations of the neutral molecules were performed using the hybrid density functional B3LYP potential in conjunction with a 6–31+G(d) basis set as implemented in GAUSSIAN03 [16]. This level was adequate for the geometry optimization of aromatic compounds. No symmetry was imposed on the molecules. Harmonic vibrations were also calculated for all the obtained structures to establish that a true minimum was observed. The scan are relaxed and were performed using the `opt = modredundant` command after freezing the value of the dihedral angle of interest every 20°. Radical anions were studied with a similar approach starting from the optimized geometry of the neutral molecules, specifying a  $-1$  charge with a spin multiplicity of 2 and unrestricted B3LYP.



**Scheme 1.** Summary of the tetrazines synthetic routes.



**Fig. 1.** CV featuring the first reduction peak of resp. tetrazines 2 (curve a) 1 (curve b) and 8 (curve c) (conditions as in exp. part). Scan rate: 100 mV/s. Electrolyte was dichloromethane with 0.1 M TEAFB, with an Ag/Ag<sup>+</sup> reference, and substrate concentration around  $5 \times 10^{-3}$  M.

### 3. Results and discussion

#### 3.1. Synthesis

The following synthetic route (see Scheme 1 below) was used for the preparation of the tetrazines.

It should be noted that so far in this work we found that nucleophilic substitution works well only with weakly hindered oxygen nucleophiles. For example the yields with imides and hindered alcohols are low, and the substitution only works well with primary alcohols and phenols. In addition, the size and the electronic characteristics of the substituents clearly affect both the electronic and the optical properties of the tetrazines, more than it could be expected.

#### 3.2. Electrochemistry

We have investigated the behaviour of all the tetrazines prepared, looking at the substituent effects, and also comparing to the generic chloromethoxy tetrazine. Fig. 1 represents the cyclic voltammograms for three different tetrazines, two of them bearing a donor alkoxy group, and the third an attractor imide group. It is clear that all compounds display reversible CV's, with potentials depending on the electron affinity of the substituent, and not on the steric hindrance as it could be expected. This is even clearer from Table 1, which gathers the standard potential values for the first redox couple of all the tetrazines studied.

While some variations of the potential can be easily correlated to the electron withdrawing or donating character of the substituent, on the other hand the steric hindrance of the substituents appears to play a smaller role, which is more complicated to attribute. All together the differences between the tetrazines bearing one chlorine and one alkoxy group appear very small, while the

presence of two alkoxy groups (in **6**) noticeably decreases the potential. Considering the behaviour of tetrazines **7** and **8**, the attracting group, although much more withdrawing than a standard alkoxy group, seems to exert a power slightly smaller than a chlorine since both potentials are more negative than dichlorotetrazine itself. It should also be noticed that electron transfer on tetrazines appears relatively slow, since the peak to peak separation values are all above 100 mV/s. This is unexpected for aromatics, and especially for the smaller member of the series like chloromethoxy tetrazine. Hindered tetrazines seem at first sight, to transfer electron more slowly, however, we show later on that the difference in their diffusion coefficients is probably responsible for the larger peak separation.

First, we have performed calculations on the structure of the neutral tetrazine and the anion radical for three typical compounds: the generic chloromethoxytetrazine, the adamantanylmethoxychlorotetrazine **5** and the bis(adamantanylmethoxy)tetrazine **6**. This choice was motivated by the fact that the adamantyl is the most bulky group of our series, and therefore that the steric hindrance regularly and noticeably increases from the first to the third compound. Fig. 2 shows the calculated energy differences related to the values of the dihedral angle N–C–O–C as shown on the figure, both for the neutral molecule and the anion-radical. The results are quite as expected in the case of the neutral compounds, the important energy variation associated with the bending of the structure resulting from the loss of the mixing of the nitrogen lone pairs to the attracting tetrazine ring. All anion-radicals also show a minimum for the 0° angle value, which was not obvious in this case, taking into account that the tetrazine ring becomes much less electron attracting once an electron has been added inside. The energy differences are slightly lower than for the neutral compounds, the difference being smaller than it could be expected. Therefore the deformation of the molecule geometry upon reduction is not likely to be the reason for the slow electron transfer.

In order to investigate more precisely the electron transfer rate for these three tetrazines, and know whether the substituents hindrance had an influence on the electron transfer rate, we performed scan rate dependant experiments in order to extract the heterogeneous rate constants  $k^0$  in the three cases. Fig. 3 displays the variations of the peak potentials with the scan rate, and Table 2 displays both diffusion coefficients and rate constants for the three compounds. Actually, despite the huge difference in the steric hindrance, the three tetrazine display almost the same rate constant, the apparent slower character of the heavier ones coming mainly from the diffusion coefficients difference. Therefore, the sluggishness of the electron transfer is likely to come in this case from solvation differences, which constitutes a difference with most of the aromatic compounds where electron transfer is usually fast [17].

One of the most interesting characteristics of tetrazine derivatives is the ability to be electrochemically reduced through a two-electrons process (similarly to most quinones) without *electrochemical*, but however, *chemical* reversibility (all tetrazines in our hands display this characteristics but dichlorotetrazine). This is exemplified in Fig. 4 which presents the CV's of compound **1** at various negative potentials. On the curves, the reoxidation of the anion radical is clearly visible whatever the negative potential limit scan. This means that the two electrons reduced electrogenerated species gives back the anion-radical in the course

**Table 1**

Standard reduction potentials and peak to peak separations for the tetrazine derivatives **1–8** (for conditions see exp. part).

	1	2	3	4	5	6	7	8
$E^{\circ}$ (V) vs. Ag <sup>+</sup> /Ag	-0.83	-0.84	-0.91	-0.88	-0.94	-1.21	-0.63	-0.60
$\Delta E_p$ (mV)	140	100	130	130	140	130	110	100

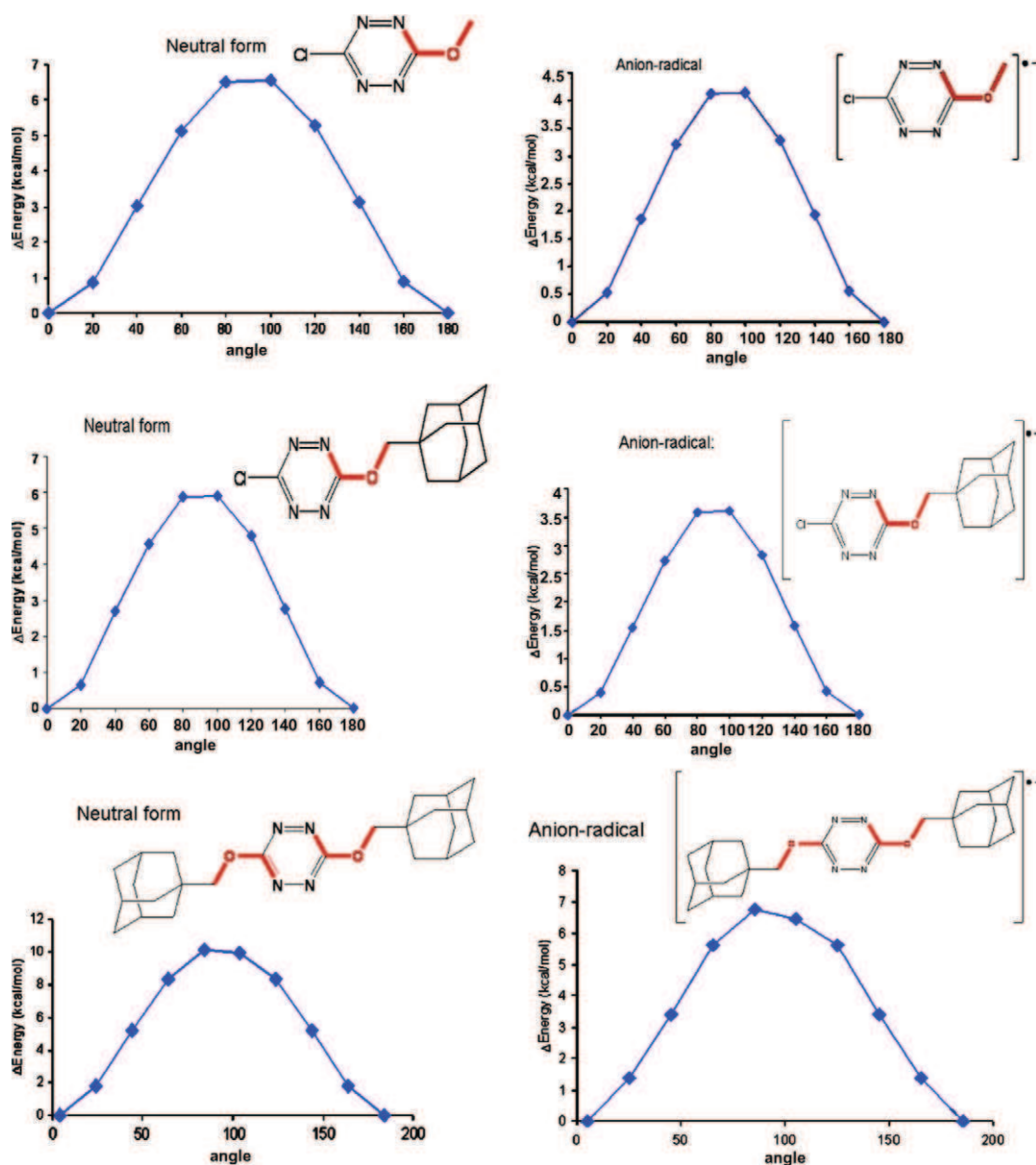


Fig. 2. Energy profiles as function of the dihedral torsion angle of one alkoxy substituent for chloromethoxytetrazine, chloro-(adamant-1-ylmethoxy)-tetrazine **5** and bis-(adamant-1-ylmethoxy)-tetrazine **6**, each for the neutral and the anion-radical forms.

of the first reoxidation process. This species is likely to be the one-time protonated dianion. This feature is quasi-general for tetrazines (only dichlorotetrazine behaves differently) and quite unexpected particularly for the monochlorotetrazines family, because it implies that no chloride ions is expelled, even from the electro-generated dianion. This behaviour reflect the particularly high electron affinity of tetrazines and is in sharp contrast with the behaviour of almost all the halogenated aromatics [14].

This shows that most tetrazines can store up to two electrons per ring, which makes them potentially interesting compounds for energy storage (most conducting polymers, for example, store a maximum of one electron over three rings). However, it should be remarked that this will not be necessarily the case for a polymer made with tetrazines; this point will be investigated further on.

### 3.3. Fluorescence

As previously reported [10–12], tetrazines bearing inductive electron-withdrawing substituents (like a chlorine or an alkoxy

moiety) are fluorescent, both in solution but also in the solid state. Fig. 5 shows the fluorescence spectrum for **1** in solution, which is typical of a chloroalkoxytetrazine, and resembles the one of the generic chloromethoxytetrazine.

The fluorescence of all the tetrazines has been investigated in solution, and the results are displayed in Table 3. Quantum yields are very dependant on the substituent nature. In the case of bulky purely alkyloxy substituents, we had expected that the yields could be higher because of some isolation of the fluorescent tetrazine core by the bulky inert alkyl groups. Actually, the yields are only very slightly higher, and therefore the size effect of the alkyl group appears unfortunately to be weak.

The case of compounds **2** and **3** bearing electron rich aromatic groups is more interesting. Quantum yields are low in these cases, most likely because of quenching by intramolecular electron transfer. We had shown before that the tetrazine fluorescence could be quenched by good electron donors, typically triphenylamines [10]. In these case the donors are weaker, since while the oxidation potential of the triaryl amines is in the +1 V (vs. SCE) range, the

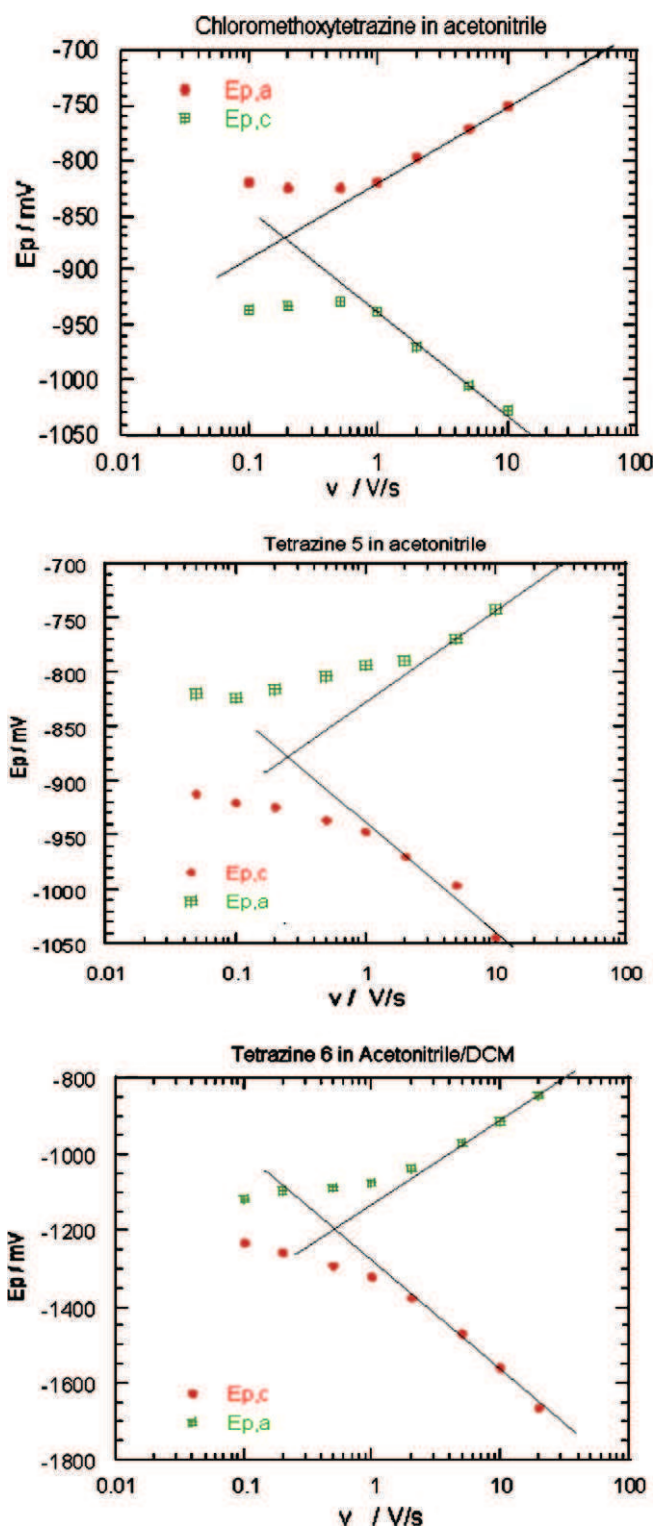


Fig. 3. Variation of the peak potentials with the scan rate for chloromethoxytetrazine, 5 and 6 (same conditions as Fig. 1).

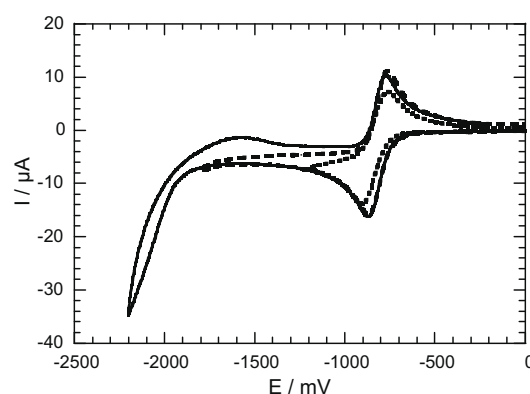


Fig. 4. CV's of tetrazine 1 at different inversion potentials. Scan rate: 100 mV s<sup>-1</sup> (same conditions as Fig. 1).

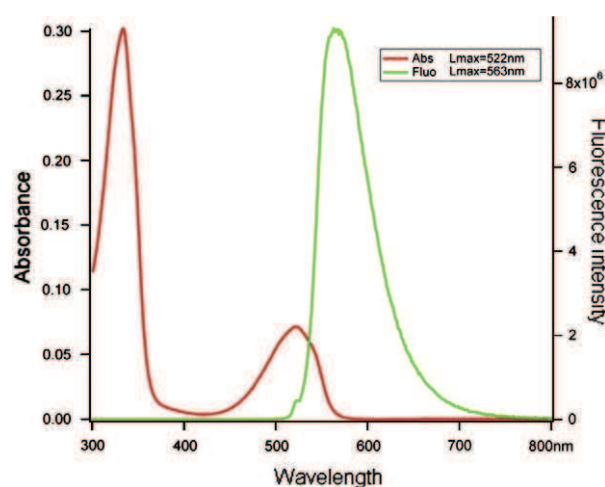


Fig. 5. Absorption and emission spectra of tetrazine 1 recorded in dichloromethane. Excitation wavelength 522 nm:

cyclophane (+1.47 V [18]) and fluorene (+1.64 V [19]) groups are oxidized at higher potentials in organic solvents. However, in this case, the proximity of the two groups in the same molecule may enhance the quenching efficiency, thus lowering the fluorescence quantum yield.

Unfortunately, tetrazines 7 and 8 bearing other electron attracting substituents display weak to very weak fluorescence quantum yields. This is somewhat surprising, especially in the case of the electron withdrawing pentachlorophenol, which owns a very low energy  $\pi$ - $n$  transition responsible for the fluorescence. However, somewhat similarly to the dichlorotetrazine case (where  $\phi_F$  is only 0.15), quantum yields decrease compared to the chloroalkoxy tetrazines. It might be therefore proposed that the existence of an appreciable dipolar moment is also a necessary condition for the existence of a relatively high fluorescence quantum yield. Finally compound 6, bearing two alkoxy substituents, display fluorescence yield in the range but slightly lower than the one of dimethoxytetrazine, and again the large size of the substituents unfortunately

Table 2  
Kinetic parameters for the electrochemical behaviour of chloromethoxytetrazine, 5 and 6.

	$u_t$ (V/s)	$D/10^{-5}$ (cm <sup>2</sup> s <sup>-1</sup> )	$\alpha$	$k^0$ (cm s <sup>-1</sup> )
Chloromethoxytetrazine	0.20 ± 0.05	1.6	0.42	0.007 ± 0.001
5	0.27 ± 0.1	0.8	0.45	0.006 ± 0.002
6	0.51 ± 0.05	0.6	0.43	0.007 ± 0.001

**Table 3**  
Fluorescence data for tetrazines reported in this paper.

Compound	$\lambda_{\text{abs, max}}$ (nm)	$\lambda_{\text{em, max}}$ (nm)	$\epsilon$ (L mol <sup>-1</sup> cm <sup>-1</sup> )	$\phi_F$
<b>1</b>	522	563	477	0.40
	334			
<b>2</b>	519	563	620	0.08
	328			
<b>3</b>	521	564	593	0.04
	326			
<b>5</b>	522	567	717	0.40
	330			
<b>6</b>	530	579	588	0.07
	351			
<b>7</b>	518	566	822	0.09
	<300			
<b>8</b>	518	546	451	0.006
	311			

does not lead to a rise of the quantum yield. However, it should be noticed that this compound is as expected nicely crystalline.

#### 4. Conclusion

We have prepared several new *s*-tetrazines and examined closely their electrochemical behaviour and more briefly their fluorescence spectroscopy. The results show that most of the alkoxytetrazine behave like the parent chloromethoxytetrazines, and that as well the electron transfer as the fluorescence behaviour is weakly affected by the size of the substituent. The substituent nature incidence is however, more important on the fluorescence properties, but bears essentially on the quantum yields rather than on the maximum emission wavelength. Preliminary results on the solid state fluorescence showing the existence of long range energy transfer are currently being obtained and will be presented in a more specialized paper.

#### Appendix A. Supplementary material

Supplementary data associated with this article can be found, in the online version, at doi:10.1016/j.jelechem.2009.03.021.

#### References

- [1] A.R. Katritzky, Handbook of Heterocyclic Chemistry, Pergamon Press, 1986.
- [2] M.A. El Sayed, J. Chem. Phys. 38 (1963) 2834;
- [3] J. Waluk, J. Spanget-Larsen, E.W. Thulstrup, Chem. Phys. 200 (1995) 201; J. Spanget-Larsen, E.W. Thulstrup, J. Waluk, Chem. Phys. 254 (2000) 135.
- [4] R. Gleiter, V. Schehlmann, J. Spanget-Larsen, H. Fischer, F.A. Neugebauer, J. Org. Chem. 53 (1988) 5756.
- [5] J.M. Lehn, Supramolecular Chemistry, VCH, New York, 1995.
- [6] N. Saracoglu, Tetrahedron 63 (2007) 4199.
- [7] (a) D.E. Chavez, R.D. Gilardi, M.A. Hiskey, Angew. Chem. Int. Ed. Engl. 39 (2000) 1791; (b) D.E. Chavez, M.A. Hiskey, J. Energy Mater. 17 (1999) 357; (c) M.Hang.V. Huynh, Mi.A. Hiskey, D.E. Chavez, D.L. Naud, R.D. Gilardi, J. Am. Chem. Soc. 127 (2005) 12537.
- [8] W. Kaim, Coord. Chem. Rev. 230 (2002) 127.
- [9] M. Chowdhury, L. Goodman, J. Chem. Phys. 38 (1963) 2979.
- [10] F. Gückel, A.H. Maki, F.A. Neugebauer, D. Schweitzer, H. Vogler, Chem. Phys. 164 (1992) 217.
- [11] P. Audebert, F. Miomandre, G. Clavier, M.C. Vernières, S. Badré, R. Méallet-Renault, Chem. Eur. J. 11 (2005) 5667.
- [12] Y.H. Gong, P. Audebert, J. Tang, F. Miomandre, G. Clavier, S. Badré, R. Méallet-Renault, J. Electroanal. Chem. 592 (2006) 147.
- [13] Y. Kim, E. Kim, G. Clavier, P. Audebert, Chem. Commun. (2006) 3612.
- [14] F. Miomandre, R. Méallet-Renault, J.J. Vachon, R. Pansu, P. Audebert, Chem. Comm. 16 (2008) 1913.
- [15] See for example J.M. Savéant, Adv. Phys. Org. Chem. 35 (2000) 117.
- [16] F. Miomandre, P. Audebert, K. Zong, J.R. Reynolds, Langmuir 19 (2003) 8894.
- [17] M.J. Frisch, G.W. Trucks, H.B. Schlegel, G.E. Scuseria, M.A. Robb, J.R. Cheeseman, J.A. Montgomery, Jr., T. Vreven, K.N. Kudin, J.C. Burant, J.M. Millam, S.S. Iyengar, J. Tomasi, V. Barone, B. Mennucci, M. Cossi, G. Scalmani, N. Rega, G.A. Petersson, H. Nakatsuji, M. Hada, M. Ehara, K. Toyota, R. Fukuda, J. Hasegawa, M. Ishida, T. Nakajima, Y. Honda, O. Kitao, H. Nakai, M. Klene, X. Li, J.E. Knox, H.P. Hratchian, J.B. Cross, C. Adamo, J. Jaramillo, R. Gomperts, R.E. Stratmann, O. Yazyev, A.J. Austin, R. Cammi, C. Pomelli, J.W. Ochterski, P.Y. Ayala, K. Morokuma, G.A. Voth, P. Salvador, J.J. Dannenberg, V.G. Zakrzewski, S. Dapprich, A.D. Daniels, M.C. Strain, O. Farkas, D.K. Malick, A.D. Rabuck, K. Raghavachari, J.B. Foresman, J.V. Ortiz, Q. Cui, A.G. Baboul, S. Clifford, J. Cioslowski, B.B. Stefanov, G. Liu, A. Liashenko, P. Piskorz, I. Komaromi, R.L. Martin, D.J. Fox, T. Keith, M.A. Al-Laham, C.Y. Peng, A. Nanayakkara, M. Challacombe, P.M. W. Gill, B. Johnson, W. Chen, M.W. Wong, C. Gonzalez, J.A. Pople, Gaussian 03, Revision C.02, Gaussian, Inc., Wallingford CT, 2004.
- [18] C.P. Andrieux, P. Hapiot, D. Garreau, J. Pinson, J.M. Savéant, J. Electroanal. Chem. 243 (1988) 321.
- [19] P. Hapiot, C. Lagrost, F. Le Floch, E. Raoult, J. Rault-Berthelot, Chem. Mater. 17 (2005) 2003.
- [20] T. Shono, A. Ikeda, S. Hakozaiki, Tetrahedron Lett. (1972) 4511.

Cite this: *New J. Chem.*, 2011, **35**, 1678–1682

www.rsc.org/njc

PAPER

## Bright fluorescence through activation of a low absorption fluorophore: the case of a unique naphthalimide–tetrazine dyad†

Zhou Qing,<sup>ab</sup> Pierre Audebert,<sup>\*ab</sup> Gilles Clavier,<sup>a</sup> Rachel Méallet-Renault,<sup>a</sup> Fabien Miomandre<sup>a</sup> and Jie Tang<sup>b</sup>

Received (in Montpellier, France) 7th February 2011, Accepted 4th May 2011

DOI: 10.1039/c1nj20100j

An original fluorescent dyad has been prepared, featuring a 1,8-naphthalimide chromophore linked to a fluorescent tetrazine. This bichromophore benefits from the good absorption coefficient of the imide, and displays a quasi complete energy transfer to the tetrazine, followed by its fluorescence emission. This allows the preparation of remarkable transparent solutions and solids displaying a strong yellow fluorescence with a long life-time.

### Introduction

The search for original fluorescent dyes has never stopped and among them, special colours or effect linked to energy transfer between chromophores have for a long time and till now received special attention.<sup>1</sup> This interest has been recently renewed due to multistate molecules and molecular calculators.<sup>2</sup> Bichromophoric dyads have also been widely investigated, especially on the point of view of the mechanisms and efficiency of energy transfer.<sup>3</sup>

However, an especially interesting situation is the activation of a weakly absorbing fluorophore by a more efficient one, which has, up to now, only been scarcely investigated.<sup>3</sup> This is likely due to the shortage of low-absorbing fluorophores, which implies that the transition responsible of the fluorescence is a forbidden or weakly allowed one. Actually, to the best of our knowledge, there are only two examples of low absorption fluorophores in the visible range, biacetyls,<sup>4</sup> and tetrazines<sup>5</sup> (see below). However, this remarkable case could lead to particularly interesting applications, like fluorescence emission from nearly transparent solutions or materials.<sup>6</sup> Another remarkable feature is that fluorescence coming from quasi-forbidden transitions has often a long life-time, which is especially interesting for fluorescence sensing, because it would leave the necessary time for the receptor/analyte interaction. Unfortunately, the sensing efficiency is often hampered by the low absorption coefficient. This problem can typically be overcome using a dyad. This is for example true for the biacetyl family since all its members have an extremely low absorption coefficient ( $\epsilon \approx 10\text{--}20 \text{ L mol}^{-1} \text{ cm}^{-1}$ ). However, they can be

activated through energy transfer and this has been extensively studied by Speiser *et al.* These authors nevertheless showed that on many occasions, energy transfer is not complete (may be due to the too low  $\epsilon$  value).

We have recently shown that *s*-tetrazines substituted with heteroatoms also display unique fluorescence properties, based on the very same process that biacetyls (the fluorescence stems from a  $n\text{--}\pi^*$  transition)<sup>5b</sup> featuring among other characteristics a very long lifetime (over 100 ns). Besides, the highly oxidizing character of their excited state makes them especially attractive for sensing electron rich pollutants. Although they absorb light more efficiently than biacetyls, unfortunately, and for a related reason, they still display a relatively low  $\epsilon$  in the 500–1000  $\text{L mol}^{-1} \text{ cm}^{-1}$  range<sup>7</sup> which limits the brilliance of these molecules. An attracting development to overcome this drawback was thus to prepare chloroalkoxytetrazines linked to an appropriate strongly absorbing chromophore which is able to absorb light with a much higher efficiency, and transfer its energy to the fluorescent tetrazine. As explained above, and as noticed before by other authors for different chromophores<sup>8</sup> this could lead to a much improved brilliance for the molecule through light harvesting,<sup>9</sup> and thus improved efficiency of any device using this family of molecules. However, the partner chromophore of the tetrazine has to be chosen carefully, because not only the absorption bands have to show some overlap, as usual when energy transfer is envisaged, but also the partner has to be devoid of, even weak, reducing properties, since the excited tetrazine is a very good electron acceptor.

We describe here the preparation of a dyad made of a chloroalkoxytetrazine linked to a naphthalimide, *N*-(2-(6-chloro-*s*-tetrazin-3-yloxy)ethyl)-naphthalimide (that will be designed later as NITZ, Fig. 1). Both partners in the dyad are electro-deficient (the only available report states that the oxidation potential of naphthalimide is higher than +2 V).<sup>10</sup> This ensures that no electron transfer can take place between

<sup>a</sup> PPSM, ENS Cachan, CNRS, UniverSud, 61 av President Wilson, F-94230 Cachan, France. E-mail: audebert@ppsm.ens-cachan.fr; Fax: +33 1 47 40 24 54; Tel: +33 1 47 40 53 39

<sup>b</sup> East China Normal University, Department of Chemistry, Shanghai, 200062, China

† Electronic supplementary information (ESI) available: Voltammogram of NITZ and NMR spectra of compounds. See DOI: 10.1039/c1nj20100j



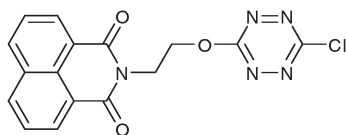


Fig. 1 Formula of NITZ.

the excited state of the tetrazine and the naphthalimide, since the redox potential of the former has been estimated between 1.2 V and 1.4 V, based on the optical gap.<sup>5a</sup> The photochemical behaviour of this new original molecule, along with the demonstration of its improved brilliance (about 10 times the one of a standard tetrazine) is presented along with its electrochemical properties. Also, we show that the compound can be inserted into a polymer and lead to a transparent and yellow fluorescent object, a unique feature that should find application in the realization of decorative objects.

## Experimental

### Materials and methods

All reagents were purchased from Sigma-Aldrich or Fluka and used as received. All solvents were obtained from Carlo-Erba. Synthesis grade ones have been dried prior to use according to standard literature procedures. All reactions were carried out under an inert argon atmosphere. Photophysical and electrochemical studies have been done in spectroscopic grade solvents. Solution NMR spectroscopy was performed on a Bruker AMX 500 MHz instrument. Mass spectrometric analyses were carried out on an Agilent 5973N apparatus. Dichloro-*s*-tetrazine was prepared as previously described.<sup>5b</sup>

### Synthesis

**Synthesis of *N*-(2-hydroxyethyl)-1,8-naphthalimide.**<sup>11</sup> 1,8-Naphthalimide (0.2g, 1 mmol) was reacted with 2-bromoethanol (0.125g, 1 mmol) in dimethylformamide (DMF, 15 ml) in the presence of potassium carbonate for 10 h (previous workers used acetonitrile but in our hands the yields were unsatisfactory). Then the resulting solution was poured in water (10 ml) and extracted with ethyl acetate; the product was purified by chromatography on silica gel using dichloromethane (DCM) as an eluant to give *N*-(2-hydroxyethyl)-1,8-naphthalimide (yield: 73%). <sup>1</sup>H NMR (400 MHz, CDCl<sub>3</sub>, ppm): 2.36 (t, 1H, *J* = 5.5 Hz, OH), 3.98 (dt, 2H, *J*<sub>1</sub> = 5.5 Hz, *J*<sub>2</sub> = 5 Hz, CH<sub>2</sub>-OH), 4.47 (t, 2H, *J* = 5 Hz, CH<sub>2</sub>-N), 7.76 (t, 2H, *J* = 7.5 Hz), 8.23 (d, 2H, *J* = 7.5 Hz), 8.62 (d, 2H, *J* = 7.5 Hz).

**Synthesis of NITZ.** The reaction of dichloro-*s*-tetrazine and *N*-(2-hydroxyethyl)-1,8-naphthalimide was conducted under previously described standard conditions<sup>12</sup> (1 eq. dichloro-*s*-tetrazine, 1 eq. alcohol, 2 eq. collidine in DCM, RT, 2 h) to give NITZ in 56% yield. <sup>1</sup>H NMR (400 MHz, CDCl<sub>3</sub>, ppm): 4.75 (t, 2H, *J* = 5 Hz), 5.06 (t, 2H, *J* = 5 Hz), 7.75 (t, 2H, *J* = 7.5 Hz), 8.23 (d, 2H, *J* = 7.5 Hz), 8.56 (d, 2H, *J* = 7.5 Hz). <sup>13</sup>C NMR (100 MHz, CDCl<sub>3</sub>, ppm): 38.1 (CH<sub>2</sub>-O), 67.6 (CH<sub>2</sub>-N), 122.3, 127.1, 128.9, 131.8, 132.3, 134.5 (naphthalene core), 163.7, 164.5, 166.7 (C=O and tetrazine). High-res ESI MS (positive ion): 355, 357 *m/z* (M<sup>+</sup>).

### Electrochemistry

Electrochemical studies were performed using DCM as a solvent and *N,N,N,N*-tetrabutylammonium hexafluorophosphate (TBAFP) as the supporting electrolyte. The substrate concentration was *ca.* 5 mM. A 1 mm diameter Pt or glassy carbon electrode was used as the working electrode, along with a Ag<sup>+</sup>/Ag (10<sup>-2</sup> M) reference electrode and a Pt wire counter electrode. The cell was connected to a CH Instruments 600B potentiostat monitored by a PC computer. The reference electrode was checked *vs.* ferrocene as recommended by IUPAC. In our case,  $E^0(\text{Fc}^+/\text{Fc}) = 0.097$  V. All solutions were degassed by argon bubbling prior to each experiment.

### Photophysical measurements

**Steady-state spectroscopy.** All the spectroscopic experiments were carried out in DCM and at concentrations *ca.* 10 μmol L<sup>-1</sup> for absorption spectra and *ca.* 1 μmol L<sup>-1</sup> for fluorescence spectra. UV-vis absorption spectra were recorded on a Varian Cary 500 spectrophotometer. Fluorescence emission and excitation spectra were measured on a SPEX fluorolog-3 (Horiba-Jobin-Yvon). For emission fluorescence spectra, the excitation wavelengths were set equal to the maximum of the corresponding absorption spectra. Only dilute solutions with an absorbance below 0.1 at the excitation wavelength λ<sub>ex</sub> were used. For the determination of the relative fluorescence quantum yields (φ<sub>F</sub>), sulforhodamine 101 in ethanol (φ<sub>F</sub> = 0.9) was used as a fluorescence standard.

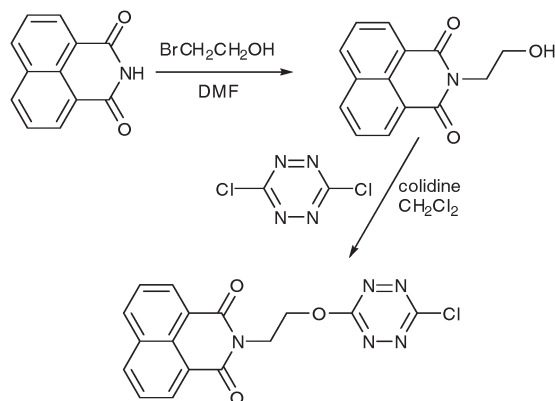
**Time-resolved spectroscopy.** The fluorescence decay curves were obtained with a time-correlated single-photon-counting method using a titanium-sapphire laser (82 MHz, repetition rate lowered to 4 MHz thanks to a pulse-peaker, 1 ps pulse width, a doubling crystal is used to reach 495 and 355 nm excitations) pumped by an argon ion laser. Data were analyzed by a nonlinear least-squares method (Levenberg-Marquardt algorithm) with the aid of Globals software (Globals Unlimited, University of Illinois at Urbana-Champaign, Laboratory of Fluorescence Dynamics). Pulse deconvolution was performed from the time profile of the exciting pulse recorded under the same conditions by using a Ludox solution. In order to estimate the quality of the fit, the weighted residuals were calculated.

### Results and discussion

The following synthetic route (Scheme 1) was used for the preparation of NITZ.

The synthesis is relatively straightforward and allows the preparation of appreciable quantities of compound if needed. We have performed the spectroscopic and electrochemical study of both *N*-(2-hydroxyethyl)-1,8-naphthalimide and NITZ in order to evaluate the properties of the imide alone, and further to be able to analyze the energy transfer in the bichromophoric NITZ. Table 1 gathers the physicochemical characteristics of *N*-(2-hydroxyethyl)-1,8-naphthalimide and NITZ, in the latter case focusing, respectively, on the imide and the tetrazine characteristics.

Regarding absorption and fluorescence, the *N*-(2-hydroxyethyl)-1,8-naphthalimide behaves like a standard naphthalimide,



Scheme 1 Synthesis of NITZ.

as shown in Fig. 2.<sup>10,13</sup> It should be noted that the fluorescence yields are usually not very high with this type of compounds. However, the situation with NITZ is more interesting. The absorption is very close to the sum of the contributions from the imide and the tetrazine behaving as independent chromophores (Fig. 2, left). NITZ when excited at 517 nm displays a classical fluorescence spectrum ( $\lambda_{\text{max}} = 567$  nm) characteristic of all chloroalkoxytetrazines associated with a long fluorescence lifetime and a relatively high quantum yield. The electrochemistry data also show that the reduction potentials are in the same range, so that, as expected electron transfer is not possible upon photochemical excitation.

However when the excitation is set at 355 nm where the naphthalimide absorbs almost exclusively, the NITZ fluorescence spectrum (Fig. 3) shows that the intrinsic fluorescence of

the imide moiety has almost disappeared, at the expense of the one of the tetrazines, evidencing the occurrence of energy transfer between the two chromophores. We have quantified the efficiency of the energy transfer, on the basis of the data reported in Table 1. On the assumption that all the fluorescence lost by the donor is transferred to the acceptor, the efficiency of the energy transfer is calculated to be:<sup>9</sup>

$$\phi_{\text{ET}} = 1 - \frac{\phi_{\text{donor}}}{\phi_{\text{donor}}^0} = 1 - \frac{0.003}{0.061} = 0.95$$

This shows that the energy transfer is quite efficient. Molecular modelization shows that the average distance between the imide donor and the tetrazine ring acceptor is about 8.5 Å. The spectral overlap between the fluorescence of the donor

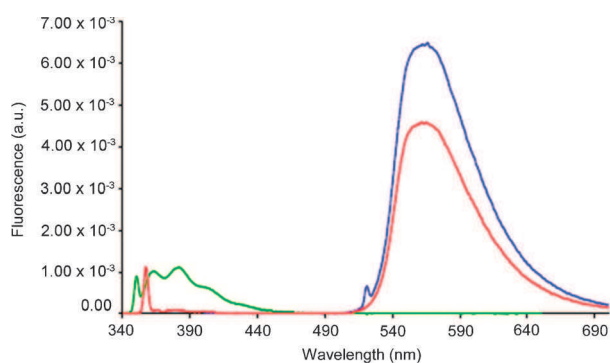


Fig. 3 Fluorescence spectra of *N*-(2-hydroxyethyl)-1,8-naphthalimide (green), NITZ with  $\lambda_{\text{ex}} = 518$  nm (blue) and NITZ with  $\lambda_{\text{ex}} = 355$  nm (red).

Table 1 Photophysical and electrochemical characteristics of compounds in dichloromethane

Compound	$\lambda_{\text{max}}/\text{nm}$	$\epsilon/\text{L mol}^{-1} \text{cm}^{-1}$	$\lambda_{\text{em}}/\text{nm}$	$\phi_{\text{F}}$	$\epsilon_{\lambda(\text{ex})} \times \phi_{\text{F}}$	$\tau_{\text{F}}/\text{ns}$	$E_{\text{red}}^0/\text{V}$
<i>N</i> -(2-Hydroxyethyl)-1,8-naphthalimide	335	8700	363 382 402 <sup>a</sup>	0.06 <sup>a</sup>	522	0.37 <sup>c</sup>	-1.70
NITZ (tetrazine data)	517	400	562 <sup>b</sup>	0.32 <sup>b</sup>	130	158 <sup>c,d</sup>	-0.86
NITZ (imide data)	334	9100 (5000 at 355 nm)	378 400 <sup>c</sup>	0.003 <sup>c</sup>	12	0.03 <sup>c</sup>	-1.70

<sup>a</sup>  $\lambda_{\text{ex}} = 350$  nm. <sup>b</sup>  $\lambda_{\text{ex}} = 517$  nm. <sup>c</sup>  $\lambda_{\text{ex}} = 355$  nm. <sup>d</sup>  $\lambda_{\text{ex}} = 495$  nm.

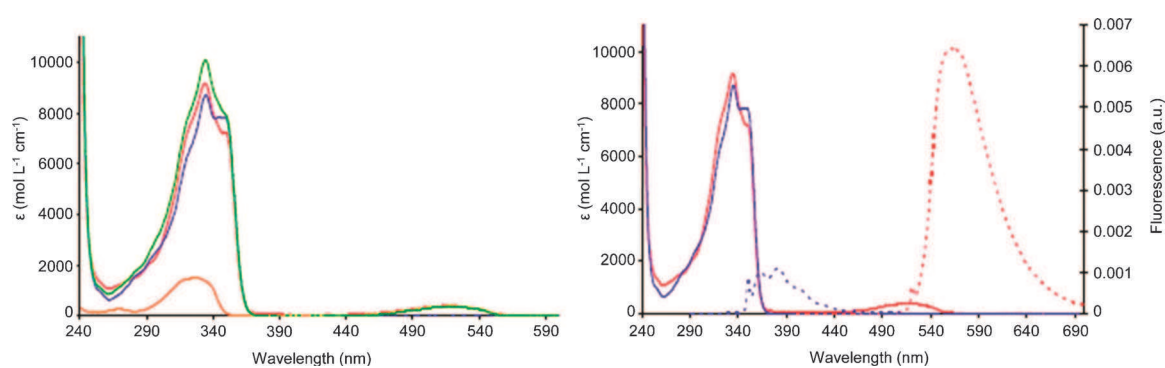
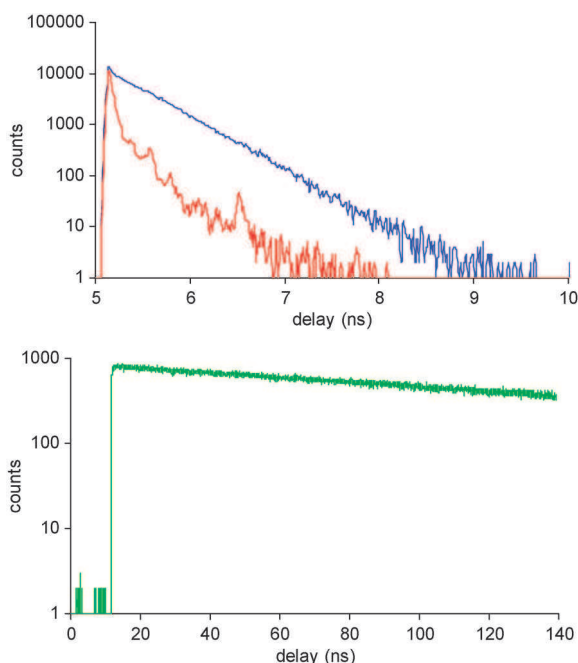


Fig. 2 Left: absorption spectra of *N*-(2-hydroxyethyl)-1,8-naphthalimide (blue), chloromethoxy-*s*-tetrazine (orange), NITZ (red) and the sum of *N*-(2-hydroxyethyl)-1,8-naphthalimide and chloromethoxy-*s*-tetrazine (green); right: absorption (full lines) and fluorescence (dotted lines) spectra of *N*-(2-hydroxyethyl)-1,8-naphthalimide (blue) and NITZ (red). The fluorescence of NITZ was obtained by direct excitation of the *s*-tetrazine ( $\lambda_{\text{ex}} = 517$  nm).



**Fig. 4** Fluorescence decay profiles upon excitation at 355 nm. Up: *N*-(2-hydroxyethyl)-1,8-naphthalimide (blue) and NITZ (red) for  $\lambda_{\text{em}} = 365$  nm; down: NITZ (green) for  $\lambda_{\text{em}} = 562$  nm.

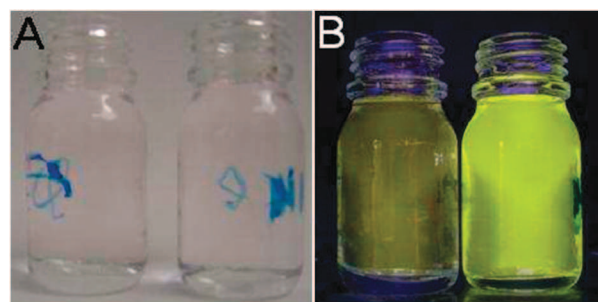
and the absorption of the acceptor being small a short Förster radius of  $R = 9.3 \text{ \AA}$  is calculated, and therefore the efficiency of the energy transfer should be only around 63%. The discrepancy between the calculated and the experimental value therefore inclines to think that the energy transfer mechanism would rather be of the Dexter type or a mixed one.

In order to refine our investigations, we recorded the fluorescence decay of the *N*-(2-hydroxyethyl)-1,8-naphthalimide and NITZ. The results (Fig. 4) give a fluorescence lifetime for the naphthalimide of 0.37 ns in the first case and 0.03 in the second, and therefore it is possible to calculate the efficiency and the rate of the energy transfer:

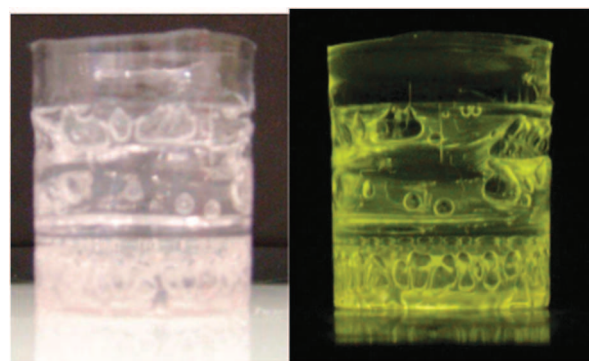
$$\begin{aligned} \phi_{\text{ET}} &= 1 - \frac{\tau_{\text{donor}}}{\tau_{\text{donor}}^0} = 1 - \frac{0.03}{0.37} = 0.92 \quad k_{\text{ET}} = \frac{1}{\tau_{\text{donor}}} - \frac{1}{\tau_{\text{donor}}^0} \\ &= 3.06 \times 10^{10} \text{ s}^{-1} \end{aligned}$$

which is two orders of magnitude higher than the radiative lifetime of the *N*-(2-hydroxyethyl)-1,8-naphthalimide ( $k_{\text{R}} = 1.65 \times 10^8 \text{ s}^{-1}$ ). It is noteworthy that the two calculated values of  $\phi_{\text{ET}}$  are in good agreement. On the other hand, the tetrazine fluorescence decay is more complex and displays a rising time. The decay could be fitted by a bi-exponential function giving a rising time of 0.06 ns similar to the fluorescence lifetime of the naphthalimide in NITZ and a decay of 158 ns typical of the tetrazine.

Finally, we have performed visual evaluation of the brilliance of our molecule, by simply comparing the brilliance of a  $5 \times 10^{-6} \text{ M}$  solution of NITZ and the one of a solution of 3-(adamant-1-ylmethoxy)-6-chloro-*s*-tetrazine, which comprises the same tetrazine emitter but without the presence of a donor. Fig. 5A shows the pictures of both solutions in white light; at these concentrations the solutions are almost colourless.



**Fig. 5** Pictures of two  $5 \times 10^{-6} \text{ M}$  solutions of, right, 3-(adamant-1-ylmethoxy)-6-chloro-*s*-tetrazine and, left, NITZ, both in (A) standard white light and (B) 365 nm UV light.



**Fig. 6** Pictures of a block of polystyrene incorporating NITZ under white (left) and UV (right) light. The dye concentration in the polymer was *ca.*  $10^{-5} \text{ M}$ .

Fig. 5B displays the fluorescence of the solution, excited at *ca.* 365 nm. It is clear that, due to the efficiency of the imide absorbance and the energy transfer, the brilliance of the NITZ solution is much higher than the one of the standard tetrazines. The quantitative evaluation of the brilliance (column  $\varepsilon_{\lambda(\text{ex})} \times \phi_{\text{F}}$  in Table 1) shows that it is 7.5 times higher when NITZ is excited at 355 nm (selective of the imide moiety) rather than 517 nm (selective of the tetrazine moiety) as is evidenced in Fig. 5.

All tetrazines, including NITZ are soluble in most organic polymers because of their moderate molecular weight. Fig. 6 shows the pictures of a block of polystyrene into which NITZ has been dispersed at a  $10^{-5} \text{ M}$  concentration. Such a low amount of dye gives a perfectly transparent object under ambient light while it exhibits a nice yellow fluorescence when exposed to UV light. In addition, the picture has been taken three weeks after the object fabrication, which demonstrates that the fluorophore does not degrade in normal conditions.

## Conclusions

We have presented a new fluorescent dyad made of a naphthalimide absorber and a tetrazine emitter. The fluorescence properties of this new molecule have been studied. The results show that, due to the efficiency of the energy transfer, the dyad is much more brilliant than a simple tetrazine irradiated in the same conditions. Application of this new molecule to fluorescent sensors is ongoing.

## Notes and references

- 1 (a) G. Weber, *Nature*, 1957, **180**, 1409; (b) M. Sirish, R. Kache and B. G. Maiya, *J. Photochem. Photobiol., A*, 1996, **93**, 129; (c) G. Hinze, M. Haase, F. Nolde, K. Mullen and Th. Basché, *J. Phys. Chem. A*, 2009, **109**, 6725; (d) Ch. Scharf, K. Peter, P. Bauer, Ch. Jung, M. Thelakkat and J. Köhler, *Chem. Phys.*, 2006, **328**, 403; (e) S. Diring, R. Ziessel, f. Barigelletti, A. Barbieri and B. Ventura, *Chem.–Eur. J.*, 2010, **16**, 9226.
- 2 (a) D. Margulies, G. Melman and A. Shanzler, *J. Am. Chem. Soc.*, 2006, **128**, 4871; (b) O. Kunetz, H. Salman, Y. Eichen, F. Remacle, R. D. Levine and S. Speiser, *J. Photochem. Photobiol., A*, 2007, **191**, 176; (c) O. Kunetz, D. Davis, H. Salman, Y. Eichen and S. Speiser, *J. Phys. Chem. C*, 2007, **191**, 176; (d) J. M. Tour, *Acc. Chem. Res.*, 2000, **33**, 79.
- 3 S. Speiser, *Chem. Rev.*, 1996, **96**, 1953.
- 4 (a) S. Speiser, R. Kataro, S. Welner and M. B. Rubin, *Chem. Phys. Lett.*, 1979, **61**, 199; (b) D. Getz, A. Ron, M. B. Rubin and S. Speiser, *J. Phys. Chem.*, 1980, **84**, 768; (c) S. Hassoon, S. Lustig, M. B. Rubin and S. Speiser, *J. Phys. Chem.*, 1984, **88**, 6367.
- 5 (a) P. Audebert, F. Miomandre, G. Clavier, M. C. Vernieres, S. Badré and R. Méallet-Renault, *Chem.–Eur. J.*, 2005, **11**, 5667; (b) Y.-H. Gong, F. Miomandre, R. Méallet-Renault, S. Badré, L. Galmiche, J. Tang, P. Audebert and G. Clavier, *Eur. J. Org. Chem.*, 2009, 6121; (c) P. Audebert and G. Clavier, *Chem. Rev.*, 2010, **110**, 3299.
- 6 This situation can only be achieved in the rare case when a fluorophore can interconvert between two structures after photon absorption. For example it has been shown through a very fast proton transfer in the remarkable paper: S. Park, J. E. Kwon, S. H. Kim, J. Seo, K. Chung, S.-Y. Park, D.-J. Jang, B. M. Medina, J. Gierschner and S. Y. Park, *J. Am. Chem. Soc.*, 2009, **131**, 14043.
- 7 Y.-H. Gong, P. Audebert, G. Clavier, F. Miomandre, J. Tang, S. Badré, R. Méallet-Renault and E. Naidus, *New J. Chem.*, 2008, **32**, 1235.
- 8 S. E. Weber, *Chem. Rev.*, 1990, **90**, 1469.
- 9 (a) J. E. Guillet, *Polymer Photophysics and Photochemistry*, Cambridge Univ. Press, Cambridge, 1985; (b) B. Valeur, *Molecular Fluorescence: Principles and Applications*, Wiley-VCH, Weinheim, 2001.
- 10 B. Ramachandram, G. Saroja, N. B. Sankaran and A. Samanta, *J. Phys. Chem. B*, 2000, **104**, 11824.
- 11 L. D. Van Vliet, T. Ellis, P. J. Foley, L. Liu, F. M. Pfeffer, R. A. Russell, R. N. Warrener, F. Hollfelder and M. J. Waring, *J. Med. Chem.*, 2007, **50**, 2326.
- 12 Y.-H. Gong, P. Audebert, G. Clavier, F. Miomandre, J. Tang, S. Badré, R. Méallet-Renault and E. Naidus, *New J. Chem.*, 2008, **32**, 1235.
- 13 (a) A. Demeter, T. Berces, L. Biczok, V. Wintgens, P. Valat and J. Kossanyi, *J. Phys. Chem.*, 1996, **100**, 2001; (b) U. C. Yoon, S. W. Oh, S. M. Lee, S. J. Cho, J. Gamlin and P. S. Mariano, *J. Org. Chem.*, 1999, **64**, 4411.

# New Tetrazines Functionalized with Electrochemically and Optically Active Groups: Electrochemical and Photoluminescence Properties.

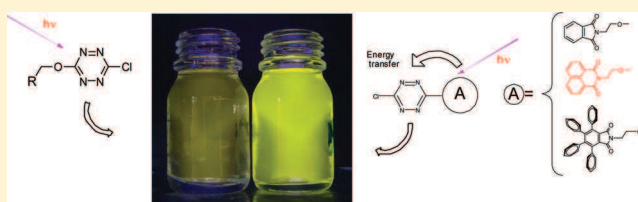
Qing Zhou,<sup>†,‡</sup> Pierre Audebert,<sup>\*,†,‡</sup> Gilles Clavier,<sup>†</sup> Rachel Méallet-Renault,<sup>†</sup> Fabien Miomandre,<sup>†</sup> Zara Shaikat,<sup>†</sup> Thanh-Truc Vu,<sup>†</sup> and Jie Tang<sup>‡</sup>

<sup>†</sup>PPSM, ENS Cachan, CNRS, UniverSud, 61 av President Wilson, F-94230 CACHAN, France

<sup>‡</sup>East China Normal University, Department of Chemistry, Shanghai, 200062, China

**S** Supporting Information

**ABSTRACT:** Original new fluorescent and electroactive compounds have been prepared, where the fluorescent moiety is a chloroalkoxy-*s*-tetrazine. Besides the tetrazine, several of these compounds possess a second active group, electroactive or able to absorb light at a lower wavelength. The electrochemical properties and photophysical properties of these bichromophoric compounds have been investigated, especially focusing on the occurrence of energy or electron transfer to the tetrazine. In one case, where the primary absorber is a naphthalimide, a quasi-complete energy transfer, followed by the tetrazine fluorescence, is observed. This allows the preparation of remarkable transparent solutions displaying a yellow fluorescence.



## I. INTRODUCTION

*s*-Tetrazines chemistry has been known for more than one century,<sup>1</sup> and their photophysical<sup>2</sup> and electrochemical<sup>3</sup> properties have been briefly recognized in the past. However, considering the recent interest in conjugated molecules and active organic materials,<sup>4</sup> the tetrazine block has been envisaged only very recently. We have shown that the *s*-tetrazine building block is indeed a very promising and fascinating one.<sup>5</sup> Very recently, the work of Ding et al. has also emphasized their remarkable potential in the field of conjugated materials for organic electronics.<sup>6</sup> *s*-Tetrazines are electroactive heterocycles, having a very high electron affinity and therefore reducible at high potentials, through a one- and sometimes two-electron process.<sup>5b,c</sup> Consequently, they have a low-lying  $\pi^*$  orbital, with a low-energy  $n\text{-}\pi^*$  transition in the visible range (this transition should normally be forbidden, but is allowed in the case of tetrazines albeit with a low absorption coefficient), which makes them colored and sometimes fluorescent. This fluorescence can be clearly perceived by the naked eye. In particular, *s*-tetrazines substituted with some heteroatoms display interesting fluorescence properties<sup>7</sup> featuring among other characteristics a very long lifetime (>100 ns), which make them especially attractive for sensing applications. For instance, it would allow more time for the receptor/analyte interaction. Furthermore, the excited state of the tetrazine has a strongly oxidant character that provides a lot of opportunities for fluorescence quenching through electron transfer.<sup>8</sup> Indeed, a slight change in lifetime would be easier to detect with a fluorophore having a long luminescence lifetime, compared with a short one (a few nanoseconds). Unfortunately, because the absorbance band responsible for fluorescence of the tetrazine is a weak transition, it has a low  $\epsilon$  (in the

500–1000 mol<sup>-1</sup> L cm<sup>-1</sup> range), which limits the brilliance of these molecules. The chemistry of *s*-tetrazines has been recently reviewed by Saracoglu and us.<sup>9</sup>

We wished to examine the influence of functional groups attached to a fluorescent tetrazine, like, for example, an aromatic group, or, more interestingly, another chromophore able to absorb light and possibly transfer the energy to the tetrazine fluorophore. This could lead to an improved brilliance for the molecule and therefore improved efficiency of any device using this family of molecules. However, the partner chromophore of the tetrazine may also have the possibility to exchange charge instead of energy because the tetrazine is a good electron acceptor and in such a case quenches the fluorescence instead of exalting it. Therefore, the redox potential of the partner chromophore has to be carefully chosen so as to avoid this situation.

Activation of low  $\epsilon$  fluorophores has already been investigated in a few cases,<sup>10</sup> and it includes only one other example of  $n\text{-}\pi^*$  fluorophore, the biacetyl family, which has been extensively investigated by Speiser et al.<sup>11</sup> Actually, they had some success in their demarche, but the rather low  $\epsilon$  of this class of compounds, however, apparently limited the efficiency for the energy transfer. The low yet clearly larger  $\epsilon$  of the tetrazine family likely opens a more promising field for tetrazine activation through chromophore “antennas”.

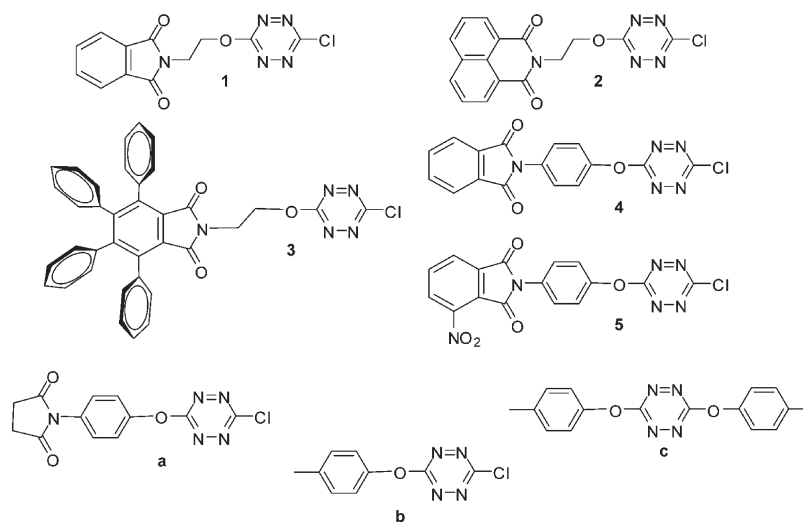
We describe here the preparation and the properties of several new tetrazines, linked to various functional groups or chromophores.

**Received:** May 26, 2011

**Revised:** June 29, 2011

**Published:** September 20, 2011

Scheme 1. Chart of Prepared Tetrazines



In most cases, we have chosen electrodeficient imide-type chromophores, which literature describes as nonoxidizable compounds<sup>12</sup> and present the best chance to forbid the charge transfer. The photochemical and electrochemical behaviors of these new original molecules are detailed, and we show that in two cases an increase in the molecule brilliance has been reached compared with a parent unmodified chloro-(1-adamantanemethoxy)-tetrazine.

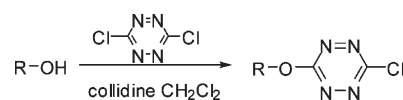
## II. EXPERIMENTAL SECTION

**1. Synthesis.** The synthesis of the compound has been made through existing procedures or modifications and is fully detailed in the Supporting Information.

**2. Electrochemical Studies.** Electrochemical studies were performed using dichloromethane (DCM) (SDS, anhydrous for analysis) as a solvent, with *N,N,N,N*-tetrabutylammonium hexafluorophosphate (TBAFP) (Fluka, puriss.) as the supporting electrolyte. The substrate concentration was ca. 5 mM. A homemade 1 mm diameter Pt or glassy carbon electrode was used as the working electrode, along with a  $\text{Ag}^+/\text{Ag}$  ( $10^{-2}$  M) reference electrode and a Pt wire counter electrode. The cell was connected to a CH Instruments 600B potentiostat monitored by a PC computer. The reference electrode was checked versus ferrocene as recommended by IUPAC. In our case,  $E^\circ(\text{Fc}^+/\text{Fc}) = 0.097$  V. All solutions were degassed by argon bubbling prior to each experiment.

**3. Photophysical Measurements.** *Steady-State Spectroscopy.* All spectroscopic experiments were carried out in DCM (spectroscopic grade from SDS) and at concentrations ca.  $10 \mu\text{mol L}^{-1}$  for absorption spectra and ca.  $1 \mu\text{mol.L}^{-1}$  for fluorescence spectra. UV–vis absorption spectra were recorded on a Varian Cary 500 spectrophotometer. Fluorescence emission and excitation spectra were measured on a SPEX fluorolog-3 (Horiba–Jobin–Yvon). For emission fluorescence spectra, the excitation wavelengths were set equal to the maximum of the corresponding absorption spectra. For the determination of the relative fluorescence quantum yields ( $\Phi_f$ ), only dilute solutions with an absorbance below 0.1 at the excitation wavelength  $\lambda_{\text{ex}}$  were used, sulforhodamine 101 in ethanol ( $\Phi_f = 0.9$ )

Scheme 2. General Synthetic Scheme for All Tetrazines (except c)



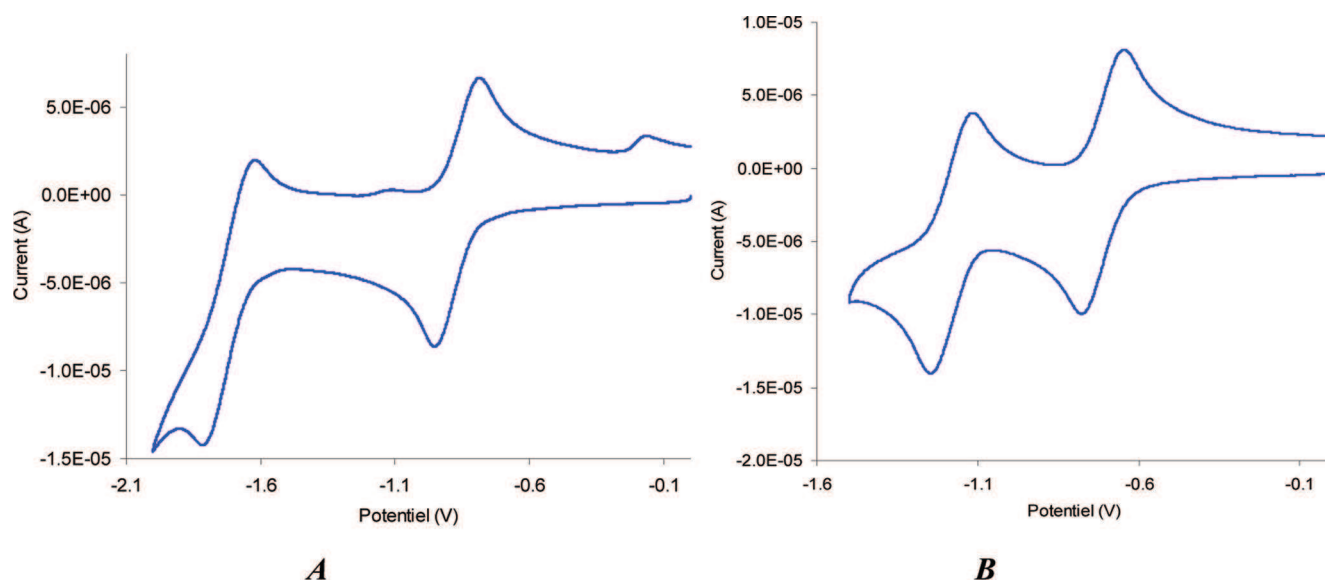
*Time-Resolved Spectroscopy.* The fluorescence decay curves were obtained with a time-correlated single-photon-counting method using a titanium-sapphire laser (82 MHz, repetition rate lowered to 0.8 MHz thanks to a pulse-peaker, 1 ps pulse width, a doubling crystals is used to reach 495 and 355 nm excitations) pumped by an argon ion laser. Data were analyzed by a nonlinear least-squares method (Levenberg–Marquardt algorithm) with the aid of Globals software (Globals Unlimited, University of Illinois at Urbana–Champaign, Laboratory of Fluorescence Dynamics). Pulse deconvolution was performed from the time profile of the exciting pulse recorded under the same conditions by using a Ludox solution. To estimate the quality of the fit, the weighted residuals were calculated. In the case of single photon counting, they are defined as the residuals, that is, the difference between the measured value and the fit, divided by the square root of the fit.  $\chi^2$  is equal to the variance of the weighted residuals. A fit was said to be appropriate for  $\chi^2$  values between 0.8 and 1.2.

## III. RESULTS AND DISCUSSION

**1. Synthesis.** We have prepared and studied the following molecules (Scheme 1).

The following synthetic route (Scheme 2) was used for the preparation of all reported tetrazines.

The synthesis is relatively straightforward with good yields and allows the preparation of appreciable quantities of compound if needed. (Full details of the experimental procedure can be found in refs 5c and 7.) The preparation of alcohols was performed following several already published procedures (Supporting Information) as well as our work.<sup>5,6a,10</sup> In some occasions, experimental procedures have been slightly modified, like, for example, changing acetonitrile to DMF as the synthesis solvent.



**Figure 1.** Cyclic voltammograms of (A) Compound 2 and (B) Compound 5 at 100 mV/s in DCM/TBAFP (pot. vs  $\text{Ag}/10^{-1} \text{ M Ag}^+$ ).

All synthetic procedures and the relevant references have been gathered in the Supporting Information, Part 1, along with a detailed report of all modified procedures as well as the NMR and MS data for all new compounds and some important precursors.

**2. Electrochemical Study.** The electrochemical study of all compounds has been performed, using cyclic voltammetry as a tool, to characterize not only the tetrazine electrochemistry but also the reduction of the functional group, which also displays a reversible behavior in several cases. Figure 1 shows the CV response of both compounds 2 and 5, where the completely reversible behavior of the tetrazine first transfer is followed at lower potentials by another wave, completely or partially reversible. In the case of the nitrophthalimide, the second wave is reversible because of the presence of the nitro group that both considerably raises the reduction potential (>500 mV) and stabilizes the anion radical on the imide moiety. We are therefore in the case of a system with two quite stable and independent anion-radicals on the same molecule, each displaying a perfectly electrochemically reversible behavior, a relatively rare occurrence in organic electrochemistry.

In the case of the naphthalimide derivative 2, the second system is less reversible, and there is a slight increase in the observed current. This is likely to be due to the existence of some overlap between the beginning of the second (sluggish and irreversible) reduction of the tetrazine and the naphthalimide reduction, which occurs at comparable potentials (from previously published data on chloroalkoxytetrazines).<sup>5a,b,6,7</sup> When considering the phthalimide derivative 4, the second reduction is almost irreversible, confirming the trend that the lower the redox potential of the second system the less reversible it behaves.

The redox potentials of all compounds are listed in Table 1. The first redox potential is ascribed to the tetrazine, whereas the second redox couple can always be assigned to the pendant group linked to the tetrazine. It can be noticed that a shift of  $\sim 100$  mV toward more positive potentials occurs for the first redox couple (located on the tetrazine) when the substituent on the tetrazine changes from an alkoxy to a phenoxy: the donor effect of the oxygen on the tetrazine is weakened by the phenyl ring through mesomery.<sup>13</sup> Both electroactive groups behave as independent redox sites in all compounds whatever the spacer.

**Table 1.** Electrochemical Data for Scheme 1 Compounds (pot. vs  $\text{Ag}/10^{-1} \text{ M Ag}^+$ )

compound	1	2	3	4	5	a	b	c
$E_{\text{red1}}^0$ (V)	-0.84	-0.86	-0.84	-0.74	-0.74	-0.74	-0.79	-0.95
$E_{\text{red2}}^0$ (V)	-1.85	-1.70	-1.80	-1.74	-1.19	<sup>a</sup>	<sup>a</sup>	<sup>a</sup>

<sup>a</sup> No second wave observable before  $-2$  V, although an increase in the background current is sometimes noticeable after  $-1.9$  V and should probably be ascribed to the second tetrazine reduction.

Also noticeable is the similar potential values for compounds 1 and 3: the unexpected very little influence on the redox potentials resulting from the five phenyl rings on the phthalimide is probably due to the fact that the phenyl rings are actually perpendicular to the phthalimide and thus do not conjugate with it. (This has been verified by calculation using Gaussian.)

In all cases, no additional wave has been observed below  $-2$  V, although an increase in the background current is sometimes noticeable around  $-1.9$  V and should probably be ascribed to the start of the second tetrazine reduction.

**3. Spectroscopic Studies.** Absorption and fluorescence studies have been performed for all tetrazines, with tetrazines a, b, and c standing for references because they do not bear pendant optically (nor electrochemically) active groups. The complete figures for each compound can be found in the Supporting Information, Part B.

The absorption spectra for tetrazines 1–5 are given in Figure 2. It is clear on all spectra that when one compares any of them to the (generic) 3-(adamant-1-ylmethoxy)-6-chloro-*s*-tetrazine spectra, all spectra from molecules 1–5 display additional bands in the UV region ascribable to the absorption of the imide group. In some cases, the imide UV band is, however, not much more intense than the band resulting of the  $\pi-\pi^*$  transition of the tetrazine at 330 nm. The  $n-\pi^*$  transition of the tetrazine is always present, with a similar intensity with all compounds, as could be expected.

The fluorescence spectra (Figure 3) show, however, that all tetrazines are fluorescent upon excitation in the visible range,

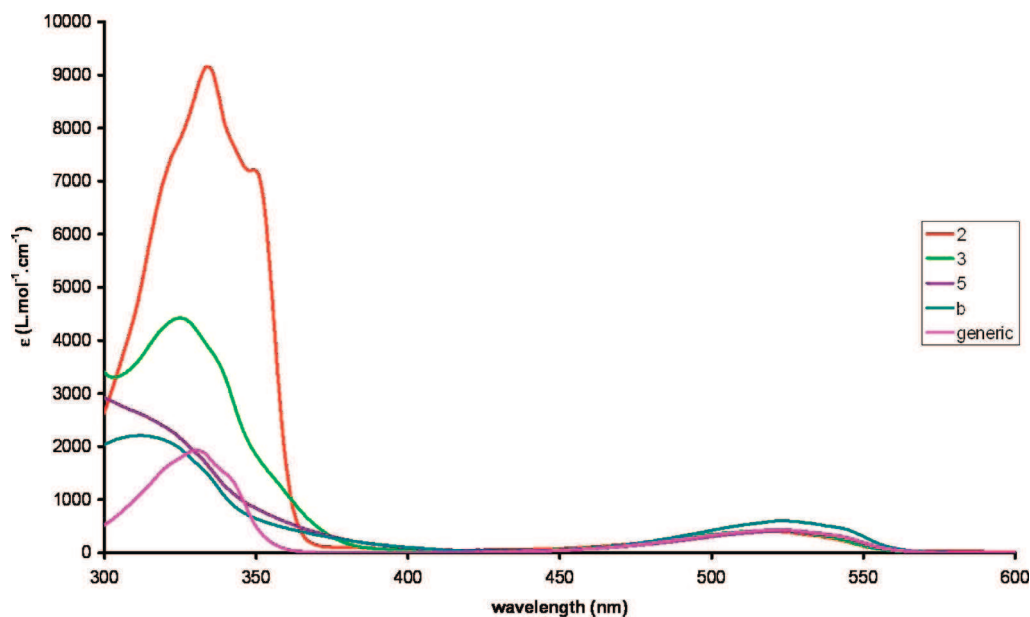


Figure 2. Absorption spectra of all compounds in Scheme 1 plus the generic 3-(adamant-1-ylmethoxy)-6-chloro-*s*-tetrazine.

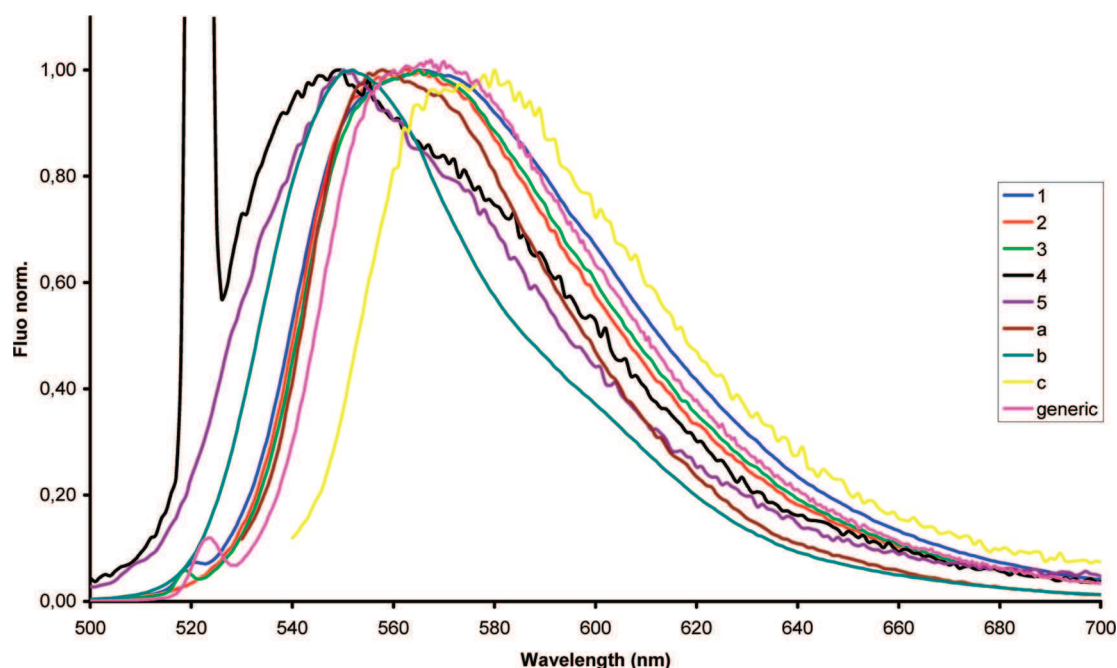


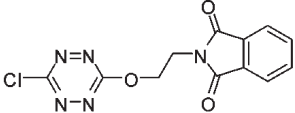
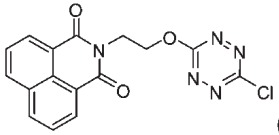
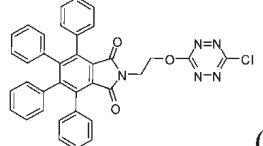
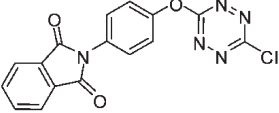
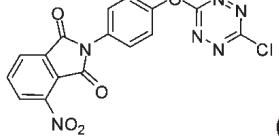
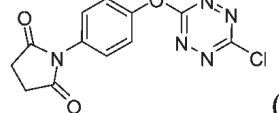
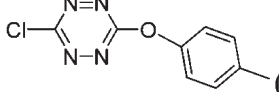
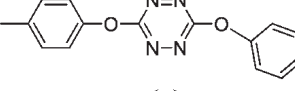
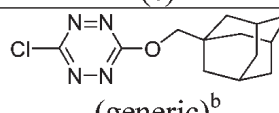
Figure 3. Normalized fluorescence spectra of all compounds in Scheme 1 plus the generic 3-(adamant-1-ylmethoxy)-6-chloro-*s*-tetrazine, focusing on the tetrazine response.

albeit with very different features. Table 2 gathers the spectroscopic characteristics of all tetrazines prepared, based on the tetrazine  $n-\pi^*$  absorption band in the visible region. (The formulas of the compounds have been added in the Table along with their corresponding numbers for easier reading.) This includes the tetrazines a–c, which bear no special group but were studied for comparison purposes because they have different linkers. We have also added to the Table the characteristics of the generic chloro(1-adamantanemethoxy)tetrazine, which are typical of any chloroalkoxytetrazine bearing only innocent alkyl groups, regardless of their steric hindrance.<sup>14</sup>

Most of the tetrazines have their fluorescence at a wavelength identical to the generic 3-(adamant-1-ylmethoxy)-6-chloro-*s*-tetrazine.<sup>6</sup> Several among the ones described here also have identical absorption and emission maxima (around 520 and 570 nm, respectively). Looking into detail, we shall compare compounds **b** and **c** with a previously published chloromethoxytetrazine.<sup>5c</sup> As already observed, a 10 nm increase in absorption band position is observed on going from chloromethoxytetrazine, to **b**, then to **c** compound. Adding the donor phenoxy group induces a 10 nm bathochromic shift. Compared with the methoxy group (5 nm), the bathochromic shift is stronger with the phenoxy (10 nm),



Table 2. Spectroscopic Characteristics of All Compounds Prepared

Molecule/data	$\lambda_{abs}^{max}$ (nm)	$\lambda_{fluo}^{max}$ (nm)	Stokes shift	$\epsilon^a$ (L.mol <sup>-1</sup> .cm <sup>-1</sup> )	$\Phi_{fluo}^a$	$\tau_{fluo}$ (ns)
 (1)	519	565	46	550	0.41	112
 (2)	518	567	49	400	0.32	158
 (3)	519	565	46	800	0.33	113
 (4)	521	549	28	600	0.02	0.3 (98.5%) 1.7 (1.1%) 11.0 (0.4%)
 (5)	522	557	35	400	0.01	2.0 (96.2%) 5.7 (3.8%)
 (a)	522	558	36	450	0.03	2.3 (99.9%) 51.8 (0.1%)
 (b)	524	565	41	600	0.001	0.1 (98.4%) 2.2 (1.4%) 21.0 (0.2%)
 (c)	534	580	46	550	0.007	2.3 (99%) 20.5 (1%)
 (generic) <sup>b</sup>	522	560	38	450	0.38	160

<sup>a</sup>Error 10%. <sup>b</sup>Data from ref 10.

which is in accordance with stronger donating properties. The same tendency is observed for the fluorescence band position (+15 nm bathochromic shift).

One striking feature is the Stokes shift evolution with the nature of the linker between the imide (or naphthalimide) group and the tetrazine core. Indeed, when an ethyl bridge is present (compounds 1–3), a 45–49 nm Stokes shift is measured, whereas when the link is a phenyl moiety, the Stokes shift is decreased to 28 nm (compounds 4–6). This might be due to the less rigid structure in the case of ethyl link compared with phenyl one, where the flexible character may allow a stronger

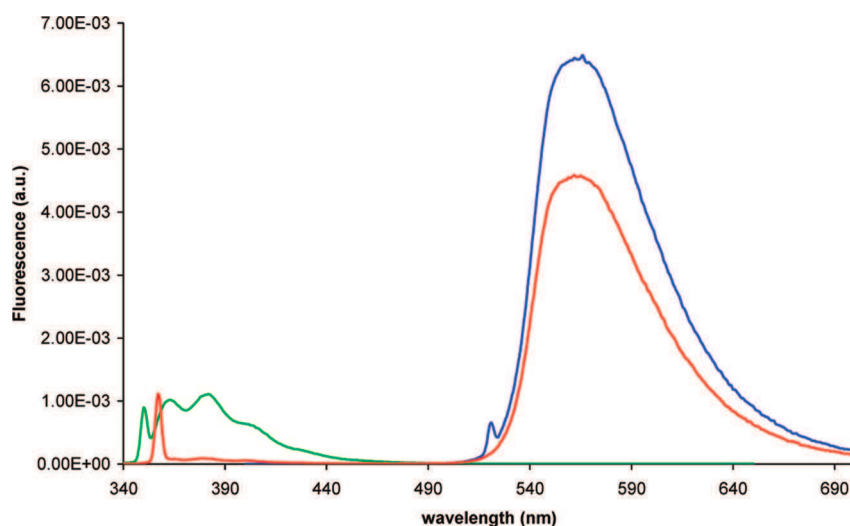
reorganization between the fundamental and excited states (larger Stokes shift).

However, the more striking differences are observed on the fluorescence quantum yields, which happen to be strongly linked to the nature of the spacer between the tetrazine and the imide group. When the spacer is a nonconjugated ethyl group, then the fluorescence of the tetrazine is practically unaffected. (Slight variations from one compound to another can be observed but are within the experimental error.) When the tetrazine is connected to a phenol spacer, not only do the fluorescence yields drop considerably but also the life times become much shorter,

**Table 3.** Detailed Spectroscopic Data for Naphthalimide-Tetrazine **2** and *N*-(2-Hydroxyethyl)-1,8-naphthalimide

molecule/data	$\lambda_{\text{abs}}$ (nm)	$\epsilon$ (L mol <sup>-1</sup> cm <sup>-1</sup> )	$\lambda_{\text{em}}$ (nm)	$\Phi_{\text{fluo}}$	$\epsilon(\lambda_{\text{ex}}) \times \Phi_{\text{fluo}}$	$\tau_{\text{fluo}}$ (ns)
<i>N</i> -(2-hydroxyethyl)-1,8-naphthalimide	335	8700	363, 382, 402 <sup>a</sup>	0.06 <sup>a</sup>	522	0.37 <sup>c</sup>
<b>2</b> (tetrazine data)	517	400	562 <sup>b</sup>	0.32 <sup>b</sup> (0.3 <sup>c</sup> )	200 (1509)	158 <sup>c,d</sup>
<b>2</b> (imide data)	334	9100	378 400 <sup>c</sup>	0.003 <sup>c</sup>	15	0.05 <sup>c</sup>

<sup>a</sup>  $\lambda_{\text{ex}} = 350$  nm. <sup>b</sup>  $\lambda_{\text{ex}} = 517$  nm. <sup>c</sup>  $\lambda_{\text{ex}} = 355$  nm. <sup>d</sup>  $\lambda_{\text{ex}} = 495$  nm.

**Figure 4.** Fluorescence spectra of *N*-(2-hydroxyethyl)-1,8-naphthalimide (green) **2** with  $\lambda_{\text{ex}} = 518$  nm (blue) and **2** with  $\lambda_{\text{ex}} = 355$  nm (red).

with the appearance of multiexponential decays. For comparison, we have prepared the three generic compounds a–c, which all own a phenol linked to the tetrazine ring, and they all display the same features with the appearance of a sharp drop of the fluorescence yields and complex fluorescence decays. This allows us to conclude that fluorescence quenching likely occurs through electron transfer from the electron-rich substituted phenolic moiety to the tetrazine ring and that the presence of an electron-withdrawing group on the para position of the phenyl ring reduces, as expected, the efficiency of the process.

We have also observed the fluorescence characteristics of molecules 1–5 upon illumination at 300 nm into the imide absorption band (at the exception of **2**, where naphthalimide absorption occurs at 350 nm and which was subjected to closer analysis, see below). Tetrazine fluorescence is also observed, but because there is overlap with the  $\pi-\pi^*$  band of the tetrazine and the absorption coefficients have comparable values, it is difficult to estimate the efficiency of the energy transfer. However, in the case of **1**, it is likely, on the basis of the spectra, that some energy absorbed by the imide is transferred to the tetrazine, and the molecule looks more brilliant upon testing with the naked eye. The especially interesting case of molecule **2** has been thoroughly investigated, especially because the much larger absorption coefficient of this molecule was expected to improve the brightness (defined by  $\epsilon\Phi_f$ ) of its fluorescence emission.

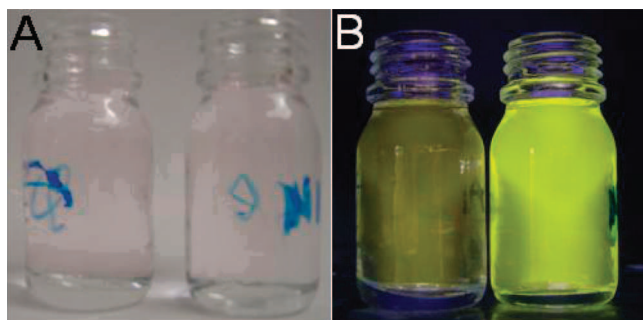
**Photophysical Study of Compound 2.** Indeed, the case of compound **2**, where the naphthalimide absorption band efficiently overlaps the  $\pi-\pi^*$  band of the tetrazine, is the most interesting because the occurrence of energy transfer between the imide and the tetrazine was highly probable. This could

occur, either into the  $\pi-\pi^*$  band of the tetrazine, followed by internal conversion, or also possibly directly into the  $n-\pi^*$  band of the tetrazine, followed by fluorescence.

We have performed the complete spectroscopic study of both the precursor *N*-(2-hydroxyethyl)-1,8-naphthalimide and **2** to evaluate the properties of the imide alone and further to be able to analyze the energy transfer in the bichromophoric compound **2**.<sup>7</sup> Table 3 gathers the spectroscopic characteristics of *N*-(2-hydroxyethyl)-1,8-naphthalimide and **2** and in the case of **2** focusing on the naphthalimide and the tetrazine response, respectively.

Regarding absorption and fluorescence, the *N*-(2-hydroxyethyl)-1,8-naphthalimide behaves like a standard naphthalimide (Supporting Information, Figure 1A). It should be noted that the fluorescence yields are somewhat low with this type of compound. However, the situation with **2** is more interesting. The absorption is close to the sum of the contributions from the imide and the tetrazine behaving as independent chromophores. Also, when **2** is excited at 518 nm, it displays a classical fluorescence spectrum characteristic of all chloroalkoxytetrazines (Supporting Information, Part 2), with an absorption due to the  $n-\pi^*$  band in the visible, associated with a long fluorescence lifetime at 567 nm and a relatively high quantum yield.

The fluorescence spectrum of both *N*-(2-hydroxyethyl)-1,8-naphthalimide and **2** upon excitation at 355 nm is quite more informative. In the first case, the classical fluorescence of *N*-(2-hydroxyethyl)-1,8-naphthalimide (violine) is observed with a low yield. (See Table 3 and Figure 4.) In the second case, almost all recorded fluorescence is emitted by the tetrazine core, with an apparent analogous relative intensity, as compared with the case



**Figure 5.** Picture of two  $5 \times 10^{-6}$  M solutions of, left, 3-(adamant-1-ylmethoxy)-6-chloro-*s*-tetrazine and, right, **2**, both in standard white light (A) and UV light (B).



**Figure 6.** Picture of, left, a solution containing a mixture of concentrated *N*-(2-hydroxyethyl)-1,8-naphthalimide ( $10^{-3}$  M) and diluted 3-(adamant-1-ylmethoxy)-6-chloro-*s*-tetrazine ( $5 \times 10^{-6}$  M) and, right, a diluted ( $5 \times 10^{-6}$  M) solution of **2**, under UV light irradiation.

of direct excitation of the fluorescence in the visible region on the  $n-\pi^*$  band of the tetrazine. This result evidences the occurrence of an energy transfer between the two chromophores. In **2**, at the exception of the very small band at 360 nm, all fluorescence is transferred to the tetrazine, and a fluorescence yield of 0.3 is obtained.

We have quantified the importance of the energy transfer on the basis of the data reported in Table 3. On the assumption that all fluorescence lost by the donor is transferred to the acceptor, the efficiency of the energy transfer is given by<sup>15</sup>

$$\phi_{\text{ET}} = 1 - \frac{\phi_{\text{donor}}}{\phi_{\text{donor}}^0} = 1 - \frac{0.003}{0.061} = 0.95$$

This shows that the energy transfer is indeed quite efficient. Standard molecular modeling shows that the average distance between the imide donor and the tetrazine ring acceptor is  $\sim 8.5$  Å. The spectral overlap between the fluorescence of the donor and the absorption of the acceptor being small, a short Förster radius of  $R = 9.3$  Å is calculated; therefore, the efficiency of the energy transfer should be only  $\sim 63\%$ . The discrepancy between the calculated and the experimental value therefore inclines us to think that the energy transfer mechanism would rather be of the Dexter type or a mixed one. To refine our investigations, we recorded the fluorescence decay of the *N*-(2-hydroxyethyl)-1,8-naphthalimide

and **2**. Results (Supporting Information, Figure 2) give a fluorescence lifetime for the naphthalimide of 0.37 ns in the first case and 0.03 in the second; therefore, using the decay times, it is possible to calculate on another basis the efficiency and the rate of the energy transfer

$$\begin{aligned} \phi_{\text{ET}} &= 1 - \frac{\tau_{\text{donor}}}{\tau_{\text{donor}}^0} = 1 - \frac{0.03}{0.37} = 0.93k_{\text{ET}} \\ &= \frac{1}{\tau_{\text{donor}}} - \frac{1}{\tau_{\text{donor}}^0} = 3.06 \times 10^{10} \text{ s}^{-1} \end{aligned}$$

This is two orders of magnitude higher than the radiative lifetime of the *N*-(2-hydroxyethyl)-1,8-naphthalimide ( $k_{\text{R}} = 1.65 \times 10^8 \text{ s}^{-1}$ ). It is noteworthy that the two calculated values of  $\phi_{\text{ET}}$  are in good agreement. It is also worth noticing that for the tetrazine fluorescence decay in the case of **2**, excitation at 355 nm is more complex and especially displays a rising time. The decay could be fitted by a biexponential function giving a rising time of 0.06 ns similar to the fluorescence lifetime of the naphthalimide in **2** and a decay of 158 ns typical of the tetrazine.

Finally, we made a visual evaluation of the improved brilliance of our molecule by simply comparing the brilliance of a  $5 \times 10^{-6}$  M solution of **2** and the one of a solution of 3-(adamant-1-ylmethoxy)-6-chloro-*s*-tetrazine, which owns the same tetrazine emitter but without the presence of an imide donor. At these concentrations, both solutions are almost colorless (only the tetrazine is colored, but its absorption is low; see Figure 5A). Figure 5B shows the fluorescence of a dilute solution ( $5 \times 10^{-6}$  M) excited with a laboratory UV lamp peaking at 365 nm (close to 355 nm, both in the imide and the tetrazine  $\pi-\pi^*$  band) of both 3-(adamant-1-ylmethoxy)-6-chloro-*s*-tetrazine (Figure 5B, left) and **2** (Figure 5B, right). It is clear that because of the efficiency of the imide absorbance and the energy transfer, the brightness of the solution of **2** is much higher than the one of the standard tetrazine. A quantitative evaluation of the brilliance (column  $\epsilon(\lambda_{\text{ex}}) \times \Phi_{\text{fluor}}$  in Table 3) shows that it should be 7.5 times higher when **2** is excited at 355 nm (selective of imide moiety) rather than 517 nm (selective of tetrazine moiety), as is evidenced in Figure 5, where the visual evaluation leads to the same appreciation.<sup>16</sup>

It should be emphasized that this situation is solely due to the proximity of the two chromophores on the dyad molecule. Upon irradiation of a mixture of concentrated *N*-(2-hydroxyethyl)-1,8-naphthalimide ( $10^{-3}$  M) and diluted 3-(adamant-1-ylmethoxy)-6-chloro-*s*-tetrazine ( $5 \times 10^{-6}$  M) under UV, no energy transfer occurs, and only the weak individual fluorescence of both compounds can be observed (Figure 6).

#### IV. CONCLUSIONS

We have presented new fluorescent dyads made of a tetrazine moiety linked to various imide moieties. The physicochemical characteristics of these new molecules, featuring especially the fluorescence, have been described, showing an original physical chemistry, like the existence, for example, of a stable double anion-radical. We have also shown that it is possible, in one particular case, to activate efficiently the energy transfer, providing a dyad that is much more brilliant than a standard tetrazine with inactive substituents. Application of this new molecule to fluorescence sensors and coloration of materials is ongoing.

## ■ ASSOCIATED CONTENT

■ **Supporting Information.** Detailed experimental procedures and spectroscopic data for the molecules prepared and complete spectra of the compounds featuring the complete absorption and fluorescence spectra for all compounds, and excitation spectra for compounds 1, 2, a, and the generic chloro-(1-adamantanemethoxy)tetrazine. This material is available free of charge via the Internet at <http://pubs.acs.org>.

## ■ AUTHOR INFORMATION

**Corresponding Author**

\*Tel: +33 1 47 40 53 13. Fax: +33 1 47 40 24 54. E-mail: [audebert@ppsm.ens-cachan.fr](mailto:audebert@ppsm.ens-cachan.fr).

## ■ REFERENCES

- (1) Katritzky, R. *Handbook of Heterocyclic Chemistry*; Pergamon Press: New York, 1986.
- (2) (a) El-Sayed, M. A. *J. Chem. Phys.* **1963**, *38*, 2834. (b) Waluk, J.; Spanget-Larsen, J.; Thulstrup, E. W. *Chem. Phys.* **1995**, *200*, 201. (c) Waluk, J.; Spanget-Larsen, J.; Thulstrup, E. W. *Chem. Phys.* **2000**, *254*, 135.
- (3) Gleiter, R.; Schehlmann, V.; Spanget-Larsen, J.; Fischer, H.; Neugebauer, F. A. *J. Org. Chem.* **1988**, *53*, 5756.
- (4) (a) Beaujuge, P. M.; Reynolds, J. R. *Chem. Rev.* **2010**, *110*, 268. (b) Audebert, P.; Miomandre, F. *Electrochemistry of Conducting Polymers*. In *Conducting Polymers Handbook*; Skotheim, T., Reynolds, J., Eds.; CRC Press: Boca Raton, FL, 2006.
- (5) (a) Audebert, P.; Sadki, S.; Miomandre, F.; Clavier, G. *Electrochem. Commun.* **2004**, *6*, 144. (b) Audebert, P.; Sadki, S.; Miomandre, F.; Clavier, G.; Saoud, M.; Vernières, M. C.; Hapiot, P. *New J. Chem.* **2004**, *28*, 387. (c) Audebert, P.; Sadki, S.; Miomandre, F.; Clavier, G.; Badré, S.; Vernières, M. C.; Méallet-Renault, R. *Chem.—Eur. J.* **2005**, *11*, 5667.
- (6) (a) Ding, J.; Song, N.; Li, Z. *Chem. Commun.* **2010**, *46*, 8668. (b) Li, Z.; Ding, J.; Song, N.; Lu, J.; Tao, Y. *J. Am. Chem. Soc.* **2010**, *132*, 13160. (c) Li, Z.; Ding, J.; Song, N.; Du, X.; Zhou, J.; Lu, J.; Tao, Y. *Chem. Mater.* **2011**, *23*, 1977.
- (7) Gong, Y.-H.; Miomandre, F.; Méallet-Renault, R.; Badré, S.; Galmiche, L.; Tang, J.; Audebert, P.; Clavier, G. *Eur. J. Org. Chem.* **2009**, *15*, 6121.
- (8) Audebert, P.; Allain, C.; Galmiche, L. French Patent, 2010. See also ref 5c.
- (9) (a) Clavier, G.; Audebert, P. *Chem. Rev.* **2010**, *110*, 3299. (b) Saracoglu, N. *Tetrahedron* **2007**, *63*, 4199.
- (10) (a) Kunetz, O.; Salman, H.; Eichen, Y.; Remacle, F.; Levine, R. D.; Speiser, S. *J. Photochem. Photobiol., A* **2007**, *191*, 176. (b) Kunetz, O.; David, D.; Salman, H.; Eichen, R. D.; Speiser, S. *J. Phys. Chem. C* **2007**, *191*, 176. (c) Speiser, S. *Chem. Rev.* **1996**, *96*, 1953.
- (11) Speiser, S.; Kataro, R.; Welner, S.; Rubin, M. B. *Chem. Phys. Lett.* **1979**, *61*, 199. (b) Getz, D.; Ron, A.; Rubin, M. B.; Speiser, S. *J. Phys. Chem.* **1980**, *84*, 768. (c) Hassoon, S.; Lustig, S.; Rubin, M. B.; Speiser, S. *J. Phys. Chem.* **1984**, *88*, 6367.
- (12) Ramachandram, B.; Saroja, G.; Sankaran, N. B.; Samanta, A. *J. Phys. Chem. B* **2000**, *104*, 11824.
- (13) Dumas-Verdes, C.; Miomandre, F.; Lepicier, E.; Galangau, O.; Vu, T. T.; Clavier, G.; Meallet-Renault, R.; Audebert, P. *Eur. J. Org. Chem.* **2010**, *16*, 2525.
- (14) Zhou, Q.; Audebert, P.; S.; Miomandre, F.; Clavier, G.; Tang, J.; Vu, T. T.; Méallet-Renault, R. *J. Electroanal. Chem.* **2009**, *632*, 39.
- (15) Valeur, B. *Molecular Fluorescence: Principles and Applications*; Wiley-VCH: Weinheim, Germany, 2001.
- (16) It is true that the spectrum of the standard laboratory UV lamp is much broader than the laser used for the measurements; nevertheless, the effect is quite discernible.

# Acknowledgement

My time at PPSM has been impactful, formative, and an extraordinary experience that I will remember with gratitude throughout my life. I must express my appreciation to who accompany with me during these years.

First of all, I would begin to thank to professor Jean-Christophe Lacroix and Jean-Manuel Raimundo for being my rapporteurs, and Céline Frochot for coming into the jury and being my examinateur.

My deepest gratitude goes first and foremost to my two supervisors: Dr. Fabien Miomandre of Ecole Normale Supérieure de Cachan in France and Prof. Jie Tang of East China Normal University in China. Words are simply not enough for expressing gratitude towards them. First, I would like to thank Dr. Miomandre for accepting me for my PhD study. I would like to thank him for everything that I have learned from him, especially the electrochemistry research, in general during my three years in France. I would like to thank Prof. Tang for his continuous support, encouragement and guide during six years since my master studies. It is a treasure for all my life.

I would to express my warm and sincere thanks to Prof. Pierre Audebert and Dr. Gilles Clavier. I would not have completed the PhD without the encouragement and sound advice of them. Thank you Pierre, your wisdom, knowledge, commitment to the highest levels inspired and motivated me, you are a good example that life is more than just science. Thank you Gilles, discussions always leave me impressed with your depth of knowledge and increase my desire to learn more. Gilles has pushed me to work harder and think more deeply about the physical processes we have studied.

Of the members of PA team past and present, Dr. Rachel Méallet-Renault, Dr. Clémence Allain, Laurent Galmiche (Ingénieur d'étude), Dr. Valérie Alain-Rizzo, Dr. Thanh-Truc Vu, Dr. Olivier Galangau, Chloé Gazon, Cassandre Quinton, Johan Saba and Jérémy Malinge have had the greatest impact on my research. As a new graduate student, Dr. Clémence Allain, Dr. Rachel Méallet-Renault and Dr. Valérie Alain-Rizzo give me suggestion when I was lost in the spectroscopic lab; Laurent Galmiche is a superman who can solve all of the problem in the lab; Thanh tutored me in the ways of fluorescence area; Olivier helped me to know how to use the instruments in the lab; Chloé, you are so nice and kind as friend (I like the traditional food from Tour ); Cassandre, because of you, I'm not lonely in tetrazine's chemistry in our lab and the cake made by yourself is always delicious; Johan, thanks for your help in electrochemistry when I was a beginner; Jérémy, tetrazine's guy, your wise suggestions (2NITZ) helped the work take off and transform into exciting novel

results.

I would like to acknowledge Prof. Joanne XIE, Prof. Keitaro Nakatani who helped me during my whole stay here. Thanks Rémi Métivier for his patient academic explanation. I would like to thank Jacky for his always kindness and help for many computer problems. I've had the privilege of working especially closely with Arnaud Brosseau on the photophysical work, Stéphanne Maisonnneuve on the NMR work, and it's been good to work with Cécile Dumas-Verdes, Carine Julien-Rabant, Isabelle Leray, Nicolas Bogliotti. Also, I would like to thank Andrée and Christian for their administrative responses and availability.

I warmly thank Prof. Fan Yang for the help in study and in life.

There are so many members of PPSM lab, including Jérémy Bell, Yibin Ruan, Aurélie, Yanhua Yu, Eva Jullien, YuanYuan Liao, Alexis Depauw, Djibril Faye, Ni Ha Nguyen, Olivier Noël, Sandrine Peyrat, Jia Su, Haitao Zhang as well as the new student yang Si. If I have forgotten anyone, I apologize.

I would like to thank Mrs. Yunhua QIAN, Mr. Haisheng LI of ECNU and Miss Xiaolin Liu for all the administrative help. Also, I would like to thank all the colleagues in ECNU. I would like to thank Ms. Bogdana Neuville, Ms. Christine ROSE, Ms. Brigitte Vidal and Aurore Patey in ENS-CACHAN.

I extend my thanks to my lifetime friends including Yonghua Gong, Yibin Ruan, Yuheng Yang, Yanchun Gong, Xiaoqian Xu, Yingying, Chen, Xiaoju Ni, Yanhua Yu, Xiao Wu, Na Li, Chun Li, Zhongwei Tang, Sanjun Zhang, Ming Zhang, Jia Su, Hui Li, Guopin Sun and Tong Wu et al, for their friendship and support over the years. Life would have been dull without you!

Finally, my greatest love and support is my family. My parents are amazing people that they are optimistic. Words can't express the blessing and rock solid support they have been all my life.

This note would be incomplete if I do not mention my thanks to the collaboration program between ENS CACHAN and ECNU which favored me to complete this thesis.